X-RAY AND NEUTRON DIFFRACTION STUDIES OF SOME RARE-EARTH DOPED BORATE GLASSES AND COATED SILICA MICROSPHERES

A Thesis Submitted to

Goa University

For the Award of the Degree of

DOCTOR OF PHILOSOPHY

in

Physics

By

WILSON AGNELO VAZ

Research Guide

Prof. J. A. E. Desa

Goa University
Taleigao Goa

2014

Declaration

It is hereby declared that this thesis entitled, "X-ray and Neutron Diffraction Studies of some Rare Earth Doped Borate Glasses and Coated Silica Microspheres" submitted to Goa University for the award of the degree of **Doctor of Philosophy in Physics** is a record of original and independent work carried out by me during January 2008 – May 2014, at the **Department of Physics, Goa University**, under the supervision of Prof. J.A.E. Desa, Department of Physics, Goa University, and that it has not formed the basis for the award of any Degree or Diploma to any candidate of this or any other University.

Goa University

30th May, 2014

Wilson Agnelo Vaz

(Research Scholar)

Certificate

This is to certify that the thesis entitled, "X-ray and Neutron Diffraction Studies of some Rare Earth Doped Borate Glasses and Coated Silica Microspheres" submitted to Goa University for the award of the degree of **Doctor of Philosophy in Physics**, is a record of original and independent work carried out by Mr. **Wilson Agnelo Vaz**, during the period, January 2008 – May 2014 at the **Department of Physics, Goa University**, under my supervision and that it has not previously formed the basis for the award of any Degree, Diploma, Associate-ship or Fellowship or any other similar title to any candidate of this or any other University.

Prof. J.A.E. Desa

DEPARTMENT OF PHYSICS

GOA UNIVERSITY

Abstract

The well known glass former B_2O_3 was chosen to be the host matrix for studies involving inclusion of rare-earth ions into this glass. The objectives were to investigate the environmental changes of both the dopant and the host as a result of such inclusions.

The work commenced with studies of absorption in the visible region by the Neodymium-Praseodymium pair of ions included in different relative proportions – from 1 to 8 mole %. It was found that the frequencies of absorption maxima of either ion type were not changed by the presence of the other rare-earth. Luminescent emissions in the range 800 to 900 nm had decay times between 1.094 to 1.225 μs. which were found to be similar to such emission times in a phosphate glass and indicated that these levels were not sensitive to the host matrix.

Neodymium oxide was included in B_2O_3 in the molar concentration range of 10% to 25%. The 1st peak at 1.366 was due to BO_3 while the BO_4 units were at 1.475 ± 0.002 Å. The percentage of 4-fold coordinated boron varied from 28% to 40% in these glasses. The Nd-O correlation distance was 2.487 ± 0.002 Å with coordination varying from 9.5 to 6 ± 0.1 in this series. It is proposed that as the Nd inclusion percentage increases, the ion is first surrounded by complex structural units of the host and then has the simpler trigonal and tetrahedral units surrounding it.

Nd and Ho ions were included together as 20 molar % but in differing relative ratios in the borate host glass. The first peak had the same constituent correlations as in the Nd borate glass but with 33% of boron atoms in BO_4 units. The combined Nd and Ho correlation with O was at 2.475 ± 0.002 Å and had coordination with O which varied from 10.5 to 5.5 ± 0.1. In this twin rare-earth included glass, both ions had complex structural units of the host surrounding them in contrast to the glass when only one rare-earth ion type is included.

Silica glass in the form of microspheres was successfully coated with Ag, Ni, ZnO and CdS. In order to increase the surface area to volume ratio adequately for X-ray and neutron diffraction studies, the coated microspheres were compacted and sintered to form rigid yet porous pellets. The coated compacts retained their surface coatings although the structure of the coating in the case of Nickel was not clearly identified. The other materials were shown to have retained their original crystalline forms prior to coating.

Acknowledgement

To know about something is not the same as understanding it. To understand something is to do a deep dive into the nuances of facts that reveal shades of meaning, challenging the seeker into connecting them into a meaningful whole.

It's in understanding the meaning of things that I could, in time, hope to find the purpose of why things are the way they are, a necessity as much a requirement for my doctoral research as for my own fulfillment.

It's this, more than anything else that made my pursuit of meaning behind the apparent complexities of nature such a rewarding journey, one that set me on myriad paths along the way, each promising and delivering a revelation that would equip me with a better understanding of why things are the way they are, nudging me further down the road of discovery – of meaning.

It's on this journey that I met with fellow riders who kept me company, steered me down the right paths, challenged me to ride a little longer on stretches abandoned by milestones, lit the road with their lamps when my own flickered uncertainly at times, alerted me to bumps in the road ahead, and braved long nights so I could ride on to the finish line.

Without them my journey as a researcher delving into the complexities of nature would've been an impossible one to chart successfully.

I take this opportunity to acknowledge my collaborators, benefactors and well wishers and express my heartfelt gratitude for their assistance rendered, and for keeping the faith.

At the outset I acknowledge the beneficence of the Almighty who worked in visible and invisible ways, providing me with opportunities, to pursue my research.

This Ph.D. thesis is as much a result of my own pursuit of meaning and purpose behind aspects of nature that fascinate and intrigue me no end, it is equally a result of my guide Prof. J.A.E. Desa, former Head, Department of Physics, and former Dean, Faculty of Natural Sciences, Goa University, extending his valuable support for the entire duration of my research work.

As a student of Prof. Erwin Desa, I've benefited greatly from his vast experience, enlightened principles and expert guidance in preparing and executing my work efficiently and effectively. In his company I learnt to look at my subject in particular and life in general in a different perspective, one that helped fill gaps in my own understanding of both.

It is difficult to express in words my deep sense of gratitude to my esteemed guide and teacher. Despite myriad commitments, official and family responsibilities and duties and other stressors, he reached out to me. I remain indebted to him for his valuable guidance, unwavering support, critical evaluation that challenged me to do better, and the tireless pursuit for perfection he demanded of me; together they inspired me throughout my Ph.D. course. His scientific approach to resolving problems systematically and logically, in-depth knowledge, personal touch, sincerity, boosting spirit, and untiring efforts proved to be immensely useful.

I am grateful to my subject experts, Prof. P.R. Sarode and Prof. K.R. Priolkar for their encouragement, guidance and support right from the inception of my research work.

This thesis would not have been completed without financial help and assistance by UGC-DAE through the projects entitled "Structural studies of coated and compacted microspheres" and "Structural and Optical studies of Rare-Earth doped borate Glasses". My sincere thanks to Dr. S.L. Chaplot, Group Director, Physics Division, B.A.R.C., Mumbai, Dr. R. Mukhopadyaya, Head, Solids State Physics Division, B.A.R.C., Mumbai, Dr. Pravin

Chaddah, Director of UGC-DAE-CSR, and also to former and present Mumbai-Centre Directors, Dr. A.V. Pimpale and Dr. V. Siruguri who have helped facilitate my work.

It is with sincere gratitude I acknowledge the valuable assistance I received from the principal collaborator in this project, Dr. P. S. R. Krishna and Mr. A. B. Shinde of Solid State Physics Division, BARC. Their prompt guidance, expertise, meaningful insight and critical discussions of data analysis, along with their vast experience were instrumental in bringing my project to fruition.

I also would like to thank Dr. Andreas Hoser and Dr. Illia Glavatskyi (Helmholtz Center, Berlin) for the Neutron diffraction data from the Flat-Cone Diffractometer and also for their hospitality.

I gratefully acknowledge the assistance of Department of Science, Technology and Environment, Government of Goa, and particularly former Director, Mr. Michael D'Souza for funding the project entitled "Structural studies of rare earth doped Borate Glasses" for a period of three years.

I wish to express thanks and gratitude to the former Deans of the Faculty of Natural Sciences, Goa University, and the present Dean, Prof. A. V. Salkar. My thanks are also due to former Head, Prof. P. R. Sarode and the present Head, Physics Department, Prof. R. B. Tangsali, for making available the department infrastructure crucial to my research.

My gratitude goes out to my fellow researcher, Dr. Bosco Lawrence and my friends Sebastiao Marcelo, Jose Pereira, Maria Gracias e Fernandes, Anil Purohit and Harish Shirodkar for being supportive and prodding me on, at all times.

I wish to express my appreciation to all my fellow research scholars – Dr. Shraddha Ganorkar, Kapil Ingle, Elaine Dias, Jason Joseph, Pranav Naik, Nilima B., and Dr. Reshma

Raut Desai for their kindness, assistance and cooperation. I cannot fail to appreciate the cooperation and assistance rendered by the non-teaching staff of the Department of Physics, namely, Ramchandra Naik, Hermina Araujo, Eva Baptista, Santosh Vaigankar and Santosh Salgaokar. I sincerely wish to thank the library staff and the administrative staff of Goa University for all the help they provided in bringing this thesis to completion.

I would also, like to thank the former and present Managements of my institution, Goa Vidyaprasarak Mandal, as well as, the former and present Principals of Smt. Nelly Joildo Aguiar Higher Secondary School, Farmagudi for the support and cooperation rendered to me.

My family and in-laws have contributed to my efforts in innumerable ways. I take this opportunity to thank my family members, for being supportive of my passion and for their encouragement. I am at loss for appropriate words to accurately describe or acknowledge their contribution and unflinching support in helping me see my work to completion.

To my wife, Yheula, and my daughters, Elishka and Annalise, I'm indebted for keeping the light in the window at all times. They anchored me in ways that helped sustain my spirit of inquiry necessary to continue my work successfully putting up with my odd schedule and eccentricities without a word of complaint, at times, saving me from duties and responsibilities so that I could devote attention to my work.

At this point, I also wish to acknowledge that there are several other people who deserve credit for having supported and assisted me. I wish to thank them, as well, even though their names have not been explicitly mentioned over here.

To sum up, to each and everyone, DEV BOREM KORUM.

Wilson Agnelo Vaz

Ponda, Goa.

Contents

List of Figures

List of Tables

Chapter 1

Introduction

1.1 Introductory Remarks

The four states of matter viz. solid, liquid, gas and plasma all have well evolved theories to describe their essential properties and structures. However, there are some special states that possess properties of more than one of these principal states. One of these special types of material is a glass. A glass is a solid in terms of rigidity and shear properties but has the properties of a liquid when the latter is viewed at a microscopic level and for very short time intervals. The challenges to the characterization of this rather unique type of material are such that many different techniques that probe its physical properties need to be brought to bear on the study of the glassy state. The work described here focuses on one type of glass i.e. the borate system when this is made to incorporate heavy ions such as the rare-earth elements. This glass is examined in terms of its structure and the way in which the included rare-earth ions are accommodated in the bulk of the glass. Also reported here is an attempt at depositing different ions on the surface of a silicate glass.

1.2 The Glassy State

In everyday occurrence, we see glass as a transparent solid that cracks easily. But there are glasses – chalcogenides and metallic – which are opaque and have high strength, some being used in armoured applications.

According to the American Society for Testing Materials (ASTM), Glass is defined as “an inorganic product of fusion which has been cooled to a rigid condition without crystallising”.

This definition of glass needs to be modified because the ‘sol-gel’ process of making glass

avoids the high temperature used for fusion of glass and a technique such as 'Chemical Vapour Deposition' does not require fusion of constituent materials.

1.2.1 The V-T Diagram

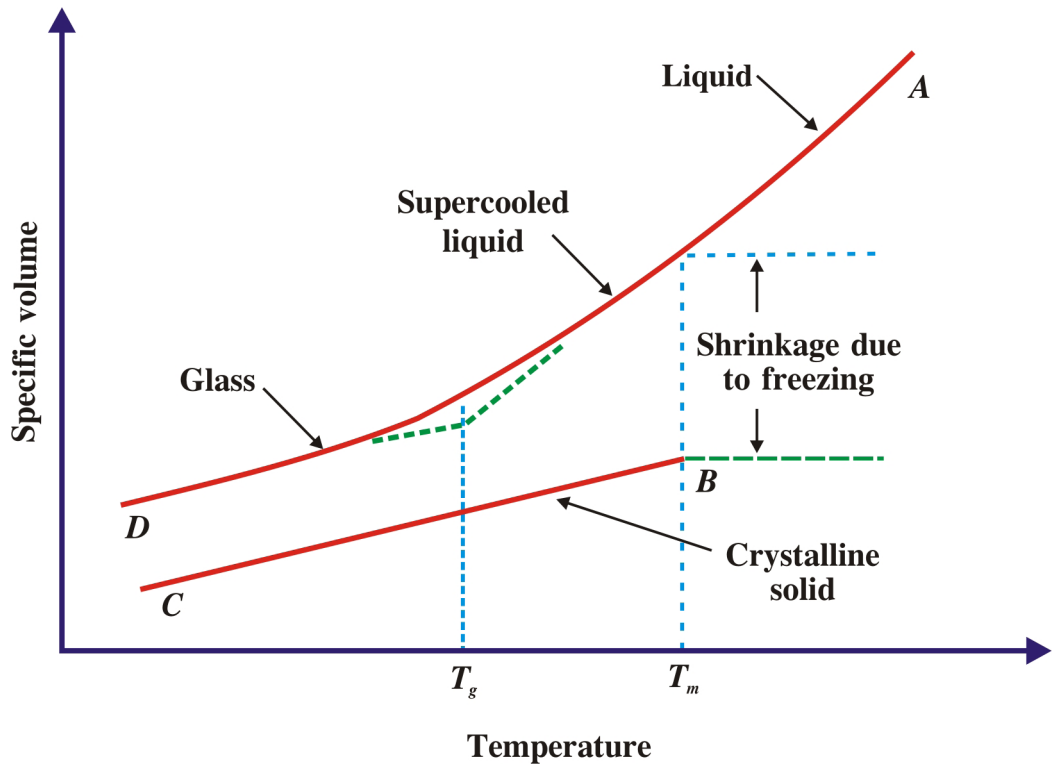

Figure 1.2.1.1: The Specific Volume-Temperature diagram for a melt as a function of temperature from the liquid to the glassy states.

If a small volume of melt is cooled slowly from a high temperature 'A', the volume decreases as shown in Figure 1.2.1.1. The point 'B' corresponds to the melting point T_m of the corresponding crystal. Crystallization will occur, when the liquid is cooled further, if there are a large number of nuclei and a large crystal growth. The crystal will shrink along the crystalline line as it cools. On the other hand, if the melt is cooled rapidly, it becomes super cooled. The molecules rapidly constitute a viscous state; as the cooling continues and behave essentially like the molecules of a solid. This is the glassy state.

1.2.2 Definition of Glass

There are many different types of glass depending on their compositions and thermal histories. However, no matter the speed with which a glass is quenched from the melt or cooled from the liquid state, a temperature known as the Glass Transition temperature, T_g, can be identified in each of these types of glasses. This temperature occurs below the crystallization temperature, T_m, at which the liquid transforms into a crystal. The glass transition temperature is that temperature range over which the super-cooled liquid cools to a rigid solid (i.e. high resistance to shear stress).

A glass may also be thought of as a solid in which there is no long-range translational symmetry - unlike the situation in a crystal. In a glass there is, nevertheless, order which is of a very short range - typically that of the chemical composition unit from which the structure can be generated. In the modeling of glassy structures, these units can be made to link together to form a continuous random network. The extent of crystallinity i.e. short and medium range order will vary according to the type of glass and its composition.

"Glass is a non-crystalline solid in which there is only a short- range order but no long-range translational symmetry."

Thus, glass structures can be constructed from the basic units which can be linked together to form a continuous three dimensional random network. In the figure 1.2.2.1, the basic structural unit is linked to each other in a random manner to form a glass as opposed to the crystal where there is long-range symmetry.

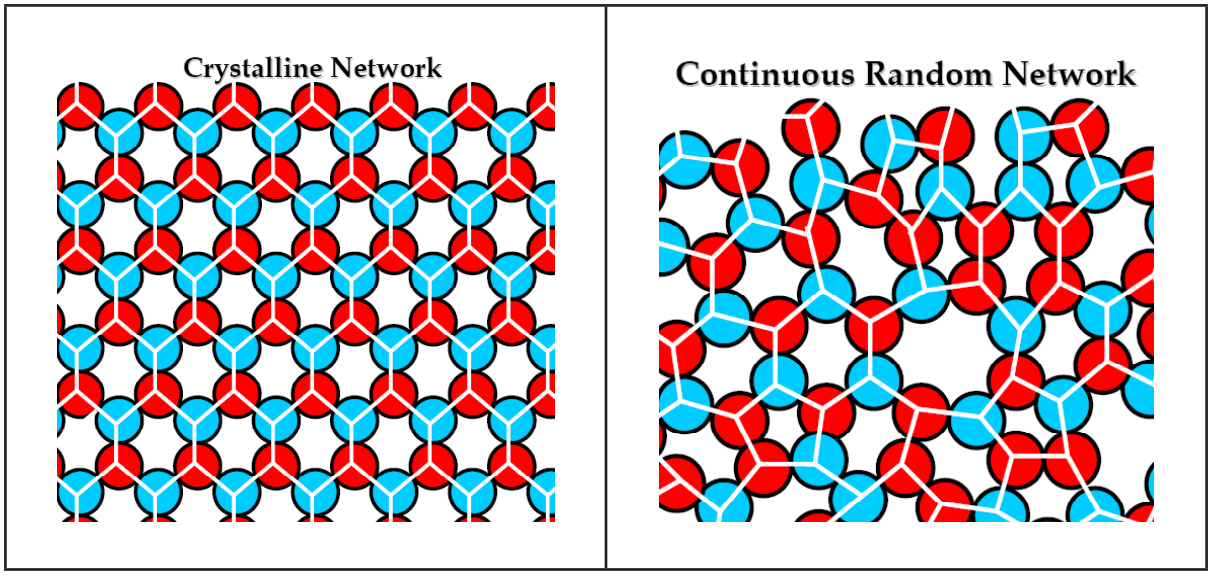

Figure 1.2.2.1: Schematic representations of a 2-D crystalline material and a glass.

1.3 Structural Theories of Glass Formation

There are many different structural theories of glass formation (Varshneya (2006)): Goldschmidt's radius ratio criterion, Zachariasen's random network theory, Smekal's mixed bonding rule, Stanworth's electro negativity rule. But the oldest and perhaps widest use is due to Zachariasen (1932).

According to Zachariasen, the mechanical properties of a glass and crystal are similar and must be so because of atomic forces being the same in both materials. X-ray diffraction of a glass shows diffuse diffraction rings and an infinitely large unit cell. The 3-D random network of bonds between atoms in the glass causes the vitreous state to have a higher internal energy as compared to a crystal. The difference of energy between a crystal and a glass must be small or else the glass would not form. Also, the glass structure must be more open than the crystal. Zachariasen suggested that the glass has a continuous random network in which there is no long-range periodicity. He proposed four rules that govern glass formation in an oxide of a cation A :

1. An oxygen atom is linked to no more than two atoms of A.
2. The oxygen coordination around A is small, say 3 or 4.
3. The cation polyhedra share corners, not edges, not faces.
4. At least 3 corners are shared.

In his view of the glassy state, the fact that atoms in the structure may not be fully ionized is not important so long as an ionic interpretation is possible.

1.4 Kinetic Theory of Glass Formation

Liquids can in principle be vitrified if the rate of cooling is adequately high to bypass crystallization. Crystallization requires the formation of nuclei and their growth. In order to determine if a system will vitrify, one needs to perform the following:

i. Calculate the rate of nucleation I, as a function of temperature.

ii. Calculate the rate of crystal growth μ, as a function of temperature.

iii. Combine (i) and (ii) to determine the volume fraction of crystallization.

1.4.1 Nucleation Rate

The barriers to crystalline nucleus formation are :

1. The kinetic barrier ΔE_D, which is the activation energy required for an atom to cross the liquid-nucleus interface.
2. The thermo-dynamic barrier ω, expressed as number of nuclei formed per unit volume per second, which is the net free energy charge in the system after a nucleus is formed.

The nucleation rate is given by

$$I = no \exp(-NW^*/RT) \exp(-\Delta E_D/RT) \quad (1.4.1.1)$$

where N = the Avogadro's number

R = gas constant

T = absolute temperature

We can define two types of nucleation:

1. Homogeneous nucleation: The random assembly of a number of atoms to form a group which leads to the lowering of the net free energy of the system.

2. Heterogeneous system: The chance assembly on pre-existing surfaces of foreign materials.

1.4.2 Crystal Growth

The crystal growth is given by

$$\mu = [f (RT/3N\pi a^2_{\mu})] [1- \exp (\Delta G_{\mu}/RT)]$$

where f is the fraction of the surface area on which growth sites may be available, a is the size of a crystallite, ΔG is the Gibb's free energy (Varshneya (2006)).

1.5 Melt-Quenched Oxide and Other Glasses with Rare-Earth and Transition Metal Oxides

Oxide glasses have been well studied (Rawson(1965), Elliott (1990)) but continue to be the subject of intensive interest on account of their wide applicability. The oxide states of Si, B, Ge, P, etc. readily form stable glasses into which a variety of different compounds may be added. These form glasses with properties with ranges of refractive index, mechanical strength, dielectric constant etc. Chalcogenide glasses are also of much relevance in conducting applications.

1.6 Models of Glass Structure

Most simple glasses whose structures are to be modeled can be categorized into either a random network structure or one that relies on generation of the full network from micro-crystallite units i.e. the crystallite theory. At present the distinction between these two approaches is small and depends on the degree to which either the basic unit is similar to that in the crystalline starting material(s) (Wright (1974)).

Glass structural work tends to focus on establishing the structural parameters of the basic chemical units and detailing the average parameters that decide on how these units link together to form a continuous random network. Much of this aspect of modeling a glass depends on knowledge of its permitted chemistry and bonding requirements.

In recent times, computer modeling of glass structures have moved from the Monte Carlo and Molecular Dynamics approaches to Reverse Monte Carlo methods in which the intensities in momentum space and their Fourier Transforms are iteratively modeled until assumed structural features are either confirmed or rejected.

1.7 Techniques of Characterization of Glasses

The various methods of probing the structures and dynamics of glasses rely on the fact that the short-range structures and the energies of vibration are similar to those of the related crystalline materials from which the glasses are melted. Structural studies tend to focus on the inter-atomic distances and nearest-neighbour coordinations of atoms in the basic chemical composition unit and the ways in which these units link together to form a continuous random network that constitutes the glass structure. Thus, structural methods such as X-ray, neutron diffraction and EXAFS are often used for first and second-neighbour structures while small angle X-ray and neutron scattering can be applied to investigate intermediate order or Mesoscopic structures. Scanning, Transmission and Atomic Force microscopy can all be put to use in examining surface structures as well.

Inelastic scattering of various radiations such as Infra-red, Raman, inelastic neutron etc. are of much value in measuring the vibrational properties of glasses and linking these to the structural models obtained from the above-mentioned structural techniques.

A variety of magnetic and electrical techniques can also be employed in measuring magnetic susceptibilities of paramagnetic glasses, semi-conducting glasses and others containing ions of magnetic and electrical importance.

1.8 Review of Literature of Structures of Borate Glass

The structure of vitreous Borate glass (v-B_2O_3) as was first suggested by Zachariasen (1932) consists of a random network of corner-linked BO_3 triangles as depicted in the 2-D in Figure 1.8.1.

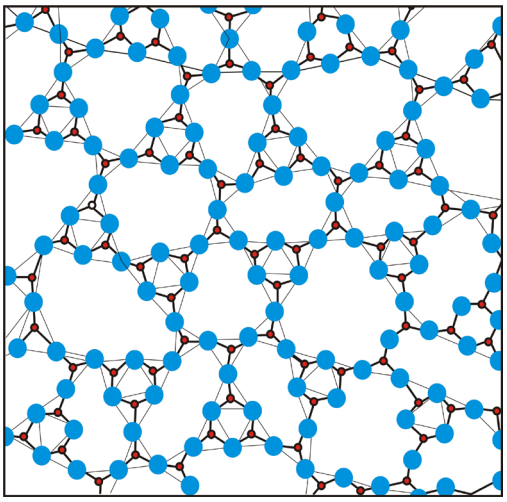

Figure 1.8.1: Schematic of a 2-D borate glass consisting only of BO_3 triangles. (after Johnson et al. (1982))

The X-ray investigation by Warren (1936), deduced the BO_3 triangle structural unit as the boron-oxygen configuration in various crystalline borates. Further X-ray studies (Green (1942), Krogh-Moe (1959), Mozzi and Warren (1970)) confirmed the triangle co-ordination of oxygen around boron, so also have the results of NMR experiments (Bray (1960), Svanson (1962) and Jellison (1976)).

Even though the model of BO_3 units in a plane was widely accepted in v-B_2O_3, the way these units were linked together remained a mystery. Some of the physical properties of v-B_2O_3 were found to be in disagreement of a network structure. It was found that the viscosity of the borate glass was less than that of silica glass by a factor of $10^{-11.6}$ at 1260^0C, which was difficult to explain on the basis of network of strong boron-oxygen bonds (Fajans and Barber (1952)).

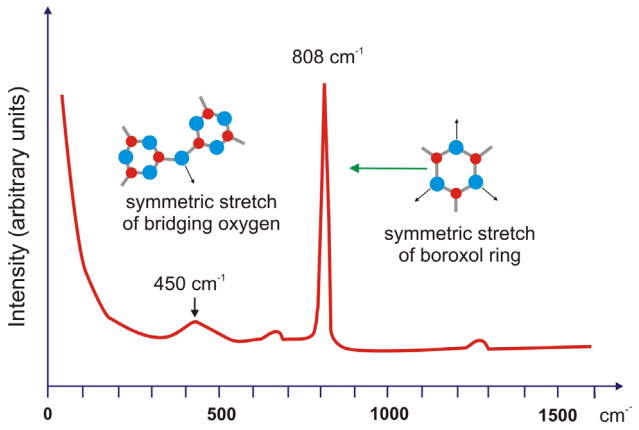

Figure 1.8.2 : Raman spectrum of vitreous B_2O_3 (adapted from Galeener (1983))

The presence of boroxol rings of B_3O_6 in the structure of v-B_2O_3 was first suggested by Goubeau et al (1953) to explain the extremely sharp lines in the Raman spectrum at 808cm^{-1} (Figure 1.8.2). Figure 1.8.3 shows a boroxol group, which consists of a three-membered ring of BO_3 triangles (6 atoms) which are planar due to delocalized π-bonding. The aromatic nature of the ring was substantiated by studies of boroxol and substituted boroxols (Barton et al 1977) and by molecular orbital calculations (Labarre et al (1968) and Serafini (1975)).

The evidence of boroxol rings in v-B_2O_3 was extracted by Krogh-Moe (1969) who reckoned that the best explanation of the data at hand supports a random three-dimensional network of BO_3 triangles with a comparatively high fraction of boroxol rings similar to that illustrated in Figure 1.8.1

The X-ray correlation function shown in Figure. 1.8.4 was interpreted by Mozzi and Warren (1970) to be in tune with a network dominated by boroxol groups. This model assumed a random network of boroxol groups, with no independent BO_3 triangles, and includes all the fixed distances defined in fig.4, along with the first inter-ring B-B correlational length assuming a bond angle β on the bridging oxygen atom between rings of 130^0.

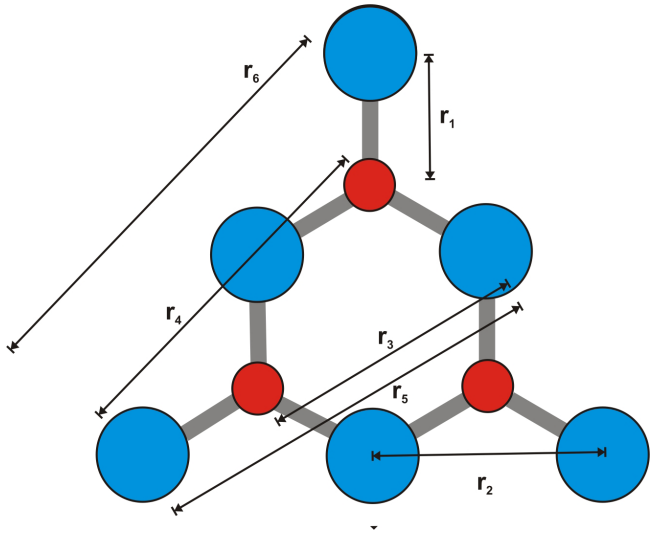

Figure 1.8.3: Boron and Oxygen atoms of a boroxol ring

(after Johnson et al. (1982))

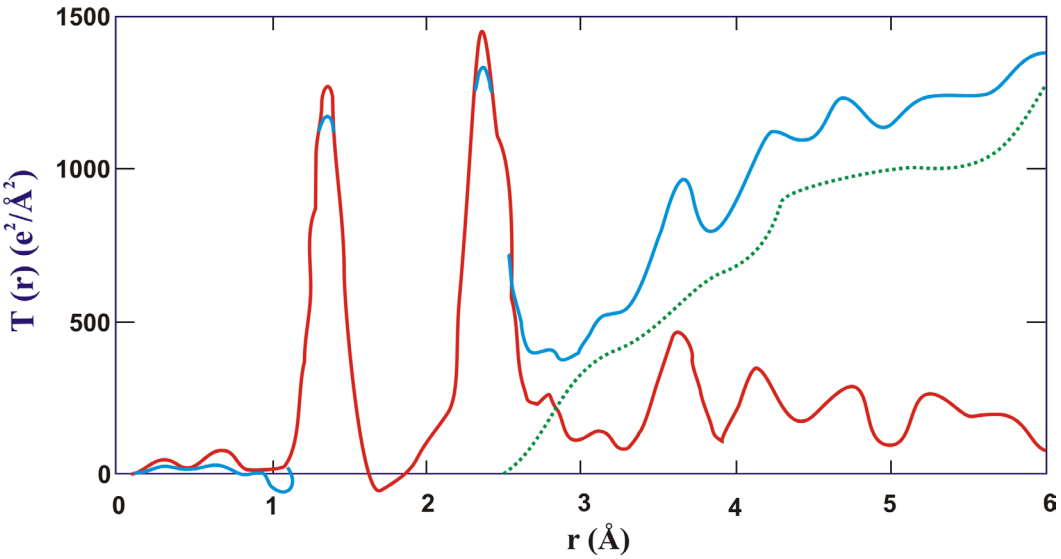

Figure 1.8.4: X-ray total correlation function T(r) of vitreous B_2O_3

(after Mozzi and Warren (1970))

The model correctly predicted all the peaks in the experimental correlation function upto 6Å including the B-O length to be 1.37Å.The structure of the model was a little too sharp implying that not all the BO_3 triangles in v-B_2O_3 form part of boroxol groups.

The presence of boroxol ring was buttressed further by the results of Jellison et al. (1977) and Bray et al. (1980), with nuclear magnetic resonance experiments. They probed the environment of ^{10}B, ^{11}B and ^{17}O nuclei in the borate glass and asserted that their data are in agreement with the boroxol ring model and from the ^{17}O spectra were able to deduce the fraction of oxygen atoms included in boroxol rings. The fraction of the boron atoms which formed the part of the boroxol rings was found to be 0.82 ± 0.08 (Jellison, 1977) and hence the boroxol group to independent BO_3 triangle ratio was found to be ~ 1.5:1. These authors also found the B-Ô-B angles for units connected to the boroxol ring and found them to be centred about 134.6^0 or 128.1^0 which was close to the value of 130^o of Mozzi and Warren (1970).

Inspite of overwhelming evidence in favour of the boroxol group, some groups begged to differ. Dunlevey and Cooper (1972, 1977) used procedures similar to Mozzi and Warren (1970) to study v-B_2O_3 and also compacted one at 21kbar. They concluded that a structural model for v-B_2O_3 does not require a great proportion of boroxol groups. This was in view of differing correlation function model and experiment around the first O-O peak at 2.4Å. The devitrification of v-B_2O_3 occurred via a rearrangement of the relative orientation of adjacent BO_3 triangles and not by an increase in the boron coordination number as occurs for the crystal at similar pressures.

Models for v-B_2O_3 were derived from hand-built models of SiO_2 (Evans and King 1966) and (Bell and Dean 1972) using geometric transformation techniques. Elliott (1978) found the coordinates of two random networks of BO_3 triangles using a decoration transformation

(Wright (1980)) of amorphous arsenic models of Greaves and Davis (1974). However the model did not contain any 3-membered boroxol rings.

Then a 1344 atom hand-built model was constructed of v-B_2O_3 without boroxol rings by Williams and Elliott (1982), with density higher than the measured value. The peaks in the experimental correlation function were introduced. Even after corrections for experimental broadening the model correlation function peak had features different to the ones obtained by X-ray and neutron diffraction. Since the torsion angles in the model were not sufficiently constrained the peak at ~3.6 Å was not narrow. The model also had a shoulder on the peak at 2.4 Å which was not observed in the data.

Wright et al (1982) built two 1200 atom ball-and-stick models containing equal number of boroxol groups and independent BO_3 triangles (f=0.75), in which one model had the two types of atoms arranged at random and the other with an alternate arrangement of units. The density of the alternate model turned out to be unstable and the correlation function did not agree with the experiment. The random model should contain larger proportion of boroxol groups since the density of the model was 17% lower than v-B_2O_3. Besides the correlation functions measured by neutrons appeared to match the random model and in particular the peak at ~3.6Å was well reproduced.

Johnson et al (1982) concluded that the neutron diffraction results and the X-ray data of Mozzi and Warren (1970) was consistent with a structure of v-B_2O_3 containing a fraction of 0.6 ± 0.2 of the B atoms in the boroxol rings. This value agreed with Jellison et al (1977) who had obtained 0.82 ± 0.08. A network containing an equal number of B_3O_6 boroxol groups and independent BO_3 triangles which had a value of 0.75, was found to be suitable for modeling purposes. The question remained whether B_3O_6 unit was linked together or exhibited topological ordering.

Nuclear quadrupole resonance experiments conducted on v-B_2O_3 showed clear evidence of

two distinct boron sites ((Gravina et al (1990), Bray et al (1991, 1992)). These results indicated that boron atoms are from the boroxol rings and independent BO_3 triangles, giving a value of $f = 0.85 \pm 0.02$ in close agreement with the previous NMR result.

Galeener and Geissberger (1982) in Raman scattering measurements on v-B_2O_3 found that the 808cm^{-1} and 470cm^{-1} lines were unshifted, indicating that they are associated with modes with little or no motion of boron atoms, the sharp 808cm^{-1} line was thus interpreted as due to the breathing mode of boroxol ring. The sharpness of the line was ascribed to a single ring and the small spread of angles in the rings. The broad 470cm^{-1} line was interpreted as being due to an inplane motion of the bridging oxygen. The breadth is ascribed to the motion being extended and to the distribution of bridging oxygen B-Ô-B angles outside the rings.

In other Raman studies Windisch and Risen (1982) and Risen (1985) found that oxygen as well as boron was isotopically substituted and showed that there was highly localized vibrational motion, characteristic of boroxol rings, and network motion, characteristic of such rings randomly connected in a network. For a $^{11}B^{16}O_{1.5}$-$^{18}O_{1.5}$ sample, the 808cm^{-1} line was found to have split into four unbroadened lines with intensities in the ratio 1:3:3:1 and that was very strong evidence that the 808cm^{-1} line is due to a localized motion of the oxygen atom in a boroxol ring. Galeener and Thorp (1983) performed central-force network dynamics calculations for v-B_2O_3 in which it was shown that a CRN of boroxol groups shows greater agreement with the richness of the spectral structure observed by Raman scattering than does a model not containing boroxol groups. These authors proposed a model having the main features of the Raman spectra and the small differences were attributed to the need to include non-central forces in the network dynamics.

Kanehisa and Elliott (1989) showed that the breathing mode of the boroxol ring is not coupled to the borate network which is to be expected from the fact that the Raman line at 808 cm^{-1} is very sharp. A relatively high resolution inelastic neutron scattering experiment was performed ((Hannon et al. 1988), and (Hannon et al. 1993) to examine the importance of the boroxol ring breathing mode in the vibrational density of states of v-B_2O_3. The inelastic neutron scattering experiment showed that the boroxol ring breathing mode is not the main feature in the vibrational density of states. The result strongly supports the model in which the majority of boron atoms are in boroxol groups ($f = 0.80 \pm 0.05$).

1.9 Objectives of the Present Work

The well known glass former B_2O_3 was chosen in this study as the host matrix for the investigation of the effect that an included heavy ion species has on the structure of the host. Although many studies have been reported on the structures of such systems, few, if any, detailed works on the effect of rare-earth ions on the structures of borate glasses have been carried out.

a. The study therefore commenced with the inclusion of Neodymium and Praseodymium oxides in varying proportions within the B_2O_3 host matrix. The optical absorption properties of rare-earth ions are well known and the purpose of these initial measurements was to examine changes – if any – in the optical spectra when the ions are included in the glass.

b. The next step in these studies was to link the observed optical spectra to the structural surroundings of the rare-earth ions. On account of the complexity of the problem, a single rare-earth viz. Neodymium was chosen to be included at various concentrations in the borate glass. The main structural tools were X-ray and neutron diffraction as these methods are known to give good representative information on bulk average structures.

c. Following the effort of incorporation of a single rare-earth ion in the borate host, it was appropriate to include pairs of these ion types. Thus, Nd and Ho were chosen as the first pair for inclusion. Different relative proportions of the two ion types were chosen. The differences in rare-earth structural environment having only one rare-earth ion type was to be examined. A second pair of rare-earth ions viz. Nd and Pr was also chosen for this part of the work.

d. All the above studies were to focus on structural environments of rare-earth dopant and boron host ions in the bulk glass. An additional insight was sought into changes of structures when ions are deposited onto the surface of a glass. In order to achieve such systems, several simple inorganic compounds were chosen for deposition onto commercially available silica microspheres. These were Ag, Ni, ZnO and CdS. In addition, one of the above mentioned Nd borate glasses was also selected to attempt deposition onto the silica surface. The special advantage of using silica microspheres was that the coated spheres could be compacted and held together by sintering, thereby, forming greatly enhanced surface areas within small volumes which would make them suitable for study by diffraction techniques. Depositions were to be made by appropriate methods : eg. the chemical bath method; electroless plating; and simple fusion of one glass onto another. In these studies of layer depositions, the focus was to be the changes in the structures of the coating materials after being deposited onto the silica microsphere surfaces.

References

1. Barton L., Brinza D., Frease R.A. and Longcor F.L., J. Inorg. Nucl. Chem. 39 (1977) 1845.
2. Bell R.J. and Dean P., Phil. Mag. 25 (1972) 1381.
3. Bray P.J. and Silver A.H., Modern aspects of the vitreous state, Vol. 1, ed., Mackenzie J.D. (Butterworths, Washington, 1960) p. 92.
4. Bray P.J., Feller S.A., Jellison G.E. Jr. and Yun Y.H., J. Non-Crystalline Solids 38-39 (1980) 93.
5. Bray P.J., Gravina S. and Lee D., in: Boron-rich Solids, ed. Emin D., Aselage T.L. and Morosin B., Al P Conf. Proc. 231 (1991) 271.
6. Davis E.A., Wright H., Doran N.J. and Nex C.M.M., J. Non-Crystalline Solids 32 (1979) 257.
7. Dunlevey F.M. and Cooper A.R., Bull. Am. Ceram. Soc. 51 (1972) 374.
8. Dunlevey F.M. and Cooper A.R., The structure of non-crystalline materials, ed., P.H. Gaskell (Taylor and Francis, London, 1977) p. 211.
9. Elliott S.R, Physics of Amorphous Materials, Longman, Harlow, 1990
10. Elliott S.R., Phil. Mag. B37 (1978) 435.
11. Evans D.L. and King S.V., Nature 212 (1966) 1353.
12. Fajans F. and Barber S.W., J. Am. Chem. Soc. 74 (1952) 2761.
13. Galeener F. L., in : The Structure of Non-Crystalline Materials, P.H. Gaskell, J. M. Parker and E. A. Davis (Eds.), Taylor and Francis, New York (1983) 343.
14. Galeener F.L. and Geissberger A.E., J. Phys. (Paris) Coll. C 9 (1982) 343.
15. Galeener F.L. and Thorpe M.F., Phys. Rev. B 28 (1983) 5802.
16. Goubeau J. and Keller H., Z. Anorg. Allg. Chem. 272 (1953) 303.
17. Gravina S.J., Bray P.J. and Petersen G.L., J. Non-Cryst. Solids 123 (1990) 165.
18. Greaves G.N. and Davis E.A., Phil. Mag. 29 (1974) 1201.
19. Green R.L., J. Am. Ceram. Soc. 25 (1942) 83.
20. Hannon A.C., Sinclair R.N., Blackman J.A., Wright A.C. and Galeener F.L., J. Non-Cryst.

Solids 106 (1988) 116.

21. Hannon A.C., Wright A.C. and Sinclair R.N., in: Fundamentals of Glass Science and Technology 1993 (Stazione Sperimentale del Vetro, Venice, 1993) p. 479 (Suppl. Riv. Staz. Sper. del Vetro XXII1 1993).
22. Jellison G.E. Jr. and Bray P.J., Sol. St. Commun. 19 (1976) 517.
23. Jellison G.E. Jr., Panek L.W., Bray P.J. and Rouse G.B. Jr., J. Chem. Phys. 66 (1977) 802.
24. Johnson P.A.V., Wright A.C. and Sinclair R.N., J. Non-Cryst. Solids 50 (1982) 281.
25. Kanehisa M.A. and Elliott R.J., Mater. Sci. Eng. B 3 (1989) 163.
26. Krogh-Moe J., Arkiv Kemi 14 (1959) 31.
27. Krogh-Moe J., J. Non-Crystalline Solids 1 (1969) 269.
28. Labarre J.-F., Graffeuil M., Faucher J.-P., M. Pasdeloup and Laurent J.-P., Theoret. Chim. Acta 11 (1968) 423.
29. Mozzi R.L. and Warren B.E., J. Appl. Cryst. 3 (1970) 251.
30. Rawson H., Inorganic Glass-Forming Systems, Academic Press (1967).
31. Risen W.M. Jr., J. Non-Cryst. Solids 76 (1985) 97.
32. Serafini A. and Labarre J.F., J. Mol. Structure 26 (1975) 129.
33. Svanson S.E., Forslind E. and Krogh-Moe J., J. Phys. Chem. 66 (1962) 174.
34. Varshneya Arun, Fundamentals of Inorganic Glasses, Soc. of glass Tech. (2006).
35. Warren B.E., Krutter H. and Morningstar O., J. Am. Ceram. Soc. 19 (1936) 202.
36. Williams S.J. and Elliott S.R., Proc. R. Soc. (London) A 380 (1982) 427.
37. Windisch C.F. Jr. and Risen W.M. Jr., J. Non-Cryst.Solids 48 (1982) 325.
38. Wright A. C., Advances in Structure Research by Diffraction Methods, 5 (1974) 1-84.
39. Wright A.C., Sumner D.J. and Clare A.G., in: The Structure of Non-Crystalline Materials 1982, ed. Gaskell P.H., Parker J.M. and Davis E.A. (Taylor and Francis, London, 1982) p. 395.
40. Zachariasen W.H., J. Am. Chem. Soc. 54 (1932) 3841.

Chapter 2

Theory and Experimental Methods

In this Chapter we consider the theory of neutron and X-ray diffraction applied to the structures of disordered materials and glasses. The formalism – after Fischer et al. (2006) and Wright (1974) - is often referred to as the Radial Distribution Method. The various experimental corrections that are necessary when dealing with either neutron or X-ray diffraction data are described. The development gives a one-dimensional average of what is essentially a three-dimensional structure and the recourse to chemical/bonding considerations is inevitable when proposing a viable structural model based on diffraction data. From the interpretation of the correlation functions, average bond lengths and coordination numbers of nearest and next-nearest neighbours can be found.

2.1 Introduction

We may begin by looking at the general properties of neutrons. The important aspects of a thermal neutron are that it is electrically neural and its wavelength is comparable to the atomic separation and energy of atomic vibrations. Hence the thermal neutron (few tens of milli electron volts) is quite unique in its ability to probe both structure and dynamics of a solid. A summary of X-ray and neutron properties is given below:

1. The special property of a thermal neutron as compared to the X-ray (i.e. a few keV from an X-ray tube) is that the neutron is able to probe the bulk microscopic volume whereas the X-ray tends to reflect off the surface.
2. The neutron has a magnetic moment and can be used to probe magnetic structures.
3. For X-rays the scattering power of a target atom is proportional to the atomic number.

4. For neutrons, the scattering length is related to the pseudo potential of the scattering process and does not vary according to any particular trend with respect to atomic number.
5. The scattering length of a neutron is angular independent whereas in X-rays it is dependent.
6. A given material will scatter differently for X-rays and neutrons. Hence, in principle the two differently weighted correlation lengths can be used to extract structural details.
7. Neutrons are sourced from either nuclear reactors or pulsed accelerators and are intrinsically more expensive than sources of X-rays which are often X-ray tubes in a laboratory.
8. Sample sizes for neutron diffraction experiments are required to be much larger than for X-ray diffraction on account of the neutral charge of the neutron and it's relatively weak interaction with solids.

2.2 Neutron Diffraction Studies of Glasses

Let a collimated beam of neutrons of wavelength λ be incident of a sample as shown in Figure 2.2.1.

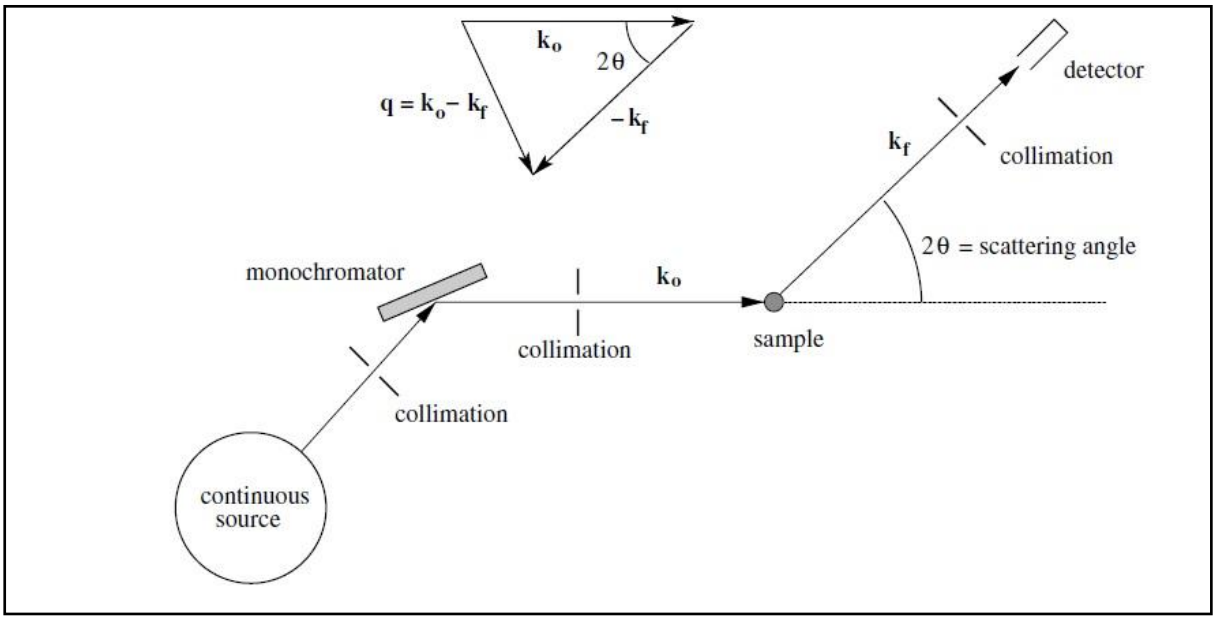

Figure 2.2.1: Schematic of neutron diffraction experiment from a continuous source of neutrons (after Fischer et al. (2006)).

Let the incident plane wave be given by equation 2.2.1

$$\psi_{inc} = \psi_{inc}\, e^{i[\boldsymbol{k}_o.\boldsymbol{r}-\omega_o t]} \equiv \psi_o\, \boldsymbol{e}^{i\boldsymbol{k}_o.\boldsymbol{r}} \qquad (2.2.1)$$

Where ψ_{inc}= amplitude of the plane wave

$\mathbf{k}_0$ = incident wavevector = $2\pi/\lambda_0$

r= position of the neutron

For a single scattering centre at the origin, the scattered wave is given by equation (2.2.2)

$$\psi_{scatt,1} = \frac{-\psi_0 b_i}{\boldsymbol{R}} e^{ik_f R} \qquad (2.2.2)$$

Where R = distance from the scattering centre

$\boldsymbol{k}_f$ = Magnitude of the final wave vector

The time dependent term exp ($-i\omega_o t$), from the incident and scattered waves is included in the ψ_0 term.

The term b_i, has dimensions of length and is called the scattering length of the scattering centre1. It has a complex value depending on the interaction between the neutrons and scattering centre.

In neutron scattering, a positive scattering length leads to a repulsive scattering potential (Squires 1978), a negative sign is used in equation (2.2.2)

If the scattering centre *i* is not the origin but at a position $\boldsymbol{r_i}$ then, we obtain a scattering vector, $\mathbf{q} = \mathbf{k}_o - \mathbf{k}_f$

If the sample contains N point like scattering centres i, with scattering length b_i,

$$\Psi_{scatt,N} = \frac{-\psi_0}{\boldsymbol{R}} e^{ik_f R} \sum_{i=1}^{N} b_i \, e^{i\boldsymbol{q}\cdot\boldsymbol{r}_i} \qquad (2.2.3)$$

at a distant point **R**, taken to be parallel to $\mathbf{k}_f$ where we place a detector of area $dS << R^2$ subtending a small solid angle $d\Omega = dS/R^2$ with respect to the sample.

The differential scattering cross section for diffraction by neutronsis defined by

$$\frac{d\sigma}{d\Omega} \stackrel{\text{def}}{=} \frac{number\ \ of\ neutrons\ \ cattered\ \ per\ second\ \ towards\ \ the\ detector\ \ into\ d\Omega}{\Phi d\Omega} \qquad (2.2.4)$$

here the flux Φ is the number of incident neutrons per second per unit crosssectional area of the incident beam.

The incident flux, after suitable normalization of the wave functions (Mott (1962)), is given by $\Phi = \psi_o \left|\psi_{inc}\right|^2 = v_o \psi_o^2$, v_o = group velocity of incident wave

The scattered flux, through area dS is given by $v_f |\psi_{scatt}|^2 dS$ where v_f is the final velocity.

If we assume $k_f \approx k_o$, for a single scattering center at the origin, we can write

$$\left.\frac{d\sigma}{d\Omega}\right|_1 = \frac{\left|\Psi_{scatt,1}\right|^2 dS}{|\Psi_{inc}|^2 d\Omega} = \frac{(\psi_0^2 |b_i|^2/R^2)(R^2 d\Omega)}{\psi_0^2 d\Omega} = |b_i|^2 or b_i^2 \qquad (2.2.5)$$

b^2 is the modulus-squared of a scattering length.

The differential scattering cross section, for N scattering centre is given by,

$$\frac{d\sigma}{d\Omega}(\boldsymbol{q}) = \overline{\langle \left|\sum_{i=1}^{N} b_i e^{i\boldsymbol{q}\cdot\boldsymbol{r}_i}\right|^2 \rangle} = \langle \sum_{i,j}^{N} \overline{b_i b_j^*}\, e^{i\boldsymbol{q}\cdot\boldsymbol{r}_{ij}} \rangle \qquad (2.2.6)$$

where $\boldsymbol{r}_{ij} = \boldsymbol{r}_i - \boldsymbol{r}_j$, the relative position of scattering centers i and j

Equation (2.2.6) was derived by assuming that the energy exchange in the interaction is very small, which is called the static approximation i.e. the target nucleus does not move.

In the experiment, the measurement equals the integration of the double scattering cross section $d^2\sigma/d\Omega dE$, at constant detector angle 2θ, over all range of energy exchange.

$$\left.\frac{d\sigma}{d\Omega}\right|_{meas} = \int_{-\infty}^{+\hbar\omega_o} d(\hbar\omega)\frac{d^2\sigma}{d\Omega dE} \in (E_f) \qquad (2.2.7)$$

where $E = \hbar w = E_o - E_f$ represents the energy loss of the neutron.

$\in(E_f)$= efficiency of the detector as a function of final energy E_f

With the static approximation the upper limit of the integral in equation (2.2.7) is extended to infinity. It can be shown that the integration over $\hbar\omega$ then occurs at constant q (Squires (1978), Lomer and Low (1965))

The equation (2.2.7) becomes,

$$\left.\frac{d\sigma}{d\Omega}\right|_{meas}^{sa} = \epsilon(E_0)\int_{-\infty}^{+\infty} d(\hbar\omega)\left.\frac{d^2\sigma}{d\Omega dE}\right|_{\boldsymbol{q}} = \epsilon(E_0)\frac{d\sigma}{d\Omega}(\mathbf{q}) \qquad (2.2.8)$$

The intensity I(**q**) measured by the detector over solid angle dΩ is obtained from equation (2.2.4)

$$I(\boldsymbol{q}) = \Phi\frac{d\sigma}{d\Omega}(\mathbf{q})d\Omega \qquad (2.2.9)$$

where φ = incident flux on the sample and $\in(E_f)$ is assumed to be 1.

The measured intensity is a function of only the scattering vector **q**. The scattering vector **q**, is obtained from the scattering triangle, as

$$q = |\mathbf{q}| = 2k_o\sin\theta = \frac{4\pi}{\lambda_o}\sin\theta \qquad (2.2.10)$$

The above equation is valid for static approximation $k_f \approx k_o$ as well as for elastic scattering $k_f = k_o$

Monoatomic System

If we suppose that there is no relation between scattering length and positions of different scattering centers, we can then consider two cases for each term in the equation (2.2.6)

$$\overline{b_i b_j^*} = \overline{b_i b_i^*} = \overline{b^2} i = j \quad (same\ site)$$

$$\overline{b_i b_j^*} = \overline{b_i b_j^*} = \overline{b}^2 i \neq j \quad (different\ sites) \tag{2.2.11}$$

$$\frac{d\sigma}{d\Omega}(\boldsymbol{q}) = \overline{b}^2 \langle \sum_{i,j\neq i}^{N} \boldsymbol{e}^{i\boldsymbol{q}\cdot\boldsymbol{r}_{ij}} \rangle + N\overline{b^2} = \overline{b}^2 \langle \sum_{i,j}^{N} e^{i\boldsymbol{q}\cdot\boldsymbol{r}_{ij}} \rangle + N(\overline{b^2} - \overline{b}^2) \tag{2.2.12}$$

The ‹› bracket represents the thermal average.In the first equality of equation (2.2.12), the first term on the RHS represents the diffraction interference from different atomic sites (distinct) and the second term, the isotropic diffraction from individual atomic sites (self).

Let's define a dimensionless interference function **H(q)** as,

$$\boldsymbol{H}(\boldsymbol{q}) \overset{\text{def}}{\equiv} \frac{1}{N} \langle \sum_{i,j\neq i}^{N} \boldsymbol{e}^{i\boldsymbol{q}\cdot\boldsymbol{r}_{ij}} \rangle \tag{2.2.13}$$

For a glass,H(q) converges to 0 as q → ∞.

Therefore the differential scattering cross section per atom is given by

$$\frac{1}{N}\left[\frac{d\sigma}{d\Omega}(\boldsymbol{q})\right] = \frac{1}{N}\left[\frac{d\sigma}{d\Omega}(\boldsymbol{q})\right]^{distinct} + \frac{1}{N}\left[\frac{d\sigma}{d\Omega}(\boldsymbol{q})\right]^{self} = \overline{b}^2 H(\boldsymbol{q}) + \overline{b^2} \tag{2.2.14}$$

The thermal de Broglie wavelength is given by

$$\Lambda = \sqrt{\frac{2\pi\hbar^2}{k_B T M}} \tag{2.2.15}$$

Where *M*= mass of atom

k_B= Boltzmann constant

T= absolute temperature

In another formulism, the second equality in equation (2.2.12) is expressed as a sum of 'coherent' and 'incoherent' parts. The scattering from all the atomic sites which include scattering from a single atom, contributes to the `coherent' part and depends on the average

scattering length. The scattering which depends on the distribution of scattering lengths in the sample, leading to the isotropic diffraction constitutes the coherent part.

The coherent and incoherent lengths are defined by

$$b_{coh} \stackrel{\text{def}}{\equiv} \overline{b} \text{and} \quad b_{incoh}^2 \stackrel{\text{def}}{\equiv} \left(\overline{b^2} - \overline{b}^2\right) = \overline{|b - \overline{b}|^2} \tag{2.2.16}$$

Let's define the (static) structure factor S(**q**) as

$$S(\boldsymbol{q}) \stackrel{\text{def}}{\equiv} \frac{1}{N}\langle \sum_{i,j}^{N} e^{i\boldsymbol{q}\cdot\boldsymbol{r}_{ij}} \rangle = H(\boldsymbol{q}) + 1 \tag{2.2.17}$$

The equation converges to 1, for q → ∞.

The differential scattering cross section per atom is

$$\frac{1}{N}\left[\frac{d\sigma}{d\Omega}(\boldsymbol{q})\right] = \frac{1}{N}\left[\frac{d\sigma}{d\Omega}(\boldsymbol{q})\right]^{coh} + \frac{1}{N}\left[\frac{d\sigma}{d\Omega}(\boldsymbol{q})\right]^{incoh}$$

$$= \overline{b}^2 S(\boldsymbol{q}) + \left(\overline{b^2} - \overline{b}^2\right)$$

$$= b_{coh}^2 S(\boldsymbol{q}) + b_{incoh'}^2 \tag{2.2.18}$$

Figure (2.2.2) shows the differential scattering cross section per atom for a typical mono-atomic glass. Using equation (2.2.8) the static structure factor S(**q**) is expressed in terms of (coherent) dynamic structure factor S(**q**,ω) (van Hove 1954)

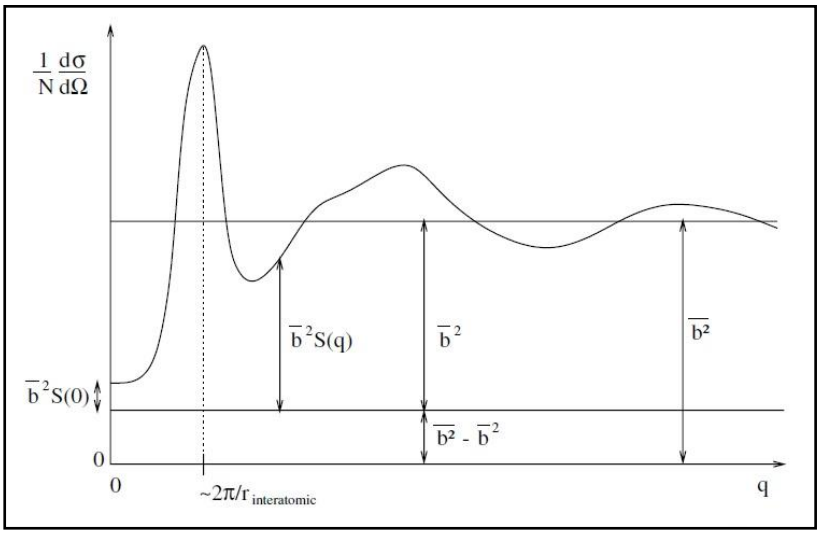

Figure 2.2.2: Differential scattering cross-section per atom for a glass (after Fischer et al.(2006)).

$$S(\boldsymbol{q}) = \int_{-\infty}^{+\infty} d(\hbar\omega) S(\boldsymbol{q}, \omega) \quad (2.2.19)$$

Here $S(\mathbf{q},\omega)$ is proportional to $d^2\sigma/(d\Omega/dE)\,|_{coh}$.

In real space the pair distribution function $g(\mathbf{r})$ is defined as the probability of finding an atom at $\mathbf{r}$ from the origin.

The function $S(\mathbf{q})$ and $g(\mathbf{r})$ are related by the Fourier transforms

$$S(\boldsymbol{q}) - 1 = \rho_0 \int [g(\boldsymbol{r}) - 1]\, e^{i\boldsymbol{q}\cdot\boldsymbol{r}} d\boldsymbol{r} \quad (2.2.20)$$

$$g(\boldsymbol{r}) - 1 = \frac{1}{\rho_o (2\pi)^3} \int [S(\boldsymbol{q}) - 1]\, e^{-i\boldsymbol{q}\cdot\boldsymbol{r}} d\boldsymbol{q}, \quad (2.2.21)$$

Where ρ_o = atomic number density

The (-1) term in the integrand of equation (2.2.20) represents the subtraction of the forward scattering at $\mathbf{q} = 0$, and

$$\rho_0 \int e^{i\boldsymbol{q}\cdot\boldsymbol{r}} d\boldsymbol{r} = \rho_0 V \delta_{\boldsymbol{q},0} = N\delta_{\boldsymbol{q},0} \quad (2.2.22)$$

Where V = volume of the sample

$\delta_{\mathbf{q},0}$= Kronecker delta

$\delta_{\mathbf{q},0}$= 1 for $\mathbf{q} = 0$ and $\delta_{\mathbf{q},0} = 0$ for $\mathbf{q} \neq 0$

In the integrand of equation (2.2.21), unity is subtracted from $S(\mathbf{q})$ in order that the Fourier transform is taken of the purely coherent part of the scattering function i.e. $H(\mathbf{q}) = S(\mathbf{q}) - 1$.

By averaging over relative orientations of r and q, the exponential terms in equation (2.2.13), (2.2.20) and (2.2.21) can be written as zeroth-order spherical-Bessel functions (Debye 1915) thereby simplifying the expression for the static structure factor.

$$S(q) = 1 + \frac{1}{N}\left\langle \sum_{i,j\neq i}^{N} \frac{\sin(qr_{ij})}{(qr_{ij})} \right\rangle \quad (2.2.23)$$

as well as the expressions for the Fourier transforms:

$$S(q) - 1 = \frac{4\pi\rho_0}{q} \int_0^\infty r[g(r) - 1] \sin(qr) dr \quad (2.2.24)$$

$$g(r) - 1 = \frac{1}{2\pi^2 r\rho_0} \int_0^\infty q[S(q) - 1] \sin(qr) dq, \quad (2.2.25)$$

where S(q→ ∞) = 1 and g(r→ ∞) = 1.

In a real diffraction experiment for a glass sample this oriental average is obtained from the sum of diffraction contributions of different coherence volumes within the sample.

For a monoatomic system, one also defines the density function D(r)

$$D(r) \stackrel{\text{def}}{=} 4\pi r\rho_0[g(r)-1] = \frac{2}{\pi}\int_0^{\infty} q[S(q)-1]\sin(qr)dq \qquad (2.2.26)$$

Where the slope at small r is proportional to ρ_o since g(r) is exactly 0, for r-values below a certain minimum interatomic distance.

The radial distribution function RDF (r), given by

$$RDF(r) \stackrel{\text{def}}{=} 4\pi r^2\rho_0 g(r), \qquad (2.2.27)$$

which when integrated can be used to get the average number of neighbouring atoms in a coordinated shell from an assumed origin atom.

$$\overline{n} = \int_{r_1}^{r_2} RDF(r)dr = 4\pi\rho_0 \int_{r_1}^{r_2} g(r)r^2 dr, \qquad (2.2.28)$$

wherer_1 and r_2 are the distances corresponding to successive minima.

The average number of atoms $\overline{n}$ in the first shell is called the coordination number around the assumed origin atom.

Due to the finite q_{max}, the Fourier transform of S(q), results in broadening of peaks in g(r) and in other r-space functions.

These truncation ripples can be minimized by modulation of S(q) by a damping function before Fourier transformation due to Lorch (1969), which results in the coarsening of the real-space resolution.

Alternatively, the step-function describing the experimental q-range, $M(q \leq q_{max}) = 1$ $M(q > q_{max}) = 0$, can be Fourier-transformed to produce the r-space modification function

$$M(r) = \frac{1}{\pi}\int_0^{q_{max}} cos(qr)dq \qquad (2.2.29)$$

Polyatomic System

Equation (2.2.14) is generalized to a system of 'n' chemical species with the self and distinct terms

$$\frac{1}{N}\left[\frac{d\sigma}{d\Omega}(q)\right] = F(q) + \sum_{\alpha}^{n} c_{\alpha}\,\overline{b_{\alpha}^{2}}, \qquad (2.2.30)$$

Where F(q) is the total interference function and C_α is the concentration of chemical species α (such that $\sum_{\alpha}^{n} c_{\alpha} = 1$).

The second term of equation (2.2.30) is therefore the mean of the scattering length squared of each chemical species as averaged over the entire sample.

$$\sum_{\alpha}^{n} c_{\alpha}\,\overline{b_{\alpha}^{2}} = \overline{b^{2}} where \overline{b_{\alpha}^{2}} = b_{coh,\alpha}^{2} + b_{incoh,\alpha}^{2}. \qquad (2.2.31)$$

Since for a polyatomic system we are generally interested in describing the distribution of one chemical species around another, it is convenient to choose the convention of Faber and Ziman (1965) for defining partial structure factors $S_{\alpha\beta}(q)$ by decomposing F(q) in the following manner

$$F(q) \stackrel{\text{def}}{=} \sum_{\alpha,\beta}^{n} c_{\alpha} c_{\beta}\,\overline{b}_{\alpha}\overline{b}_{\beta}^{*}\left[S_{\alpha\beta}(q) - 1\right], \qquad (2.2.32)$$

where each $S_{\alpha\beta}(q)$ is a function that is dependent only on the distribution of α atoms around β (or vice-versa)

$$S_{\alpha\beta}^{AL}(q) = \delta_{\alpha\beta} + (c_{\alpha} c_{\beta})^{1/2}\left[S_{\alpha\beta}(q) - 1\right], \qquad (2.2.33)$$

by analogy with equation (2.2.23), the FZ partial structure factors for an isotropic system can be written as

$$S_{\alpha\beta}(q) = S_{\beta\alpha}(q) = 1 + \frac{1}{c_{\alpha} c_{\beta} N}\left\langle \sum_{i,j\neq i}^{N_{\alpha},N_{\beta}} \frac{\sin(q r_{ij})}{(q r_{ij})} \right\rangle \qquad (2.2.34)$$

where $N_\alpha = C_\alpha N$ is the number of α atoms and i and j refer to sites among the α and β atoms, respectively.

Evidently the equivalence of sites i = j is only possible within a single chemical species (i.e. for α=β)

Fourier transformation of $S_{\alpha\beta}(q)$ leads to the partial pair-distribution functions $g_{\alpha\beta}(r)$

$$S_{\alpha\beta}(q) - 1 = \frac{4\pi\rho_0}{q}\int_0^\infty r\left[g_{\alpha\beta}(r) - 1\right]\sin(qr)\,dr \qquad (2.2.35)$$

$$g_{\alpha\beta}(r) - 1 = \frac{1}{2\pi^2 r\rho_0}\int_0^\infty q\left[S_{\alpha\beta}(q) - 1\right]\sin(qr)\,dq \qquad (2.2.36)$$

Where ρ_o is still the total number density of atoms.

The $g_{\alpha\beta}(r)$ are a measure of the probability of finding a β atom at a distance r from an α atom (Fournet 1957).

The partial coordination number $\bar{n}^{\beta}_{\alpha}$ (i.e. the average number of β atoms in a spherical shell around an α atom) is found through integration of a partial radial distribution function

$$\bar{n}_\alpha^\beta = 4\pi\rho_0 c_\beta \int_{r_1}^{r_2} g_{\alpha\beta}(r) r^2 dr. \qquad (2.2.37)$$

A Fourier transform of F(q) defines the total pair-correlation function G(r) as

$$G(r) \stackrel{\text{def}}{=} \frac{1}{2\pi^2 r\rho_0}\int_0^\infty qF(q)\sin(qr)\,dq = \sum_{\alpha,\beta}^n c_\alpha c_\beta\, \bar{b}_\alpha \bar{b}_\beta^*\left[g_{\alpha\beta}(r) - 1\right] \qquad (2.2.38)$$

which is a simple weighted sum of the $g_{\alpha\beta}(r)$ only in the case of neutron 'N' diffraction for which the scattering lengths are q-independent.

For neutron diffraction of glasses, the *total correlation function* T(r) is defined as

$$T(r) \stackrel{\text{def}}{=} 4\pi r\rho_0\left[G(r) + \sum_{\alpha,\beta}^n c_\alpha c_\beta\, \bar{b}_\alpha \bar{b}_\beta^*\right] \qquad (2.2.39)$$

where

$$\sum_{\alpha,\beta}^n c_\alpha c_\beta\, \bar{b}_\alpha \bar{b}_\beta^* = \left|\sum_\alpha^n c_\alpha \bar{b}_\alpha\right|^2 = \bar{b}^2 \qquad (2.2.40)$$

and $\bar{b} = \sum_\alpha^n c_\alpha \bar{b}_\alpha$ is the mean scattering length as averaged over the entire sample.

The T(r) function is theoretically zero below a certain minimum distance between atoms and has the advantage of peaks that are symmetrically broadened by finite q_{max} (Wright 1980).

It leads directly to a total radial distribution function N(r)

$$N(r) \stackrel{\text{def}}{=} rT(r) \qquad (2.2.41)$$

In practice, experimental results for diffraction by glasses should be compared with theory/simulation in both r-space and q-space as well as with results from other experimental techniques, so as to fully appreciate the significance of single features such as 'first sharp diffraction peak' FSDP (Salmon (1994)).

By taking the limit as r→0 in equation (2.2.38) we obtain a sum-rule that can be useful for checking the normalization of partial structure factors

$$\int_0^\infty q^2\left[S_{\alpha\beta}(q)-1\right]dq = -2\pi^2\,\rho_0 \qquad (2.2.42)$$

where ρ_o = total atomic number density.

The area of peak in N(r) is related to partial coordination number N_{ij}, the average number of j-type atoms around any i-type atoms within the range of integration (Ramesh Rao et al. (1998)), is given by,

$$C_e = \frac{1}{\langle b\rangle^2}\sum_{i,j} c_i\ \bar{b}_i\bar{b}_j N_{ij}$$

Since $c_i\ N_{ij} = c_j\ N_{ji}$

$$C_e = c_1\left|\frac{\overline{b_1}}{\langle\bar{b}\rangle}\right|^2 N_{11} + 2\,c_1 Re\left(\frac{\overline{b_1}\ \bar{b}_2}{\langle\bar{b}\rangle^2}\right)N_{12} + c_2\left|\frac{\overline{b_2}}{\langle\bar{b}\rangle}\right|^2 N_{22} \qquad (2.2.43)$$

$$C_e = W_{11}N_{11} + W_{12}N_{12} + W_{22}N_{22} \qquad (2.2.44)$$

2.2.1 X-ray diffraction

The purely coherent part of the scattering function i.e. (S(q) – 1) in neutron diffraction is replaced by the same function divided by a sharpening function $f_e(q)^2$ for X-rays. The form factor per electron $f_e(q)$ is defined as:

$$f_e(Q_0) = \frac{\Sigma_j f_j(Q_0)}{\Sigma_j Z_j} \qquad (2.2.1.1)$$

The same equations that apply to neutron diffraction (equations 2.2.3 to 2.2.42) may be used to analyze and interpret data from X-ray diffraction with the neutron scattering lengths b_j or b_k being replaced by the X-ray form factors $f_j(q)$ and $f_k(q)$.

2.3 Neutron Diffraction Measurements:

Neutron diffraction was initially used for complementing and extending X-ray measurements. Over the last 60 years, neutron diffraction has been increasingly used in the characterization and structural studies of wide variety of materials.The interaction of neutrons with the atomic site is either elastic or inelastic. Inelastically scattered neutrons are useful in probing vibrational properties through energy transfer measurements. On the other hand, elastically scattered neutrons are used for the structural studies of materials.

The present study is limited to the structural studies of glasses.The High-Q diffractometer at Dhruva Reactor, Bhabha Atomic Research Center, Mumbai has been used for the total scattering of the neutronsfrom the glass samples to obtain the scattering diffractogram.The maximum flux at the center is about $1.3x10^{14}$ neutrons/cm^2/s.The energetic neutrons produced in the fuel core are thermalised by the D_2O moderator. These neutrons are then permitted to stream through the neutron beam holes in the reflector and shielding. The typical flux in a beam hole is of the order of 10^8n/cm^2/s. In the process of monochromatisation and collimation, the flux becomes 10^4-10^5n/cm^2/s at the sample position. Due to the low incident flux, large specimen samples and longer acquisition times become necessary for improved statistics of scattered neutrons.

2.3.1 High-Q Diffractometer

The neutron beam from the reactor is monochromatised by reflection off a Copper crystal. The wavelength of the neutrons can be selected from 0.783Å and 1.27Å by the orientation of the Copper monochromator. The number of neutrons in the beam is monitored by a low efficiency BF_3 counter placed in the beam. A sample table of 300cm diameter accommodates the sample as well as the 5 positions sensitive detectors. The 5 PSDs, cover a Q range of $0.3Å^{-1}$ to 15 $Å^{-1}$. An oscillating Radial Collimator (ORC) placed before the detector assembly decreases the background and the contributions arising from the sample environment.

High-Q Diffractometer specifications:

Q-range	: $0.3Å^{-1}$ to 15 $Å^{-1}$
Resolution ($\Delta Q/Q$)	: 4%
Incident wavelengths	: 0.783Åor1.278Å
Monochromator	: Cu(220) or Cu(111)
Monochromator take off angle $2Q_M$	: 34.66°
Detectors	: $5He^3$ PSDs
Beam size at sample	: $1.5x4cm^2$
Flux value at sample	: $1.1x10^6$ $n/cm^2/s$ at $\lambda = 1.278$ Å
	10^5 $n/cm^2/sec$ at $\lambda = 0.783$ Å

2.3.2 Flat Cone Diffractometer

The scattered neutron momentum space can be scanned in less than five steps by combining the “off-plane Bragg-scattering” and the flat-cone layer concept while using a computer-controlled tilting axis of the detector bank. Parasitic scattering from cryostat or furnace walls is reduced by an oscillating "radial" collimator. A software package (TVneXus) deals with the raw data sets, the transformed physical spaces and the usual data analysis tools (e.g. MatLab). TVneXus can convert to various data sets e.g. into powder diffractograms, linear detector projections, rotation crystal pictures or the 2D/3D reciprocal space. A list of the main parameters of this diffractometer is given below :

Flat Cone Diffractometer specifications

Monochromator	• Cu (220) • Ge (311) • PG (002)
Wave length	• λ=0.091 nm [Cu (200)] • λ=0.121 nm [Ge (311)] • λ=0.241 nm [PG (002)]
Flux	$2 \cdot 10^6$ n/cm^{2}s (flat PG monochromator without collimation)
Range of scattering angles	$-10° < 2\Theta < 107°$
Angle resolution	• horizontal resolution: 0.2° - 0.1° • vertical resolution: 0.5° - 0.1° • pixel size 0.1°x0.1°
Detector	four 2D delay-line detectors (PSD 300 x 300 mm^2)
Instrument options	• single crystal mode • powder diffraction mode

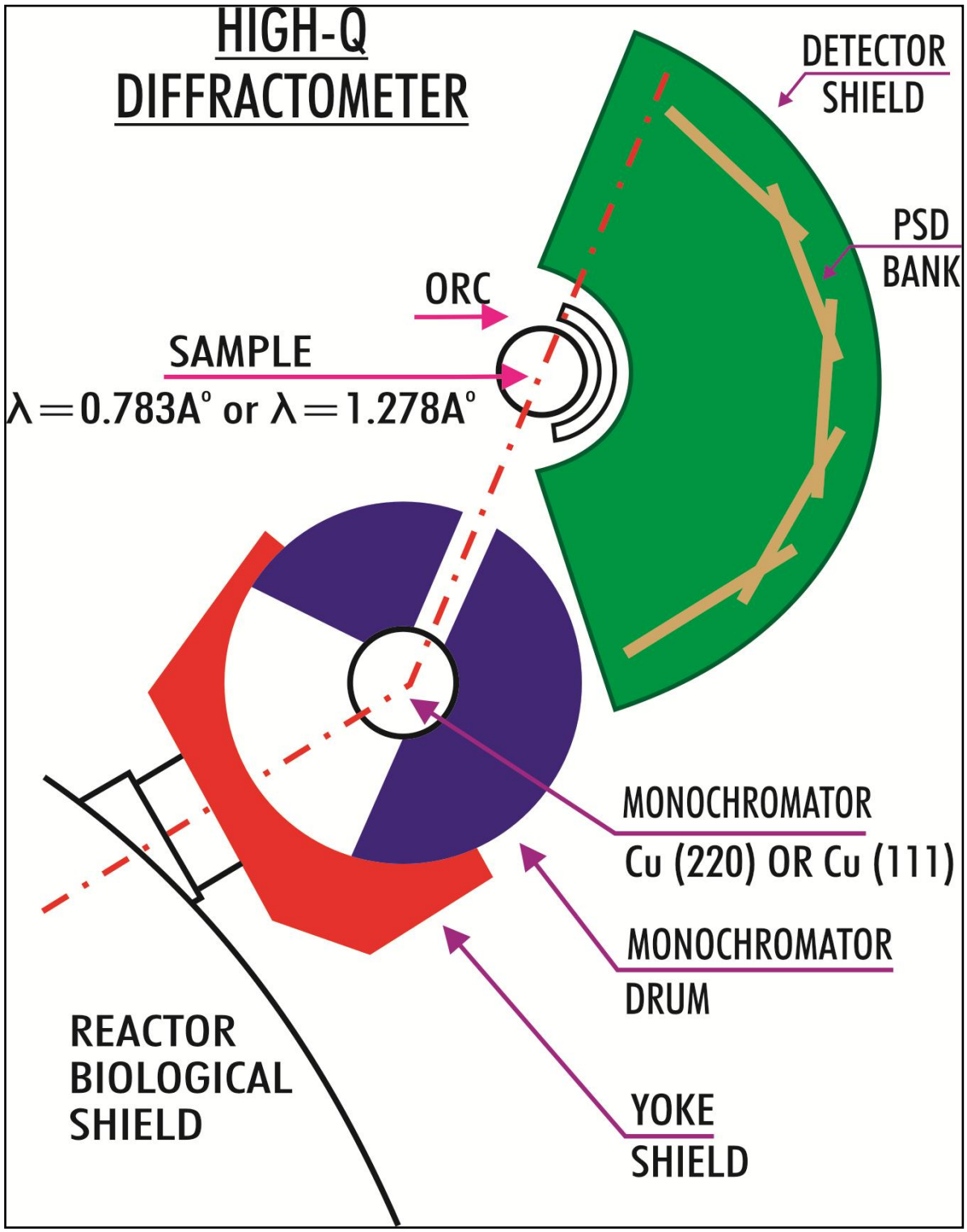

Figure 2.3.1.1: Schematic of High-Q Diffractometer at Dhruva, BARC, Mumbai.

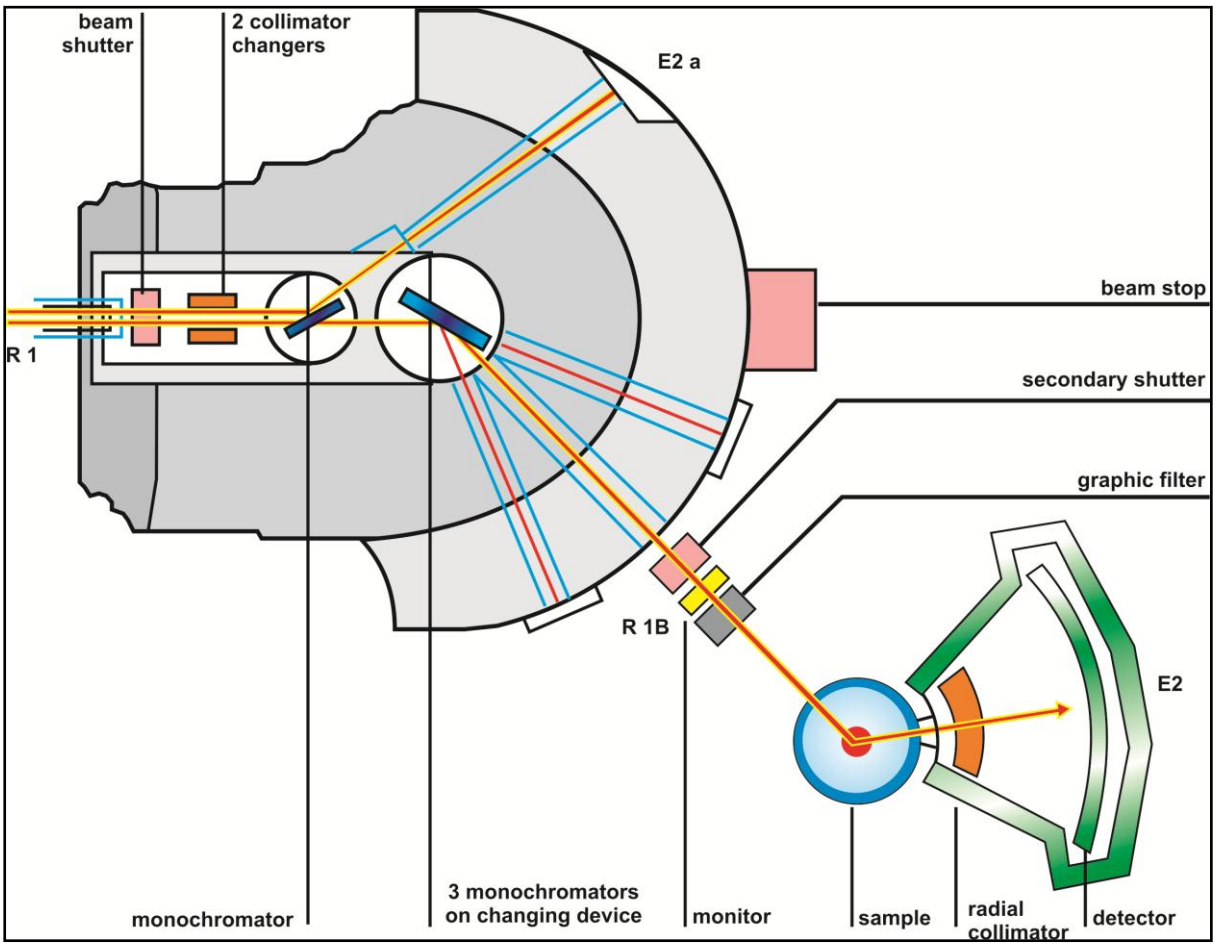

Figure 2.3.2.1: Schematic of Flat Cone Diffractometer at HZB, Berlin, Germany.

2.3.3 Corrections Involved in the Analysis of Neutron Data

The experimental setup which consists of sample and diffractometer geometry will determine the type of correction which is required for the neutron data. The scattering data needs to be corrected for various experimental effects before being normalized to a vanadium standard since the measured intensity depends on the instrumental resolution functions which are dependent on angle and wavelength. Thereafter, renormalization of the data is necessary on account of errors in cross-sections of sample constituents and composition of the sample.

2.3.3.1 Sample Container, Air and Electronic Background

Sample container size is decided by:

1. The beam dimensions at the sample position.
2. Expected absorption and multiple scattering which decide the optimum thickness of the sample.

The above factors determine the length of the experimental counting time. The sample container is chosen such that 10 percent or less of the incident flux is scattered. Thus large, thin-walled cylindrical sample containers are often used in these experiments. Thin-walled containers having plate geometry are not favoured. Container dimensions need to be accurately known for the calculation of the number of scattering atoms in the container. Cylindrical cans are preferred for use as sample containers. For small can diameters, the total sample scattering is relatively low making the signal to background ratio also small. Containers are normally of vanadium or any other null-matrix material having an isotropic incoherent scattering.

After correcting for container transmission factor, the container scattering is usually subtracted from the sample-in-container data. When no container is used, air background is subtracted from the sample scattering intensities.

2.3.3.2 Absorption Correction and Multiple Scattering

In the case of cylindrical and annular geometries for X-rays, Paalman and Pings (1962) have evaluated the expressions for absorption - which can be applied to neutrons. The scattering from the sample and container modify the absorption coefficient. The absorption correction for a cylindrical sample without a container, is given by Wright (1974) :

$$A(Q) = \frac{I}{I_0} = \exp[-(1.7133 - 0.0368\sin^2\theta)\mu_a R + (0.0927 + 0.0375\sin^2\theta)(\mu_a R)^2] \qquad (2.3.3.1)$$

where R is the radius of the sample and the absorption coefficient $\mu_a = \sum_k \rho_k \sigma_k^a$

When multiple scattering is less than 10% and samples are cylindrical, this correction is equally made up of self-shielding and multiple scattering (Wright (1974)). Multiple scattering corrections for cylindrical samples have also been discussed by Blech and Averbach (1965) and were further modified by Soper and Eglstaff (1980). For a cylindrical sample:

$$I_m = I_1\left(\frac{\exp(2\partial)}{2\partial} - 1\right) \qquad (2.3.3.2)$$

Where I_m and I_1 are respectively the multiple and singly scattered intensities and δ is the ratio of secondary to primary scattering I_2/I_1. Values of δ are listed by Blech and Averbach (1965). The appropriate values from this list have been used for these samples.

2.3.3.3 Normalization

Normalization of the experimentally corrected scattered intensities is achieved by comparing them to the data from a sample having a known cross-section. As Vanadium scatters incoherently (σ_{incoh} = 5.13 barns) and isotropically, it is used for this purpose. Certain systematic errors of the instrument are also removed by normalization to a standard sample. Both numbers of scattering atoms of the sample and of vanadium must be known accurately. In order to reduce errors in the interpretation of correlation functions, neutron scattering lengths must be known correctly. The normalized intensity of the sample is then given by:

$$I_N(Q) = \frac{I_s^c(Q).C_R}{I_v^c(Q)/S_v(Q)} \qquad (2.3.3.3)$$

where I_s^c and I_v^c are the intensities corrected for background, absorption and multiple scattering of sample and vanadium respectively; $S_V(Q)$ (equal to $\Sigma_j < b_j^2 >$) is the calculated self-scattering for vanadium and C_R is the ratio of composition units per unit volume of sample to vanadium.

2.3.3.4 Renormalisation

Errors in scattering lengths of the constituent atoms of the sample and composition may cause the normalized intensities to not oscillate perfectly about the self-scattering level. In such cases, renormalization is necessary. The Krogh-Moe (1956) and Norman (1957) integration method assumes both the self and the distinct parts to be in error. There are several sources of systematic error such as background subtraction, sample density, neutron cross sections which contribute to uncertainty in the normalization. Thus if α and β are constants, S(Q) is the Placzek-corrected self-scattering, and $I_R(Q)$ is the renormalized intensity function;

$$I_R(Q) = \propto I(Q) - \beta S(Q) \qquad (2.3.3.4)$$

If one of the constants is assumed to be unity, the other may be evaluated. It may be shown that when α = 1;

$$\beta = \frac{\int_0^\infty Q^2 I(Q) dQ + 2\pi^2 \rho^\circ (\sum_j \overline{b_j})^2}{\int_0^\infty Q^2 S(Q) dQ} \qquad (2.3.3.5)$$

And when β = 1;

$$\alpha = \frac{\int_0^\infty Q^2 S(Q) dQ - 2\pi^2 \rho^\circ (\sum_j \overline{b_j})^2}{\int_0^\infty Q^2 I(Q) dQ} \qquad (2.3.3.6)$$

Where ρ^o is the average number density of composition units within the sample. The geometric mean of α and β is used to find $I_R(Q)$ from equation (2.3.3.1) and typically has a value of one percent or less.

2.3.3.5 Placzek Corrections

In the the static approximation, the assumption is made that the atoms do not move during the scattering process. The repercussion of this assumption is that the integration of intensity is performed along a constant value of Q in ω-Q space.

This approximation leads - in first order - to distortions of the self-scattering level. These may be removed by the method employed by Placzek (1952) who assumed a 1/v detector law.

This work was further extended to arbitrary detector efficiencies by Yarnel et al. (1973). In the present work the latter formalism has been adopted since gas detectors follow an exponential law where the efficiency is assumed to have the form

$$\varepsilon(k) = 1 - e^{-ak/k_o} \qquad (2.3.3.7)$$

where 'a' is a constant dependent on detector constant. The effective integrated cross-section measured with a detector having an energy dependent efficiency is given by

$$\frac{d\sigma}{d\Omega_{meas}} = Nb^2 \int_{-\infty}^{\infty} \frac{|k|}{|k_o|} e(k) S\left(\underline{Q},\ \omega\right) d\omega \qquad (2.3.3.8)$$

where $h\omega = E_i$ (incident energy)

Neutrons have a non negligible mass m compared to the mass M of the scattering atom. The departure of $| k/k_o |$ from unity and the variation of $\varepsilon(k)$ give rise to corrections of the order of m/M at large scattering angles. If only the first order terms in m/M are considered (since the mass of the scattering atom is much greater than the neutron mass) the effective differential cross sections can be written for first order recoil effects as:

$$\frac{d\sigma^{coh}}{d\Omega} = b_{coh}^2 [S(Q) + P(Q)] \qquad (2.3.3.9)$$

$$\frac{d\sigma^{inco\ h}}{d\Omega} = b_{inco\,h}^2 [1 + P(Q)] \qquad (2.3.3.10)$$

with,

$$P(Q) = \frac{m}{M}\left[\frac{k_B T}{2E_o} - \left(c_1 + c_3\left(\frac{k_B T}{E_o}\right)\right)\frac{Q^2}{k_o^2}\right] \qquad (2.3.3.11)$$

Here E_o and k_o are the energy and wavevector of the incident neutron respectively and $k_B T$ is the mean kinetic energy of the atom. C_1 and C_3 are the detector constants depending on the detector law.

$$c_1 = 1 - \frac{ae^{-a}}{2(1-e^{-a})} \qquad (2.3.3.12)$$

$$c_3 = \frac{a(1+a)e^{-a}}{4(1-e^{-a})} \qquad (2.3.3.13)$$

2.4 X-ray Diffraction Measurements

A schematic representation of a typical X-ray diffractometer that was used in this work is shown in Figure 2.4.1. The real space correlation functions were obtained by using RAD (program) from Petkov (1989).

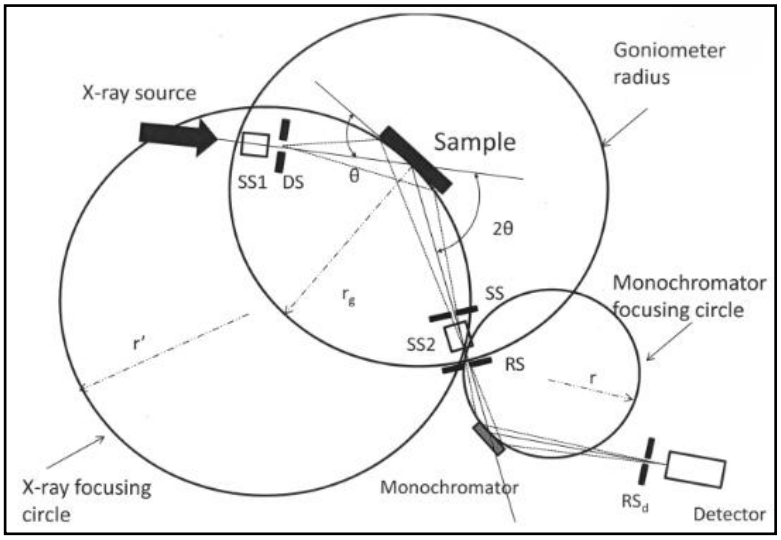

DS : Goniometer divergence slit.
SS : Soller slit
θ : Incident angle of the X-ray
2θ : Diffracted angle of the X-ray
SS : Goniometer scatter slit.
RS : Monochromator receiving slit.
RS_d: Detector receiving slit.
r' : Primary focal circle radius.
r_g: Goniometer radius.
r : Secondary focal circle.

Figure 2.4.1: Schematic of a typical X-ray Diffractometer (http://lipidlibrary.aocs.org/physics/xray)

2.4.1 X-ray Data Corrections

2.4.1.1 Background

The samples measured here all required correction for absorption of X-rays (1.54 Å). The samples were all in powder form, mounted on the usual glass slides and counted in reflection geometry. Reflection from the glass slide itself was negligible. The main background was scattering from air in the sample environment and along the scattered beam path. Thus, only air background subtraction from the sample scattering was made.

2.4.1.2 Absorption

For X-rays in Bragg-Brentano reflection geometry, it can be shown that, for planar samples the following absorption factor A(Q) can be applied (Milberg (1958)):

$$A(Q) = \frac{I}{I_o} = \frac{\sin\theta}{2\mu t}\left[1 - e^{-2\mu t / \sin\theta}\right] \qquad (2.4.1.1)$$

normalized to unit volume where μ is the absorption coefficient, of the sample. For the samples studied here, scattering of X-rays was considerably less than absorption and multiple scattering was thus negligible.

2.4.1.3 The Polarization Factor

The X-rays produced by an X-ray tube are unpolarized. However, after scattering the X-rays are polarized and this polarization factor is a function of scattering angle (Compton and Allison (1935)). The polarization factor P(θ) is used to correct for the loss of intensity and is given by;

$$P(\theta) = \frac{1 + x\cos^2 2\theta}{1 + y} \qquad (2.4.1.2)$$

where 2θ is the scattering angle, $x = \cos^2 2\alpha$, α being the Bragg angle of the monochromator. In the above expression, x = y when the monochromator is set in the incident beam and y = 1 when the monochromator is located in the diffracted beam. When a filter is used in place of the monochromator, x = y = 1 .

2.4.1.4 Form Factor Calculation

The theoretical form factor can be calculated from the expression,

$$f(\sin\theta/\lambda) = \sum_{i=1}^{4} a_i exp[-b_i \sin^2\theta/\lambda^2] + c \qquad (2.4.1.3)$$

Values of a, b and c have been tabulated (Cromer and Mann (1968)).

In the calculation of coherent scattering, the energy of the incident X-ray is assumed to be much greater than the absorption edge of the constituents present in the specimen.

In instances when there is appreciable absorption of the X-rays, anomalous dispersion corrections are necessary. The form factor calculated considering this effect has the form

$$f_i(Q) = f_i^o(Q) + \Delta f_i^{'}(Q) + i\Delta f_i^{''}(Q) \quad (2.4.1.4)$$

$$< f >^2 = (< f^o + \Delta f^{'} >)^2 + < \Delta f^{''} >^2 = [\sum_i C_i f_i(Q)]^2 \quad (2.4.1.5)$$

$$< f^2 >= < (f^o + \Delta f^{'})^2 > + < (\Delta f^{''})^2 >= [\sum_i C_i f_i^2(Q) \ ] \quad (2.4.1.6)$$

where Δf' and Δf'' are the real and imaginary additions of the anomalous dispersion term to the form factor (Cromer (1968)).

2.4.1.5 Correction to Incoherent Scattering

A fraction of the scattered radiation may be due to Compton scattering and has a longer wavelength. This change in the wavelength is known as the Compton Shift ($\Delta\lambda_C$) which increases at high angles. The incoherently scattered Compton intensity can be calculated and the analytical expressions have the form (Thijsse (1984)) :

$$I_{inc}(Q) = \left(\frac{\lambda}{\lambda'}\right)^2 \sum_{j=1}^{n} \frac{C_j Z_j (b_j Q)^{a_j}}{1+(b_j Q)^{a_j}} \quad (2.4.1.7)$$

Where $\lambda' = \lambda + \Delta\lambda_c$,A' Z_j 3 is the atomic number of atom-type j and

$$a_j = 2.6917\, Z_j^{-1} + 1.245 \quad (2.4.1.8)$$

$$b_j = 1.1870\, Z_j^{-1} + 0.1075 + 0.00436 Z_j - (0.01543 Z_j)^2 + (0.01422 Z_j)^3 \quad (2.4.1.9)$$

$I_{inc}(Q)$is added to the calculated form factor.

2.4.1.6. Normalization

After all the corrections for background, polarization and absorption, $I^{cor}(Q)$ can be expressed as:

$$\alpha I^{cor}(Q) = I_{eu}^{coh} + I_{eu}^{inc}(Q) \quad (2.4.1.10)$$

where h$I_{eu}^{coh} and I_{eu}^{inc}(Q)$ are the coherent and incoherent scattering intensities in electron units and α is the normalization constant given by;

$$\alpha = \frac{\int_{Q_{min}}^{Q_{max}} [<f^2> + I_{eu}^{inc}(Q)]dQ}{\int_{Q_{min}}^{Q_{max}} [I^{cor}(Q)]dQ} \quad (2.4.1.11)$$

A generally acceptable value of Q_{min} is $0.75Q_{max}$. This method of normalizing the intensity is referred to as the High Angle Method. The normalizing constant α depends on the chosen range (Q_{max} - Q_{min}) and the value of Q_{min} may in turn be chosen such that the following expression is satisfied,

$$\int_{Q_{min}}^{Q_{max}} Q^2 I(Q)dQ = -2\pi\rho^o \quad (2.4.1.12)$$

2.5 MCGR Analysis

MCGR is a program for determining total or partial radial distribution functions from one or more total structure factors measured by neutron or X-ray diffraction, by an inverse method (Pusztai and McGreevy (1997)).

MCGR uses a 1-dimensional version of RMC to produce a radial distribution function g(r). The corresponding structure factor A(q) for g(r) is then compared to the measured structure factor S(q) and depending on the sum of squares of differences, a decision to accept or reject g(r) is made before the next iteration commences.

The inverse method has considerable advantages over the conventional direct methods; for instance, they avoid truncation errors and allow the estimation of errors in radial distribution function (http://www.isis2.isis.rl.ac.uk/RMC/mcgr.htm).

.

In MCGR, the $g_{\alpha\beta}(r)$ are generated by a Monte Carlo method. The set of $g_{\alpha\beta}(r)$ are defined as histograms of n_r points with spacing dr. In addition to the measured structure factors, some constraints can be applied to the modeling of g(r). There is always a minimum distance below which g(r) has to be zero (closest approach between atoms). MCGR can be run so that no $g(r)<0$ below this limit will be allowed.

If the coordination number of some peak in g(r) is known, it can be used as a constraint. It is also possible to constrain g(r) to be positive within certain r limits (or for all r). It is also possible to use a polynomial background when fitting MCGR.

2.6 Fourier Transform Infra Red Spectroscopy

The total energy of a molecule has rotational, translational, vibrational and electronic components. The vibrational energy of a molecule is mostly in the infra-red part of the EM spectrum. Electronic energies may be probed by the absorption or emission of ultraviolet and visible radiation. Electronic states may thus be studied by UV/ Visible spectroscopy while vibrational states of a molecule in a given matrix of a solid or liquid may be studied with IR spectroscopy.

IR absorption takes place when a vibrational mode is excited through a change in dipole moment associated with that state. The dipole moment vector M is proportional to the displacement μ_l andcan be written as (Alben and Boutron (1975)):

$$M = \sum_{i(j.k)}\left[\left(r_{ik} - r_{ij}\right)\left(u_i - u_j\right).r_{ij} - (u_i - u_k).r_{ik}\right] \qquad (2.6.1)$$

where u_i are displacement vectors and r_{ij} is a unit vector joining sites i and j. In terms of bond compression;

$$C_{ij} = (u_i - u_j) r_{ij} \quad (2.6.2)$$

$$M = 2 \sum_i \left(\sum_j C_{ij} \right) \left(\sum_k r_{ik} \right) \quad (2.6.3)$$

A dipole moment arises due to an asymmetric atomic charge distribution. An induced dipole moment can be zero such as for perfect tetrahedral symmetry since $\Sigma_{ij} r_{ij} = 0$.

IR spectroscopic measurements generally employ a grating together with a source and a detector. If the monochromator is replaced by a Michelson interferometer, the measured transmitted spectrum is Fourier transformed into a frequency spectrum and the instrument is then called a Fourier Transform Infra-Red Spectrometer (FTIR). This spectroscopy has the following three advantages: multiplex advantage; aperture advantage; and wavenumber precision advantage. FTIR measures a spectrum of all wavenumbers in a single scan. A spectrum with high signal-to-noise ratio can be obtained by scanning for a longer period. This is known as the multiplex advantage. A large aperture can be used on the FTIR offering a large beam source area and is the analogue of a bright optical system. This helps in creating a spectrum having a high signal-to-noise ratio and is known as aperture advantage. The FTIR uses a He-Ne laser in sampling the interferogram. The use of monochromatic light helps in obtaining a spectrum with a high wavenumber precision.

The schematic of the IR spectrophotometer is shown in Fig. 2.6.1. The instrument uses black coated heated wire as the source of infra-red radiation. A KBr plate coated with Ge is used as a beam splitter. The transmitted radiation is measured by a high sensitivity pyroelectric detector in the range 4600 cm^{-1} to 400 cm^{-1}. In the measurements reported here, the powdered glass samples were mixed with KBr and pelletized under 6 tons pressure (6.12 x 10^6Pa).

2.7 UV-Visible Spectroscopy

UV-Visible absorption spectra of rare-earth glasses were studied using a Shimadzu spectrophotometer (Figure 2.7.1). The instrument covers a range of 200 to 1000 nm and uses a tungsten-halogen lamp for the visible range (i.e. 340 to 1000 nm), while a deuterium lamp is used as a source of UV light (200 to 340 nm). The transmitted beam is detected by a solid state silicon detector. The glass samples were measured in transmission mode in the sample position with no sample in the reference position. Data were presented as Absorbance in arbitrary units as normalization was not performed on these data.

According to Judd- Ofelt theory (Judd (1962), Ofelt (1962)) the oscillator strength f_{cal} of an induced electric dipole transition between the states ψJ and $\psi' J'$ is given by:

$$f_{cal} = \frac{8\pi^2 mc\,\nu}{3h(2J+1)} \frac{(n^2+2)^2}{9n} \sum_{\lambda=2,4,6} \Omega_\lambda (\psi J \| U^\lambda \| \psi' J')^2 \qquad (2.7.1)$$

Where n is the refractive index of the glass ν is the wave number of the absorption peak, Ω_λ are the host dependent intensity parameters, $\|U^\lambda\|$ are the square reduced matrix elements which do not depend on the host. By comparing f_{cal} with the measured oscillator strengths f_{meas}, Ω_j can be found. These Ω_j intensity parameters give information on bonds between rare-earth ion and the ligands in its vicinity as well as the symmetry of the environment of the ion. Thus f_{meas} or absorption line intensity is dependent on the rare-earth's structural environment (Shin and Heo (1999)).

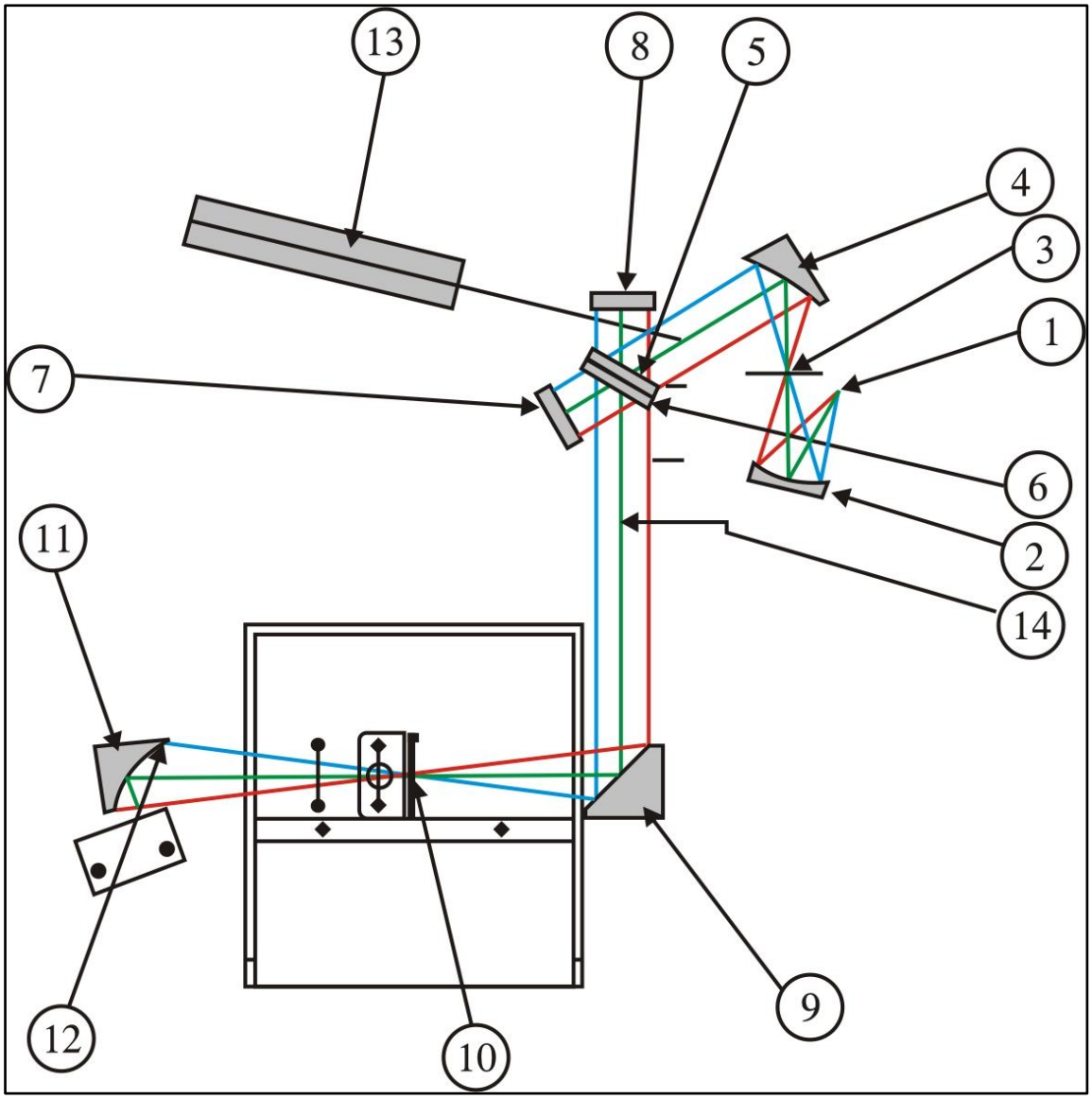

1. Source
2. Spherical Mirror
3. Aperture
4. Collimator Mirror
5. Beam Splitter
6. Compensator
7. Fixed Mirror
8. Moving Mirror
9. Paraboloidal Mirror
10. Collecting Mirror
11. High Sensitive Pyroelectric Detector
12. He-Ne Laser
13. 1/8 Wavelength Plate
14. He-Ne Laser Half Mirror
15. Polarized Beam Splitter
16. He-Ne Laser Detector
17. He-Ne Laser Beam Introducing mirror

Figure 2.7.1: Schematic of the FTIR – 8001 spectrophotometer.

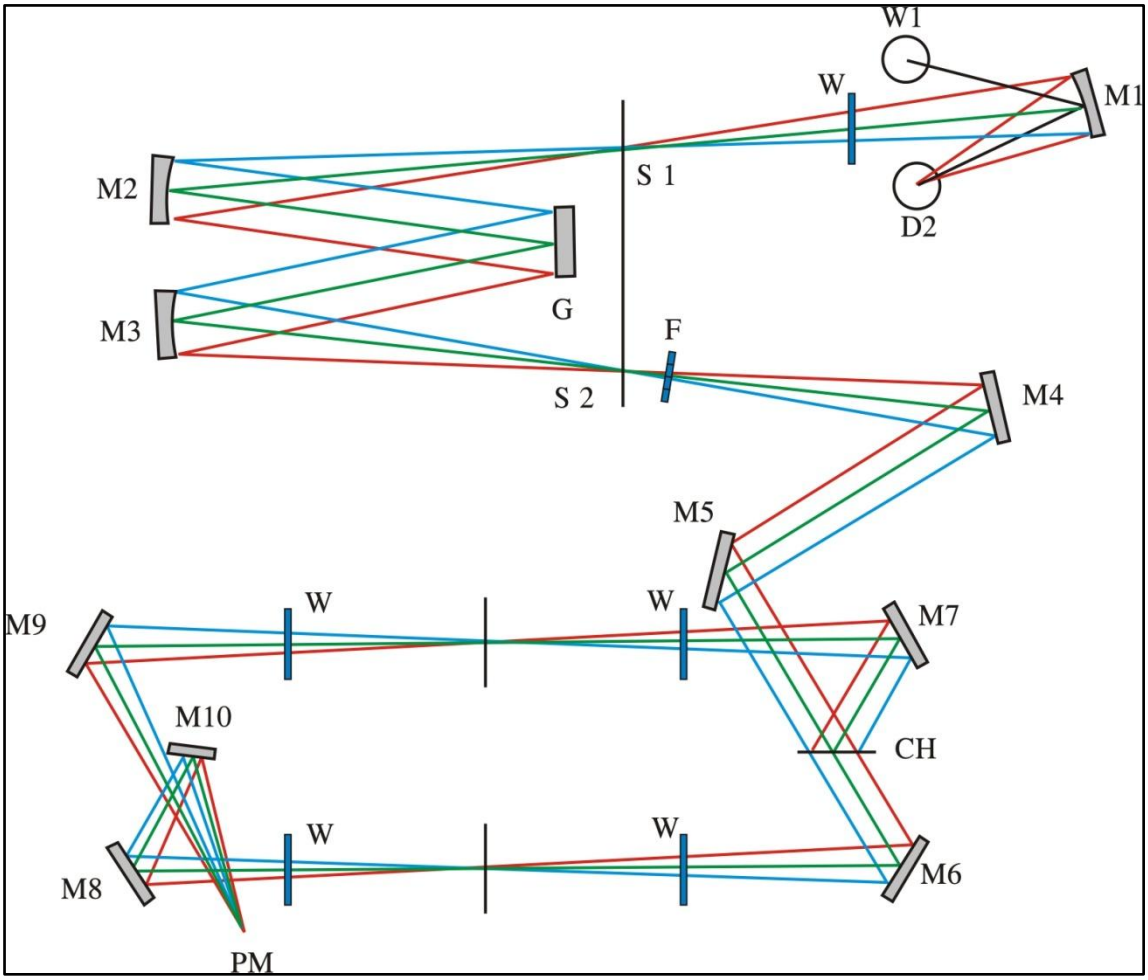

D2	: Deuterium Lamp	G	: DiffractionGrating
W1	: Halogen Lamp	S2	: Exit Slit
S1	: Entrance Slit	F	: Filters
W	: Quartz Windows	CH	: Beam Choppers
M1-M10	: Mirrors	PM	: Photomultiplier

Figure 2.7.2: Optical system of the UV-2401 Spectrometer.

(from Shimadzu UV-2401 Manual)

References

1. Alben R. and Boutron P., Science, 187 (1975) 430
2. Blech I.A. and Averbach B.L., Phys. Rev. 137 (1965) A 1113
3. Cocking S.J. and Heard C.R.T., U.K.A.E.A., Rept. A.E.R.E. (1965) 5016
4. Compton A.H. and Allison S.K., X-rays in Theory and Experiment, Van Nostrand Rainhold, New York, (1935)
5. Cromer D.T and Mann J.B., Acta Cryst. A24 (1968) 321
6. Debye P., Ann. Phys. 46 (1915) 809
7. Enderby J.E., Physics of Simple Liquids, (1968) Eds. Temperly H.N.V., Rowlinson J.S. and Rushbrooke G.S. (North-Holland, Amsterdam), Chap. 14
8. Faber T. E. and Ziman J. M., Phil. Mag. 11 (1965) 153
9. Fischer H. E., Barnes A. C and Salmon P. S., Rep. Prog. Phy. 69 (2006) 233-199
10. Fournet G., Handbuch der Physik vol 32 (Berlin: Springer) (1957) pp 238–320
11. Krogh-Moe J., Acta Cryst. 9 (1956) 951
12. Lomer W. M. and Low G. G., Thermal Neutron Scattering ed P A Egelstaff (London and New York: Academic) (1965) chapter 1
13. Lorch E., J. Phys. C: Solid State Phys. 2 (1969) 229
14. Milberg M.E., J. Appl. Phys. 29 (1958) 64
15. Mott N. F., Elements of Wave Mechanics (Cambridge: Cambridge University Press), (1962)
16. Norman N., Acta Cryst., 10 (1957) 370
17. Paalman N.H. and Pings C.J.; J. Appl. Phys. 33 (1962) 2635
18. Petkov V., J. Appl. Cryst. 22 (1989) 387
19. Placzek G., Phys. Rev. 86 (1952) 377

20. Pusztai L. and McGreevy R.L., Physica B 357 (1997) 234-236
21. Ramesh Rao N., Krishna P.S.R., Basu S., Dasannacharya B.A., Sangunni K.S. and Gopal E.S.R., J. Non-Crystalline Solids, 240 (1998) 221-231
22. Salmon P. S., Proc. R. Soc. Lond. A (1994) 445 351–65
23. Shin Y.B. and Heo J., J. Non-Cryst. Solids, 253 (1999) 23
24. Soper A.K. and Egelstaff P.A., Nucl. Instrum. Meth. (1980) 415
25. Squires G.L., Introduction to the Theory of Thermal Neutron Scattering (Cambridge: Cambridge University Press) (1978)
26. Thijsse B.J., J. Appl. Cryst. 17 (1984) 61
27. van Hove L., Phys. Rev. 95 (1954) 249–62
28. Vineyard G.H., Phys. Rev. 96 (1954) 93
29. Wright A. C., Advances in Structure Research by Diffraction Methods, (1974) 1
30. Wright A. C., Nucl. Instrum. Methods, 176 (1980) 623–5
31. Yarnel J.L., Katz M.J., Wenzel R.G. and Koenig S.H., Phys. Rev. A7 (1973) 2130
32. http://www.isis2.isis.rl.ac.uk/RMC/mcgr.htm

Chapter 3

Optical Studies of Rare-Earth Doped Borate Glasses

A set of rare-earth doped borate glasses are examined here from a consideration of their optical properties. The glasses that contained the rare-earth elements were taken singly as well as in pairs such that the relative concentrations of each ion type varied in the glasses of the series. Optical absorption and luminescent spectra were collected and analyzed to check for any effect that the host matrix – in this case a B_2O_3 glass – has on the optical spectra. The study also checked for possible mutual interaction between the rare-earth ion types in the optical data.

3.1 Introduction

There are many different applications of rare-earth oxide glasses that derive from their chemical properties, high refractive index (Chakraborty (1984) and Chakraborty (1985)) and well-defined visible absorption resonances. These uses include optical filters, optical waveguides, fibres, laser-host materials etc (Shikerkar et al. (2000), Moorthy et al. (2004) and Moorthy et al. (2005)). The incorporation of some of the rare-earth oxides in borate glass was attempted here and the glasses obtained were measured for their infra-red spectra, UV-Visible absorption and luminescence properties. The motivation was to check for structural effects on the optical properties – especially absorption spectra.

In Judd-Ofelt theory (Judd (1962), Ofelt (1962)) absorption, refractive index and density measurements can be used in calculating spontaneous emission probabilities of forced electric dipole transitions in rare-earth ions. These probabilities can be used to calculate aspects such as induced-emission cross-section, lifetime and branching ratios (Krupke (1974)). The type of

network former also affects spontaneous emission probability (Jacobs and Weber (1976)) in which small variations occur depending on the content and type of network-modifier (Izumitani et al. (1982), Marion and Weber (1991), Tanabe et al. (1992)). However, the dependence of emission probability on type of host glass and local structure around the rare-earth ion is not as yet understood.

3.2 Sample Preparation

Five borate glasses containing oxides of La, Pr and Nd were prepared. Lanthanum oxide was used with the intention of increasing the total rare-earth content of these glasses without adding to the magnetic component of scattering in the structural measurements that were to follow the present optical experiments. The initial powder mixture proportions that were used are as shown in Table 3.2.1 (Rare-earth oxides (99.9%) from Indian Rare Earths Ltd., Al_2O_3 (99.8%) and B_2O_3 (99%) both from Aldrich Chemical Company Inc.).

All samples were melt-quenched in air from approximately 1300 ^oC to room temperature in batch sizes of 15 g of the starting oxide mixtures using alumina crucibles (De Sousa and Singh (2004), Kumari and Pereira (2003). Homogeneous bubble-free glasses were formed having colours from purple for sample 1 to green for sample 5 and intermediate colours for the other glasses (samples 2, 3, 4) as shown in Figure 3.2.1

Table 3.2.1: Initial powder mixture proportions of the glass samples

Sample No.	Components (Molar %)				
	La_2O_3	Nd_2O_3	Pr_6O_{11}	Al_2O_3	B_2O_3
1	7	8	0	5	80
2	9.19	3.06	0.99	5.10	81.66
3	10.56	2.29	2.64	5.28	79.23
4	9.19	0.99	3.06	5.10	81.66
5	10.73	0	3.46	5.36	80.45

Figure 3.2.1: Photographs of the glass samples doped with Nd and Pr.

3.3 Results

X-ray diffraction patterns were taken with incident CuK_{α} in reflection mode in the 2θ angular range of 10^{o} to 140^{o} and are shown in Figure 3.3.1. Continuous lines in the latter and subsequent plots in this work are drawn linking data points and are intended as guides to the eye. FTIR data (Shimadzu spectrometer) on the five glass samples in the range 400 cm^{-1} to 1000 cm^{-1} are shown in Figure 3.2.2. UV-Visible absorption spectra of the glasses were measured with a Shimadzu spectrophotometer between 300nm to 900nm and are stacked together in Figure 3.3.3. For the luminescence measurements, the excitation wavelength for the rare-earth ions was 445 nm. The resulting emission spectra for Nd and Pr transitions were measured in the range 800 to 950 nm. Lifetime measurements from the latter emission peaks (relating to $^{4}F_{3/2}$ to $^{4}I_{9/2}$ transitions (Ajroud et al. (2000)) yielded the purely exponential decay functions shown in Figure 3.3.4.

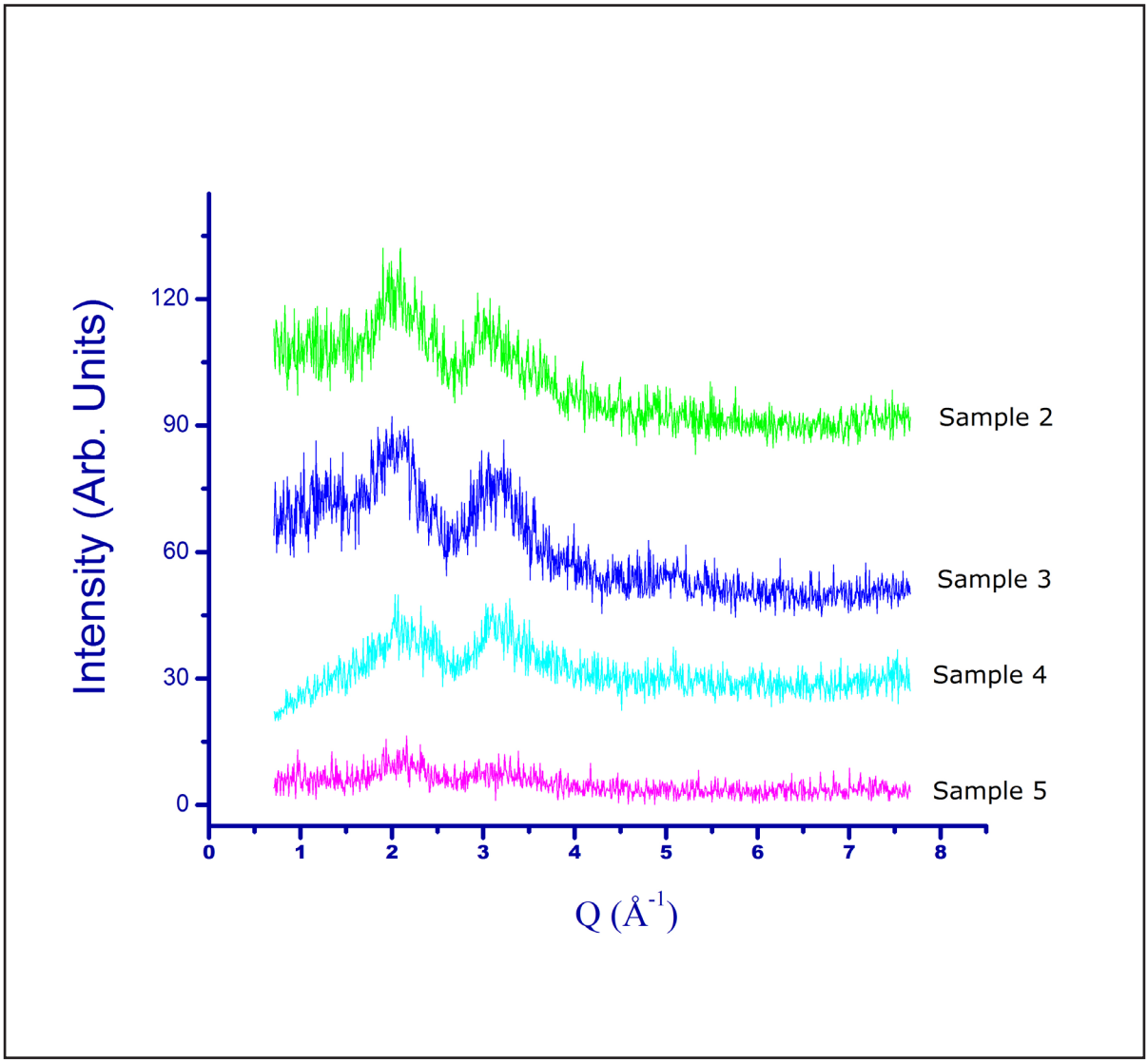

Figure 3.3.1: X-ray diffraction patterns of the borate glasses.

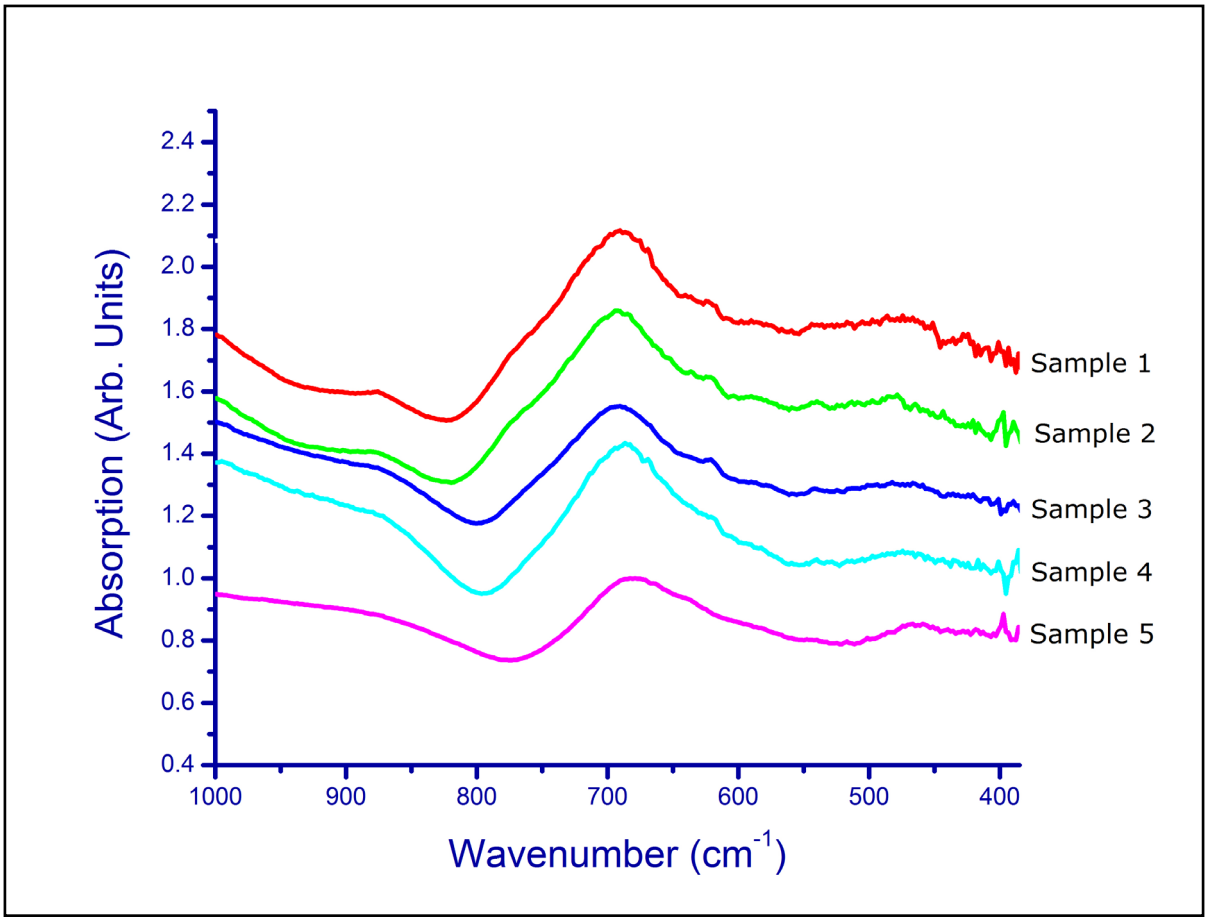

Figure 3.3.2: FTIR Absorption spectra of the glasses.

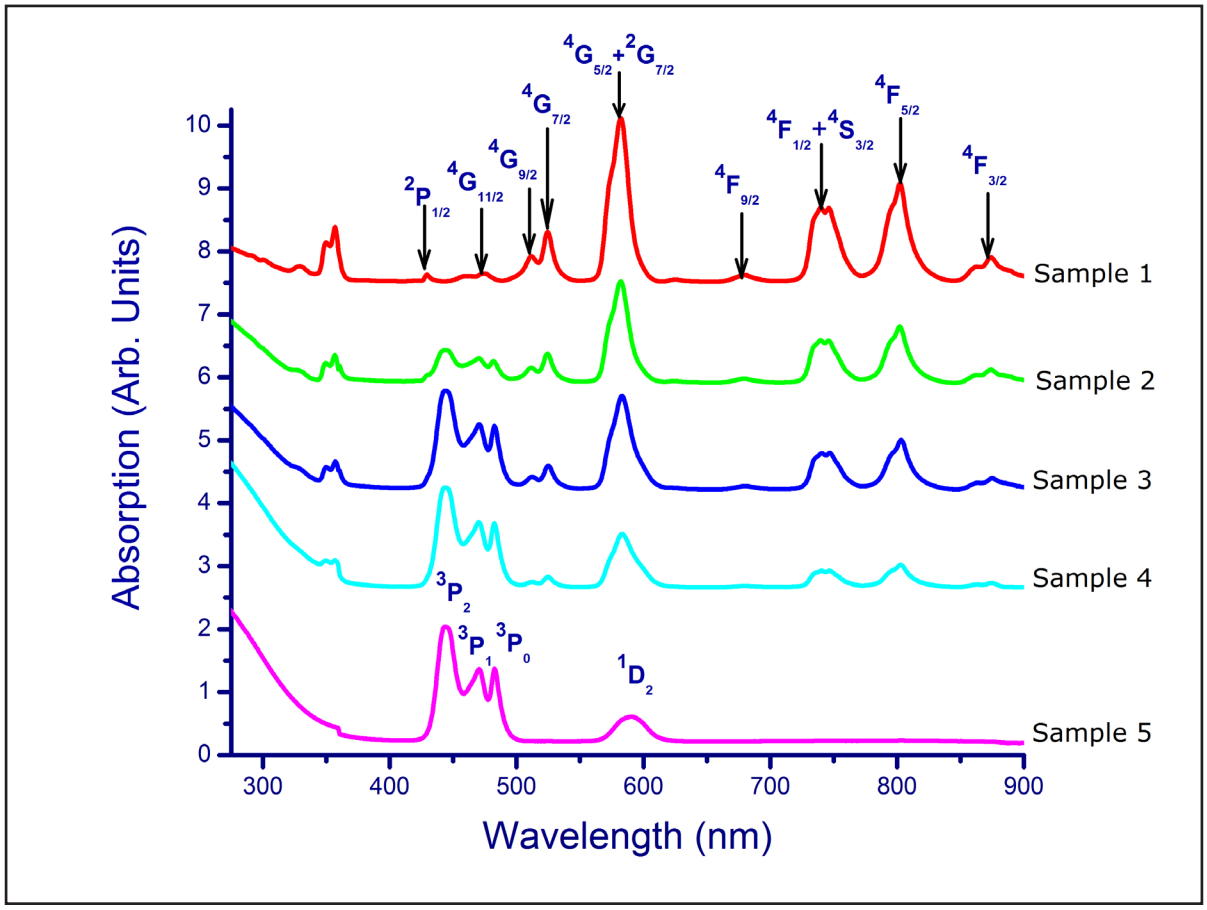

Figure 3.3.3: Comparison of UV-Vis absorption spectra of the borate glasses.

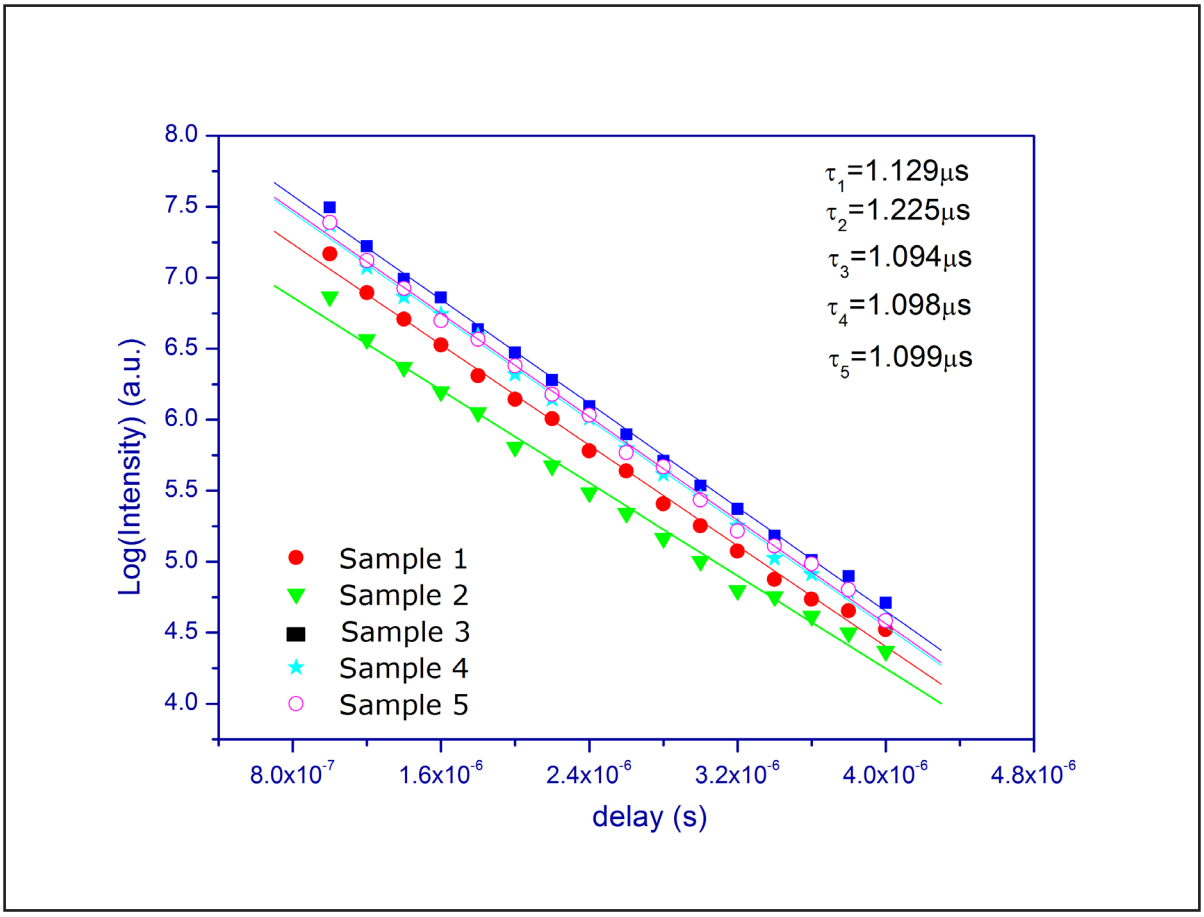

Figure 3.3.4: Lifetimes of luminescent emission from Nd, Pr in the borate glasses.

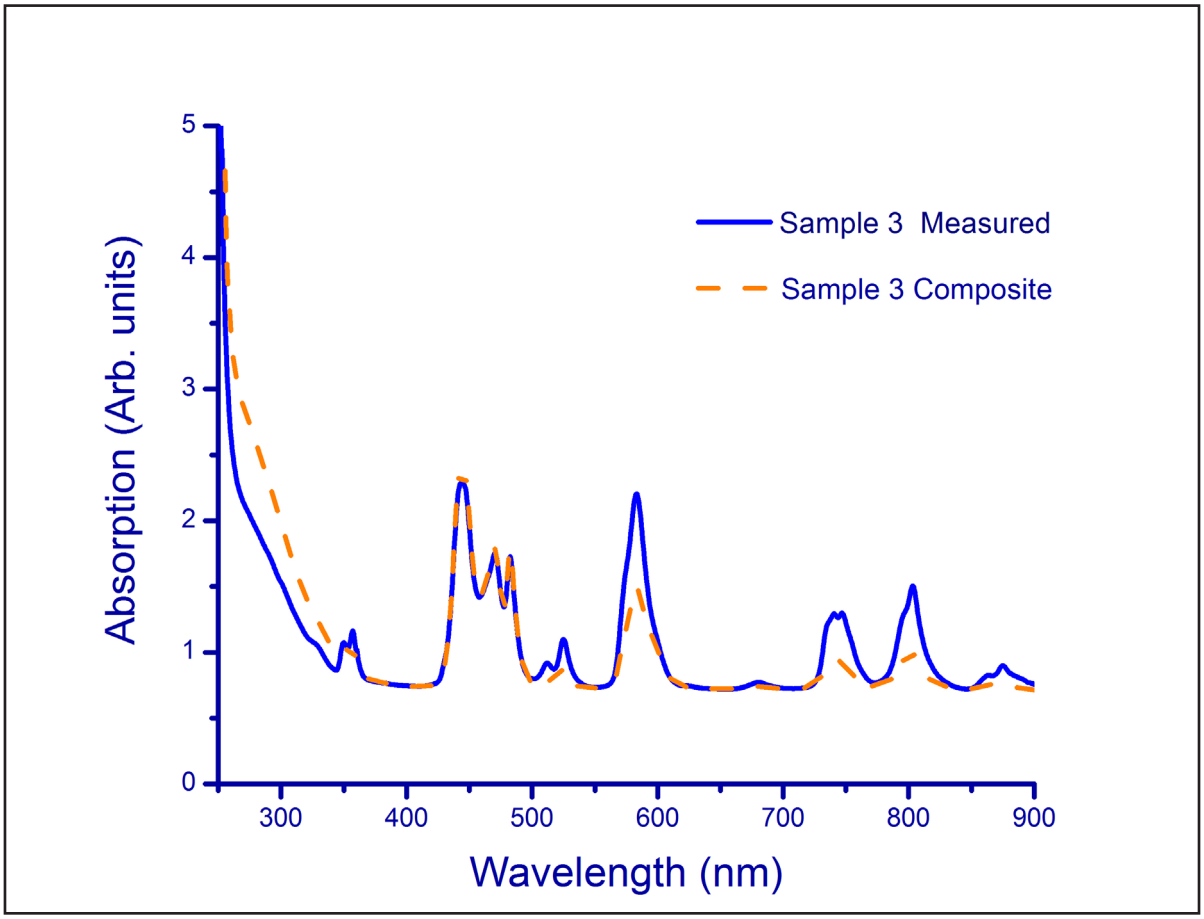

Figure 3.3.5: Comparison of measured and calculated composite UV-Vis spectra of sample 3 scaled to the Pr peaks at 450 nm.

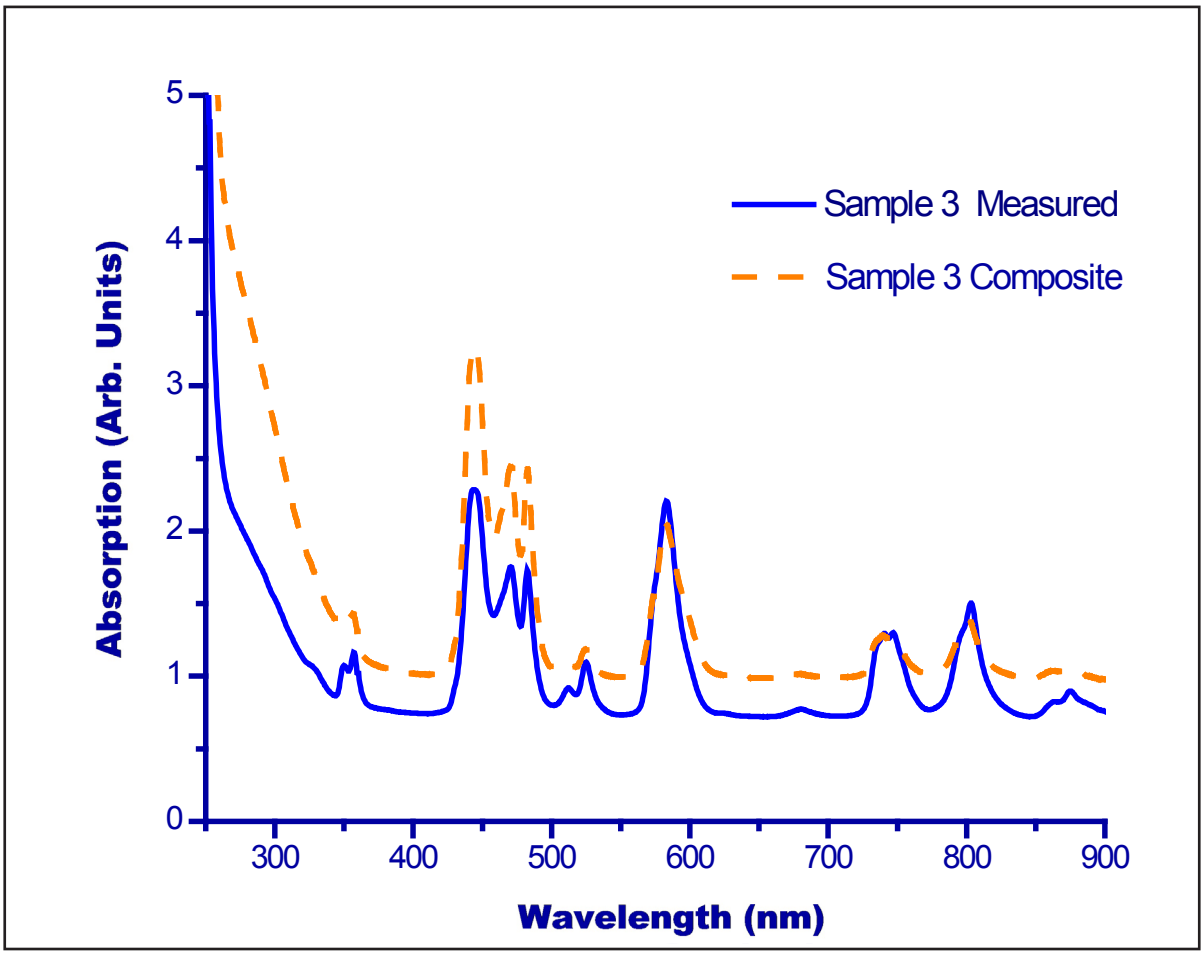

Figure 3.3.6: Comparison of measured and calculated composite UV-Vis spectra of sample 3 scaled to the Nd peak at 750 nm.

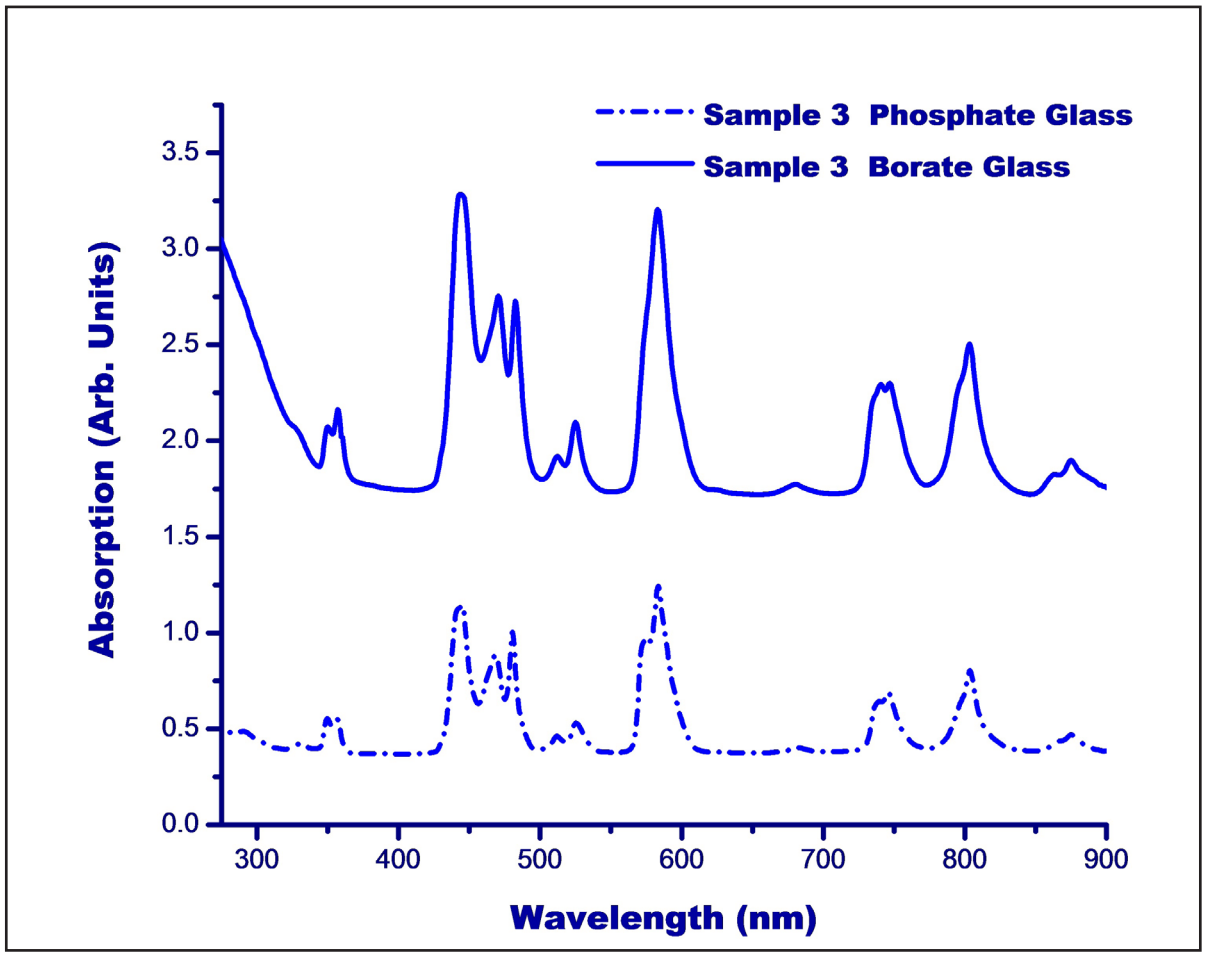

Figure 3.3.7: Comparison of UV-Vis spectra of a borate and equivalent phosphate glass with the same rare-earth ion compositions.

3.4 Discussion

The essentially vitreous nature of the samples was confirmed from the X-ray diffraction data of Figure 3.3.1.

The B-O stretching mode due to BO_4 tetrahedra at 900 cm^{-1} and the B-O-B bond bending mode at 700 cm^{-1} are also observed in the glasses indicating the presence of BO_4 units and their linkages.

The absorption peaks in both glass types were spectroscopically identified ((Moorthy et al. (2004), Moorthy et al. (2005), Ajroud et al. (2000), Lowther (1974)) as being from the 4f electronic levels of Nd, Pr. The spectra of the two samples that had either Nd_2O_3 (sample 1) or Pr_6O_{11} (sample 5) but not both oxides were added together in the same relative ratios that these components occur in samples 2, 3 and 4 to yield three calculated spectra. The latter were then compared to the measured spectra from these glasses by multiplicative scaling of the calculated spectra until the peak heights due to the Pr transitions (at 450 nm) matched. The comparison is shown for sample 3 in Figure 3.3.5. This procedure was also tried by using the Nd transitions, but this resulted in an offset and apart from a particular chosen Nd peak (eg. at 750 nm) the other peak heights in the spectra did not match (Figure 3.3.6). Scaling by using the Nd peaks was thus not pursued further. This scaling procedure (using the Pr peaks) resulted in agreement to within 2 nm of all peak positions and about 2% of peak height for the Pr peaks. Peak wavelengths relate to energies of electronic transitions and the fact that these wavelengths remain approximately unchanged strongly suggests that the 4f states of the rare-earth ions (at these concentrations) in all these glasses interact only weakly with the host glass structure. The extent that this is true is emphasized when the absorption spectra for phosphate glasses having the same rare-earth concentrations (as for example in sample 3) are compared to each other (Figure 3.3.7). The main absorption features are present in both glass-types but relative peak intensities which relate to transition probabilities are, as expected, slightly different. However,

for the Nd absorption peaks the heights of the measured peaks were upto 60% higher than the calculated, indicating that the presence of Pr in the actual glasses (samples 2, 3, 4) enhances the intensities of these Nd absorption lines. It is possible that a certain degree of interaction between the Pr and Nd ions' energy levels in each glass seems to be taking place affecting their relative transition probabilities but not their energies of transition. The theory of electronic transitions of these states in rare-earth elements has been dealt with by Judd and Ofelt (1962). In the latter, the detailed transition probabilities are dependent on the structural environment of the rare-earth ion. In particular, next-nearest neighbor correlations are known to have an effect on these transitions. Thus a detailed structural study of these glasses would help in estimating relative transition probabilities and thus relative peak heights in the absorption spectra.

The energies of emission states for both Nd and Pr gave rise to a single peak in the range of measurement (800 nm to 950 nm). These measured emissions of Nd and Pr yielded exponential decay life-times in the range 1.094-1.225 μs for these borate glasses. The errors associated with these measurements were of the order of the size of the symbols of the data points in Figure 3.3.4. These values were similar for an equivalent set of phosphate glasses (3.3.7). The similarity of decay times from all these samples indicates that the luminescent states are only weakly affected by the host structures.

3.5 Conclusions

Upto 15 mole % of rare-earth ions La, Pr and Nd have been incorporated in a B_2O_3 glass matrix to produce homogeneously coloured bubble-free glasses.

From FTIR data, the presence of BO_4 tetrahedra and a continuous random network with B-O-B linkages are both supported.

UV-Visible absorption spectra on these glasses have shown the energies of the 4f electronic levels of the Nd and Pr ions (at these concentrations) to be only weakly linked to the surrounding host glass network be it borate or phosphate. Intensities of optical absorption transitions in the Nd ions were enhanced by the presence of Pr ions in these glasses possibly due to interaction between the 4f levels of these two ions in these glasses. Thus, while the probabilities of transitions between the 4f levels of these rare-earth ions are affected by their environment and neighbours, the energies of transition between the states remain essentially unchanged. Structural studies of these glasses by X-ray and neutron diffraction using B-11 B_2O_3 would be useful in estimating the necessary input parameters for the calculation of the transition probability matrix of 4f electrons around the rare-earth ions.

Life-times of luminescent emissions from the rare-earth ions are similar and of the order of 1 μs from these borate glasses as well as from a similar set of phosphate glasses. This indicates that the structural surroundings of the rare-earth ions do not greatly affect the luminescent levels of these ions.

References

1. Ajroud M., Haouari M., Ben Ouada H., Maaref H., Brenier A. and Garapon C., J. Phys.: Condens. Matter, 12 (2000) 3181-3193
2. Chakraborty I.N., Shelby J.E., and Condrate R.A. Sr., J. Am. Ceram. Soc., 67 (1984) 782
3. Chakraborty I.N., Day D.E., Lapp J.C., and Shelby J.E., J. Am. Ceram. Soc., 68 (1985) 368
4. De Sousa B., and Singh M., M.Sc. Project Report, 2004, Goa University
5. Izumitani T., Toratani H. and Kuroda H., J. Non-Cryst.Solids 47 (1982) 87
6. Jacobs R.R. and Weber M.J., IEEE J. Quantum Electron.QE-12 (1976) 102
7. Judd B.R., Phys. Rev. 127 (1962) 750
8. Krupke W.F., IEEE J. Quantum Electron. QE-10 (1974) 450

9. Kumari S. and Pereira N., M.Sc. Project Report, 2003, Goa University

10. Lowther J.E., J. Phys. C, 7 (1974) 4393-4402

11. Marion J.E. and Weber M.J., Eur. J. Solid State Inorg. Chem. 28 (1991) 271

12. Moorthy L.R., Rao T.S., Jayasimhadri M., Radhapathy A., & Murthy D.V.R., Spectrochimica Acta Part A, 60 (2004) 2449-2458

13. Moorthy L.R., Jayasimhadri M., Radhapathy A. & Ravikumar R.V.S.S.N., Mater. Chem. Phys., 93 (2005) 455-460

14. Ofelt G.S., J. Chem. Phys. 37 (1962) 511

15. Shikerkar A.G., Desa J.A.E., Krishna P.S.R., and Chitra R., J. Non-Cryst. Solids, 270 (2000) 234- 246

16. Tanabe S., Ohyagi T., Soga N. and Hanada T., Phys. Rev. B46 (1992) 3305

Chapter 4

Neodymium Dopant Ions in Borate Glass

In order to examine the effect of inclusion of rare-earth ions on the structure of the host matrix, it was decided to commence the study with the inclusion of a single ion type at different concentrations in the glass. This led to the measurements described in the present chapter. The motivation for this structural work was some differences in expected intensities in the visible absorption spectra. According to the Judd-Ofelt (1962) description, details of peak intensities are dependent on structural features beyond the nearest neighbor, as these affect transition probabilities in the 4f electronic states.

4.1 Literature Survey of Doped Borate Glass Structures

The basic model of the atomic structure of vitreous B_2O_3 (v-B_2O_3) was proposed by Zachariasen (1932) as a three-dimensional continuous random network formed by sharing BO_3 structural units. With the help of X-ray diffraction, Warren et al. (1936) confirmed this model. Johnson et al. (1982) using neutron diffraction proved that the v-B_2O_3 consisted of a larger structural unit called the boroxol group (see figure 4.1.1). The extremely intense, narrow and highly polarized Raman peak at 808cm^{-1} had led Goubeau and Keller (1953) to the existence of the boroxol group for the first time. On the basis of the study of a large range of experimental results, Krogh-Moe(1969) proposed that the v-B_2O_3 structure consists of a continuous random network with a high fraction of boroxol groups. Comparing the measured real space correlation function from X-ray data with a model correlation function, Mozzi and Warren (1970) were correctly able to predict all the peaks upto 6Å.

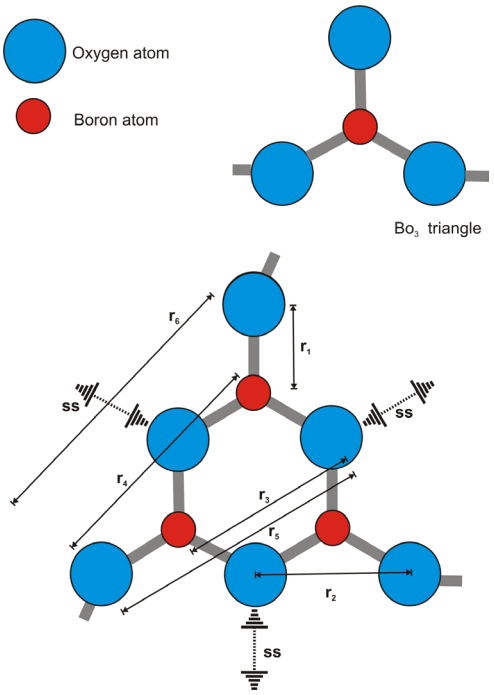

Figure 4.1.1: Boroxol ring structure (after Hannon et al. (1994)

The frequency of presence of boroxol group (Hannon et al. (1994)) is given by

$$f = \frac{3r}{(1+3r)} \qquad (4.1.1)$$

where r = ratio of number of boroxol groups to the number of independent BO_3 triangles.

Table 4.1.1 lists the distances within a boroxol group, along with the non-ring distances which are fixed if the B-Ô-B bond angle β is fixed (figure 4.1.2).

The constituents of the silicate glasses were classified as either network former or network modifiers. The classification arises from the fact that the network modifying cations are more ionic in character.

Table 4.1.1: Boron – Oxygen distances in BO_3 and the B_3O_6 boroxol ring.
(after Hannon et al.(1994))

Distance	Type	$\Sigma_j\Sigma_k n_{jk}$	r_{jk}/r_1	r_{jk}	$\langle u_{jk}^2 \rangle^{1/2}$
r_{jk}	j-k			(Å)	(Å)
r_1	B-O	12	1	1.365	0.043
r_2	B-B	4*f*	√3	2.364	0.07
	O-O	12			
r_2'	B-B	6-4*f*	2 sin(β /2)	2.474	0.07
r_3	B-O	4*f*	2	2.730	0.07
r_4	B-O	8f	√7	3.611	0.07
r_5	O-O	4*f*	3	4.095	0.07
r_6	O-O	4*f*	2√3	4.728	0.07
r_7	B-O	4*f*	√(10-6 cos β)	5.081	0.07

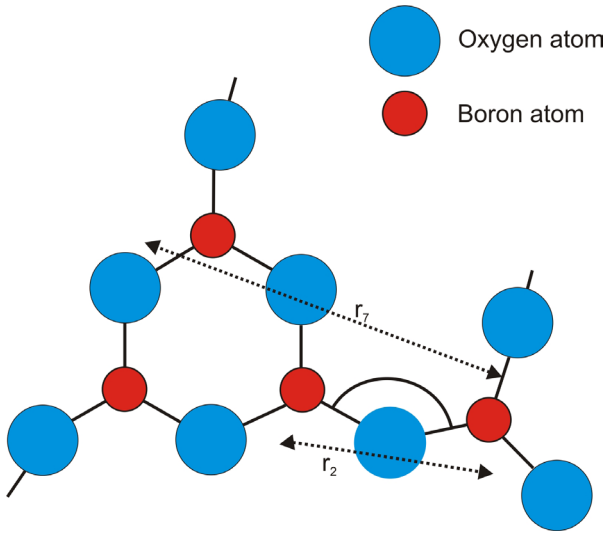

Figure 4.1.2 : Distances within the boroxol ring for a given B-O-B angle β .
(after Hannon et al.(1994))

The continuous 3-D random network of a glass former is modified by an included modifier which modifies the structure and leads to the presence of non-bridging oxygen atoms. The presence of the modifier in the B_2O_3 glass structure causes conversion of some of the basic BO_3 trigonal units to BO_4^- tetrahedral:

$$\frac{1}{2} M_2O + BO_3 \rightarrow M^+ + BO_4 \qquad (4.1.2)$$

or

$$M_2O + 2BO_3 \rightarrow 2M^+ + 2BO_4 \qquad (4.1.3)$$

The network becomes more compacted as the number of tetrahedra increase. When there are no non-bridging oxygen atoms the fraction of tetrahedra is like that for hydrated borates (Edwards and Ross (1960)) and is given by (Krogh-Moe (1962)) :

$$N_4 = B_4 / (B_4 + B_3) \qquad (4.1.4)$$

where B_4 is the fraction of all Boron atoms in four-fold coordination, B_3 is the fraction of all B atoms in three-fold coordination. The BO_4^- tetrahedron has a delocalized electronic charge which makes it energetically unattractive to connect to a neighbouring tetrahedron. The concentration of non-bridging oxygen atoms increases as the modifier concentration increases.

Krogh-Moe (1965) in dealing with $xM_2O.B_2O_3$ glasses proposed that the entire network is made up of different structural units that exist in the crystalline compounds. These units can be complex and are schematically shown in Figure 4.1.3. The proposed model of Krogh-Moe was given support by several different authors using a variety of techniques : NMR (Feller et al. 1982), (Chiodilli et al. (1982), (Kim and Bray (1974), (Hayashi and Hayamizu (1989) ; Raman Scattering (Galeener et al. (1980) and (Lorsch et al. (1984) and Infra-red absorption experiments (Kamitos et al. (1990) and (Tuller and Button (1985)).

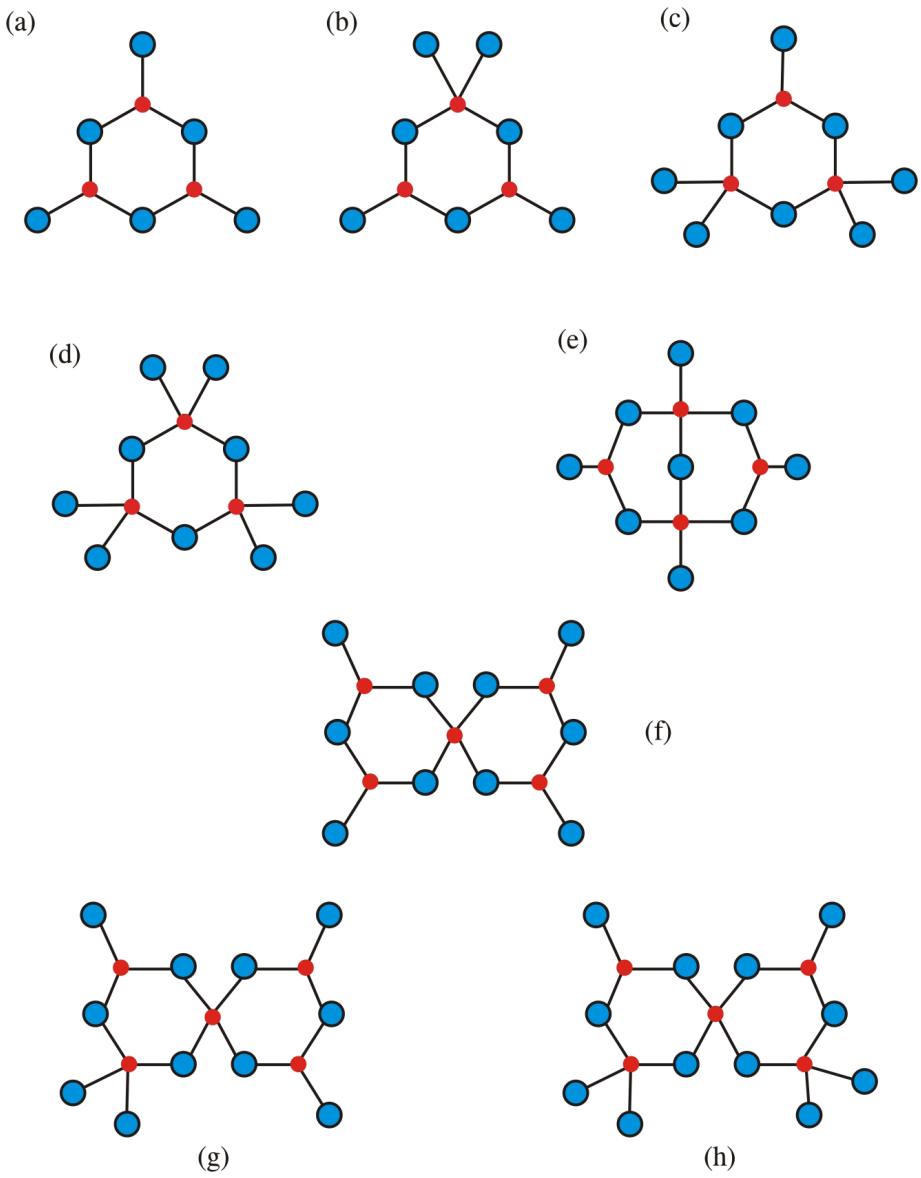

Figure 4.1.3 : Schematic representations of the different superstructural units in a borate glass having doped cation (after Wright (2010)) :
(a) boroxol ring B_3O_6 (b) triborate B_3O_7 (c) di-triborate B_3O_8
(d) meta-borate B_3O_9 (e) di-borate B_4O_9 (f) bicyclic metaborate B_5O_{10}
(g) di-pentaborate B_5O_{11} (h) tri-pentaborate B_5O_{12}

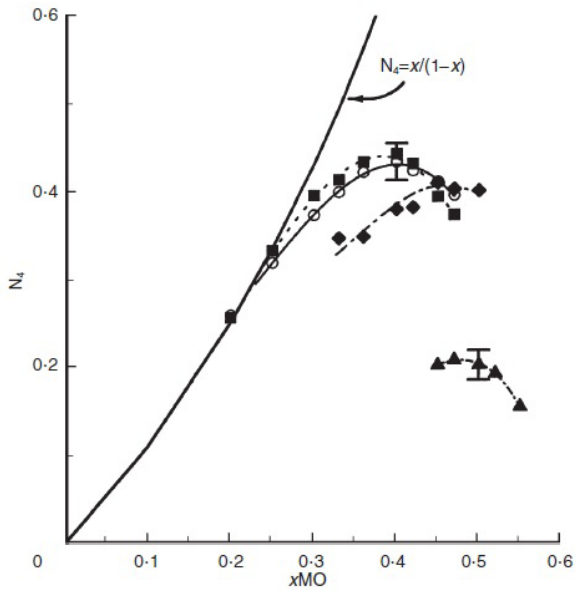

Figure 4.1.4: Fraction of four coordinated boron atoms, N4, as function of MO mole fraction in xMO.(1-x)B_2O_3 glasses. (after Y. D. Yiannopoulos et el. (2001))

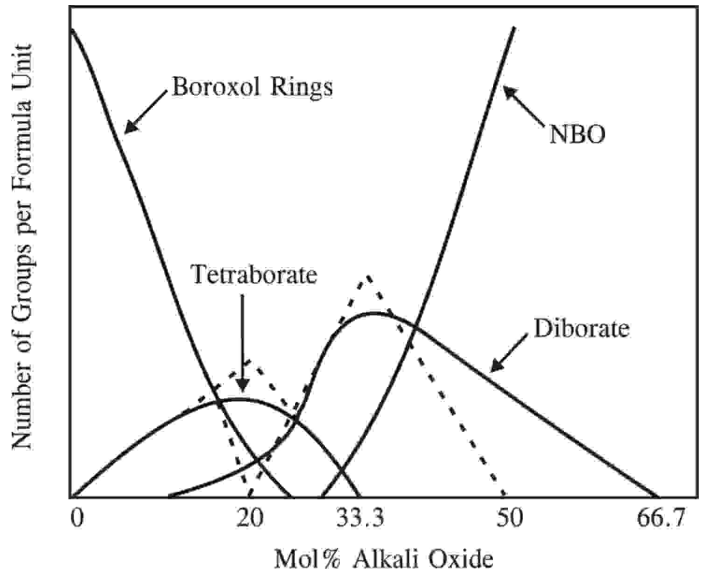

Figure 4.1.5: Fraction of superstructural units with composition of dopant cation. (after Griscom (1978))

Yiannopoulos et el. (2001) have shown that as a metal cation is added to the B_2O_3, there is a growth of four-fold coordinated Boron at the expense of the number of 3-fold coordinated B as shown in Figure 4.1.4. There are changes in the borate structure as the metal ion concentration grows with increasing numbers of new types of borate structural groups being formed – as shown in Figure 4.1.5 . Metal cation coordinations with oxygen have been studied by a number of authors and methods viz. X-ray diffraction by Licheri et al. (1986) and Pashina et al. (1984) ; Extended X-ray Absorption Fine Structure (EXAFS) (Dalba et al. (1987), Dalba et al. (1990)). There is a coordination of the metal ions with the BO_4^- tetrahedral groups. These authors do not however assert that the cations and the BO_4^- tetrahedral tend to cluster into certain pathways which would make them suited to ion diffusion. Also, it is not clear if the cations are homogeneously distributed in the glass.

4.2 Sample Preparation

A set of 5 glasses were prepared in which B_2O_3 obtained from ^{11}B boric acid (Sigma Aldrich 99 % B-11) was used as the host network as shown in Table 4.2.1.

Table 4.2.1: Proportions of Nd_2O_3 doped borate glasses.

Sample No.	Sample Name	Components (Molar %)	
		Nd_2O_3	B_2O_3
1	Nd - 0	0	100
2	Nd - 10	10	90
3	Nd - 15	15	85
4	Nd - 20	20	80
5	Nd - 25	25	75

The method of preparation was that of fusion of a starting powdered mixture of the constituent components. The initial charge consisted of the individual component oxides which were weighed out in the appropriate amounts with increasing molar concentration of Nd ions (Thomas Baker 99.9%). A summary of the starting compositions and weights of constitutents of the powder mixtures is shown in Table 4.2.2.

The mixtures were thoroughly ground and homogenized before being heated (in air) in stages in a Carbolite muffle furnace from room temperature to 1450 ^{0}C over a period of 1 hour with appropriate care being taken to permit the decomposition of boric acid into boron oxide (B_2O_3) in the temperature range 350 to 500 ^{0}C.

The thermal history of the samples is shown in Figure 4.2.1. The crucible, made of alumina, was removed and the melt poured onto a metal plate at room temperature. Coloured transparent glass beads were formed (shown in Figure 4.2.2). An undoped borate glass was prepared in order to relate structural features to the presence of the rare-earth ion.

Table 4.2.2 : Initial powder mixture compositions of the Nd_2O_3 doped borate glasses.

Sample No	Compound	gram-mole	Mole%	Corr.wt	Desired in 1 gm	Desired in 5 gm
1	Nd2O3	336.48	0	0	0	0
	B2O3	69.62	100			0
	H3BO3	62.03	200	124.06	1	5
				124.06	1	5
Sample No	**Compound**	**gram-mole**	**Mole%**	**Corr.wt**	**Desired in 1 gm**	**Desired in 5 gm**
2	Nd2O3	336.48	10	33.64782	0.2315719	1.15786
	B2O3	69.62	90			0
	H3BO3	62.03	180	111.654	0.7684281	3.84214
				145.30182	1	5
Sample No	**Compound**	**gram-mole**	**Mole%**	**Corr.wt**	**Desired in 1 gm**	**Desired in 5 gm**
3	Nd2O3	336.48	15	50.47173	0.3236971	1.618485
	B2O3	69.62	85			0
	H3BO3	62.03	170	105.451	0.6763029	3.381515
				155.92273	1	5
Sample No	**Compound**	**gram-mole**	**Mole%**	**Corr.wt**	**Desired in 1 gm**	**Desired in 5 gm**
4	Nd2O3	336.48	20	67.29564	0.4040721	2.020361
	B2O3	69.62	80			0
	H3BO3	62.03	160	99.248	0.5959279	2.979639
				166.54364	1	5
						0
Sample No	**Compound**	**gram-mole**	**Mole%**	**Corr.wt**	**Desired in 1 gm**	**Desired in 5 gm**
5	Nd2O3	336.48	25	84.11955	0.4748103	2.374051
	B2O3	69.62	75			0
	H3BO3	62.03	150	93.045	0.5251897	2.625949
				177.16455	1	5

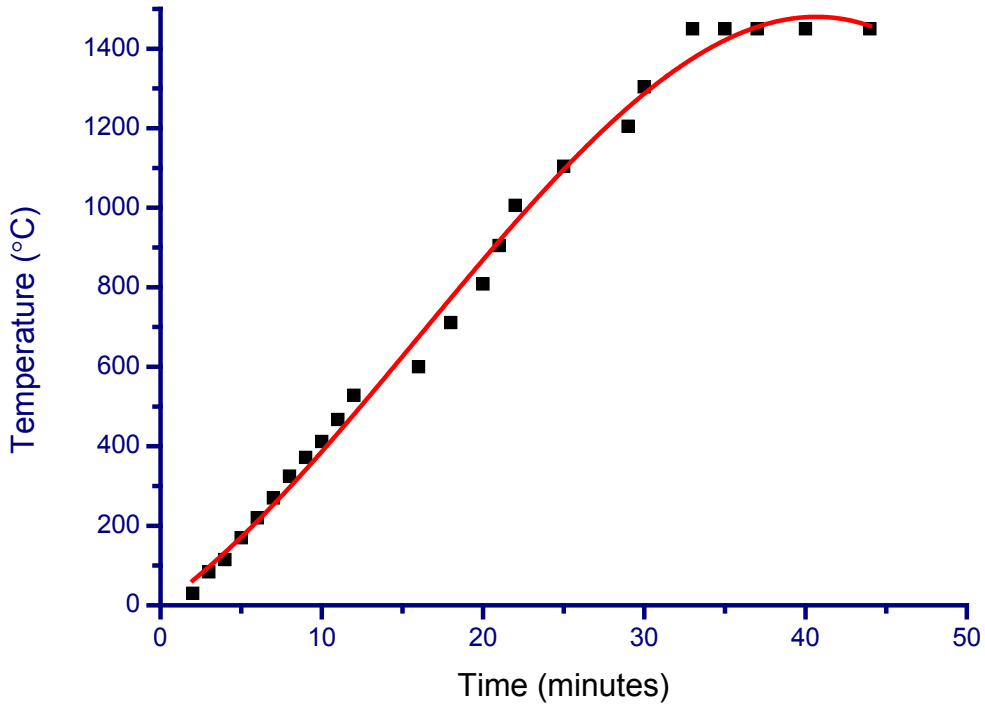

Figure 4.2.1: Typical heating schedule in the preparation of the Nd_2O_3 doped borate glasses..

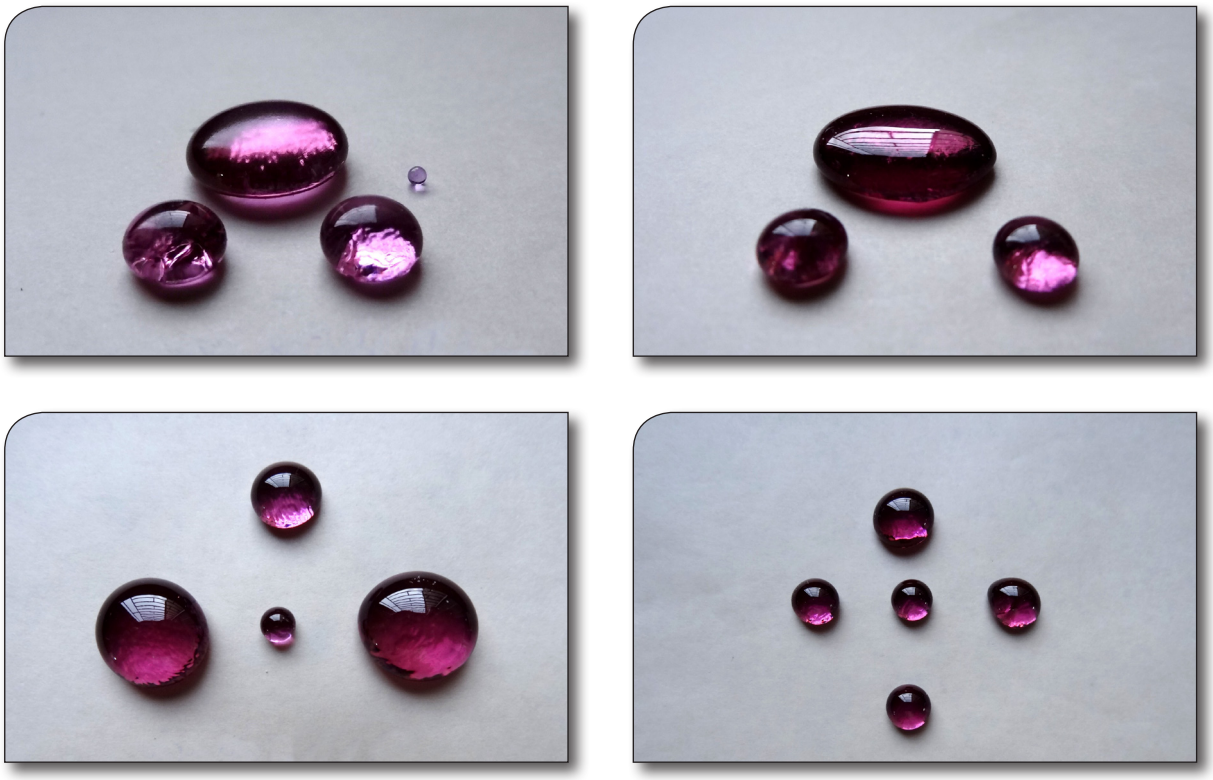

Figure 4.2.2: Photographs of Nd_2O_3 doped borate glasses with 10% to 25% molar concentration of Nd ions.

4.3 Density Measurement

The densities of the samples were measured by the water displacement method. On account of the fact that most of the prepared glass samples were of irregular shapes and sizes and could not fit into a standard specific gravity bottle, an alternative receptacle was made to suit these samples as described in Chapter 2. The density of the samples is shown in Figure 4.3.1

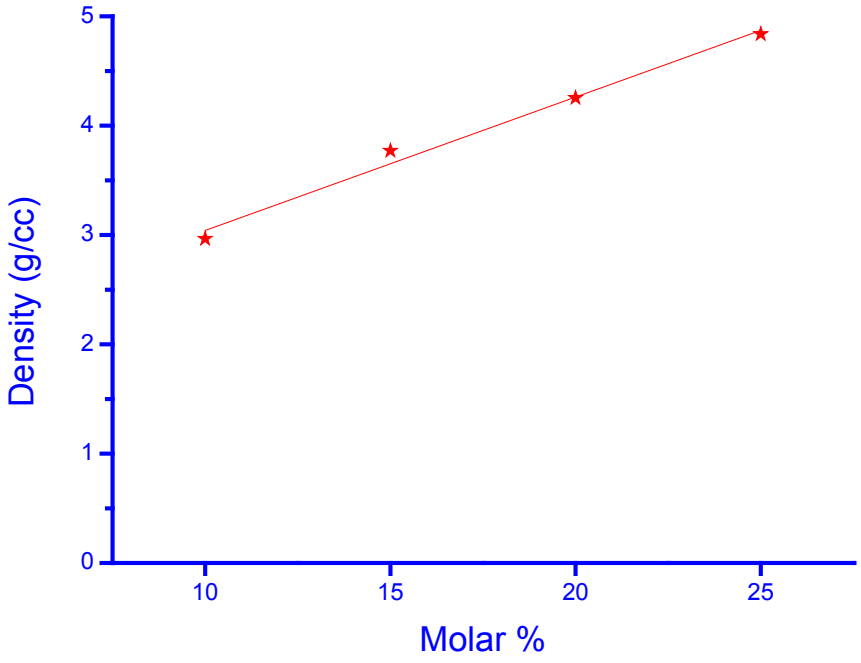

Figure 4.3.1: Variation of density of the Nd doped borate glasses with molar concentration of Nd_2O_3 .

It is observed that as the molar percentage of Nd ions in the sample increases, the bulk density also increases as would be expected from the increasing mass of Nd ions in the samples.

4.4 X-Ray Diffraction Data of Nd Doped Borate Glasses

X-ray diffraction data were measured using a Rigaku D-MAX/B rotating anode diffractometer with Cu Kα incident X-rays and counted in the angular range of 3^0 to 145^0 . The intensity data are shown in Figure 4.4.1. Experimental corrections and normalization were performed before Fourier inversion to obtain the pair distribution functions, total correlation functions and total radial distribution functions as shown in Figures 4.4.2, 4.4.3 and 4.4.4.

4.5 Neutron Diffraction

Neutron diffraction measurements on the glasses were performed using 0.783 Å incident neutrons. The high Q diffractometer at Dhruva Reactor, B.A.R.C., Mumbai was used. The instrument has a fixed arc of linear position sensitive detectors covering the Q range up to 15 Å-1. The glass samples were ground to a powder and filled into 6 mm. diameter vanadium cans of height 5.15 cm. Neutron beam height was 4 cm and width was considerably more than the can diameter thus ensuring uniform illumination of the sample by the beam. The S(q) data may be seen in Figure 4.5.1. The pair distribution functions G(r) are shown in Figure 4.5.2. The total correlation functions T(r) are plotted on the same axes for comparison in Figure 4.5.3 and as a stack in Figure 4.5.4. The total radial distribution function N(r) can be seen in Figure 4.5.5.

The MCGR method was used to fit the S(q) functions in an iterative fashion as described in Chapter 2. The total pair distribution functions from these calculations are displayed in Figure 4.5.6. The stack of T(r) is given in Figure 4.5.7. The fits to the first, second and higher peaks in T(r) are shown in Figures 4.5.8 to 4.5.11. The latter functions were used to determine the average correlation lengths / bond distances. Similarly, the total radial distribution functions N(r) as a stack are given in Figure 4.5.12. The fits to the first few peaks in these functions which were used in obtaining coordination numbers are displayed in Figures 4.5.13 to 4.5.16.

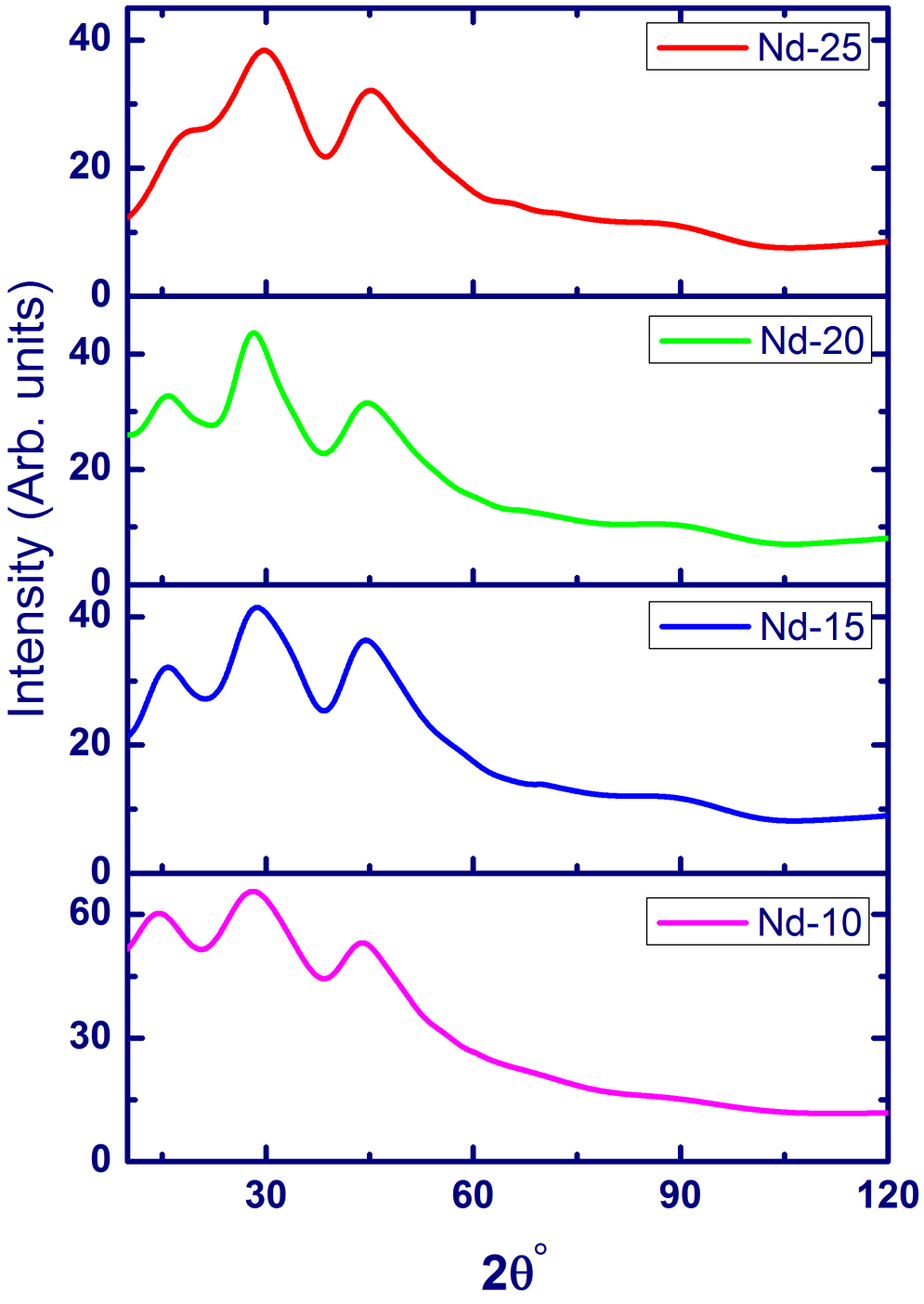

Figure 4.4.1: Measured X-Ray diffraction patterns of the Nd_2O_3 doped borate glasses.

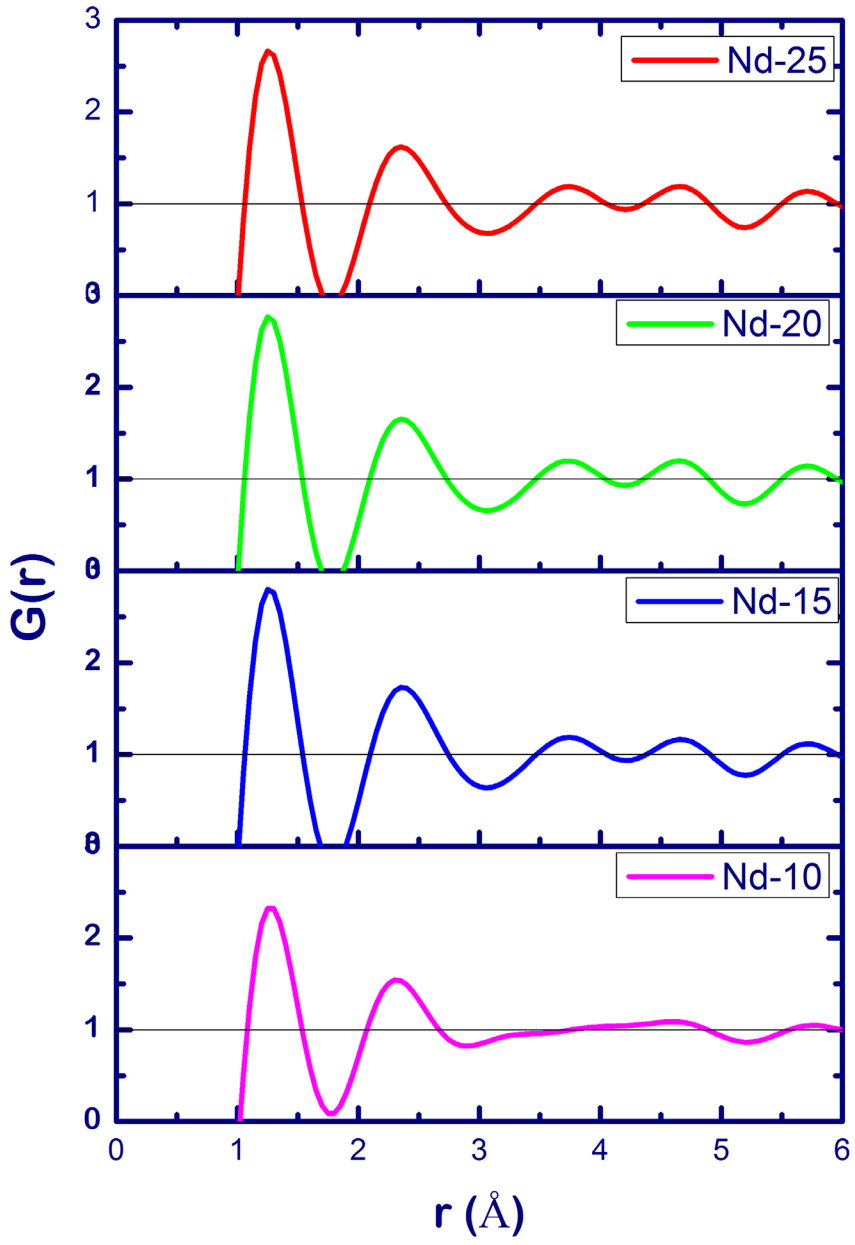

Figure 4.4.2: Pair-Correlation Function of the Nd_2O_3 doped borate glasses from the X-ray data.

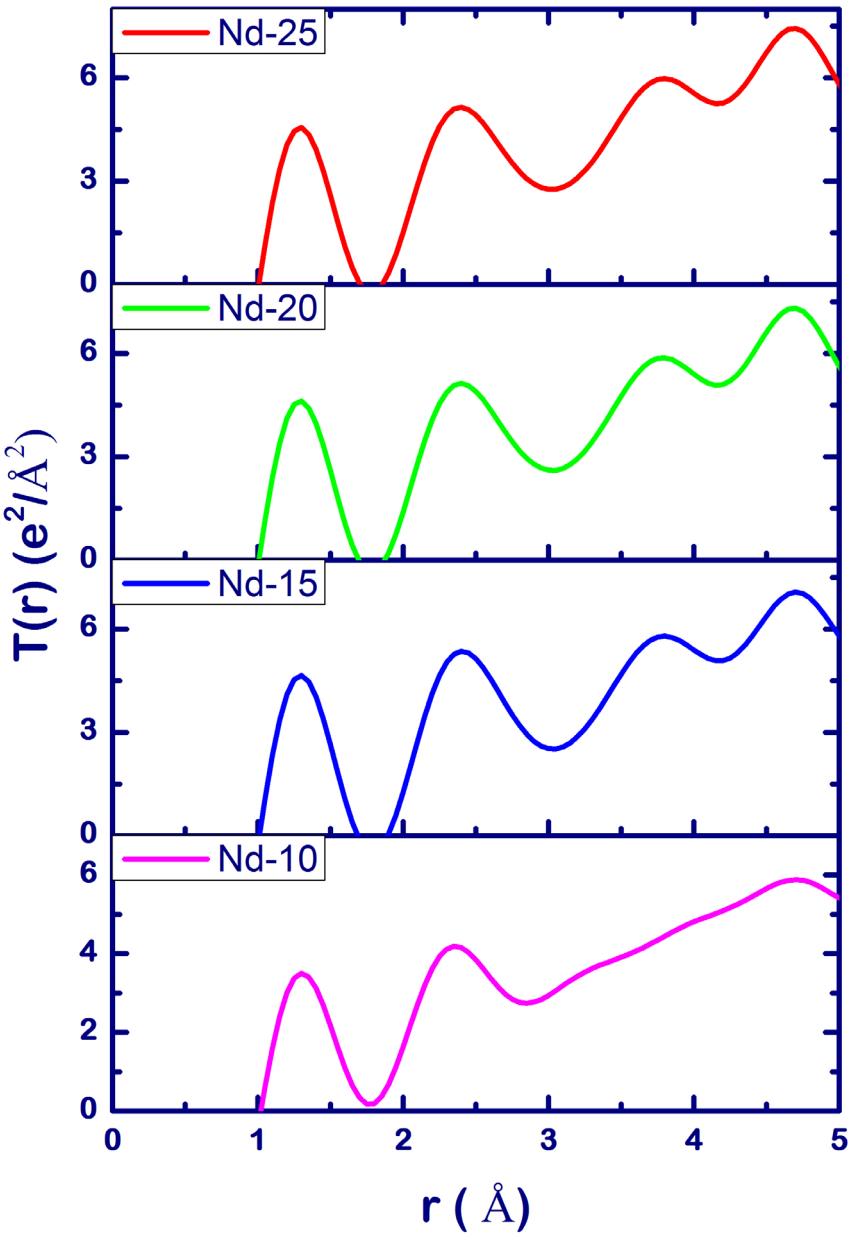

Figure 4.4.3: Total Correlation Function of the Nd_2O_3 doped borate glasses from the X-ray data.

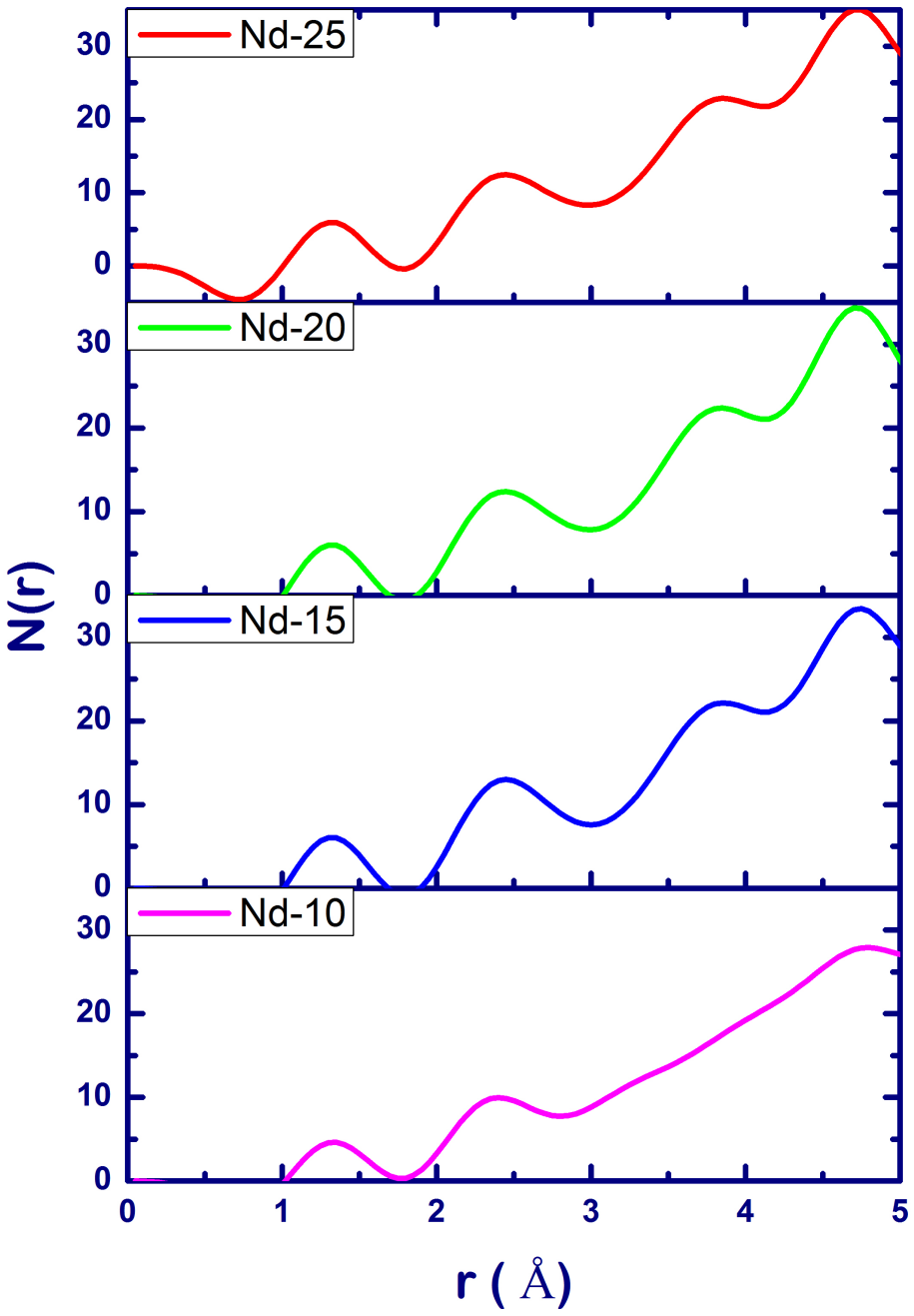

Figure 4.4.4: Radial Distribution Function of the Nd_2O_3 doped borate glasses from the X-ray data.

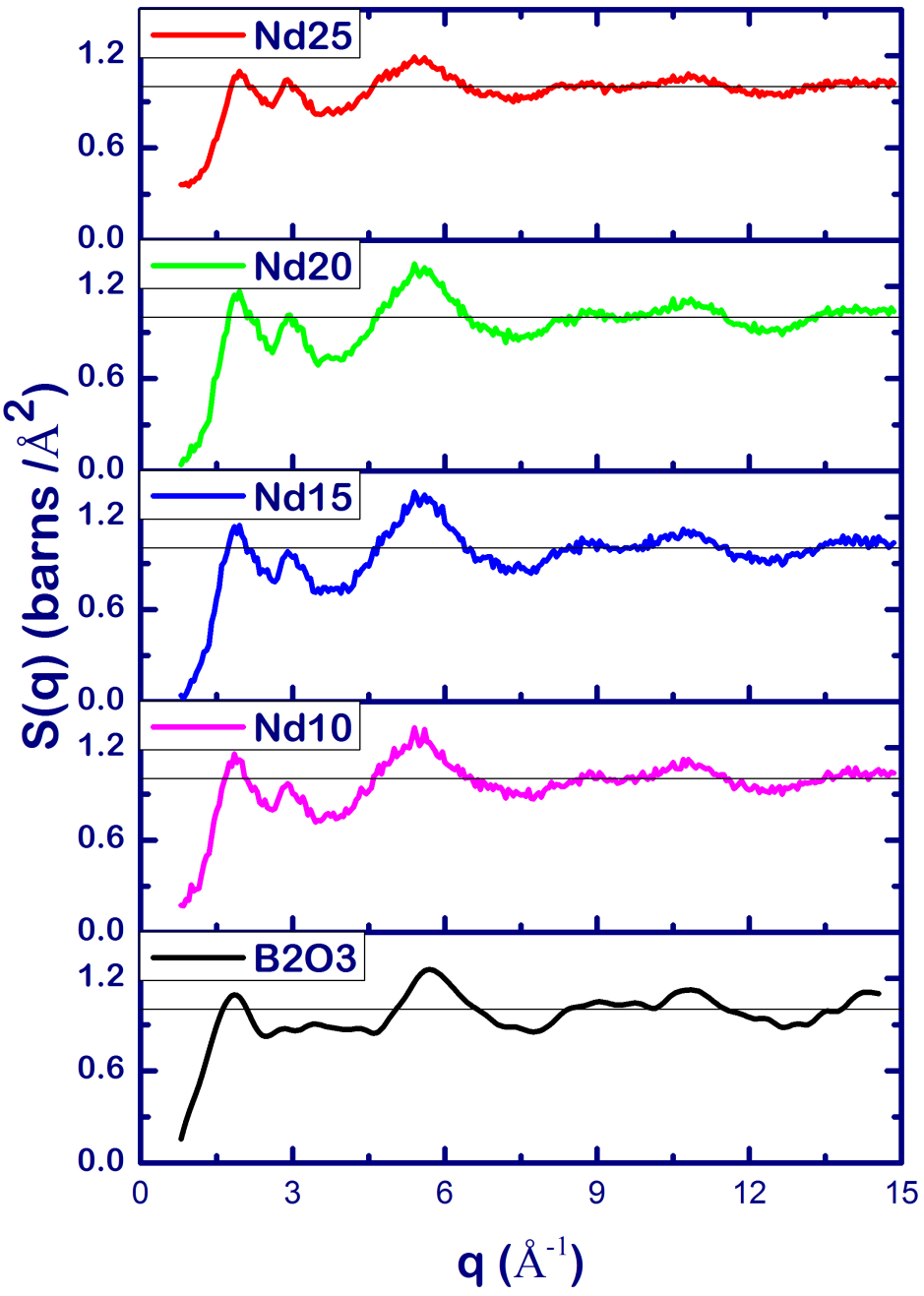

Figure 4.5.1: Measured structure factors of the Nd_2O_3 doped borate glasses from the neutron data.

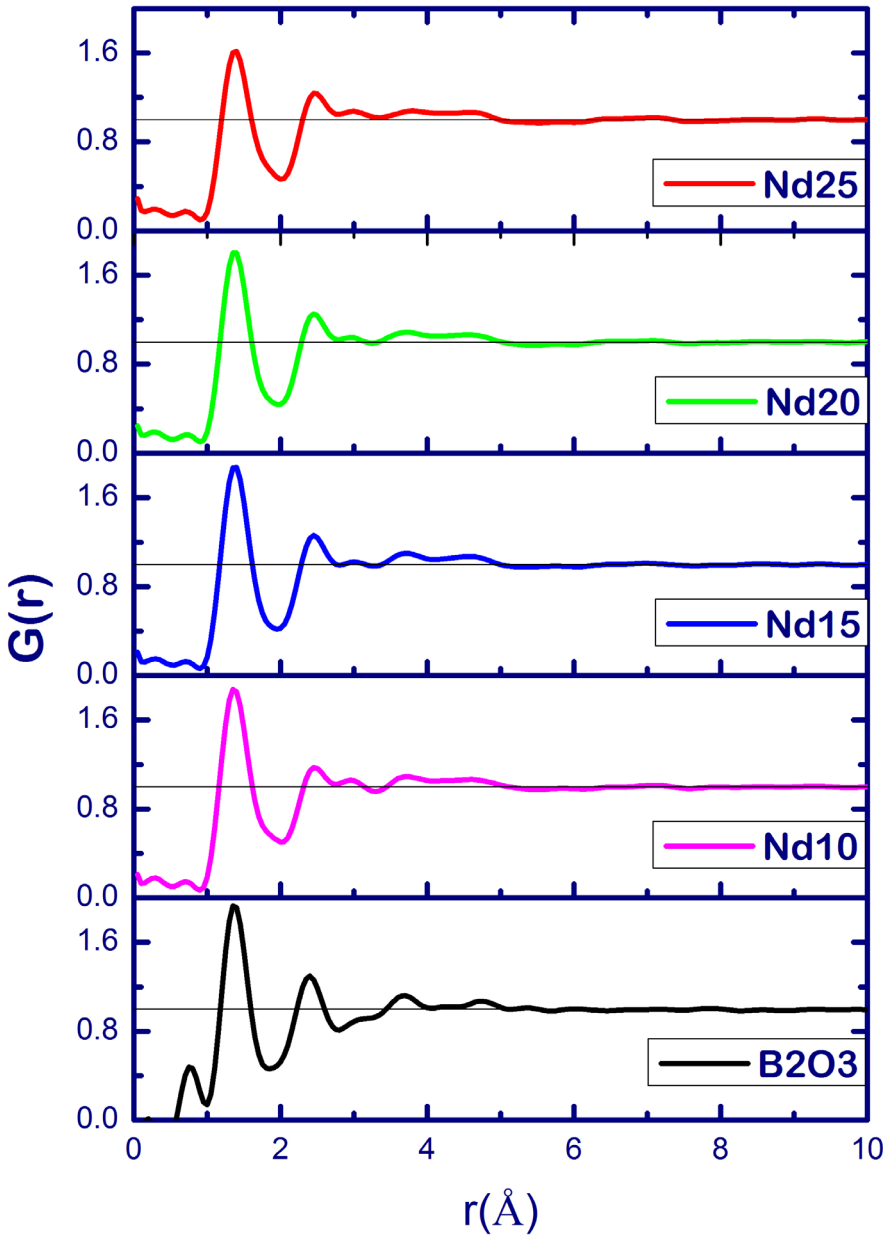

Figure 4.5.2: Pair-Correlation Function of the Nd_2O_3 doped borate glasses from the neutron data by Fourier Transformation of S(q)

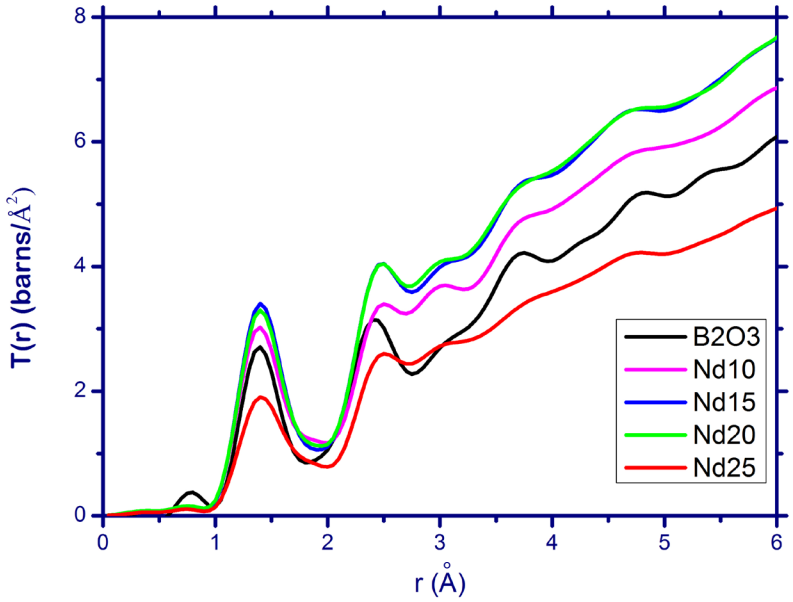

Figure 4.5.3: Overlay of Total Correlation Function of the Nd_2O_3 doped borate glasses from the neutron data by Fourier Transformation of S(q).

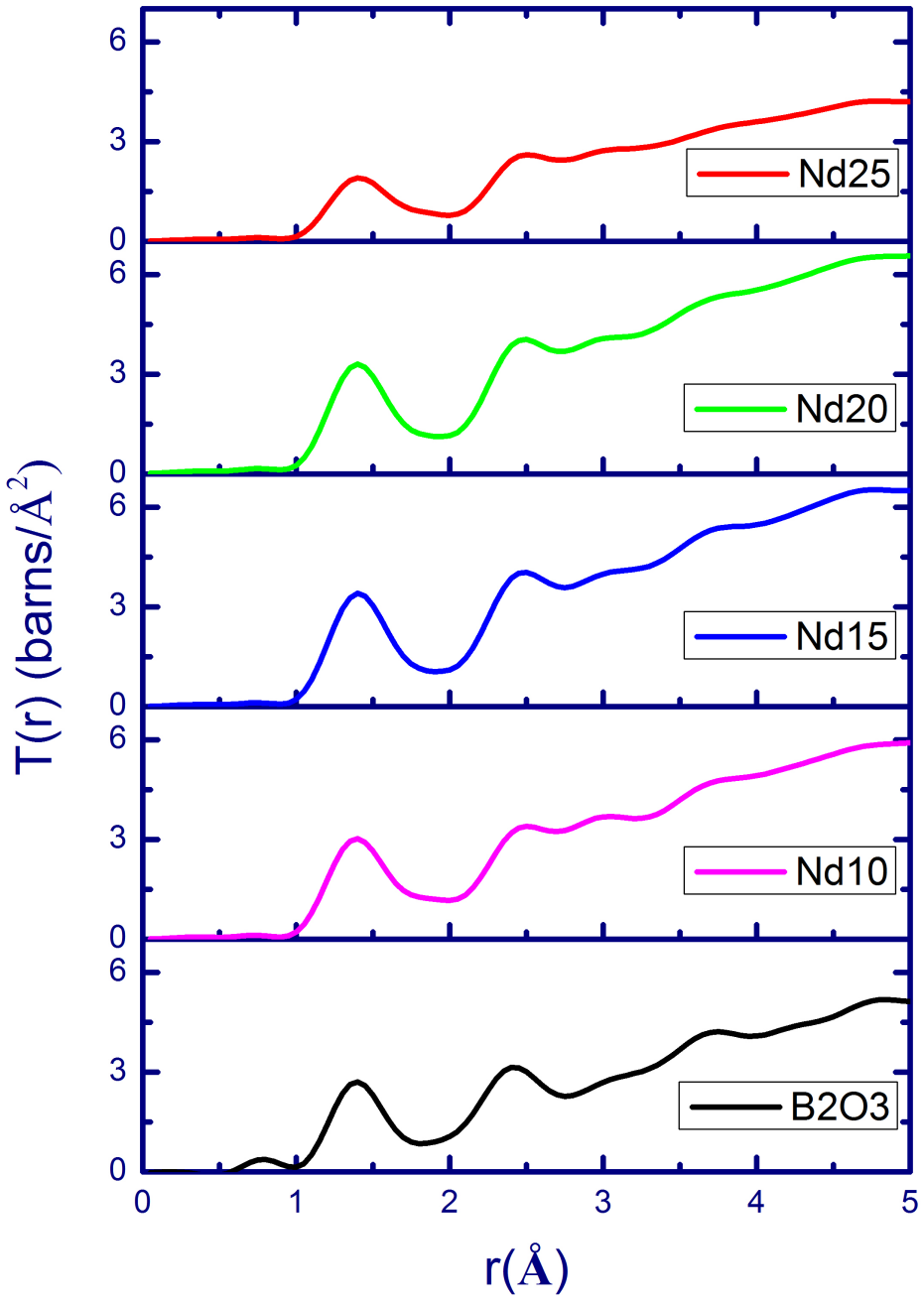

Figure 4.5.4: Total Correlation Function of the Nd_2O_3 doped borate glasses from the neutron data by Fourier Transformation of S(q).

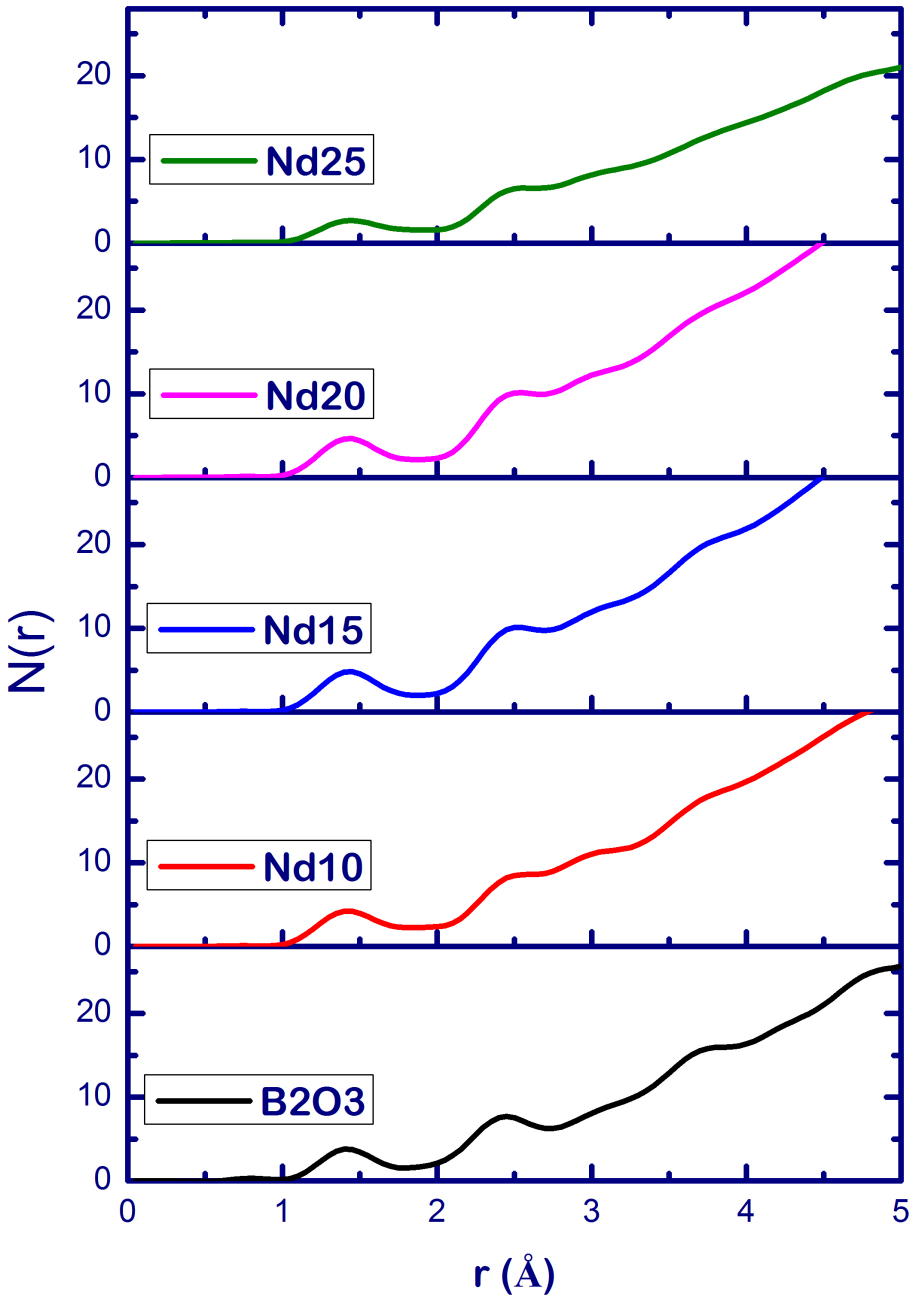

Figure 4.5.5: Radial Distribution Function of the Nd_2O_3 doped borate glasses from the neutron data by Fourier Transformation of S(q).

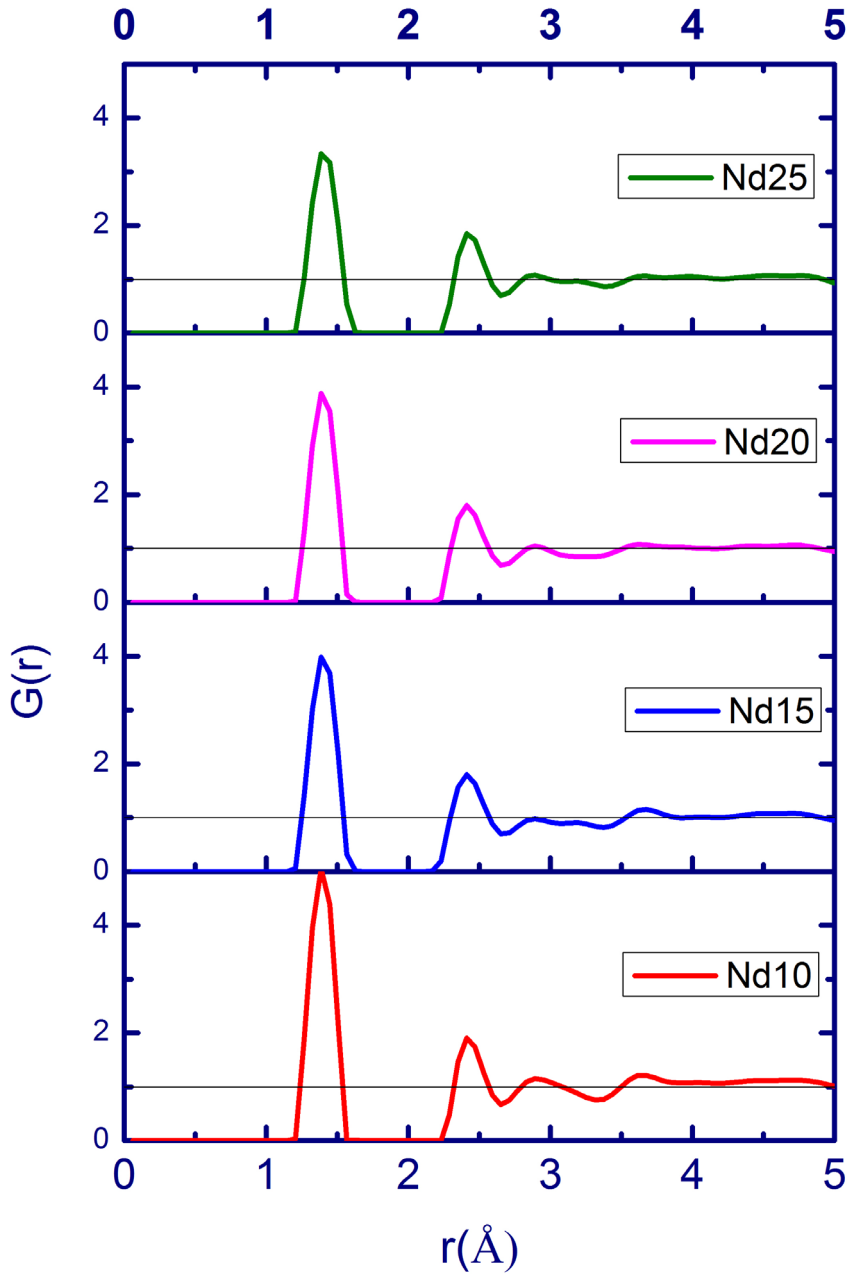

Figure 4.5.6: Pair-Correlation Function of the Nd_2O_3 doped borate glasses from the neutron data by MCGR.

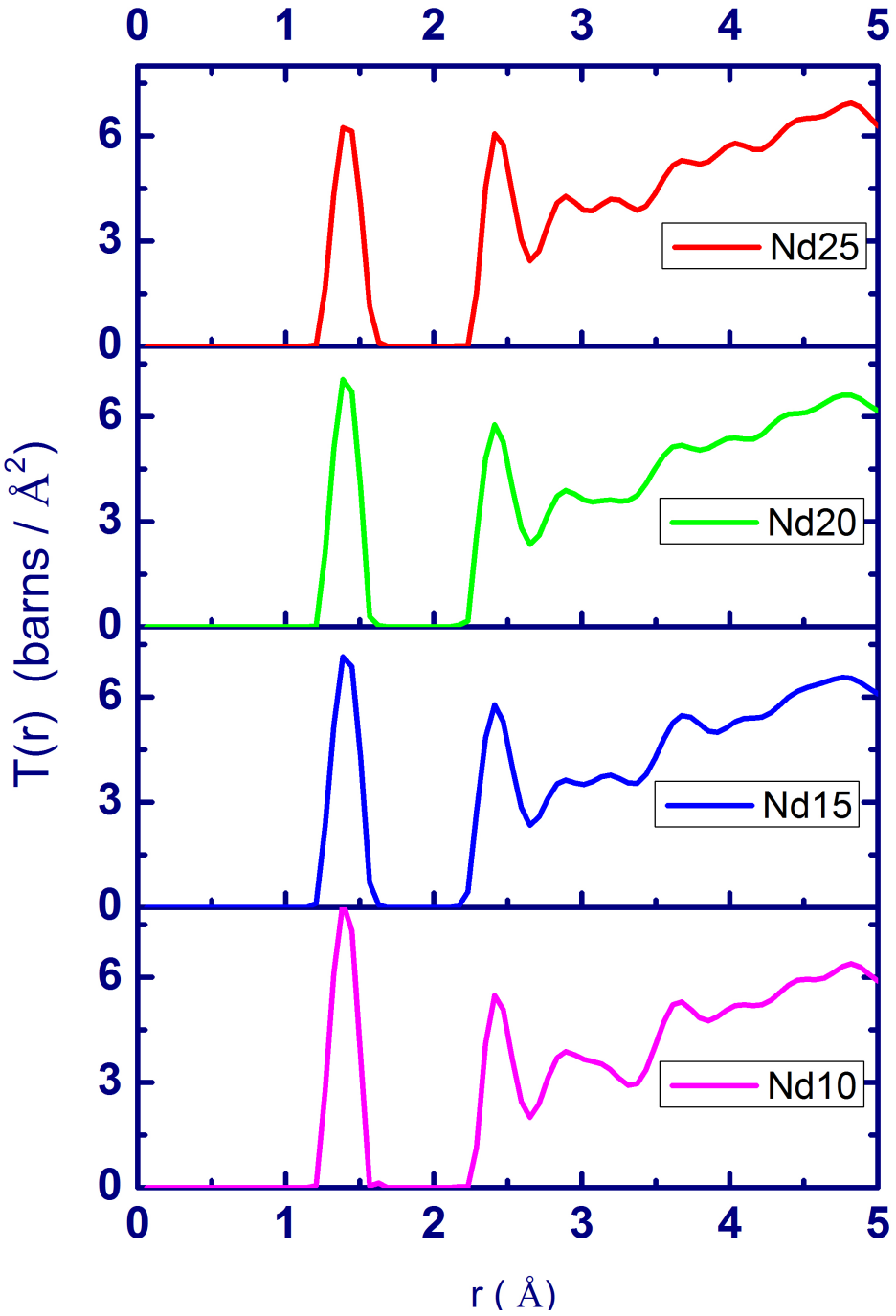

Figure 4.5.7: Total Correlation Function of the Nd_2O_3 doped borate glasses from the neutron data by MCGR.

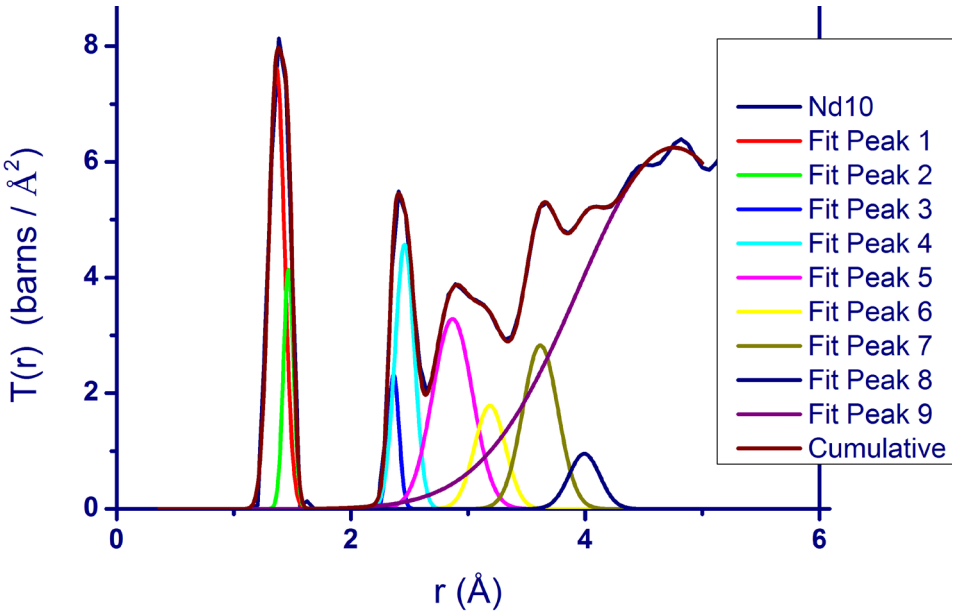

Figure 4.5.8: Total Correlation Function of the 10% Nd_2O_3 doped borate glass, peaks fitted to obtain peak positions.

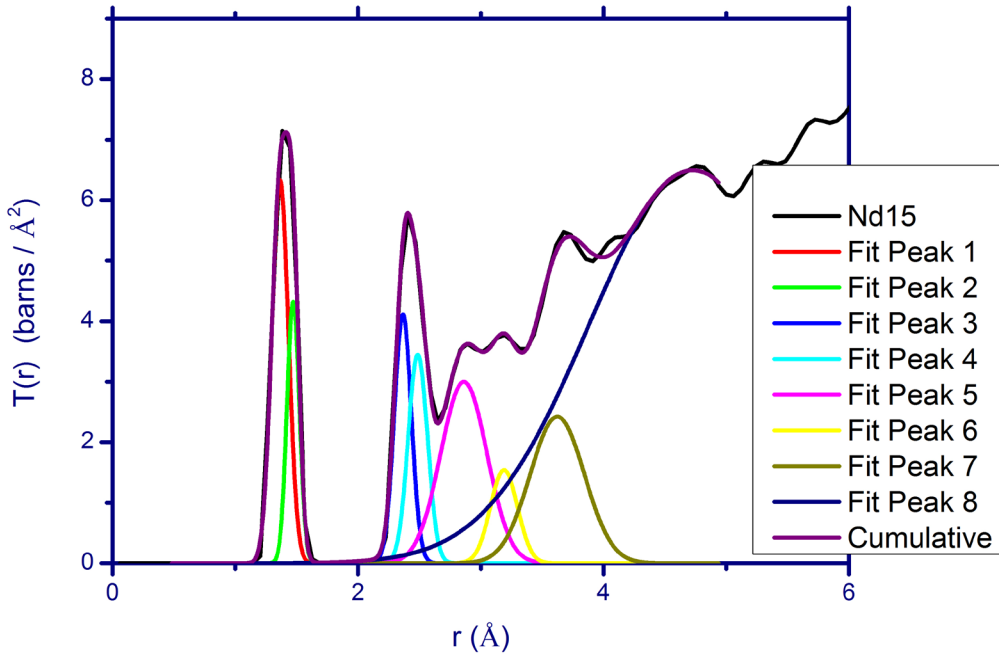

Figure 4.5.9: Total Correlation Function of the 15% Nd_2O_3 doped borate glass, peaks fitted to obtain peak positions.

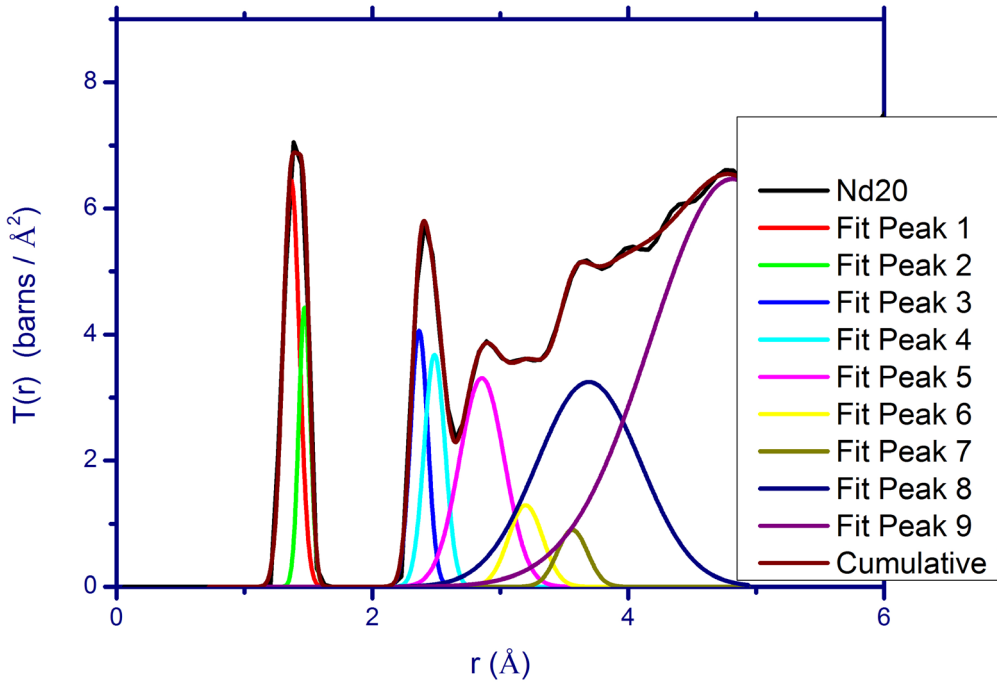

Figure 4.5.10: Total Correlation Function of the 20% Nd_2O_3 doped borate glass, peaks fitted to obtain peak positions.

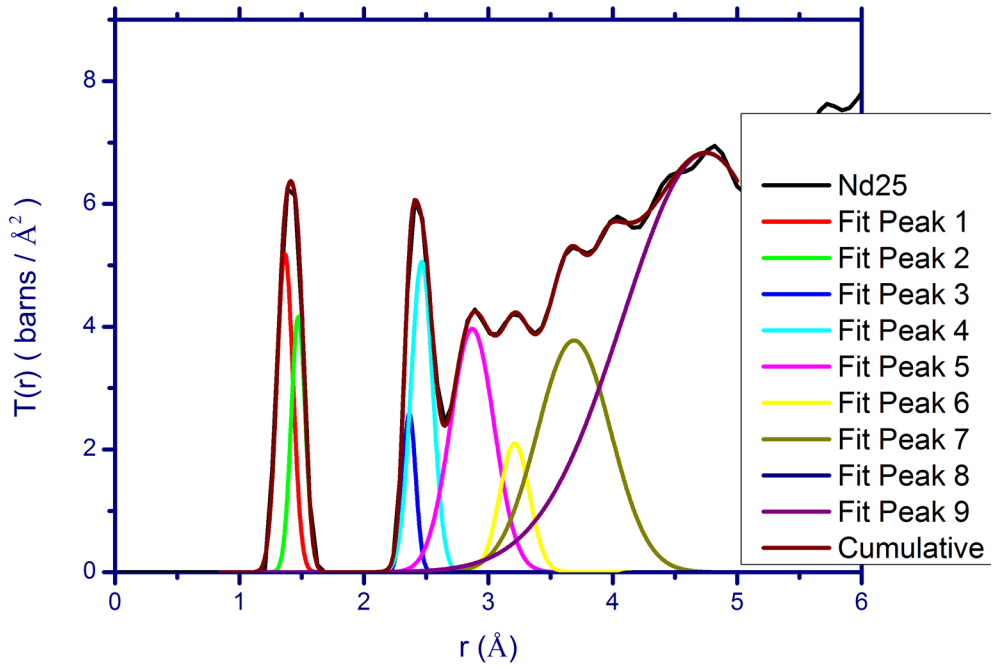

Figure 4.5.11: Total Correlation Function of the 25% Nd_2O_3 doped borate glass, peaks fitted to obtain peak positions.

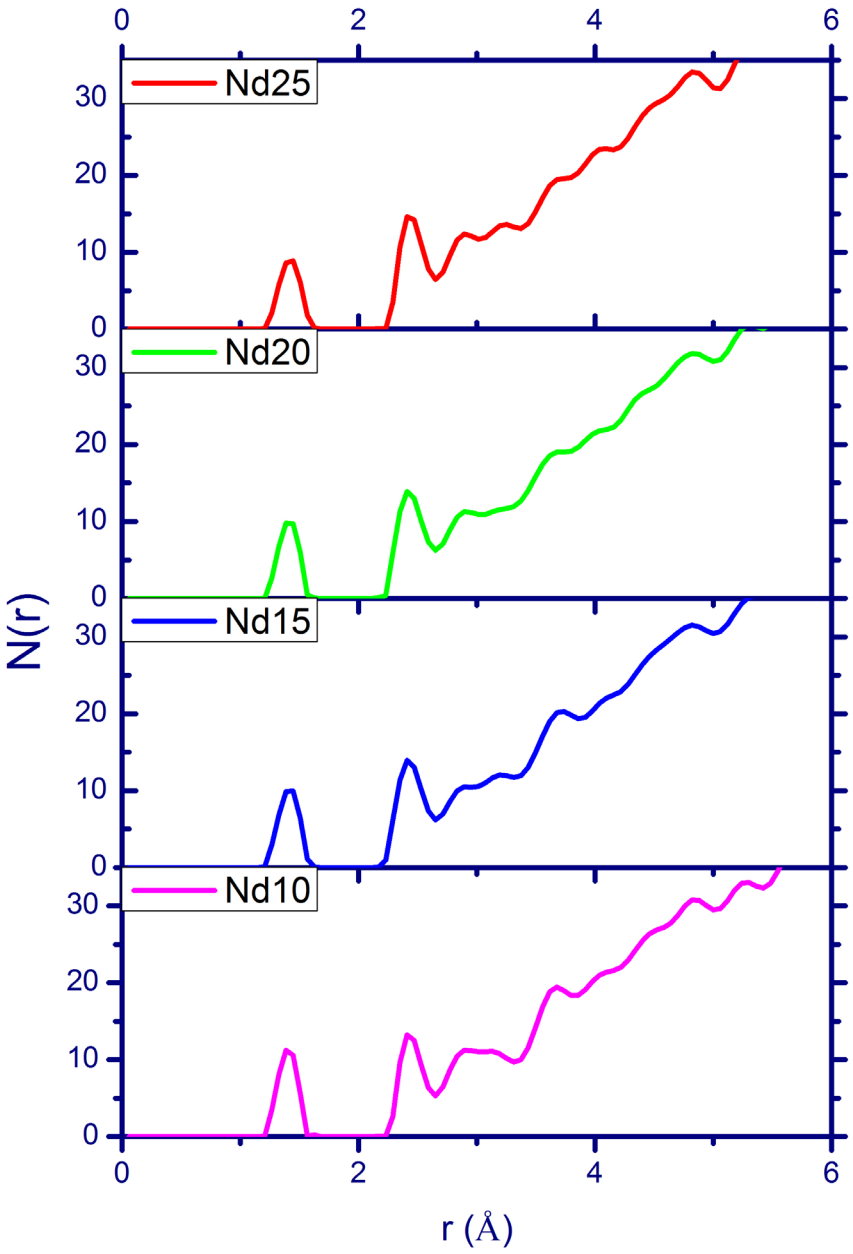

Figure 4.5.12: Radial Distribution Function of the Nd_2O_3 doped borate glasses from the neutron data by MCGR.

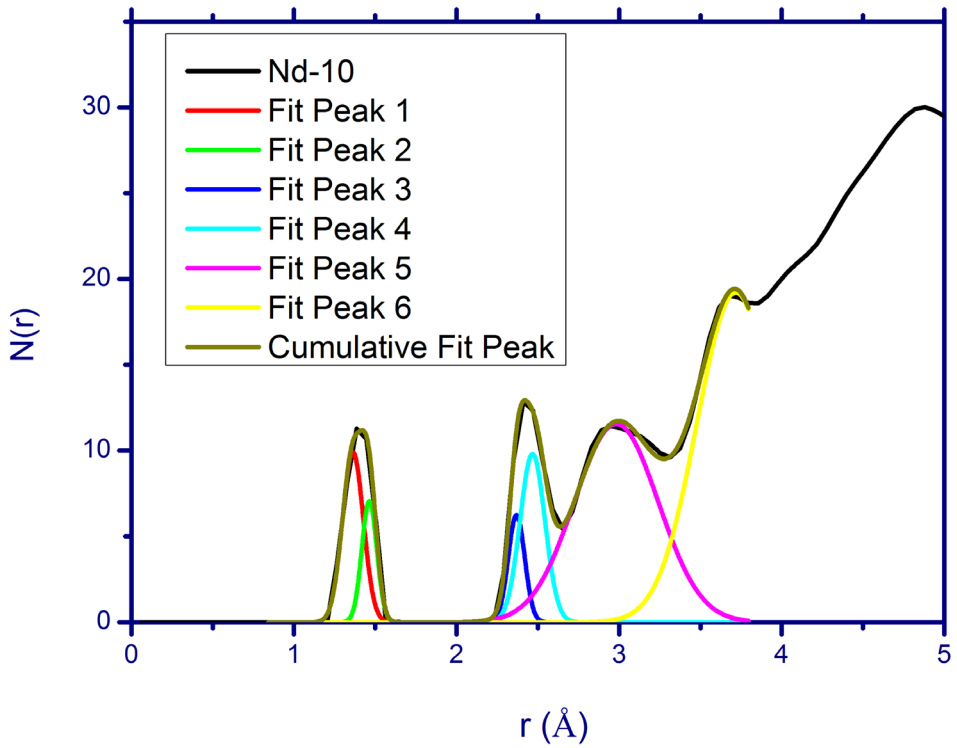

Figure 4.5.13: Radial Distribution Function of the 10% Nd_2O_3 doped borate glass, peaks fitted to obtain coordination numbers.

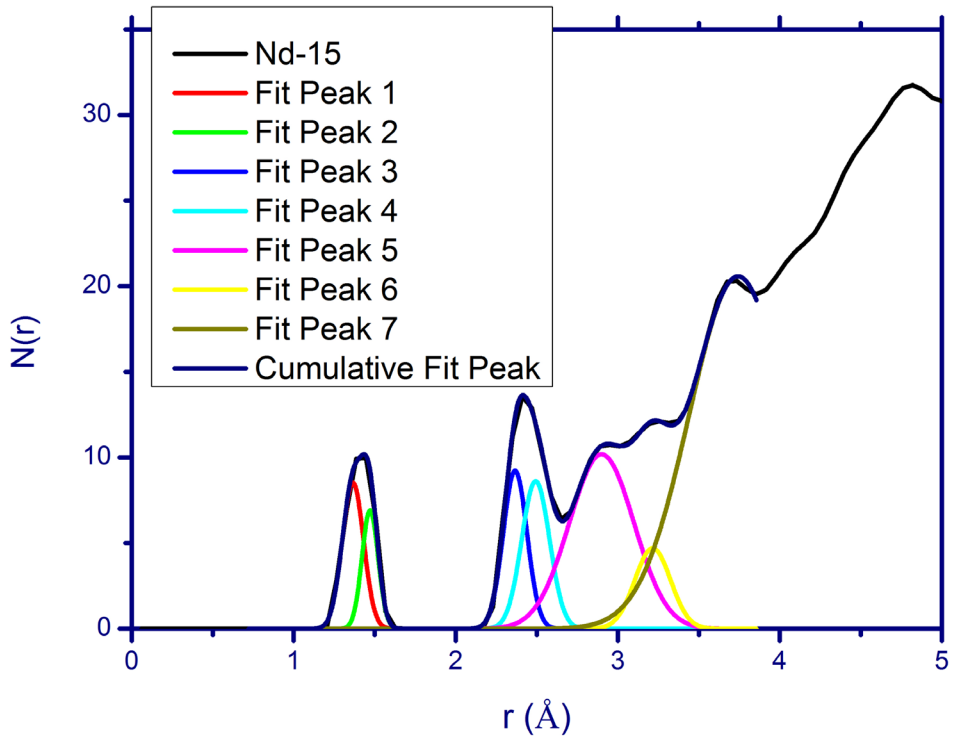

Figure 4.5.14: Radial Distribution Function of the 15% Nd_2O_3 doped borate glass, peaks fitted to obtain coordination numbers.

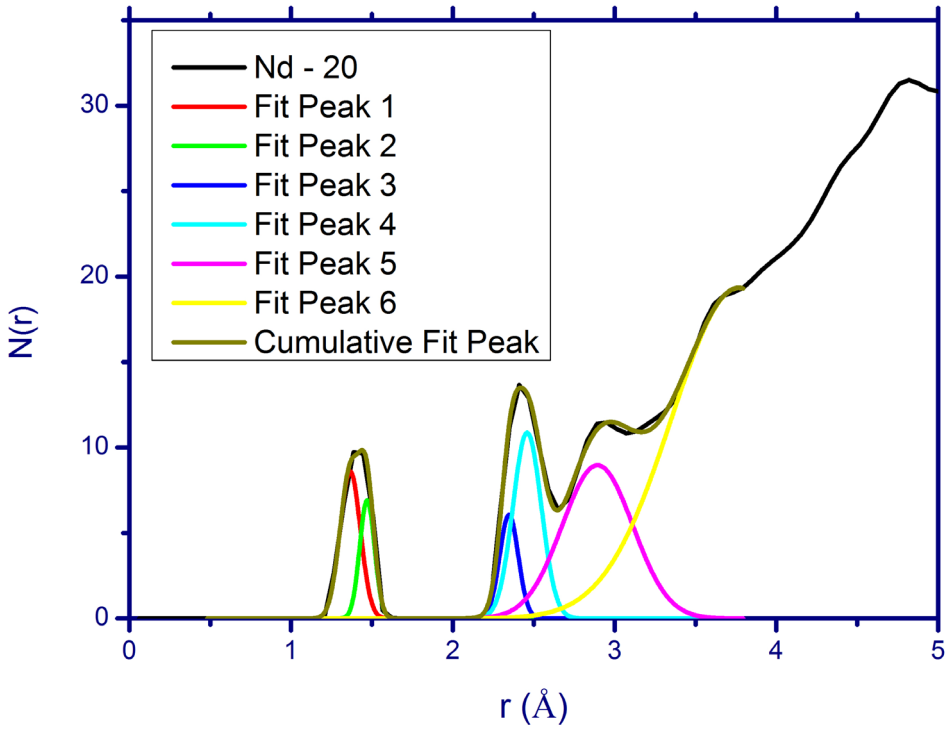

Figure 4.5.15: Radial Distribution Function of the 20% Nd_2O_3 doped borate glass, peaks fitted to obtain coordination numbers.

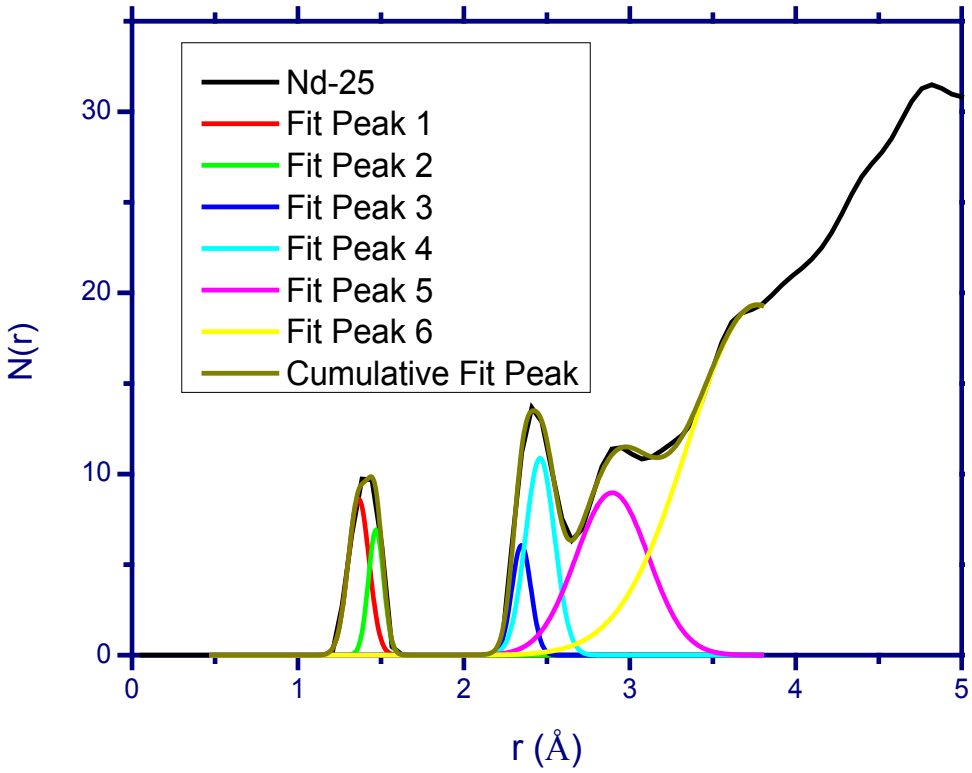

Figure 4.5.16: Radial Distribution Function of the 25% Nd_2O_3 doped borate glass, peaks fitted to obtain coordination numbers.

4. 6 Results and Discussion

The X-ray diffraction patterns of this set of glasses are shown in Figure 4.4.1. By use of the program RAD, the pair correlation functions G(r), total correlation functions T(r) and radial distribution functions N(r) were calculated and are displayed in Figures 4.4.2, 4.4.3 and 4.4.4 respectively. The neutron diffraction patterns corrected for absorption, multiple scattering, Placzek correction and normalized to vanadium are shown in Figures 4.5.1. These corrected patterns are referred to as S(q) and were Fourier transformed while applying the Lorch modification function, to obtain the real space correlation functions of Figures 4.5.2, 4.5.3 (overlaid), 4.5.4. (stack) and Figure 4.5.5. Also shown are the correlation functions calculated by the Monte Carlo G(r) as described in section 2.5 in Figures 4.5.6 to 4.5.16.

The first peak in T(r) relates to the B-O correlation in the glass. It may be seen that a slight asymmetry in this first peak is present for the doped glasses. The area under this first peak in the N(r) was found for each of the set of these Nd doped glasses. Assuming this area comes from the B-O correlations, the coordination of oxygen around boron was found to be 3.28 in the Nd-10 sample and similar values for other members of the set (see Table 4.6.1 and Figure 4.5.17) . Many different authors have reported the presence of BO_4 tetrahedral structural units in borate glasses. The first peak was thus assumed to be composed of two Gaussian peaks – one to be at 1.366 Å due to the B-O of BO_3 (Johnson et al. (1982)) and the second due to the B-O of the BO_4 tetrahedron which was at 1.45 Å for a correct fit to the profile of the first peak. In the Nd-10 sample for example, these two Gaussian fits may be interpreted to mean that there are about 28% of all borons in tetrahedral coordination while 72% are in trigonal BO_3 coordination.

The second peak in N(r) is taken to be composed of three different correlations viz. first neighbours B-B, O-O and Nd-O. The positions of the B-B and O-O were assumed to be the same at 2.366 Å as calculated from the B_3O_6 boroxol ring (Johnson et al. (1982), Hannon et al. (1994)). The calculation of both the position of the Nd-O correlation and its coordination with

oxygen were found to be critically dependent on the coordination numbers of B-B and O-O. In order to choose appropriate values of the latter numbers, the two dimensional scheme of linked boroxol rings in which the nearest neighbour B-B correlation is 5 while the nearest neighbour O-O is 6. Although the glass network is three dimensional, these first estimates were assumed. The resulting Nd-O positions and coordination numbers for the members of the set of glasses is summarized in Table 4.6.1. These calculations were repeated for B-B and O-O coordination numbers obtained from Hannon et al. (1994) in which 80% of boron atoms are assumed to be located within boroxol rings. These authors state the B-B coordination in the glass as 4 x 0.8 = 3.2 while the O-O in the glass would be 80% of the 9-fold nearest neighbour O-O correlation of the boroxol ring i.e. 7.2 . With the latter values, the Nd-O correlation length and coordination numbers are also found to vary between about 10 and 6 for the different Nd concentrations. These calculations are also shown in Table 4.6.2.

In order to understand the decrease in coordination of oxygen around Nd in going from the Nd-10 to the Nd-25 sample, it is proposed that for the lower Nd concentrations it is the superstructural units such as boroxol rings, diborates, di-pentaborate units etc. which surround the Nd ions. This would account for the larger oxygen coordination numbers for the Nd-10 and Nd-15 glasses. For the higher concentrations of rare-earth i.e. Nd-20 and Nd-25, it would appear that the Nd ions are mostly found in octahedral coordination with oxygen. The latter is in keeping with the view of author like Krogh-Moe (1962) in which it is asserted that the presence of added cations to the glass former encourages the formation of tetrahedral coordinations of B with O from the BO3 units. For the higher concentrations of Nd, the number of superstructural units around the rare-earth ions would thus diminish with a concomitant increase in the number of simpler tetrahedral and trigonal units surrounding the rare-earth ion .

The constituent correlations of the higher peaks at 2.86 Å and 3.18 Å are thought to be due to B-O and Nd-B respectively. As the peak at 3.18 Å is absent in the neutron data of the pure B_2O_3

glass, its presence in the Nd containing glasses is ascribed to an Nd-containing correlation. The resultant coordination numbers are shown in Table 4.6.1 for B-O with Nd-B.

It may be noted that the Nd-B coordination for the Nd-10 glass is about double that of the Nd-O. This could be due to the fact that each oxygen around the Nd at this lower concentration is linked to two B atoms of a superstructural unit. At higher Nd concentrations, in which there would - on average - be mainly smaller units such as BO_3 and BO_4 around the Nd ions, each oxygen in the octahedral coordinated sites would on average have only one nearest neighbour B nearest to it. The latter would make the Nd-B coordination at these higher Nd concentrations comparable to the 6 fold coordinations of the Nd-O correlation.

It may thus be concluded that at lower concentrations of Nd in this set of glasses, the Nd ions are mainly surrounded by complex superstructural units, while at higher Nd concentrations the oxygen environment of these rare-earth ions are likely to be simpler units such as trigonal and tetrahedral units surrounding the cation and causing it to have approximately an octahedral coordination with oxygen.

Table 4.6.1: Peak positions and Coordination number of first four correlations of Nd doped borate glasses

Correlation type	Sample	av. b sqr	Area	Peak Positions	Coord. No.
				(±0.002)	(±0.01)
B-O	Nd-10	0.3823	2.3846	1.366, 1.468	3.28
1st Peak	Nd-15	0.3849	2.2554	1.366, 1.472	3.30
	Nd-20	0.3875	2.1295	1.366, 1.471	3.34
	Nd-25	0.3901	2.0238	1.366, 1.473	3.40
Nd-O	Nd-10	0.3823	0.9305	2.366, 2.460	9.96
2nd peak	Nd-15	0.3849	1.1223	2.366, 2.488	8.06
2nd Gaussian	Nd-20	0.3875	1.1336	2.366, 2.487	6.15
	Nd-25	0.3901	1.3759	2.366, 2.486	6.01
Nd-O	Nd-10	0.3823	0.8728	2.366, 2.460	9.34
2nd peak	Nd-15	0.3849	1.0857	2.366, 2.488	7.80
2nd Gaussian	Nd-20	0.3875	1.1178	2.366, 2.487	6.06
	Nd-25	0.3901	1.3806	2.366, 2.486	6.03
	Nd-10	0.3823	4.4176	2.867	6.07
B-O	Nd-15	0.3849	4.3881	2.862	6.43
3rd Peak	Nd-20	0.3875	4.5310	2.886	7.10
	Nd-25	0.3901	5.0671	2.871	8.53
	Nd-10	0.3823	2.2179	3.187	20.72
Nd-B	Nd-15	0.3849	2.0054	3.189	12.57
4th Peak	Nd-20	0.3875	0.8822	3.198	4.17
	Nd-25	0.3901	1.9288	3.211	7.35

Table 4.6.2: Areas of the second peak calculated by assuming coordination numbers.

Correlation type	Sample	Conc	Boron	Oxygen	av. b sqr	Coord. No.	Area
		Cb	b1	b2			Ce
B-B	Nd-10	0.3600	0.6650	0.6650	0.3823	3.2000	1.3324
2nd peak	Nd-15	0.3400	0.6650	0.6650	0.3849	3.2000	1.2500
	Nd-20	0.3200	0.6650	0.6650	0.3875	3.2000	1.1686
	Nd-25	0.3000	0.6650	0.6650	0.3901	3.2000	1.0883
Correlation type	**Sample**	**Conc.**	**Oxygen**	**Oxygen**	**av. Bsqr**	**Coord. No.**	**Area**
		Cb	b1	b2			Ce
	Nd-10	0.6000	0.5803	0.5803	0.3823	7.2000	3.8048
O-O	Nd-15	0.6000	0.5803	0.5803	0.3849	7.2000	3.7794
2nd peak	Nd-20	0.6000	0.5803	0.5803	0.3875	7.2000	3.7541
	Nd-25	0.6000	0.5803	0.5803	0.3901	7.2000	3.7292
Correlation type	**Sample**	**Conc.**	**Boron**	**Boron**	**av. Bsqr**	**Coord. No.**	**Area**
		Cb	b1	b2			Ce
	Nd-10	0.3600	0.6650	0.6650	0.3823	5.0000	2.4983
B-B	Nd-15	0.3400	0.6650	0.6650	0.3849	5.0000	1.9531
2nd peak	Nd-20	0.3200	0.6650	0.6650	0.3875	5.0000	2.1911
	Nd-25	0.3000	0.6650	0.6650	0.3901	5.0000	2.0405
Correlation type	**Sample**	**Conc.**	**Oxygen**	**Oxygen**	**av. Bsqr**	**Coord. No.**	**Area**
		Cb	b1	b2			Ce
	Nd-10	0.6000	0.5803	0.5803	0.3823	6.0000	3.1707
O-O	Nd-15	0.6000	0.5803	0.5803	0.3849	6.0000	3.1495
2nd peak	Nd-20	0.6000	0.5803	0.5803	0.3875	6.0000	3.1284
	Nd-25	0.6000	0.5803	0.5803	0.3901	6.0000	3.1076

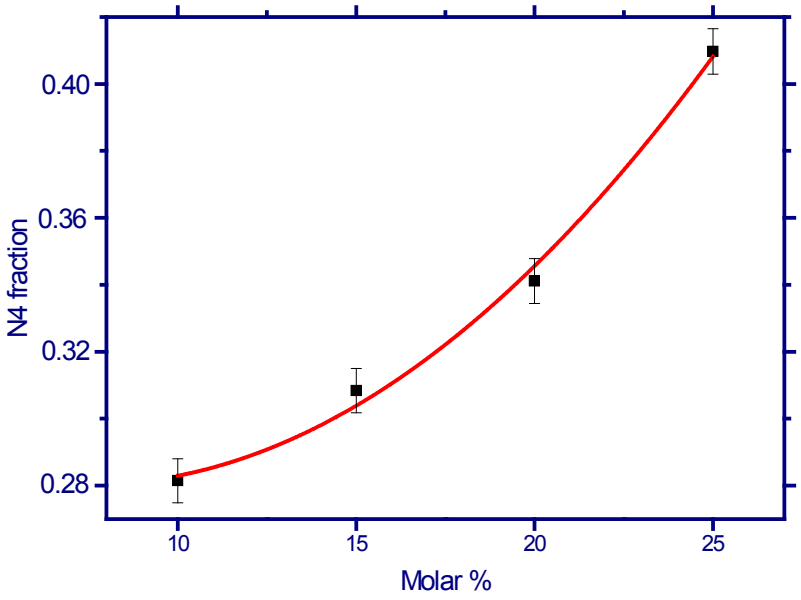

Figure 4.5.17: Increase of fraction of 4-fold coordinated Boron as a function of molar concentration of Nd in the Nd-Borate glasses.

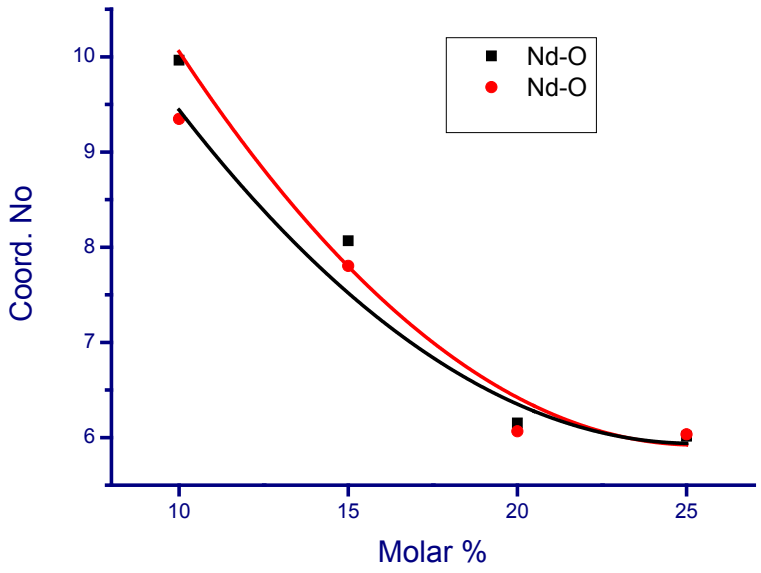

Figure 4.5.18 : Decrease of Nd-O coordination number from the 2nd peak in N(r) with increase in Nd concentration in the Nd-Borate glasses when : B-B, O-O was 5,6 and when these were 3.2, 7.2.

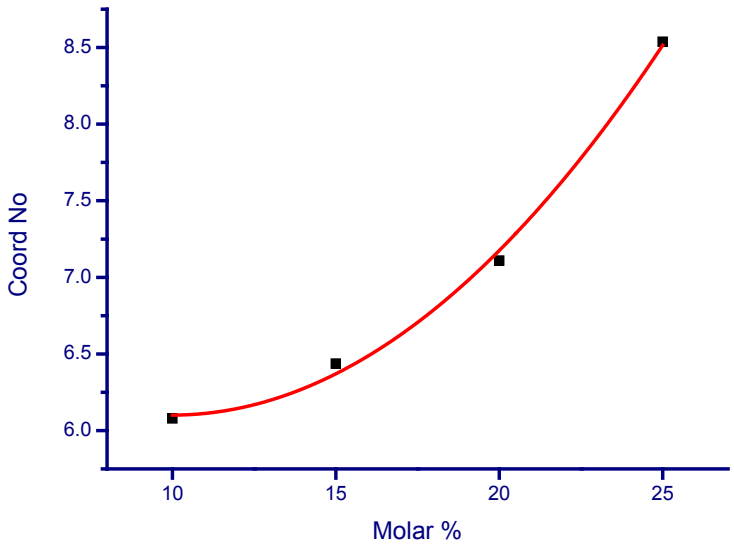

Figure 4.5.19: Increase of B-O coordination number from 3rd peak in N(r) with increase in Nd % in the Nd-Borate glasses.

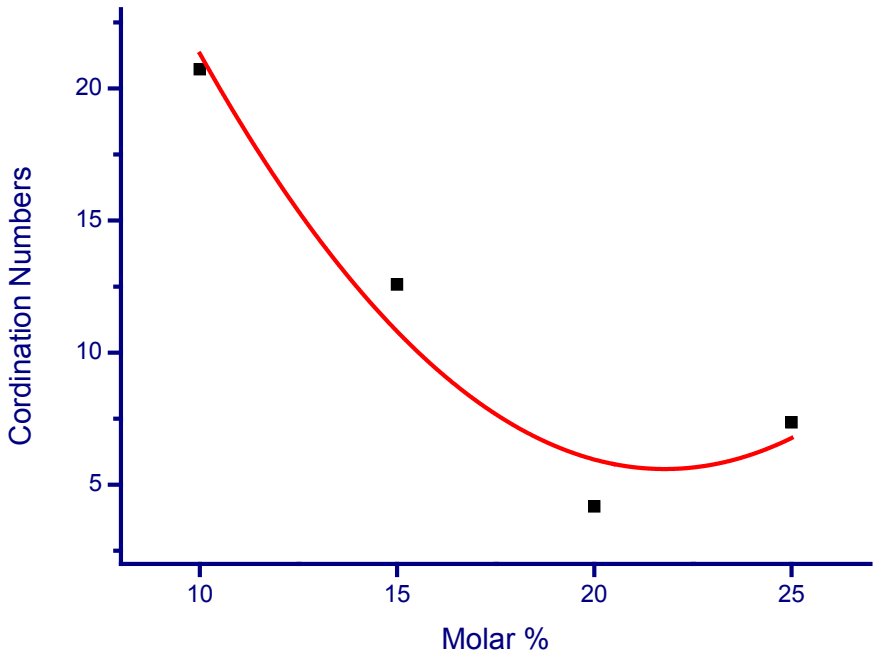

Figure 4.5.20: Decrease of Nd-B coordination number from 4th peak in N(r) with Nd% in glasses.

References

1. Chiodelli C., Magistris A., Villa M., and Björkstam J.L., J. Non-Cryst. Solids 51 (1982) 143
2. Dalba G., Fornasini P., Rocca F., Bernieri E., Burratini E., and Mobilio S., J. Non-Cryst. Solids, 91 (1987) 153
3. Dalba G., Fornasini P., Rocca F., J. Non-Cryst. Solids, 123 (1990) 310
4. Edwards J.O. and Ross V.J., J. Inorg. Nucl. Chem. 15 (1960) 329
5. Feller S.A., Dell W.J., and Bray P.J., J. Non-Cryst. Solids 15 (1982) 21
6. Galeener F., Lucovsky G., and Mikkelsen J.C., Jr., Phys. Rev. B8 (1980) 3983
7. Goubeau J. and Keller H., Z. Anorg. Allg. Chem. 272 (1953) 303
8. Griscom D.L., in: Borate Glasses: Structure, Properties, Applications, Eds. Pye L.D., Frechette V.D. & Kreidl N.J., Plenumney York (1978) 11
9. Hannon A.C., Grimly D.I., Hulme R.A., Wright A.C., Sinclair R.N., J. Non-Cryst. Solids, 177 (1994) 299-316
10. Hayashi S. and Hayamizu, J. Non-Cryst. Solids 11 (1989) 214
11. Johnson P.A.V., Wright A.C. and Sinclair R.N., J. Non-Cryst. Solids 50 (1982) 281
12. Judd B.R., Phys. Rev. 127 (1962) 750
13. Kamitsos E.I., Patsis A.P., Karakassides M.A., and Chryssikos G.D., J. Non-Cryst. Solids 126 (1990) 52
14. Kim K.S. and Bray P.J., J. Nonmetals, 2 (1974) 95
15. Krogh-Moe J., Phys. Chem. Glasses, 3 (1962) 1
16. Krogh-Moe J., Phys. Chem. Glasses, 6 (1965) 46
17. Krogh-Moe J., J. Non-Cryst. Solids, 1 (1969) 269
18. Licheri G., Musini A., Pashina G., Piccaluga G., Pinna G., and Magistris A., J. Chem. Phys. 85 (1986) 500
19. Lorösch J., Couzi M., Pelous J., Vacher R., and Levasseur A., J. Non-Cryst. Solids, 69 (1984) 1

20. Mozzi R.L. and Warren B.E., J. Appl. Crystallogr. 3 (1970) 251

21. Ofelt G.S., J. Chem. Phys. 37 (1962) 511

22. Pashina G., Piccaluga G., and MAgini M., J. Chem. Phys. 81 (1984) 6201

23. Tuller H.L. and Button D.P., in Transport-Structure Relations in Fast Ion and Mixed Conductors, ed. by Poulsen F.W., Hessel-Andersen N., Clausen K., Skaarup S., and Toft Soerensen O., (Risø National Laboratory, Denmark, (1985)

24. Warren B.E., Krutter H. and Morningstar O., J. Am.Ceram. Soc. 19 (1936) 202.

25. Wright A.C., Phy.Chem. Glasses: Eur. J. of Glass Sci. Technol. B, 51(1) (2010) 1-39

26. Yiannopoulos Y. D., Chryssikos G. D. & Kamitsos E. I., Phys. Chem. Glasses, 42 (3) (2001) 164–72

27. Zachariasen W.H., J. Am. Chem. Soc. 54 (1932) 3841

Chapter 5

Mixed Rare-Earth Types in Borate Glass

The structural interaction of a single rare-earth ion with its host glassy network was examined in some detail in Chapter 4. Evidence for the presence of some longer B-O bonds when the rare-earth was included in the glass was found. In the present Chapter, the structural modifications were investigated when a second type of rare-earth ion was added to the first. The results are presented and discussed. It was observed in Chapter 3 that in a glass in which there are two rare-earth types, - in both the visible and luminescent spectra – the presence of one type affects the emission probability of the other. An attempt is made here to find a structural correlation to the optical transitions.

The two rare-earth types were Nd and Pr in one set and Nd and Ho as another pair in a borate glass host. As with the single rare-earth ion, neutron and X-ray diffraction methods were used here and the changes in the correlations of one type as a result of the second type being added to the glass were investigated.

5.1 Introduction

Most glass applications use more than one network former. Properties of glasses can be fine tuned by choice of a combination of network formers. In the sodium borophosphate glass, $(Na_2O)_x[(P_2O_5)_{1-y}(B_2O_3)_y]_x$, if the alkali content is kept constant while the relative ratios of phosphorous oxide to boron oxide change, the glass transition temperatures and ion conducting properties can be made to alter appreciably (Branda et al. (1995), Constantini

et al. (1994), Takebe et al. (2006), and Ahoussou et al. (2006)). The understanding of such effects depends on structural data. Raman and multinuclear solid-state NMR studies of borophosphate glass have been reported (Yun and. Bray (1978), Feng and Linzhang (1989) and Villa et al. (1987)). Advanced dipolar NMR involving high magnetic fields and magic angle spinning have helped in these structural investigations. The correlation between physical properties and structures has been made by this technique (Zeyer-Dusterer et al. (2005) and Elbers et al. (2005)). Local structural environments can be described in terms of numbers of non-bridging oxygens and hetero-atomic bridges of each network former type. In multicomponent phosphate glasses, X-ray photoelectron spectroscopy has been used to distinguish between bridging and non-bridging oxygen atoms. XPS together with Raman and NMR spectroscopy can be used to propose a structural model for the $(NaPO3)_{1-x}$ $(B2O3)_x$ glass system.

Isard (1969) and Day (1976) have reviewed the mixed alkali effect in alkali glasses. Properties such as ionic conductivity, ionic diffusion, dielectric relaxation, mechanical loss and internal friction change non-linearly with addition of the 2^{nd} alkali type, while other macroscopic properties such as molar volume and density, refractive index, thermal expansion coefficient and elastic modulii show linear variation with 2^{nd} alkali type. Models to explain the mixing of two alkali ion types causing anomalous conductivity in these glasses have been proposed (Isard (1969) and Ingram (1987)) but no structural support for them is available.

The motivation for the work reported in this chapter was to investigate structural changes in mixed rare-earth glasses. The objective of this work was therefore to examine the local structures around rare-earth ions in borate host glassy networks in which an additional rare-earth ion viz. Nd and then Ho was added to the starting mixtures. Subsequently the Nd-Pr

pair of ions was included in the borate host glass. In other words, the effect of mixed rare-earth ions on the host glassy matrix was studied.

5.2 Sample Preparation

5.2.1 Nd-Ho Doped Borate Glasses

A set of 5 glasses were prepared in which B_2O_3 was obtained from ^{11}B boric acid (Sigma Aldrich 99 % B-11) was used as the host network. In this part of the study glasses of the following composition were prepared:

$$0.2((1-x)Nd_2O_3\text{-}xHo_2O_3)\text{-}0.8B_2O_3 \qquad (x=0.0,0.2,0.4,0.6,0.8,1.0)$$

The proportions of the components are shown in Table 5.2.1.1.The method of preparation was that of fusion of a starting powdered mixture of the constituent components. The initial charge consisted of the individual component oxides which were weighed out in the appropriate amounts for a total rare-earth molar composition of 20%. The mixtures were thoroughly ground and homogenized before being heated (in air) in stages in a Carbolite muffle furnace from room temperature to 1450 ^{0}C over a period of 1 hour. The cucible was removed and the melt poured onto a metal plate at room temperature. Coloured transparent glass beads were formed as shown in Figure 5.2.1.1. A summary of the starting compositions and weights of the powder mixtures is shown in Table 5.2.1.2. Most of the beads were crushed to fine powders for use in X-ray and neutron diffraction. In the latter measurements, the powders were packed into hollow vanadium cans (6 or 8 mm diameter, 5 cm tall). The different colours of the glasses were related to the optical absorption bands of their rare-earth constituents as well as the luminescent emission bands in the visible.

5.2.2 Nd-Pr Doped Borate Glasses

A set of two Borate glasses doped with Nd and Pr were also prepared by the method outlined in the previous section with proportions as shown in Table 5.2.2.1. Coloured transparent glass beads were formed as shown in Figure 5.2.2.1. A summary of the starting compositions and weights of constituents of the powder mixtures is shown in Table 5.2.2.2.

Table 5.2.1.1: Proportions of Nd_2O_3 in borate glasses.

Sample No.	**Sample Name**	**Components (Molar %)**		
		Nd_2O_3	Ho_2O_3	B_2O_3
1	Ho-0	20	0	80
2	Ho-5	15	5	80
3	Ho-10	10	10	80
4	Ho-15	5	15	80
5	Ho-20	0	20	80

Table 5.2.2.1: Proportions of Nd_2O_3 and Pr_6O_{11} in borate glasses.

Sample No.	Sample Name	Components (Molar %)			
		Nd_2O_3	Pr_6O_{11}	Al_2O_3	B_2O_3
1	Nd-Pr	18	2	5	75
2	Pr-Nd	8.15	8.15	4.15	79.61

Table 5.2.1.2: Starting compositions and weights of the powder mixtures of Nd – Ho doped borate glass samples.

Sample No	Compound	gram-mole	Mole%	Corr.wt	Desired in 1 gm	Desired in 10 g
1	Nd2O3	336.48	20	67.2956	0.40407	4.04072
	HoO3	377.86	0	0	0	0
	B2O3	69.62	80			0
	H3BO3	62.03	160	99.248	0.59593	5.95928
				166.544	1	10
2	Nd2O3	336.48	15	50.4717	0.29934	2.99335
	HoO3	377.86	5	18.893	0.11205	1.1205
	B2O3	69.62	80			0
	H3BO3	62.03	160	99.248	0.58862	5.88615
				168.613	1	10
3	Nd2O3	336.48	10	33.6478	0.19714	1.97138
	HoO3	377.86	10	37.786	0.22138	2.21383
	B2O3	69.62	80			0
	H3BO3	62.03	160	99.248	0.58148	5.8148
				170.682	1	10
4	Nd2O3	336.48	5	16.8239	0.09739	0.97388
	HoO3	377.86	15	56.679	0.3281	3.28097
	B2O3	69.62	80			0
	H3BO3	62.03	160	99.248	0.57452	5.74515
				172.751	1	10
5	Nd2O3	336.48	0	0	0	0
	HoO3	377.86	20	75.572	0.43228	4.32285
	B2O3	69.62	80			0
	H3BO3	62.03	160	99.248	0.56772	5.67715
				174.82	1	10

Sample 1

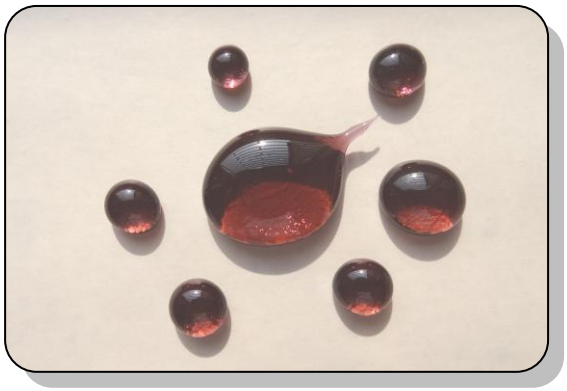

Sample 2

Sample 3

Sample 4

Sample 5

Figure 5.2.1.1: Photographs of Nd – Ho doped borate glasses from Sample 1 to Sample 5.

Table 5.2.2.2: Starting compositions and weights of the powder mixtures of Nd-Pr doped borate glass samples.

Sample Name	Compound	gram-mole	Mole%	Corr.wt	Desired in 1 gm	Desired in 10 gm
Nd-Pr	Al2O3	101.96	5	5.098	0.02846	0.28459
	Nd2O3	336.48	18	60.5661	0.3381	3.38098
	Pr6O11	1021.44	2	20.4288	0.11404	1.1404
	B2O3	69.62	75			
	H3BO3	62.03	150	93.045	0.5194	5.19404
	Total		175	179.138	1	10
Pr-Nd	Al2O3	101.96	4.07738	4.15729	0.01946	0.19457
	Nd2O3	336.48	8.15475	27.439	0.12842	1.28423
	Pr6O11	1021.44	8.15475	83.2959	0.38985	3.89852
	B2O3	69.62	79.6131			
	H3BO3	62.03	159.226	98.768	0.46227	4.62267
	Total		100	213.66	1	10

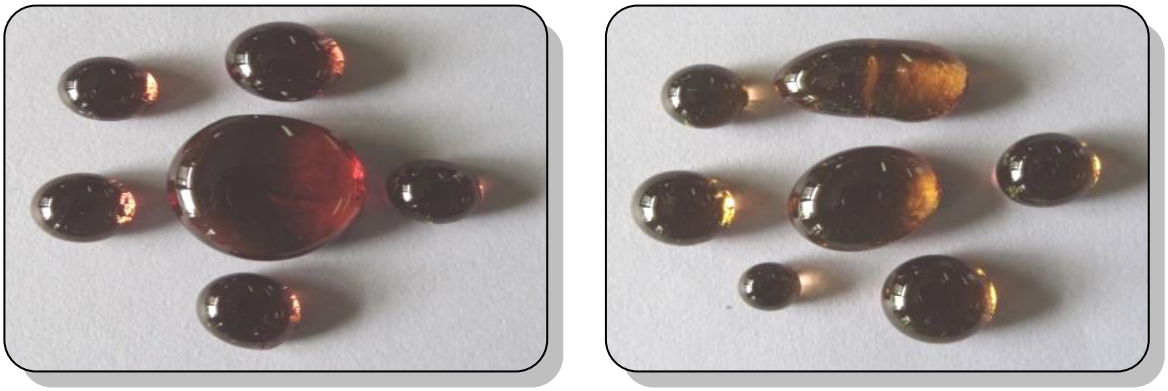

Sample 1 **Sample 2**

Figure 5.2.2.1: Photographs of Nd-Pr and Pr-Nd doped Borate Glasses

5.3 Density Measurement

The densities of the glass samples were measured using the water displacement method. A linear least square fit to the Density versus sample no. is shown in Figure 5.3. It is seen that densities increase by a mere 5% in going from sample 1 to 5.

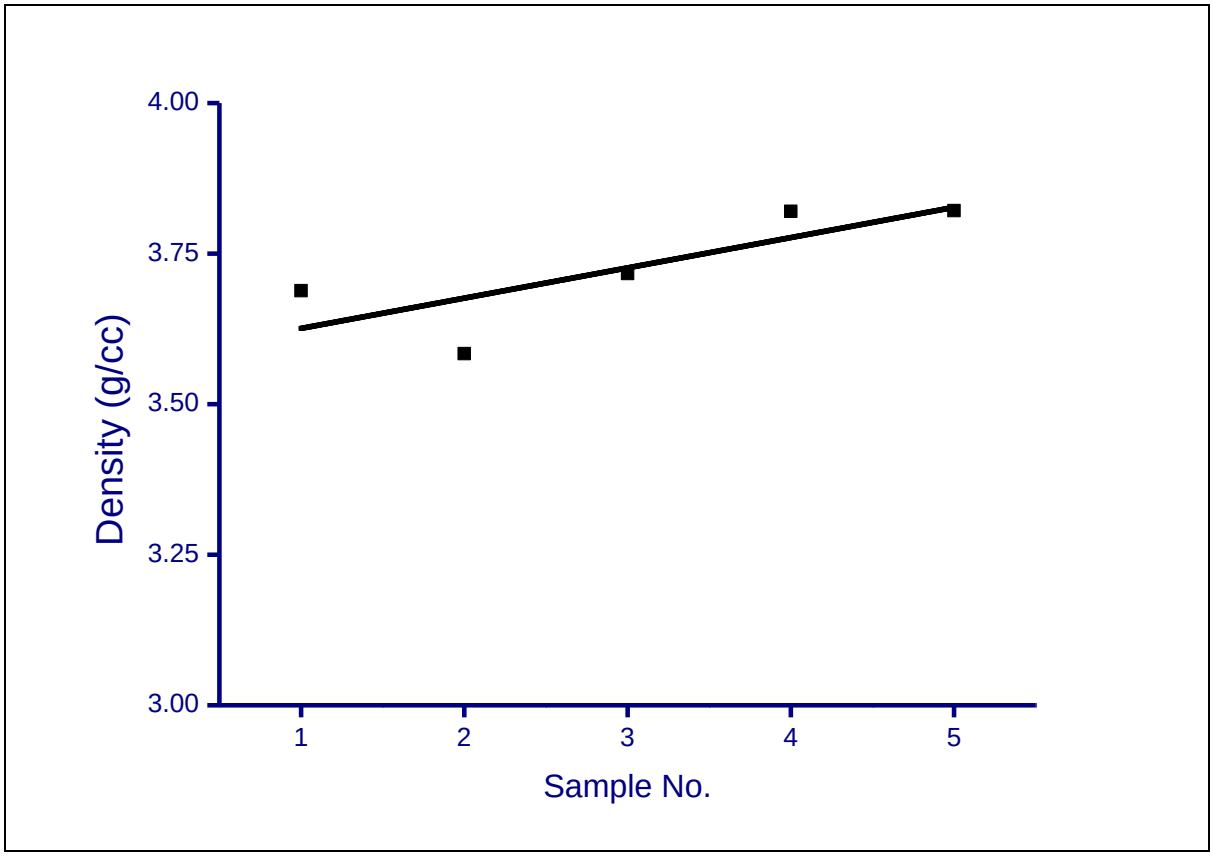

Figure 5.3: Density of Nd – Ho doped borate glasses from Sample 1 to Sample 5

(Errors are of the size of the symbols)

5.4 DTA measurement

The glass transition temperatures of three members of the set of glasses in Table 5.2.1.1 viz. Samples 1,3 and 5 were measured by Differential Thermal Analysis (Shimadzu) and Differential Scanning Calorimetry (Netzsch Proteus Thermal Analyser). The data are shown in Figures 5.4.1 and 5.4.2. The transition temperatures were found to be ~ 950 ^{o}C for the Nd-20 glass, ~ 970 ^{o}C for the Ho-20 glass and 780 ^{o}C for the Nd-10:Ho-10 glass.

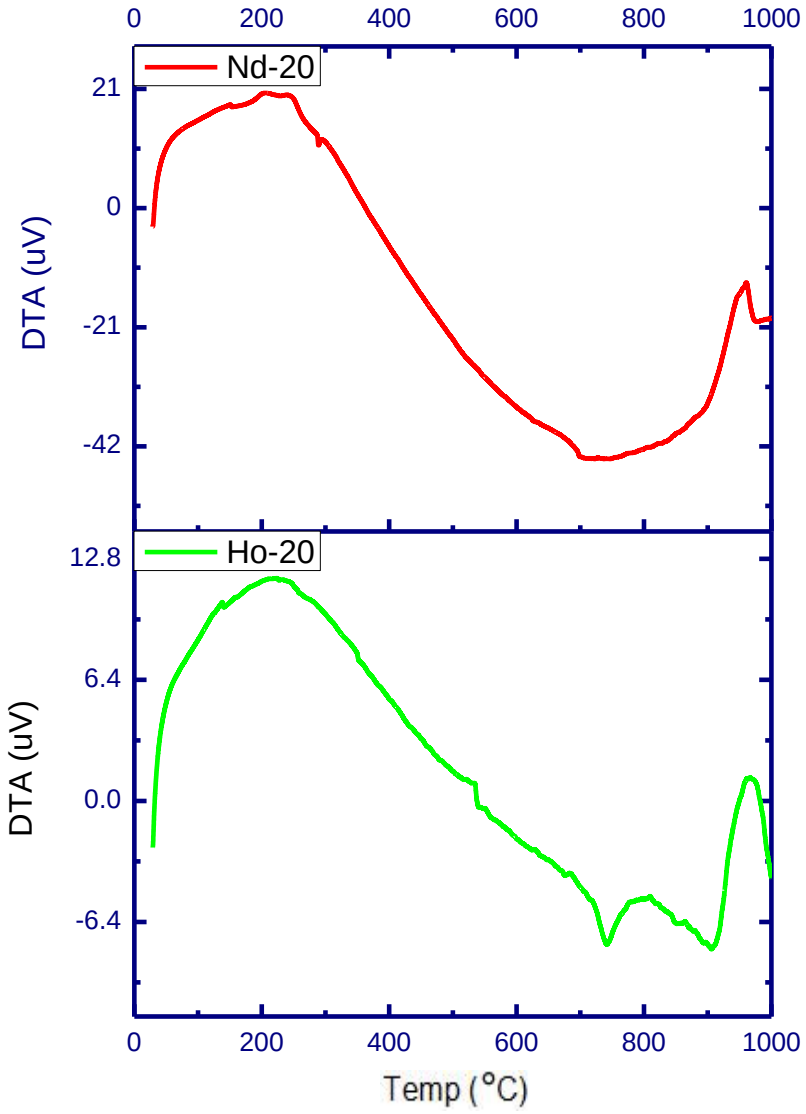

Figure 5.4.1: DTA measurement of 20%Nd and 20% Ho doped borate glasses.

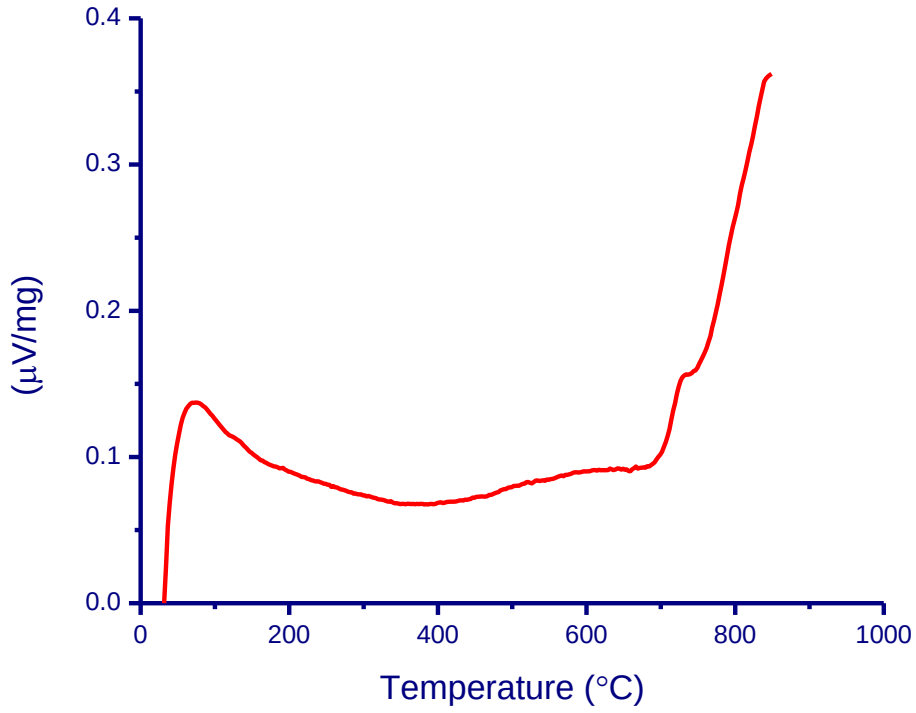

Figure 5.4.2: DSC measurement of the 10% Nd – 10% Ho doped borate glass.

5.5 X-Ray Diffraction Data

5.5.1 Nd - Ho Doped Borate Glasses

X-ray diffraction data were measured using a Rigaku D-MAX/B rotating anode diffractometer with Cu K_α incident X-rays and counted in the angular range of 3^0 to 145^0. The intensity data are shown in Figure 5.5.1.1. The pair distribution functions, total correlation functions and total radial distribution functions shown in Figures 5.5.1.2, 5.5.1.3and 5.5.1.4 were obtained after experimental corrections and normalization.

Before the X-ray diffraction of the samples of Table 5.2.1.1 was measured, these glasses were used in neutron diffraction experiments at HZB, Berlin, Germany. In the latter measurements, the 10 % Nd_2O_3 – 10% Ho_2O_3 sample was measured at room temperature and at two temperatures in the glass transition region before being returned to room temperature. As the cooling was slow, it is expected that this particular glass devitrified – as evidenced by the crystalline reflections in Figure 5.5.1.1.

5.5.2 Nd – Pr Doped Borate Glasses

X-ray diffraction data on these samples were also obtained with a Rigaku D-MAX/B rotating anode diffractometer with Cu K_α incident X-rays and the angular range of 3^0 to 145^0. The intensity data are shown in Figure 5.5.2.1.

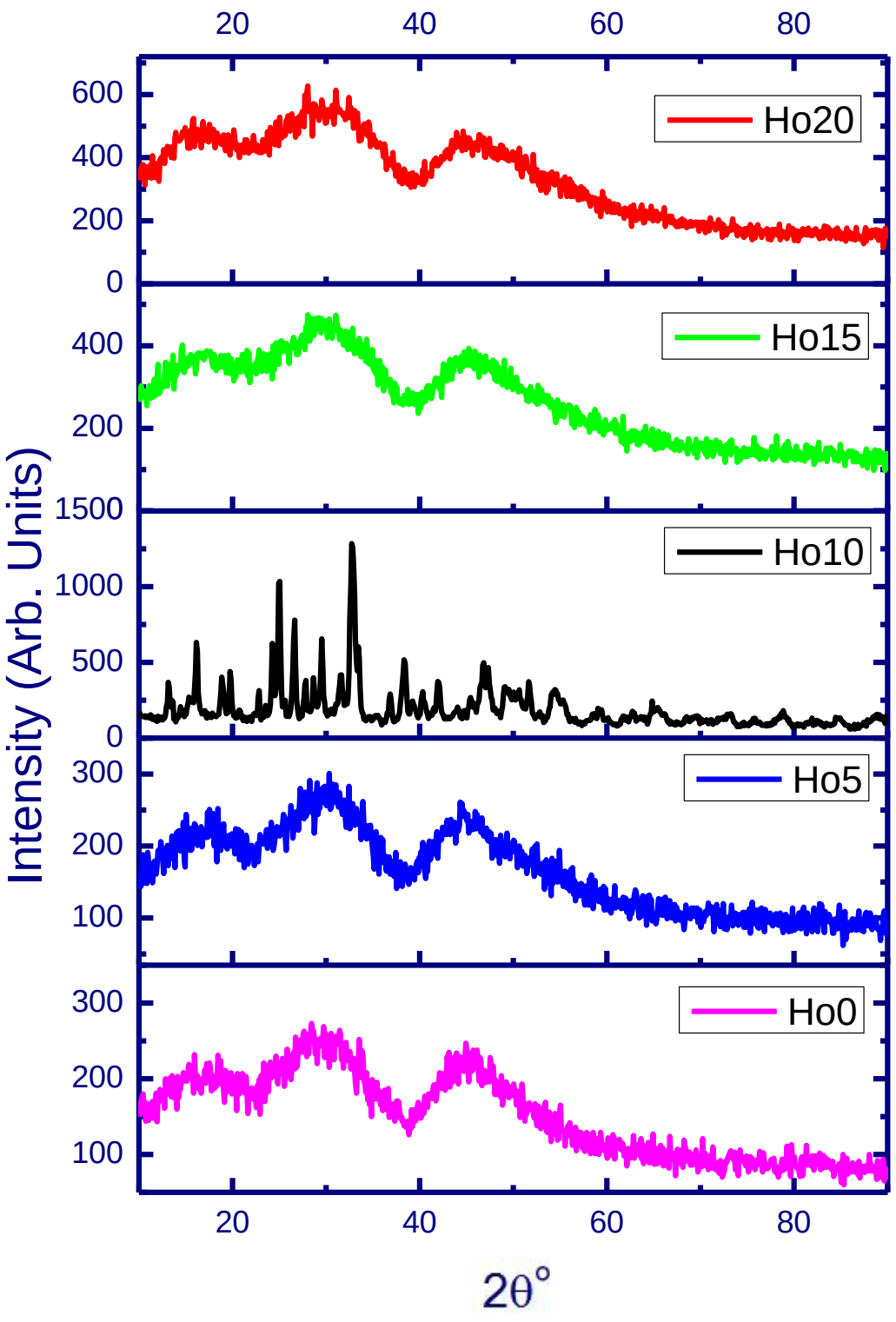

Figure 5.5.1.1: Measured X-Ray diffraction pattern of the Nd_2O_3 - Ho_2O_3 doped borate glasses.

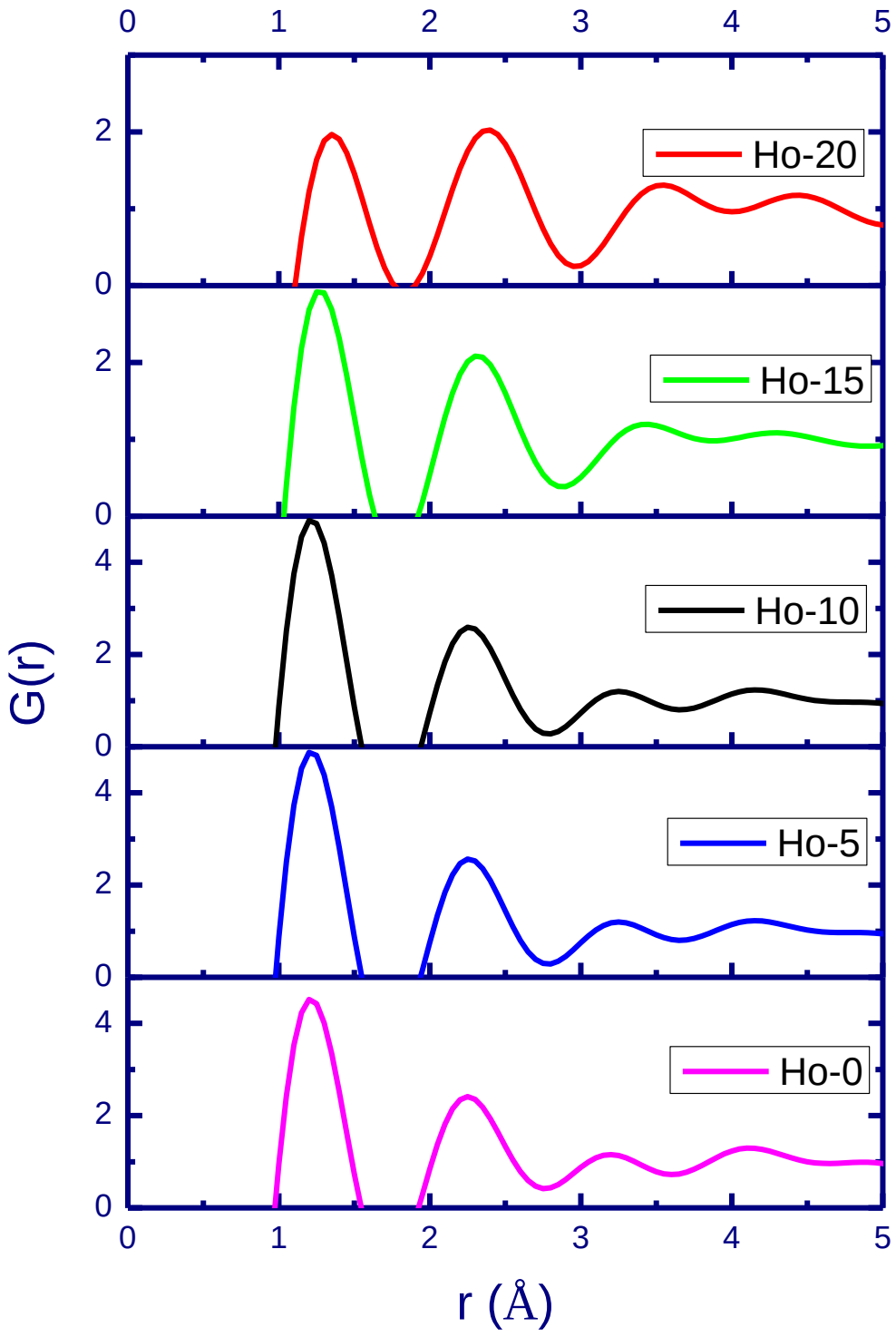

Figure 5.5.1.2: Pair-Correlation Function of the Nd_2O_3 - Ho_2O_3 doped borate glasses from the X-ray data

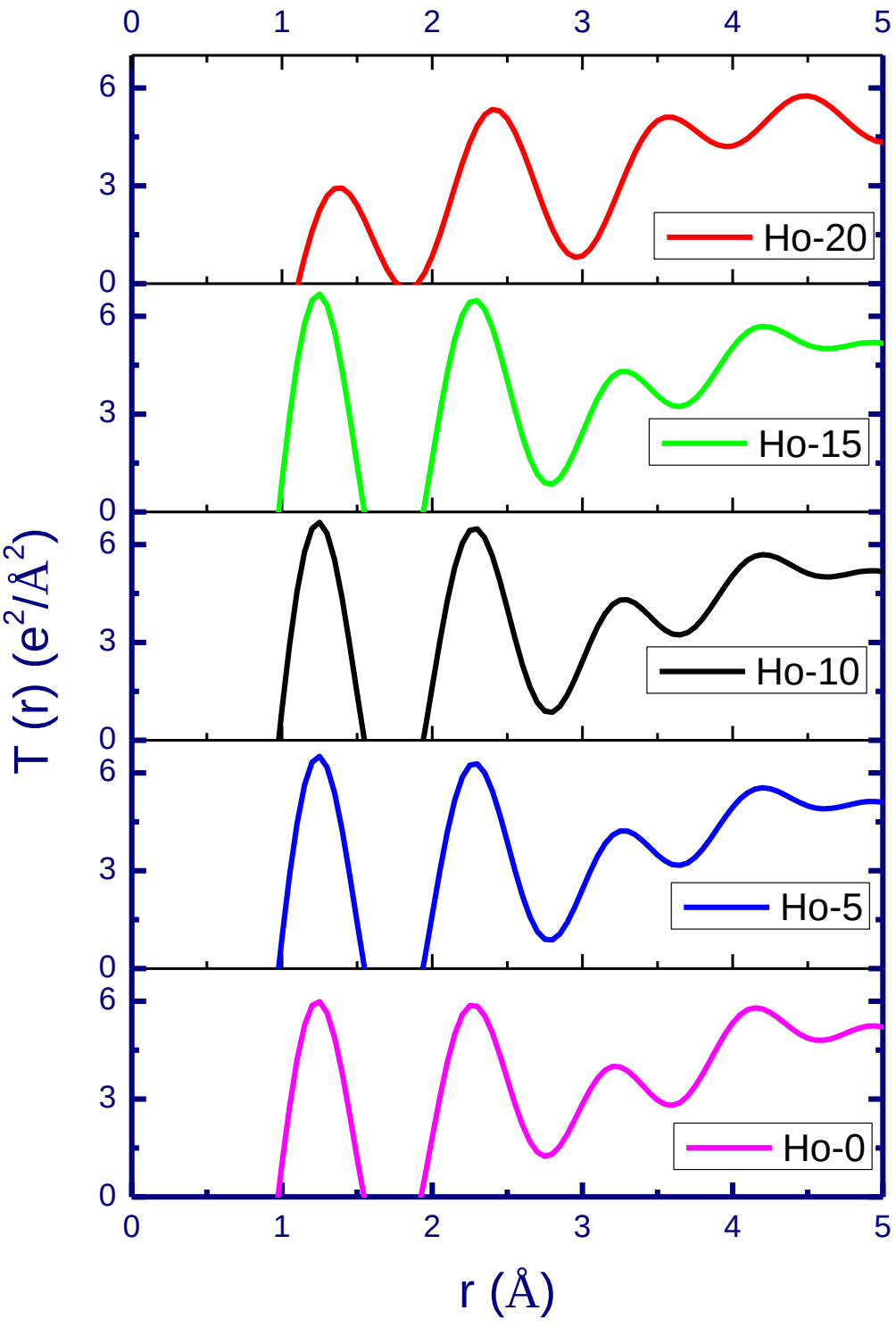

Figure 5.5.1.3: Total Correlation Function of the Nd_2O_3 - Ho_2O_3 doped borate glasses from the X-ray data.

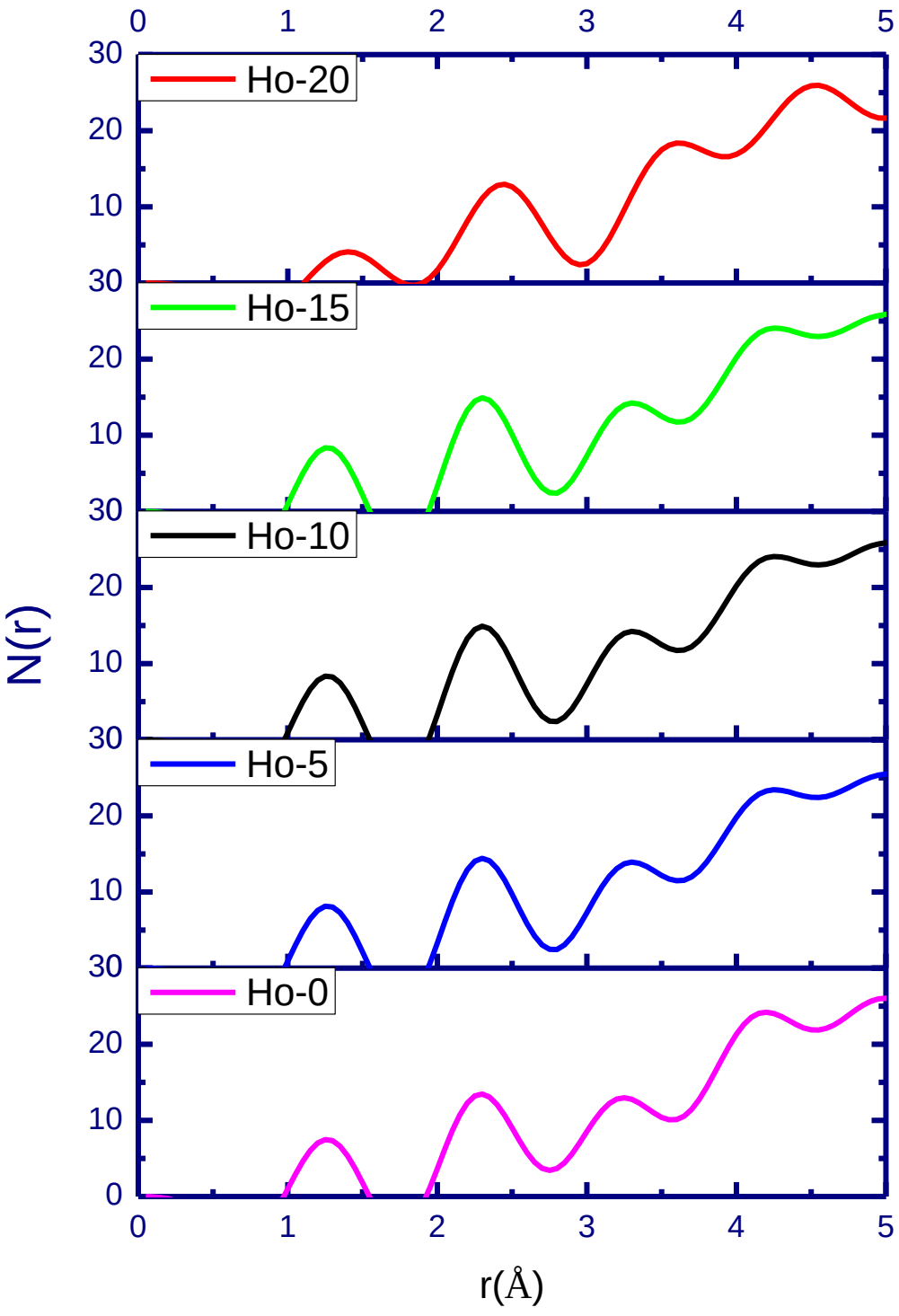

Figure 5.5.1.4: Radial Distribution Function of the Nd_2O_3 - Ho_2O_3 doped borate glasses from the X-ray data.

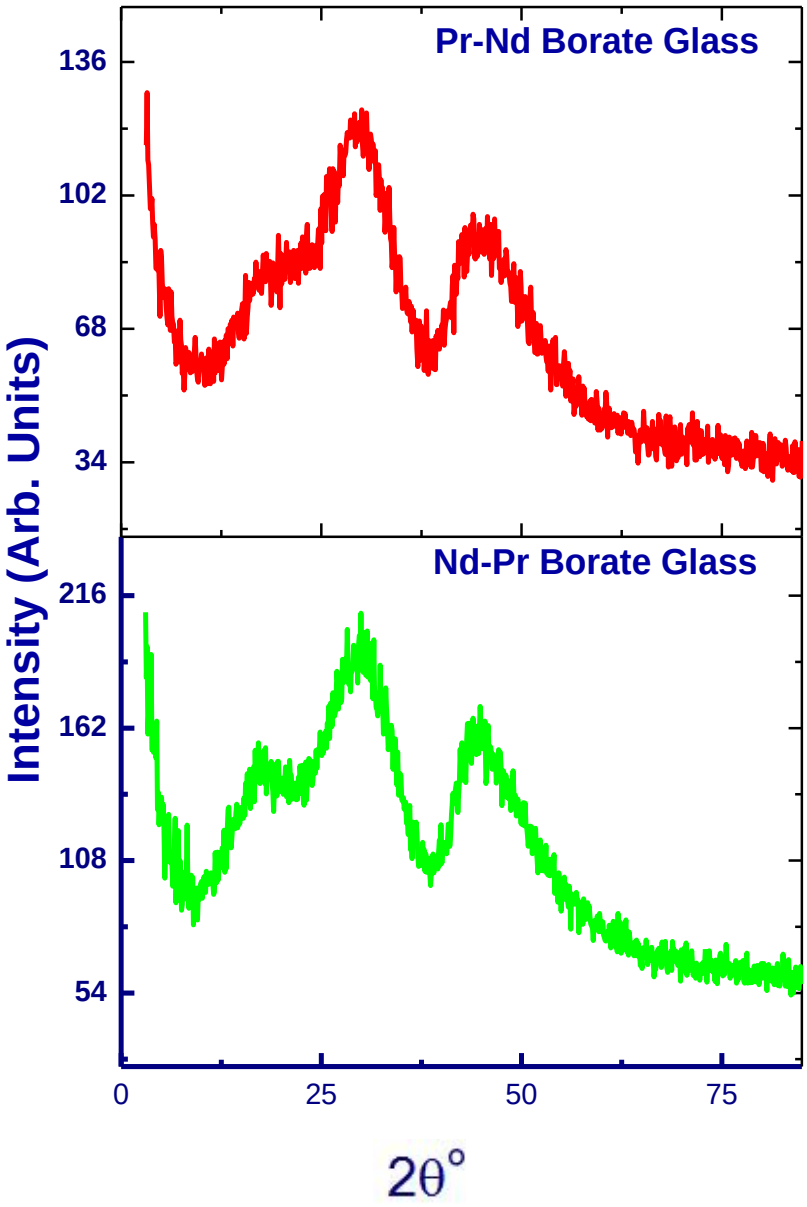

Figure 5.5.2.1: Measured X-ray diffraction patterns of the Nd_2O_3 – Pr_6O_{11} doped borate glasses.

5.6 Neutron Diffraction Data

5.6.1 Nd-Ho Doped Borate Glasses

Neutron diffraction measurements on the glasses were performed using 0.783 Å incident neutrons on the High Q diffractometer at Dhruva Reactor, B.A.R.C. and with 0.91 Å incident neutrons on the Flat Cone diffractometer (E2 beamline) at HZB, Berlin, Germany. The intensities from neutron diffraction data were corrected for absorption, multiple scattering and normalized to vanadium before being Fourier transformed to yield the real space correlation functions.

5.6.2 Nd-Pr Doped Borate Glasses

Neutron diffraction data was obtained on these glasses using 0.783 Å incident neutrons on the High Q diffractometer at Dhruva Reactor, B.A.R.C.

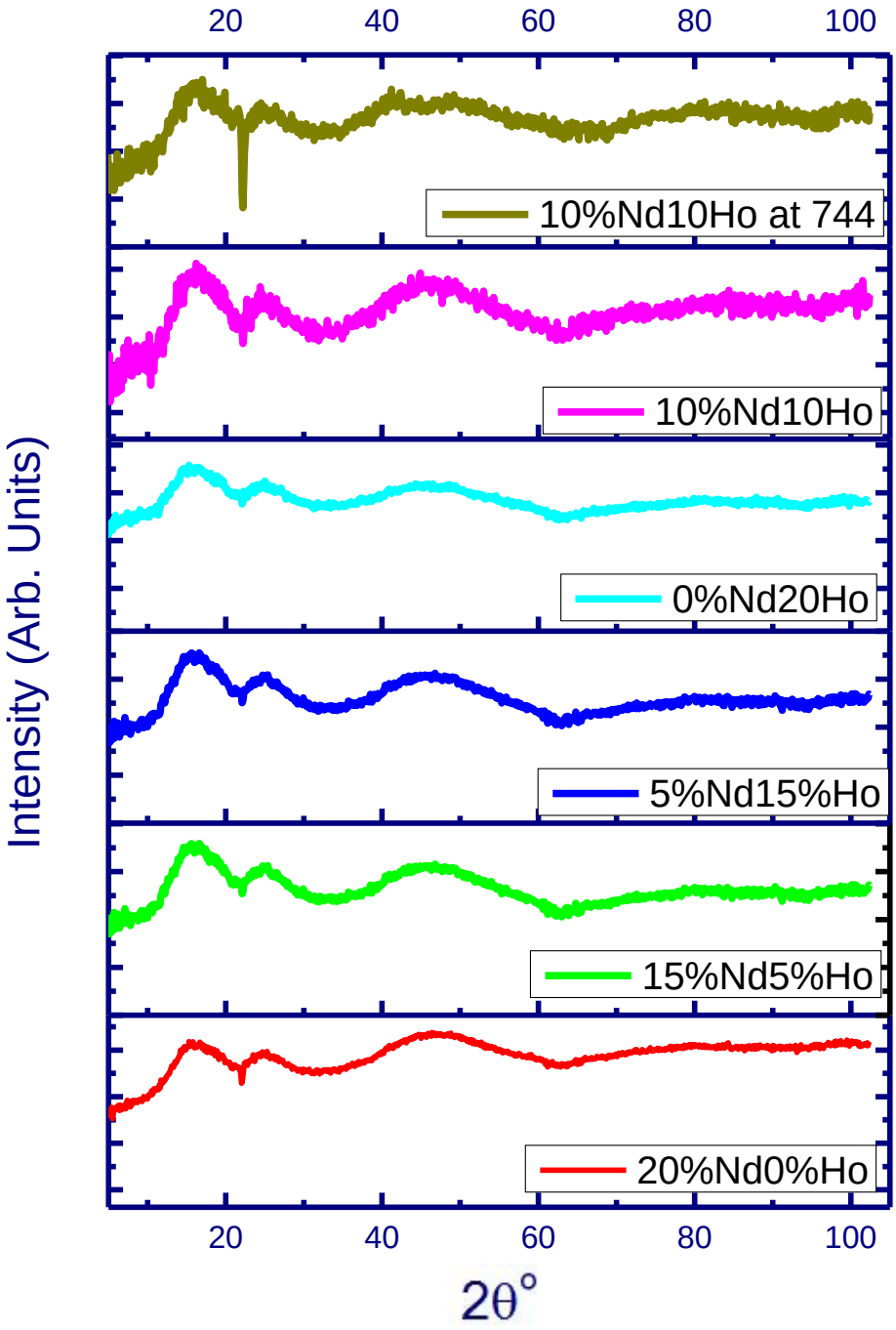

Figure 5.6.1.1: Measured Intensity of the Nd_2O_3 – Ho_2O_3 doped borate glasses from neutron data obtained from HZB, Berlin.

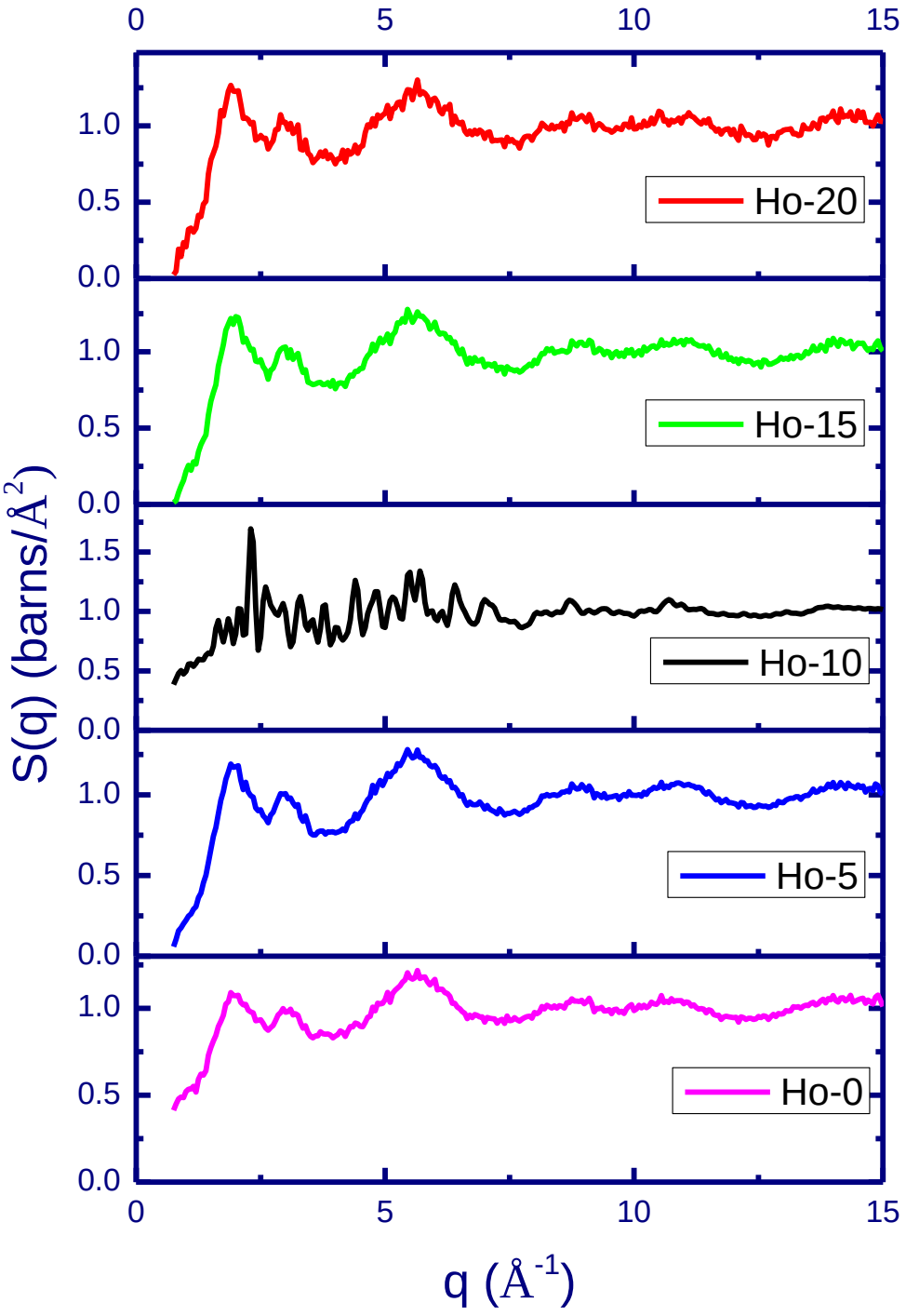

Figure 5.6.1.2: Measured structure factors of the Nd_2O_3 - Ho_2O_3 doped borate glasses from neutron data.

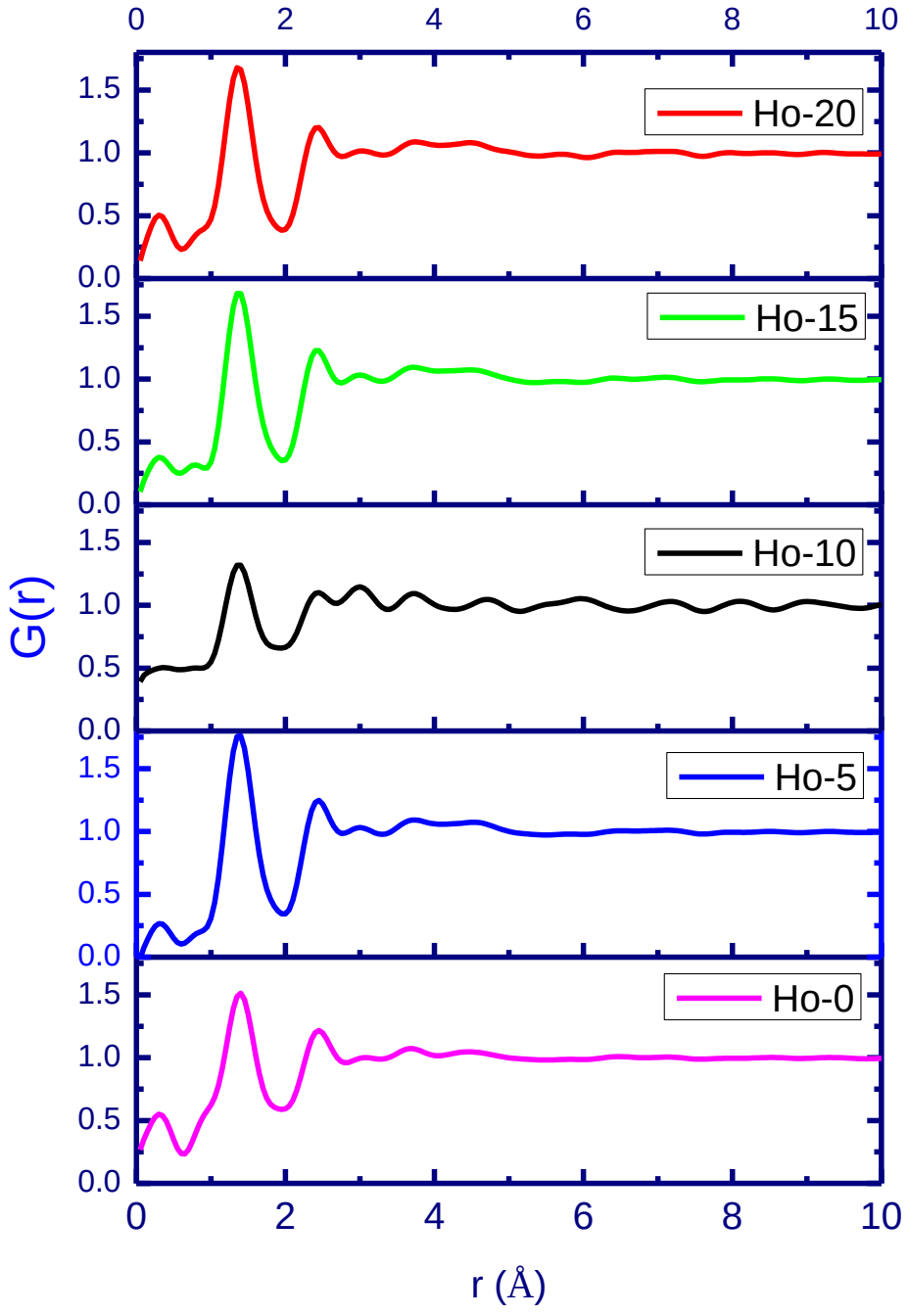

Figure 5.6.1.3: Pair-Correlation Function of the Nd_2O_3 – Ho_2O_3 doped borate glasses from the neutron data by Fourier Transformation of S (q).

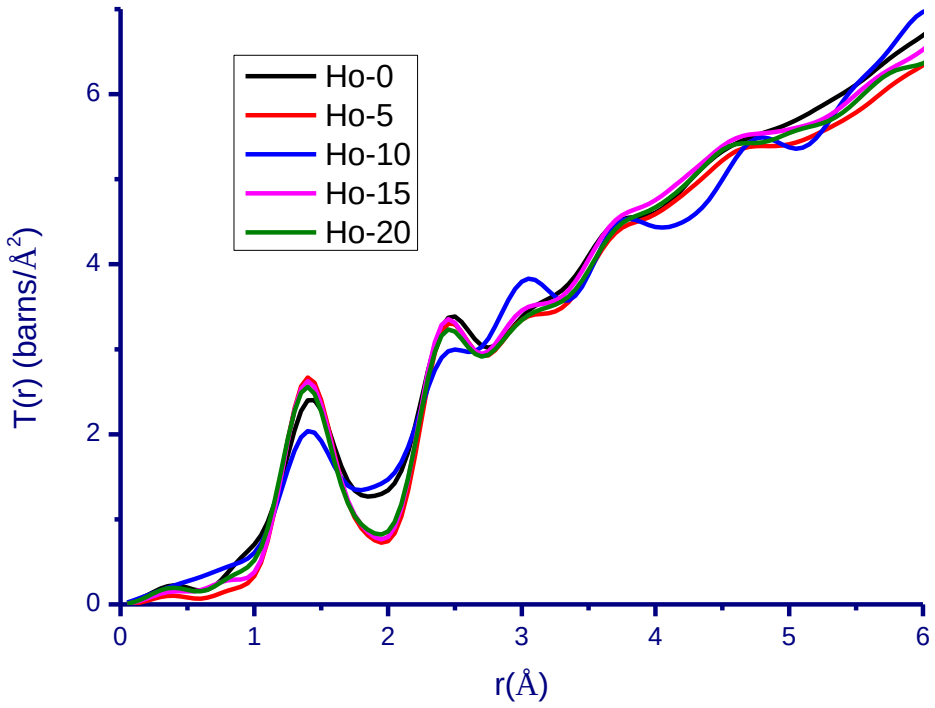

Figure 5.6.1.4: Overlay of Total Correlation Function of the Nd_2O_3 – Ho_2O_3 doped borate glasses from the neutron data by Fourier Transformation of S(q).

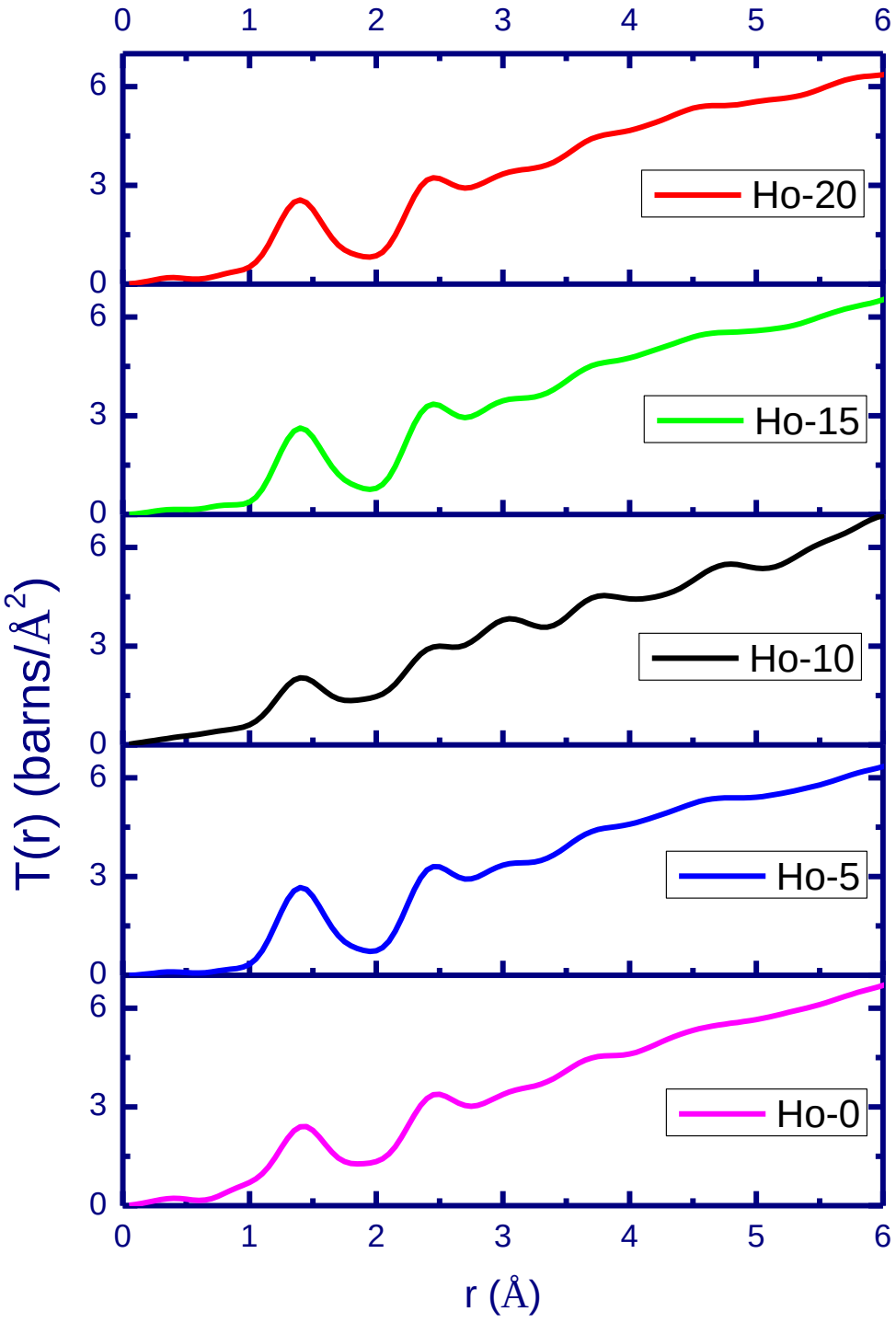

Figure 5.6.1.5: Total Correlation Function of the Nd_2O_3 – Ho_2O_3 doped borate glasses from the neutron data by Fourier Transformation of S(q).

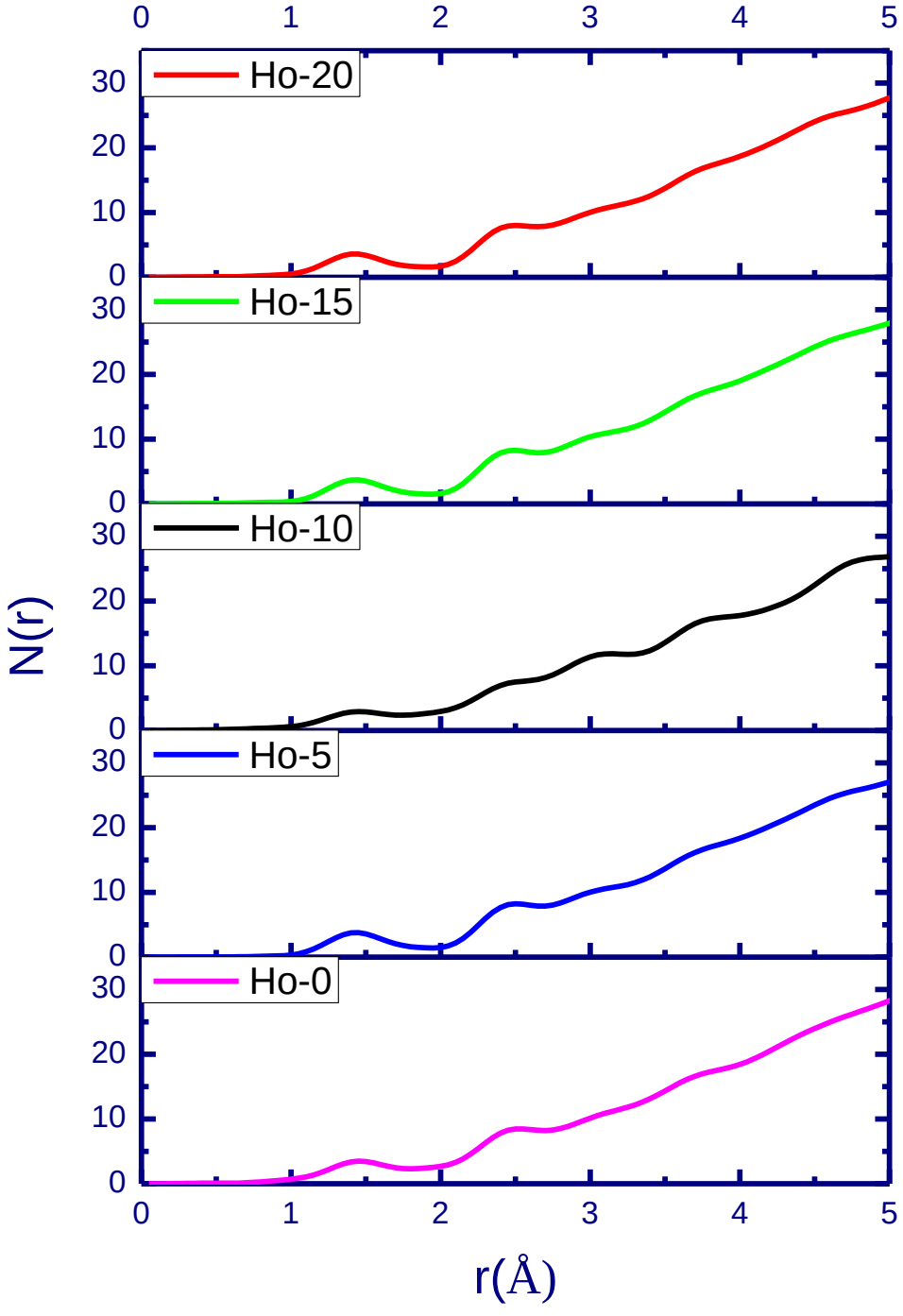

Figure 5.6.1.6: Radial Distribution Function of the Nd_2O_3 – Ho_2O_3 doped borate glasses from the neutron data by Fourier Transformation of S(q).

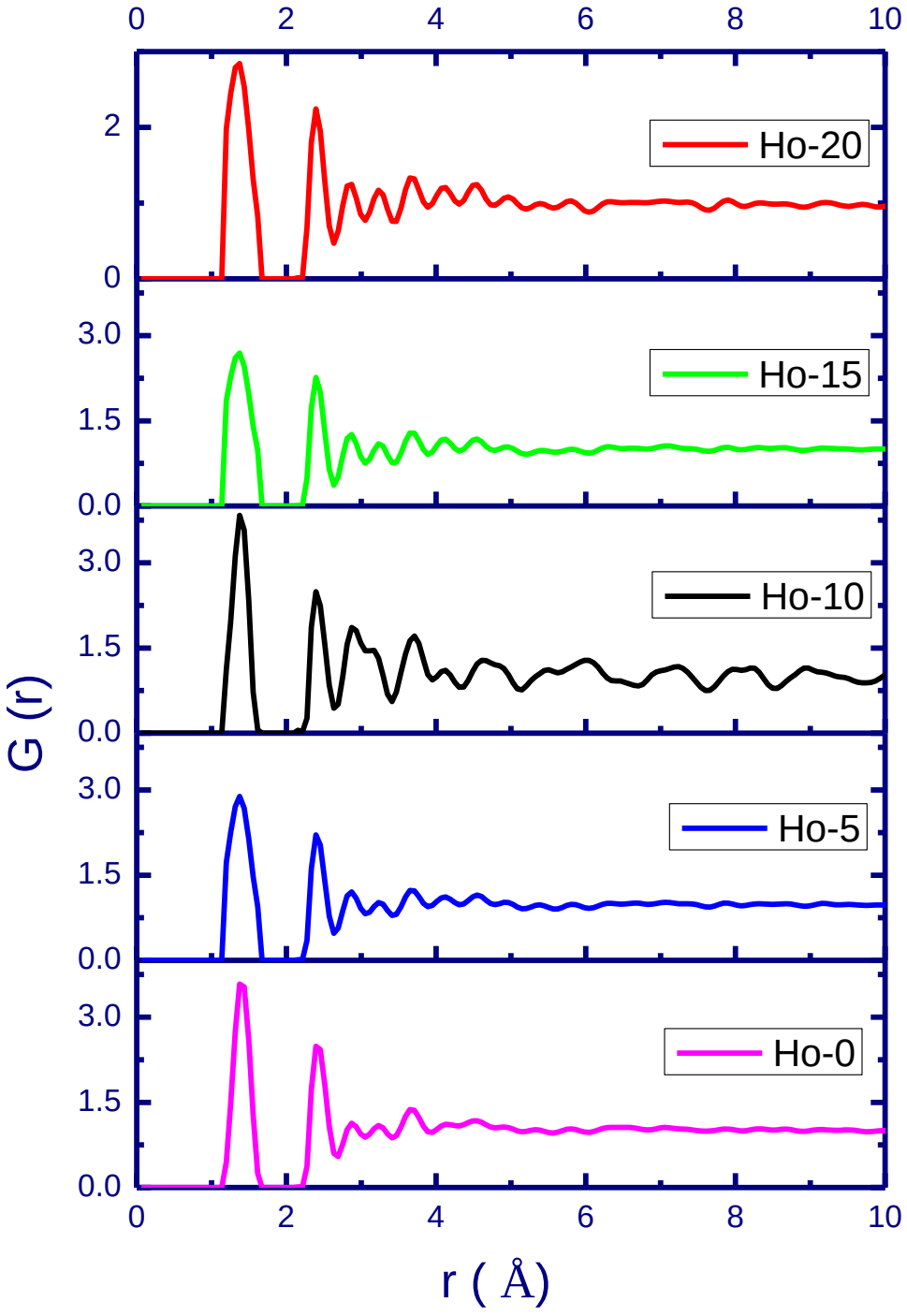

Figure 5.6.1.7: Pair-Correlation Function of the Nd_2O_3 – Ho_2O_3 doped borate glasses from the neutron data by MCGR

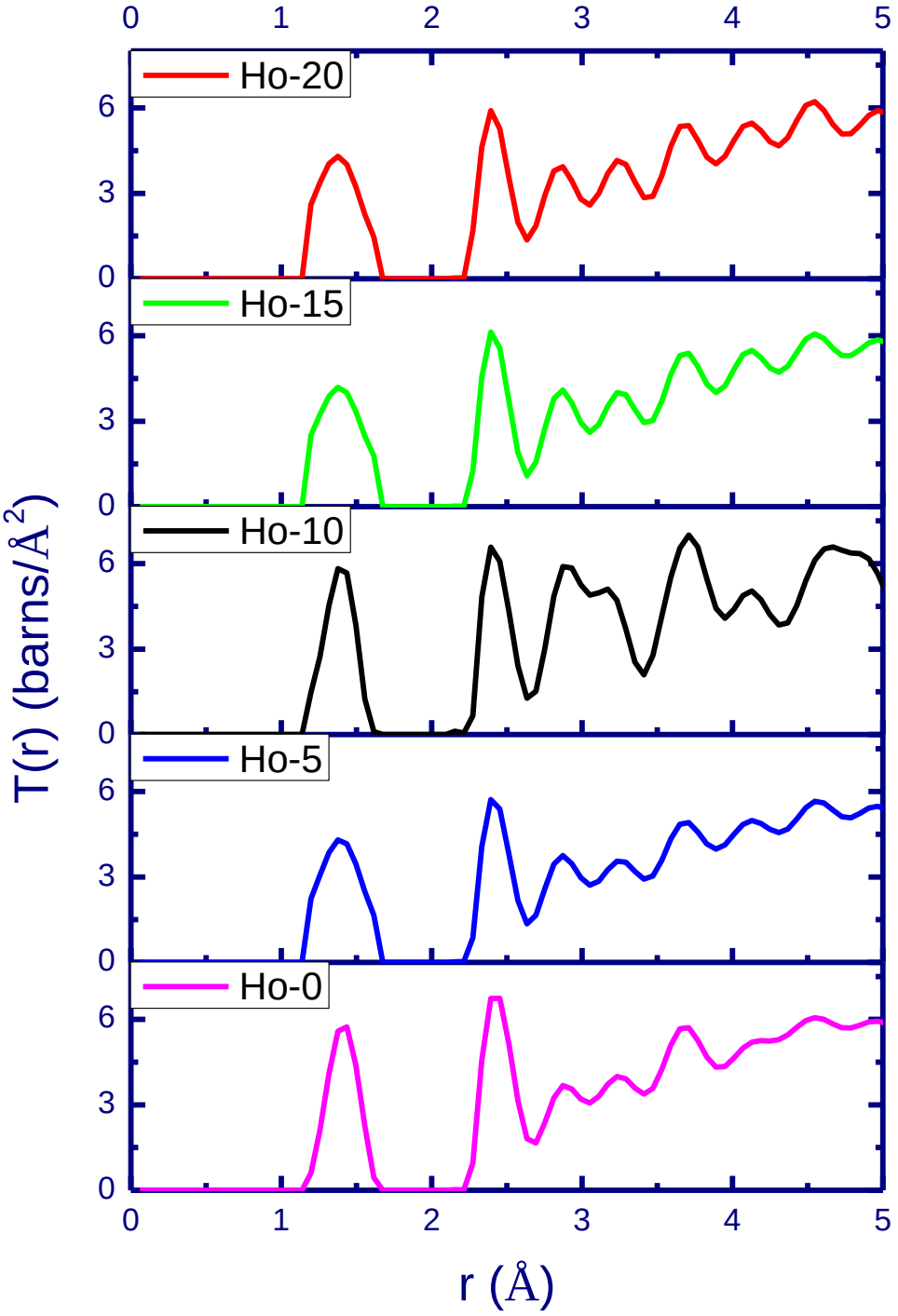

Figure 5.6.1.8: Total Correlation Function of the Nd_2O_3 – Ho_2O_3 doped borate glasses from the neutron data by MCGR

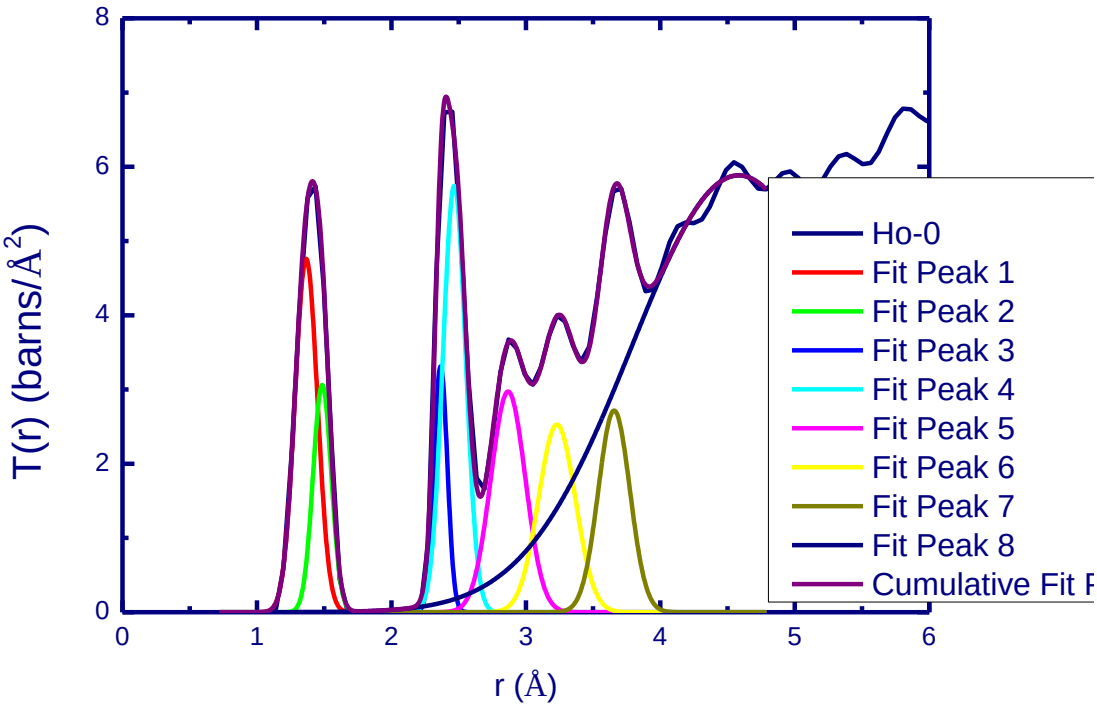

Figure 5.6.1.9: Total Correlation Function of the 20% Nd_2O_3 doped borate glass peaks fitted to obtain peak positions

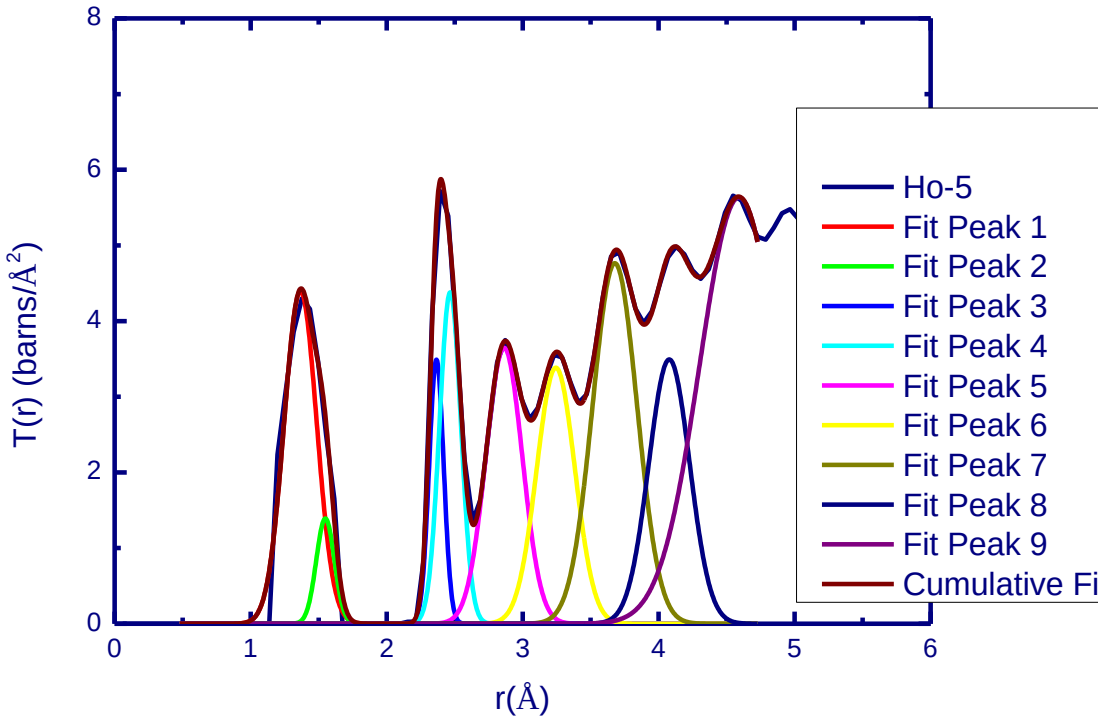

Figure 5.6.1.10: Total Correlation Function of the 15% Nd_2O_3 – 5% Ho_2O_3 doped borate glass peaks fitted to obtain peak positions

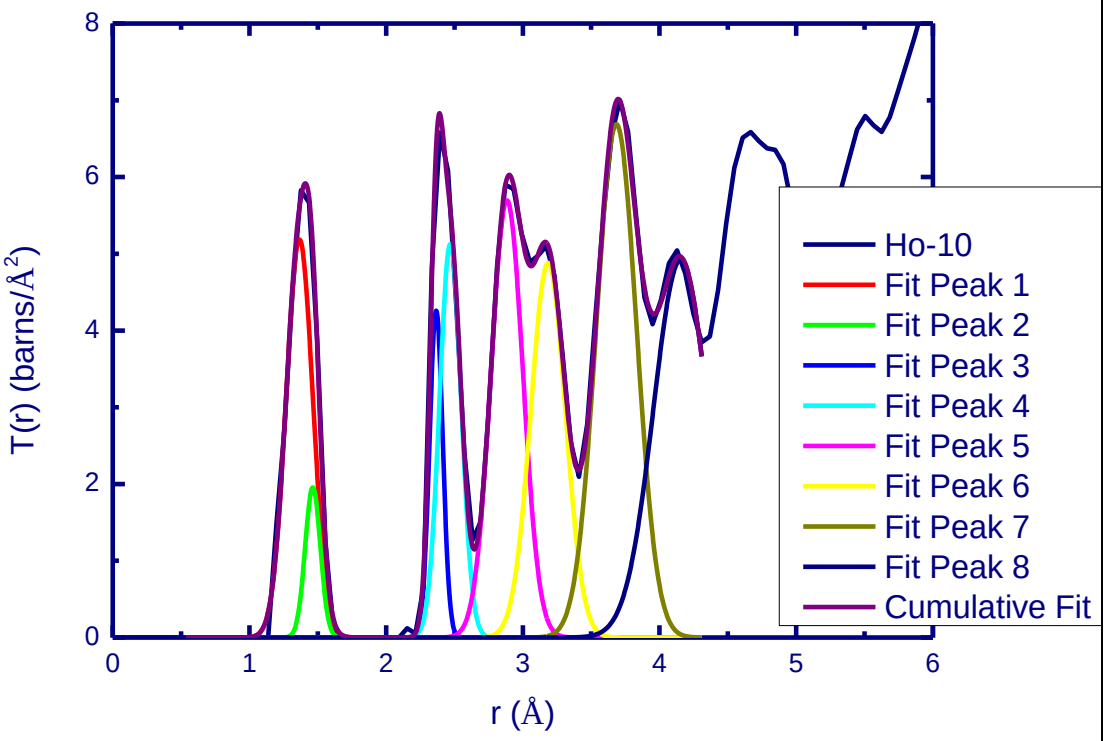

Figure 5.6.1.11: Total Correlation Function of the 10% Nd_2O_3 - 10% Ho_2O_3 doped borate glass peaks fitted to obtain peak positions

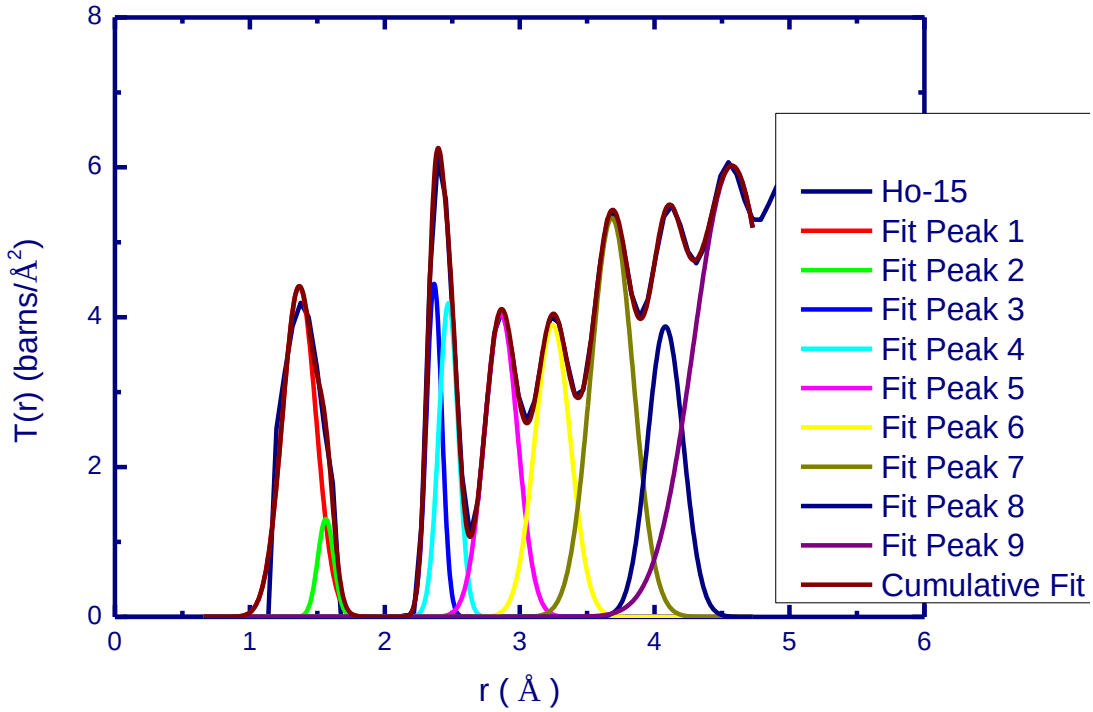

Figure 5.6.1.12: Total Correlation Function of the 5% Nd_2O_3 - 15% Ho_2O_3 doped borate glass peaks fitted to obtain peak positions

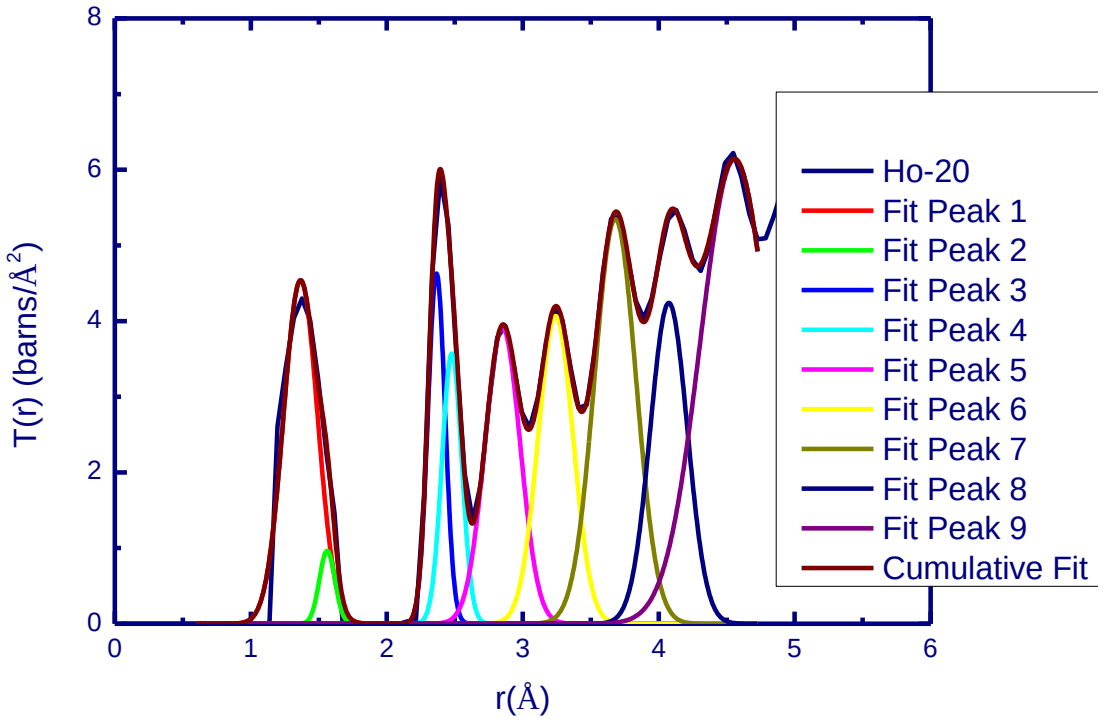

Figure 5.6.1.13: Total Correlation Function of the 20% Ho_2O_3 doped borate glass peaks fitted to obtain peak positions

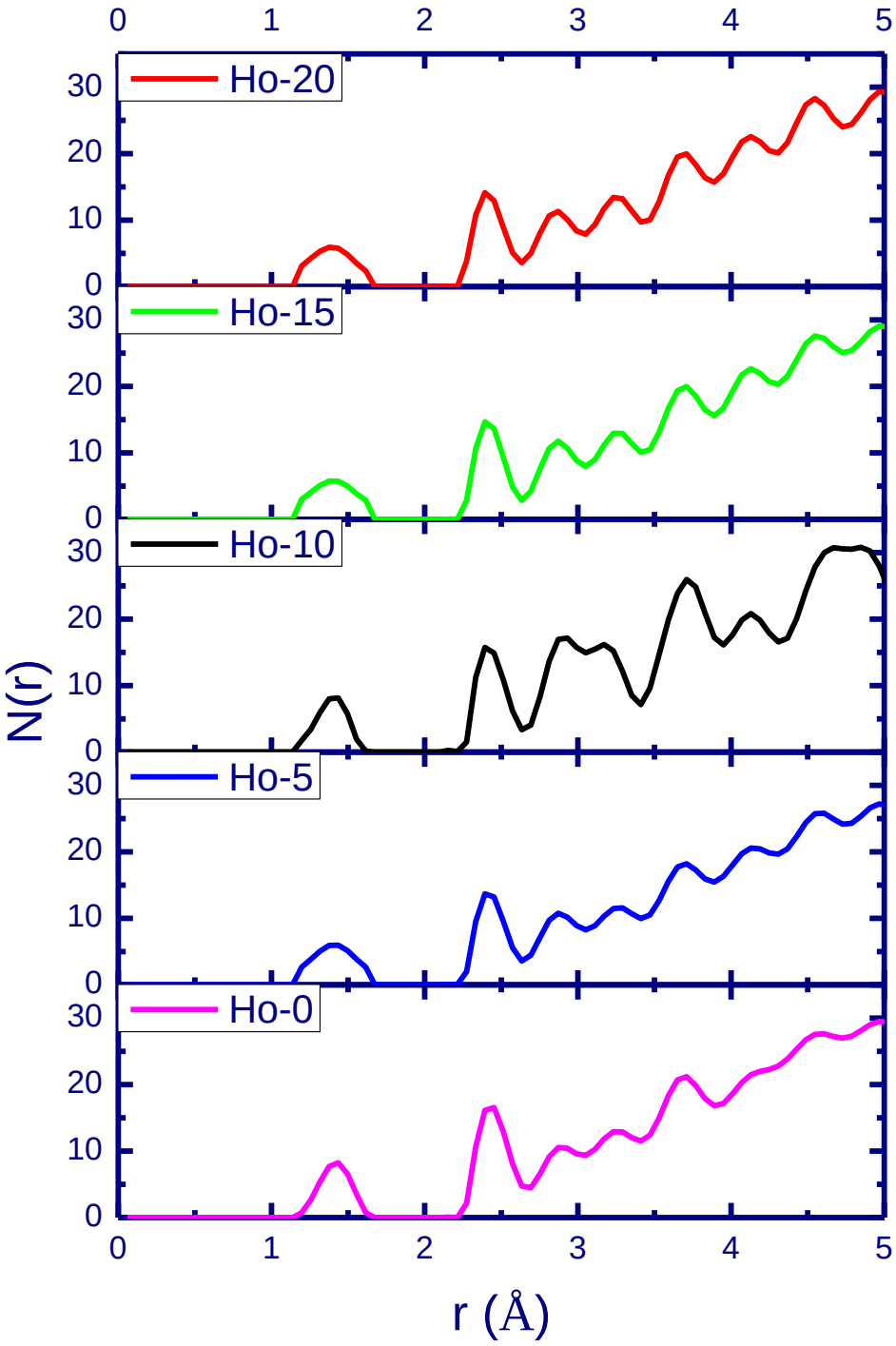

Figure 5.6.1.14: Radial Distribution Function of the Nd_2O_3 - Ho_2O_3 doped borate glasses from the neutron data by MCGR

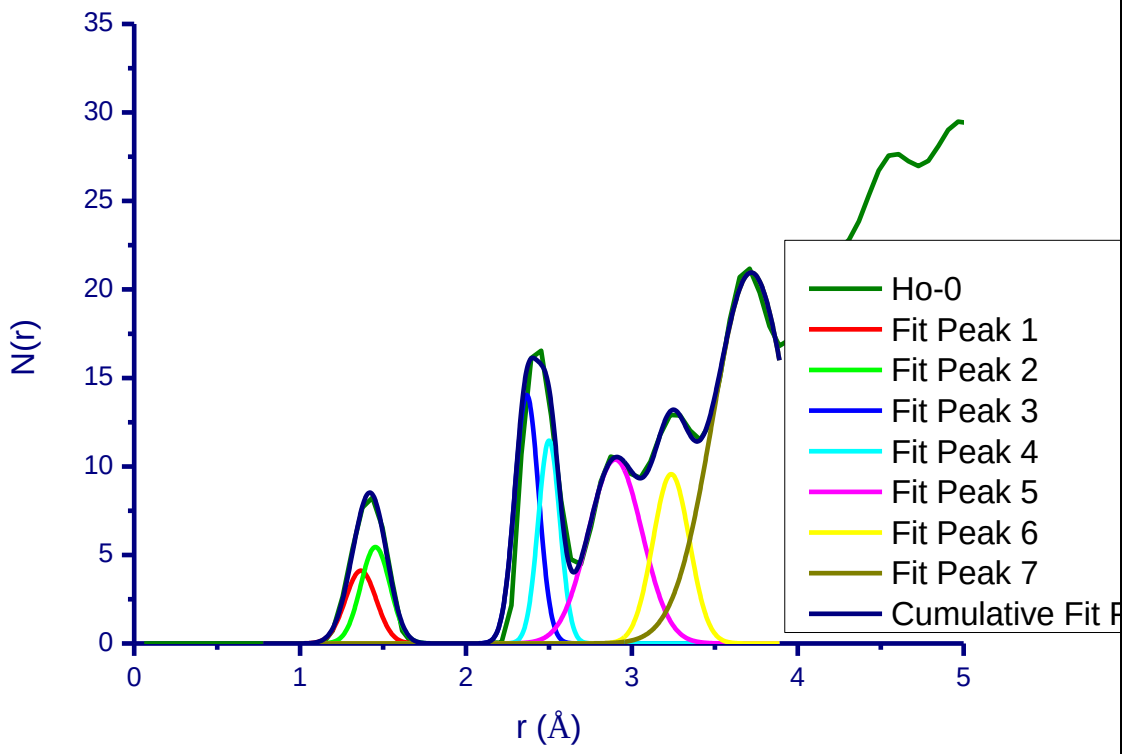

Figure 5.6.1.15: Radial Distribution Function of the 20% Nd_2O_3 doped borate glass peaks fitted to obtain coordination numbers

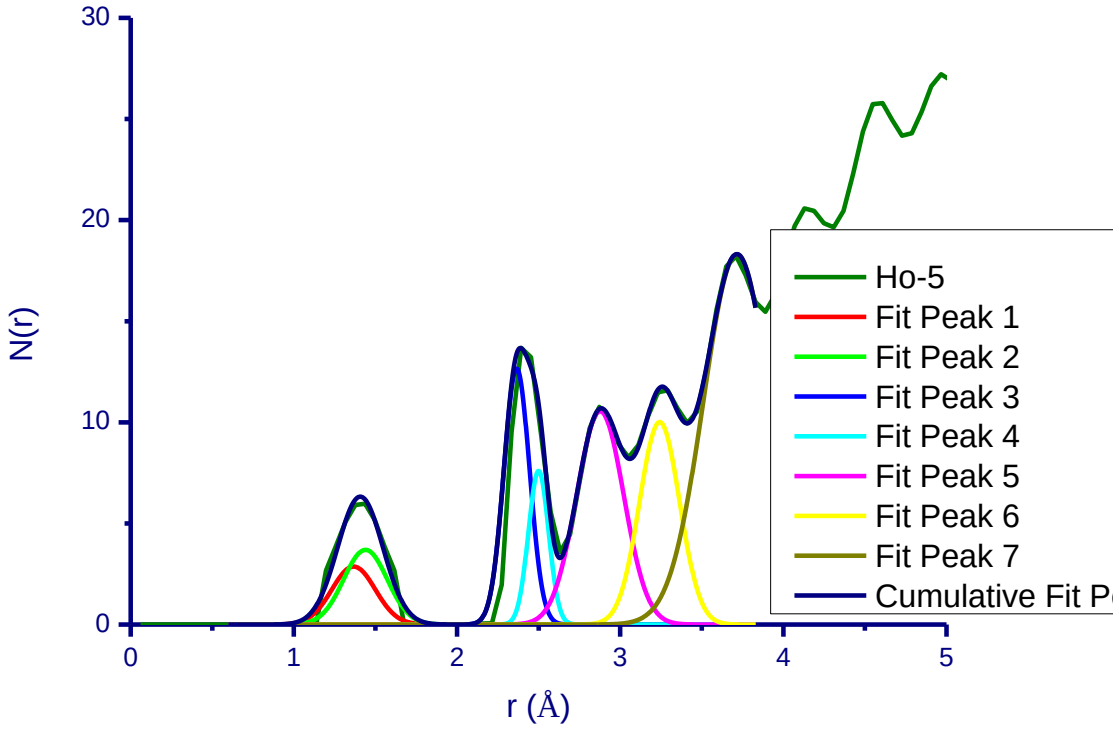

Figure 5.6.1.16: Radial Distribution Function of the 15% Nd_2O_3 - 5% Ho_2O_3 doped borate glass peaks fitted to obtain coordination numbers

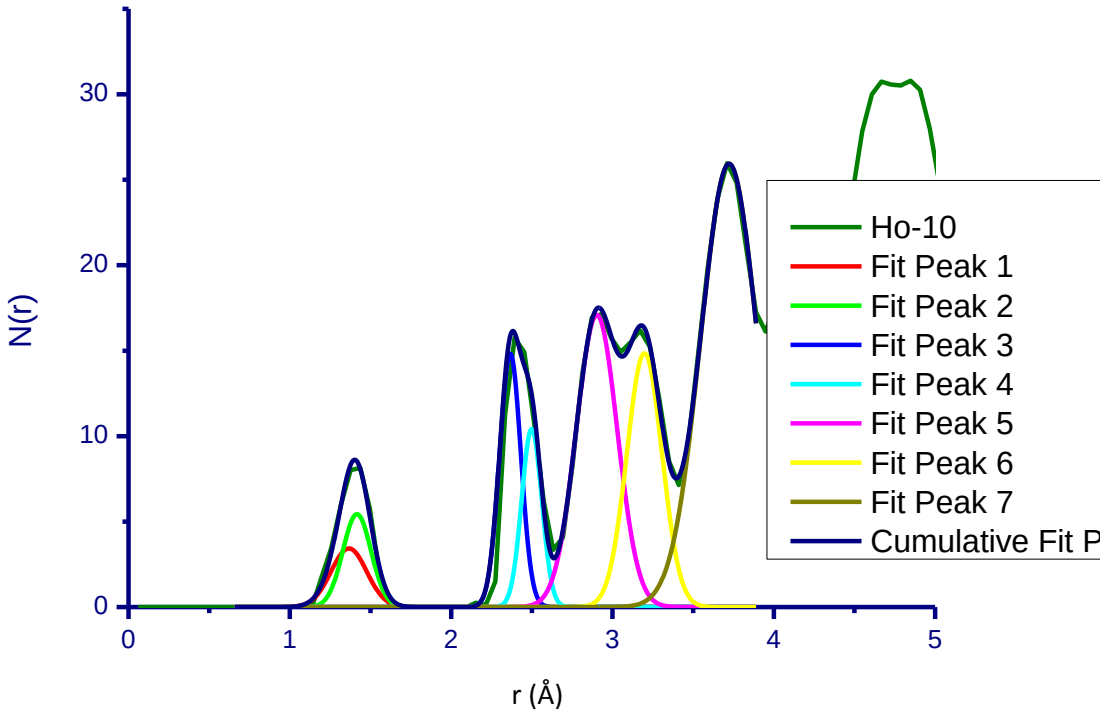

Figure 5.6.1.17: Radial Distribution Function of the 10% Nd_2O_3 - 10% Ho_2O_3 doped borate glass peaks fitted to obtain coordination numbers

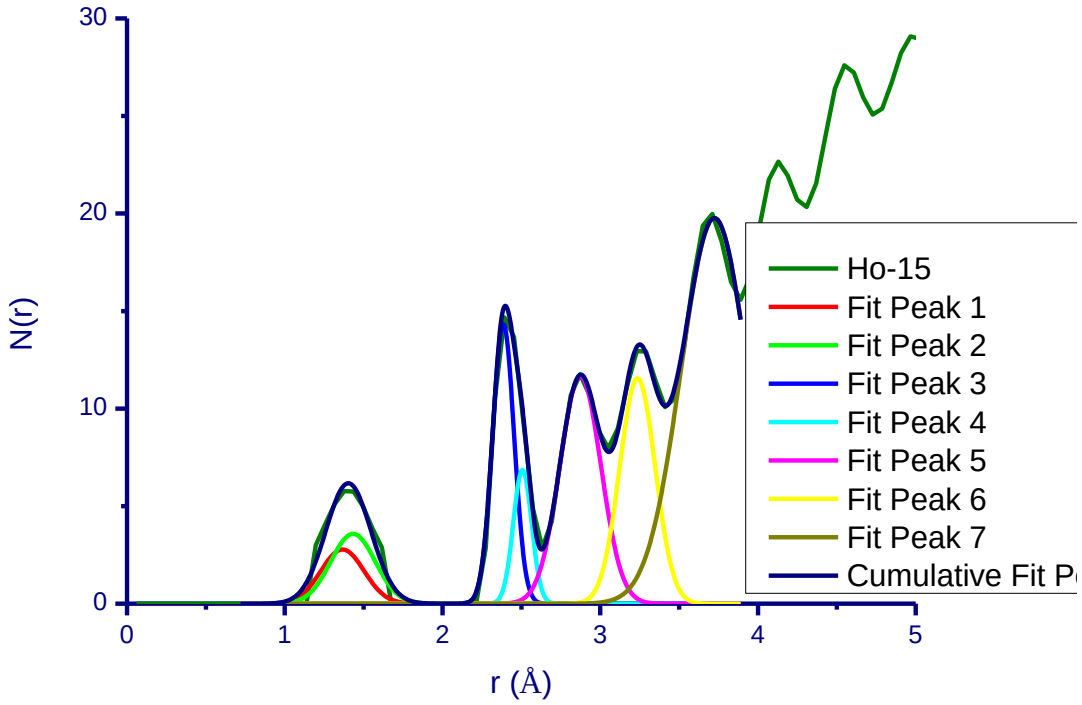

Figure 5.6.1.18: Radial Distribution Function of the 5% Nd_2O_3 - 15% Ho_2O_3 doped borate glass peaks fitted to obtain coordination numbers

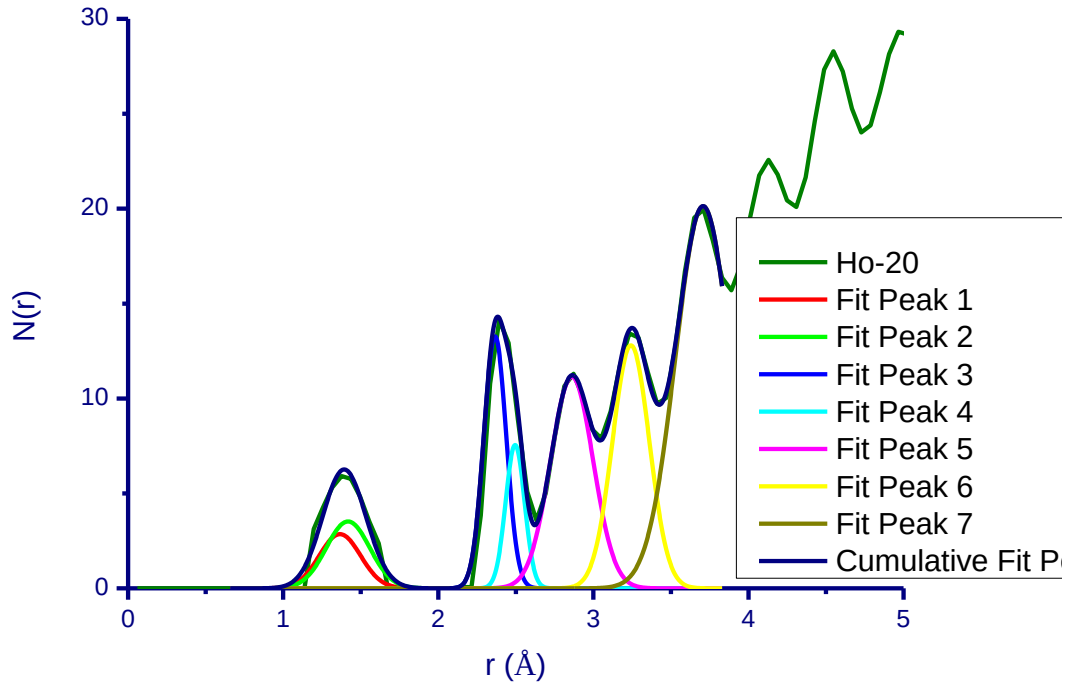

Figure 5.6.1.19: Radial Distribution Function of the 20% Ho_2O_3 doped borate glass peaks fitted to obtain coordination numbers

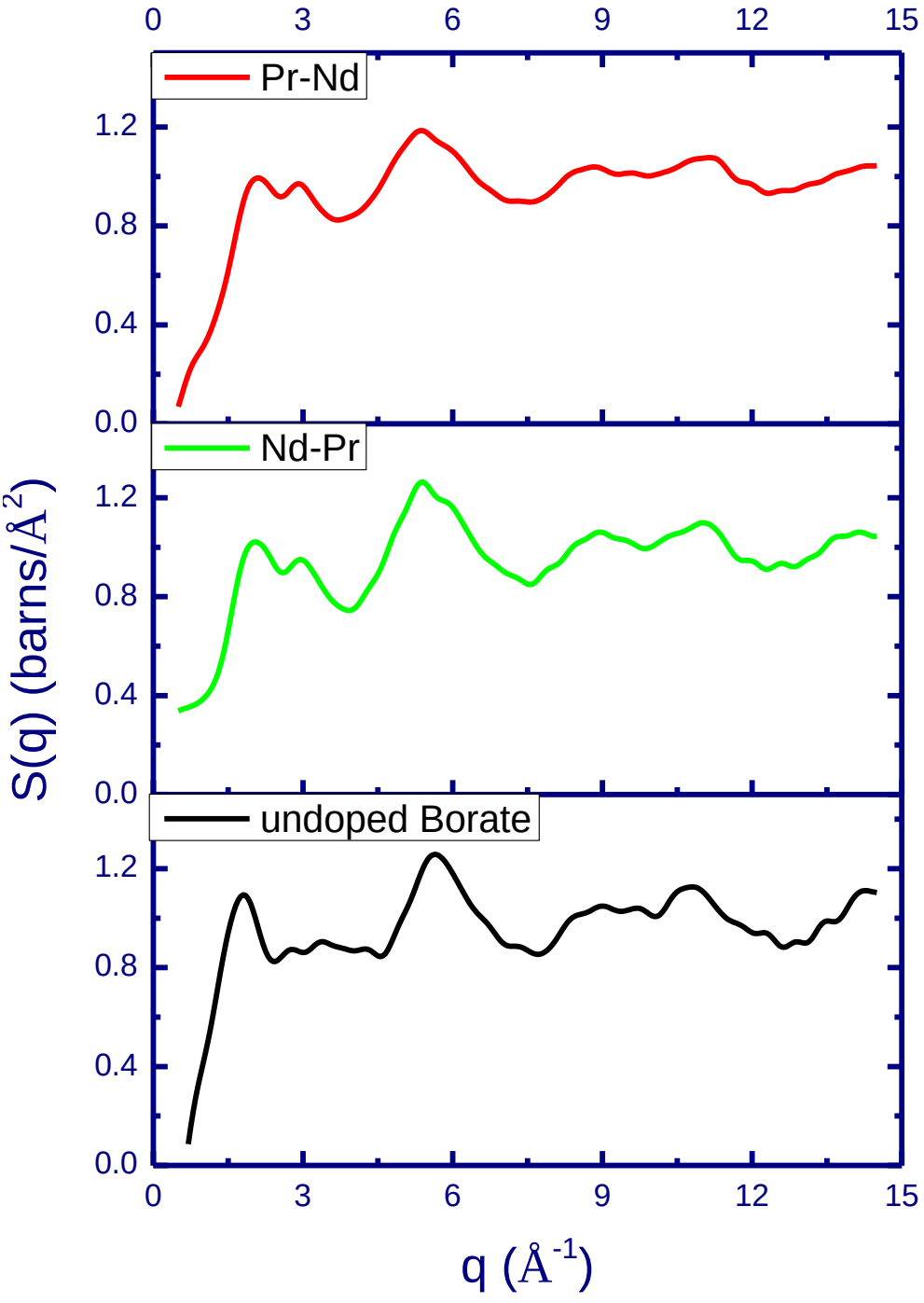

Figure 5.6.2.1: Measured structure factors of the Nd_2O_3 – Pr_6O_{11} doped and undoped borate glasses from neutron data

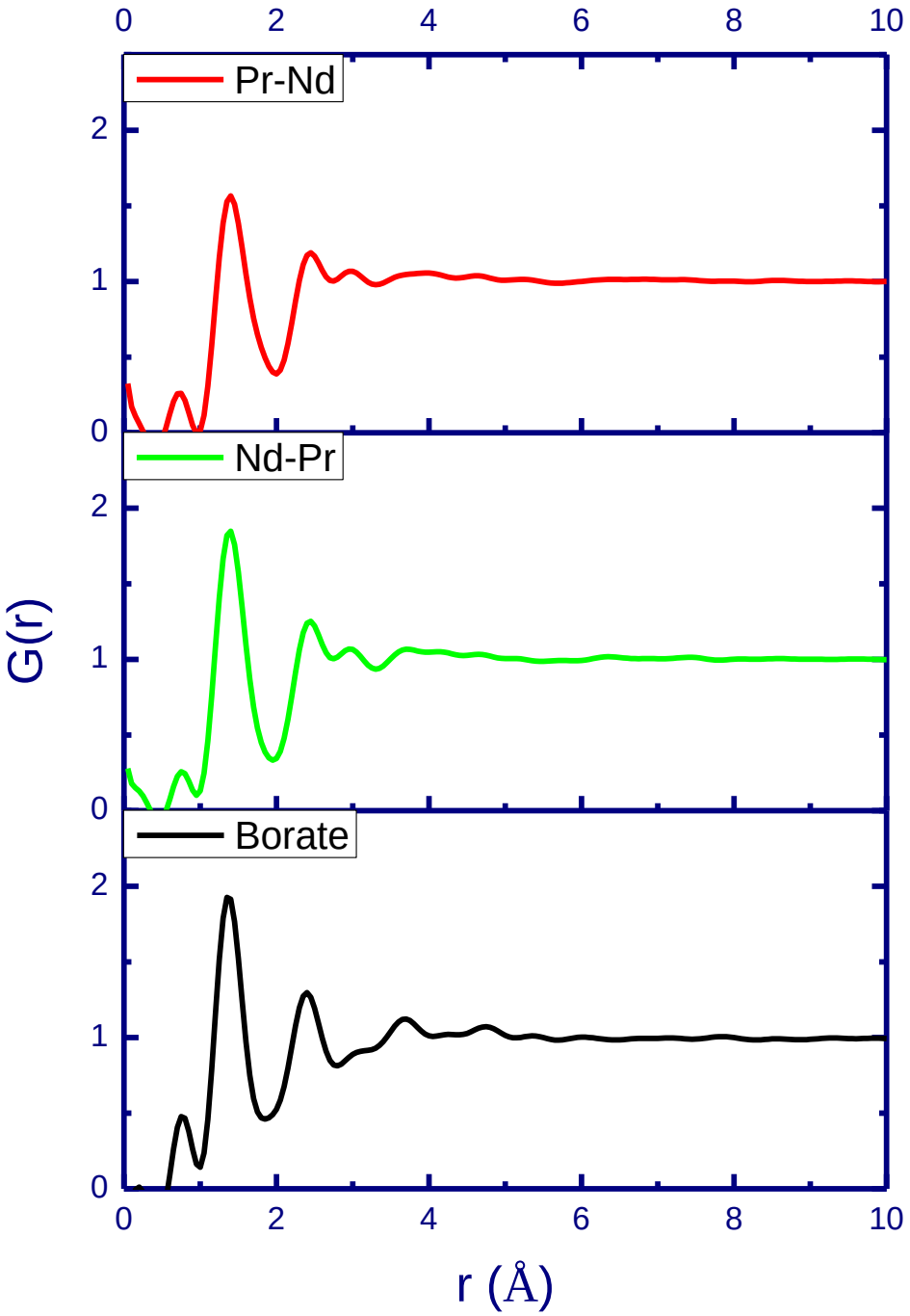

Figure 5.6.2.2: Pair-Correlation Function of the Nd_2O_3 – Pr_6O_{11} doped and undoped borate glasses from neutron data Fourier Transformation of S(q)

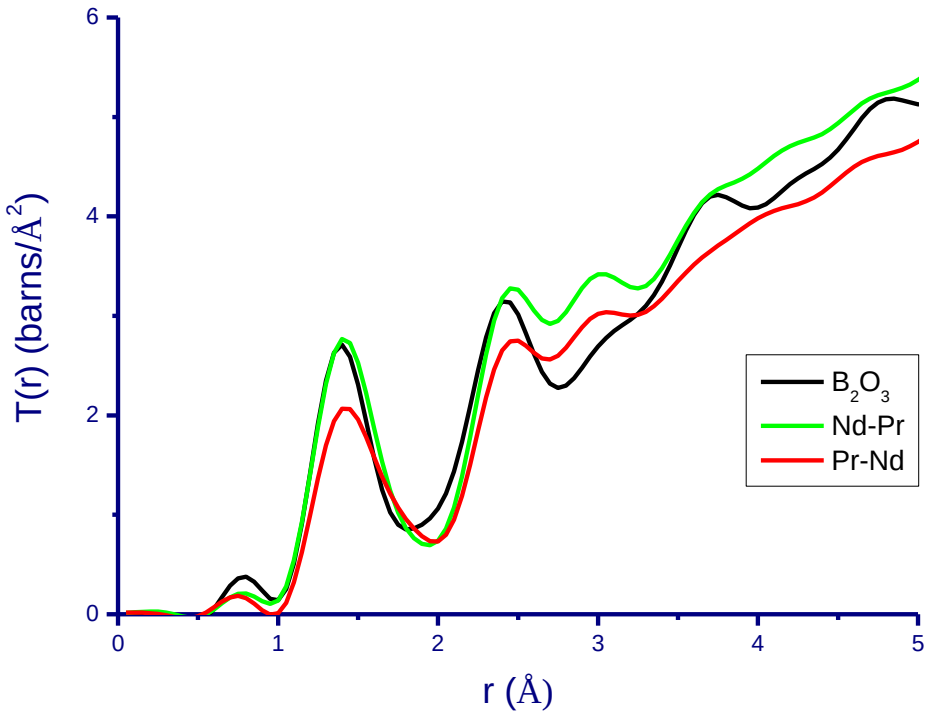

Figure 5.6.2.3: Overlay of Total Correlation Function of the Nd_2O_3 – Pr_6O_{11} doped and undoped borate glasses from neutron data by Fourier Transformation of S(q).

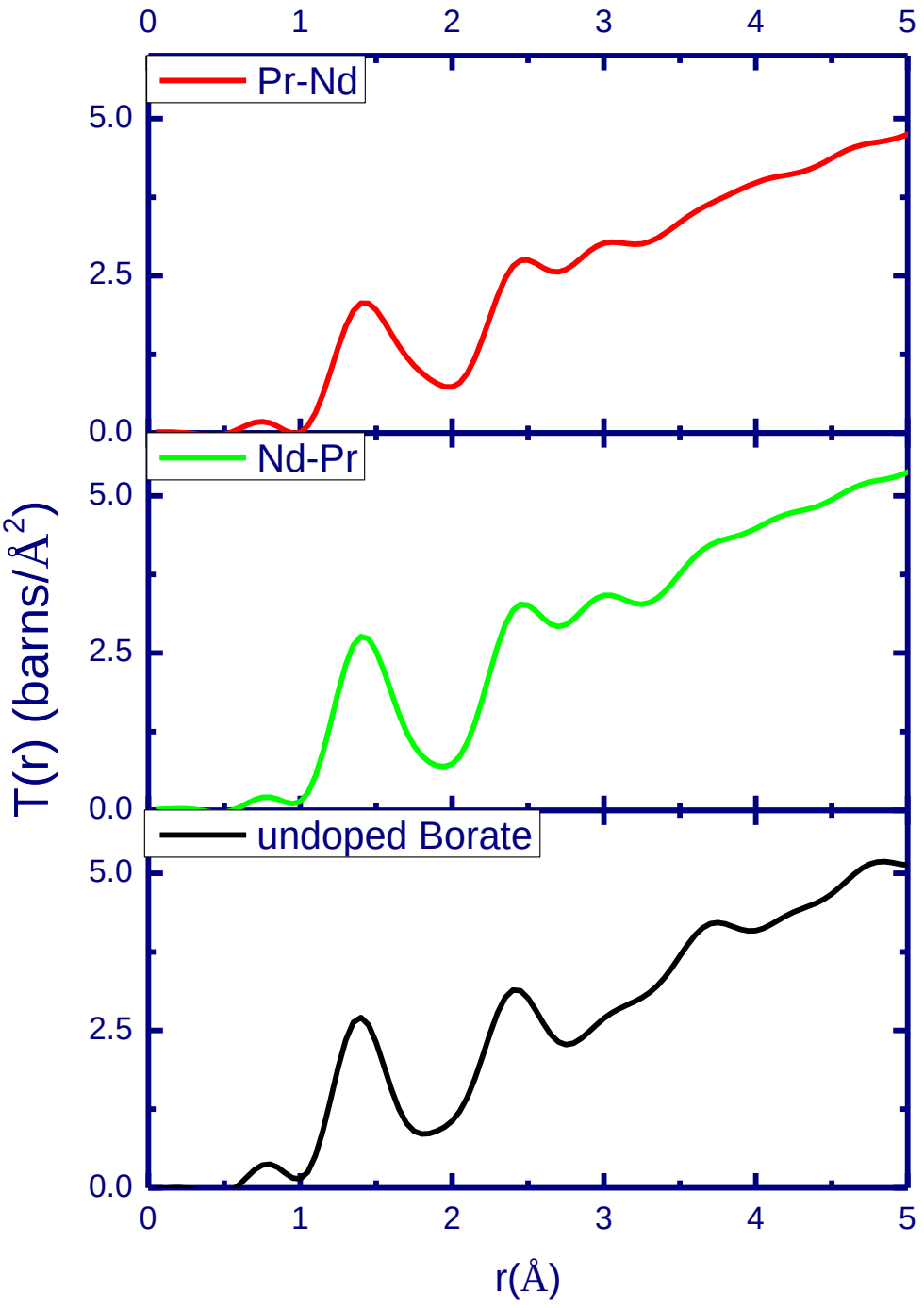

Figure 5.6.2.4: Total Correlation Function of the Nd_2O_3 – Pr_6O_{11} doped and undoped borate glasses from neutron data by Fourier Transformation of S(q).

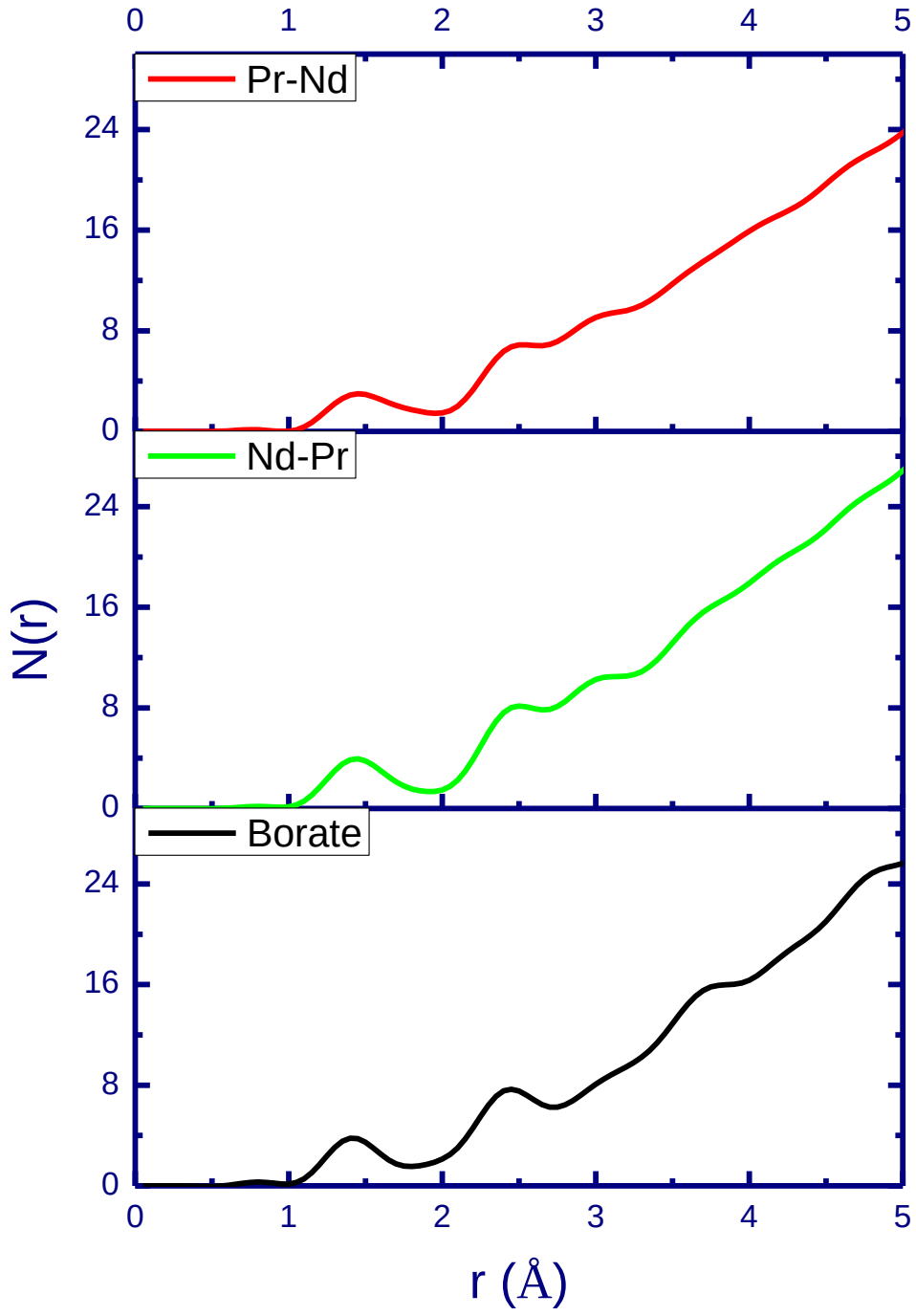

Figure 5.6.2.5: Radial Distribution Function of the Nd_2O_3 – Pr_6O_{11} doped and undoped borate glasses from neutron data by Fourier Transformation of S(q).

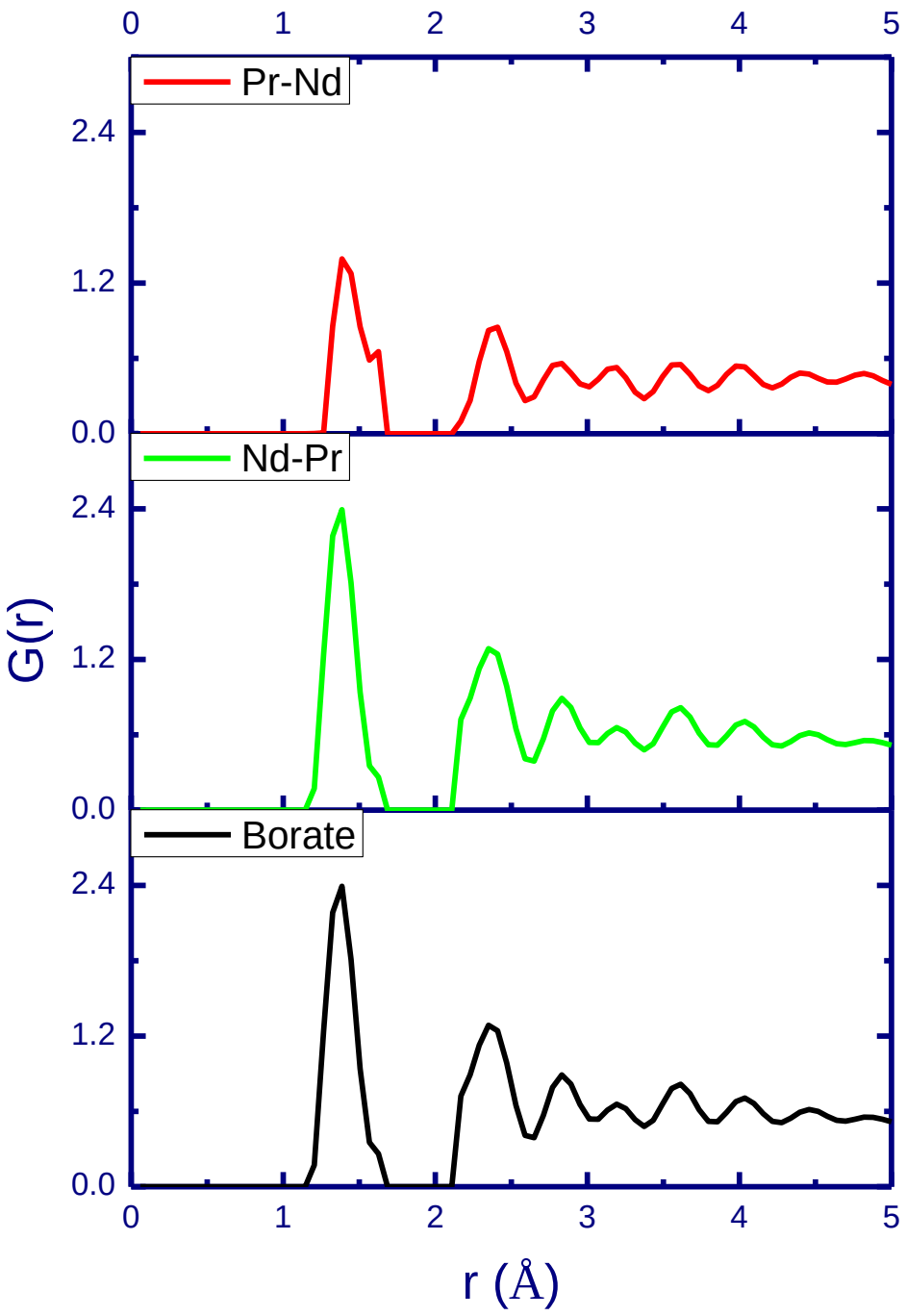

Figure 5.6.2.6: Pair-Correlation Function of the Nd_2O_3 – Pr_6O_{11} doped and undoped borate glasses from neutron data by MCGR.

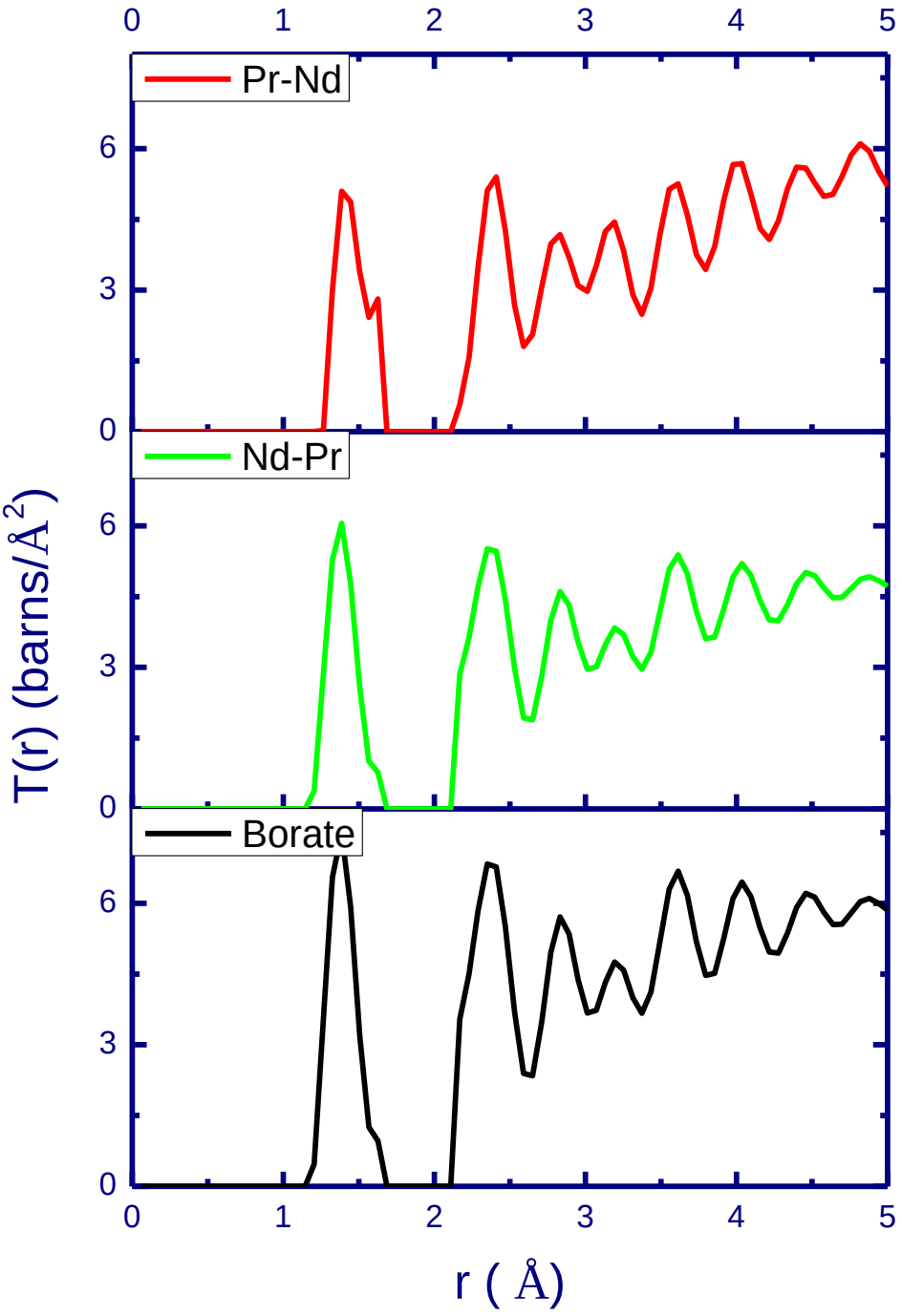

Figure 5.6.2.7: Total Correlation Function of the Nd_2O_3 – Pr_6O_{11} doped and undoped borate glasses from neutron data by MCGR.

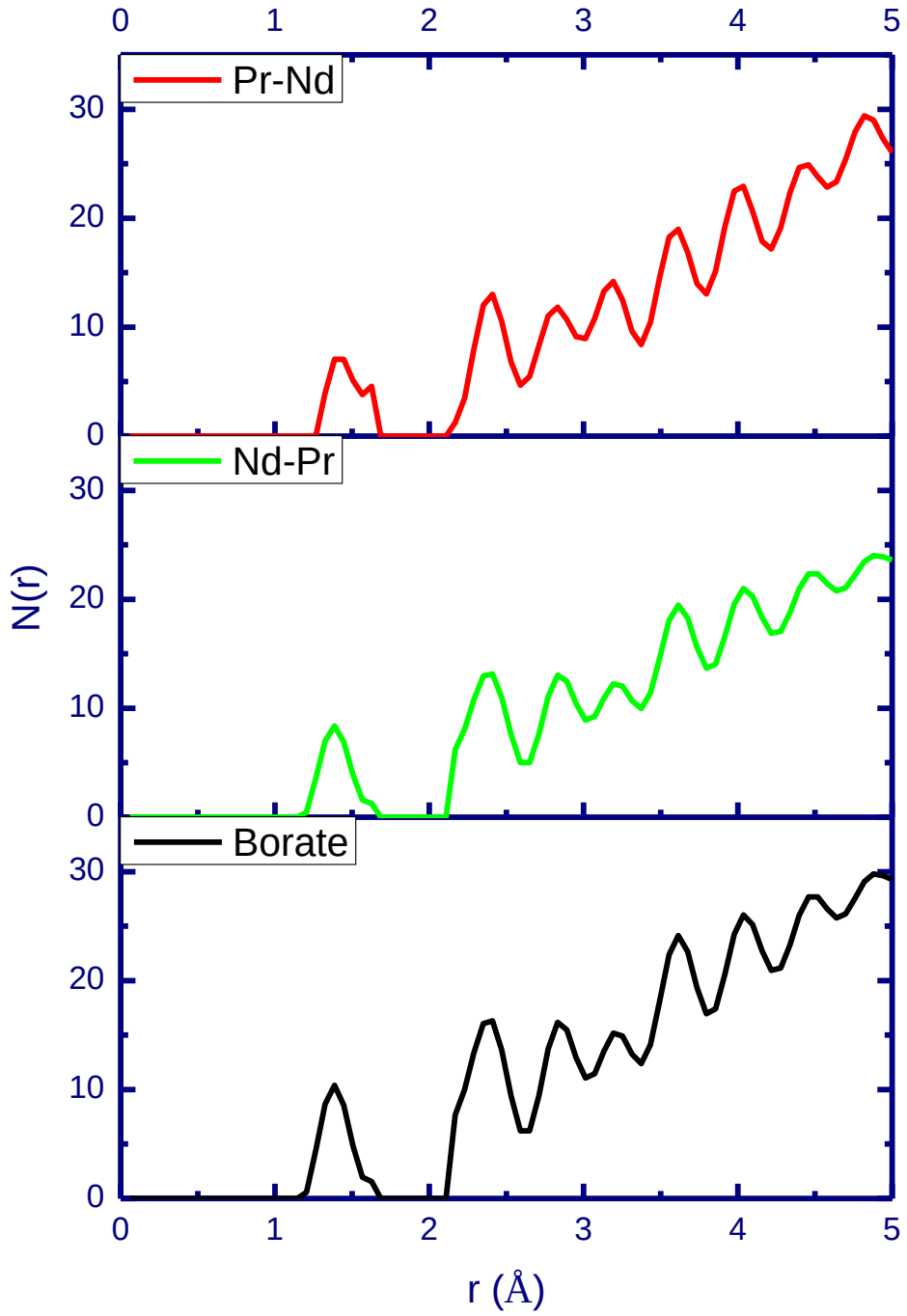

Figure 5.6.2.8: Radial Distribution Function of the Nd_2O_3 – Pr_6O_{11} doped and undoped borate glasses from neutron data by MCGR.

5. 7 Results and Discussion

5.7.1 Nd-Ho doped Borate Glasses

The initial neutron diffraction data on the Neodymium-Holmium borate glasses were measured using the E-2 neutron spectrometer at the HZB Reactor (see section 2.3.2). The data are shown in Figure 5.6.1.1. One of the glasses viz. the Nd10-Ho10 sample was measured at room temperature, and at three temperatures in the vicinity of the glass transition temperature (~ 780 ^{o}C) : below, at T_G , and above T_G . Although the data have not been analyzed due to unavailability of appropriate vanadium data by which the measured patterns could be normalized, it is clear that the samples were vitreous and that there are discernible differences in the patterns taken at different temperatures on the Nd10-Ho10 sample. These differences pertain to the Q range above 5 $Å^{-1}$. It is expected that medium to short-range differences in real space correlation functions will be observed once the data is fully analyzed for this particular sample. The purpose of these temperature - dependent diffraction patterns was to examine possible changes in nearest-neighbour correlations and coordinations as a glass cools from the liquid through T_G and into the glassy state. Such differences must await quantification on completion of the data analysis.

X-ray diffraction data on the same set of glasses as were used in the above-mentioned experiments at HZB were collected using CuK_{α} incident X-rays of the Rigaku D-MAX/B rotating anode X-ray diffractometer at B.A.R.C., Mumbai. The data are displayed in Figure 5.5.1.1. It may be noted that for sample Nd10-Ho10, the pattern is clearly from a crystalline sample. This was expected due to the fact that this particular sample had been held progressively at temperatures approaching the glass transition temperature for several hours at a time and was finally permitted to cool slowly at the highest of these temperatures. This caused it to devitrify as the presence of Bragg reflection peaks clearly confirm. The real space

correlation functions are shown in Figures 5.5.1.2, 5.5.1.3 and 5.5.1.4. Although coordination numbers have not been calculated from these data, they are useful in deciding important features such as the position of the Rare-earth-to-oxygen component correlation function – given that the X-ray data is more sensitive to the scattering from the rare-earth atoms than to the borate ions.

Neutron diffraction measurements using the High Q spectrometer at the Dhruva Reactor, B.A.R.C. were carried out on these glasses up to a maximum of 15 $Å^{-1}$. The structure factor functions are shown in Figure 5.6.1.2. All necessary experimental corrections and Fourier transformation with a Lorch modification function gave the pair distribution functions, total correlation functions and radial distribution functions displayed in Figures 5.6.1.3, 5.6.1.4, 5.6.1.5 and 5.6.1.6. The MCGR method was used in calculating G(r), N(r) and T(r) shown in Figures 5.6.1.7, 5.6.1.8 and 5.6.1.14 respectively. The peaks of T(r) in Figures 5.6.1.9, 5.6.1.10, 5.6.1.11, 5.6.1.12 and 5.6.1.13 were fitted to obtain the correlation lengths whereas the peaks of N(r) in Figures 5.6.1.15, 5.6.1.16, 5.6.1.17, 5.6.1.18 and 5.6.1.19 were fitted to obtain the coordination numbers.

The analysis of coordination numbers followed a similar approach as used in analyzing the Neodymium borate glasses (chapter 4). Calculation of coordination numbers from peak areas was made using the same expression as in Section 2. 2 (Equation 2.2.43). The first peak was assumed to be composed of B-O correlations from the BO_3 trigonal unit together with the BO_4 tetrahedra and is summarized in Table 5.7.1.1. The variation of four-fold coordination with rare-earth composition is shown in Figure 5.7.1.1. As expected in these glasses, the tetrahedral coordinated boron atoms is similar in all members of this series on account of the fact that there is no variation of total percentage of rare-earth in going from one member to

the next in this set. When the modifier cation is of a particular percentage, the number of tetrahedral-coordinated boron atoms remains the same.

In the second peak of N(r), the B-B and O-O correlations were assumed to have the same distances and coordinations as in the Nd-borate glasses of chapter 4. The scattering length for this particular correlation was calculated as a weighted average of the Nd and Ho values of scattering length based on their compositional percentages Table 5.7.1.2.

Table 5.7.1.1 lists the results of these estimations of coordination number. The Re-O coordination was found to generally decrease with increasing Ho content as shown in Figure 5.7.1.2. As the devitrified sample Nd10-Ho10 was not a glass, it was not included as a datum point in the latter Figure. The implication of Figure 5.7.1.2 is that as the percentage of Ho ion increases in the glass, there is a tendency for formation of octahedral oxygen coordination around the rare-earth ion.

The third peak in the calculated N(r) of the MCGR plot (Figure 5.7.1.3) was taken to be due to the next nearest B-O correlations and the values of coordination are shown in Table 5.7.1.1. The variation of the coordination numbers of 2^{nd} B-O with molar percentage of Holmium in the glasses is seen to slightly decrease from 6.6 to 6 as shown in Figure 5.7.1.3. The average value of each of these coordination numbers is a few percent lower than for the Nd glasses (of chapter 4) and since they relate to coordinations in the bulk, these numbers could be related to the extent to which the structures are compacted. The bulk densities of these Nd-Ho glasses were also measured to be a few percent lower than the Nd glasses.

The Re-B coordination number shows a clearly increasing trend with Holmium concentration in the composition unit of the glass as can be verified in Figure 5.7.1.4 and Table 5.7.1.1. The increasing trend of a larger boron coordination around the rare-earth ion could be arising

from a tendency for larger superstructural units to surround the Holmium ions, while the simpler units having only about one boron each could be surrounding the Neodymium ions. In such a configurational scheme, the number of borons around the Nd ions (~12.5) would be about the same as the oxygen atoms around the rare-earth (~ 10.5) while the number of borons (~17) would be about three times the number of oxygen neighbours of Ho (~5.5).

In summary, it may be said that these Nd-Ho glasses appear to ; leave the smallest structural BO_3 and BO_4 units unchanged; have less compacted structures than the Nd borate glasses; and have more complex superstructural units surrounding the Ho ions with the simpler units of the borate host surrounding the Nd ions.

5.7.2 Nd-Pr doped Borate Glasses

The measured S(q) data of the Nd-Pr and Pr-Nd glasses together with the pure or undoped borate glass are shown in Figure 5.6.2.1 and the Fourier transformed real space functions are shown in Figures 5.6.2.2, 5.6.2.3, 5.6.2.4 and 5.6.2.5 . Although the pure borate glass did not have a smooth shiny appearance, the diffraction data confirmed it to be a vitreous sample. The small undulations in S(q) at the higher values of q for all three samples are likely to have caused an additional peak in the correlation functions at 1.86 Å. The origin of these minor maxima in q space is not known. It was found that if the data was smoothed out, the peak at 1.86 Å was not obtained. This peak was fitted to a Gaussian and assumed to be a B-O correlation in the MCGR fit to the S(q). The coordination number was found to be approximately unity. Referring to the various structural units of B_2O_3 shown in Chapter 1, this particular peak could be ascribed to the B-O correlation in the diborate unit of approximately 1.86 Å.

The G(r), T(r) and N(r) functions obtained from the MCGR fits to the S (q) functions are displayed in Figure 5.6.2.6, 5.6.2.7 and 5.6.2.8. The coordination number of the first B-O correlation at 1.366 Å was found to be unacceptably low. A second attempt at calculating the total radial distribution function N(r) while suppressing the feature at 1.86 Å yielded a first coordination B-O shell of an even lower value. It is noted that in the region between 2.56 Å to 3.29 Å, these two glasses have different features in N(r) (Figure 5.6.2.8). In order to understand how these differences could have originated, it is necessary to examine the equation linking the area of a correlation function to its coordination number as given in Equation (2.2.43). In the latter, it can easily be shown that the weighting function of the Re-B coordination number (where Re stands for Nd and Pr) is 0.21956 for the Pr-Nd glass and 0.22464 for the Nd-Pr glass. If the coordination number of Re-B is approximately the same in the two glasses, then the area due to this particular correlation should be approximately the same. In order to explain the relative differences of the N(r) functions, the Re-B peak was taken to have the same area in each of the two glasses. With this valid assumption, the total N(r) was shown to be approximately reproduced in the region 2.56 to 3.29 Å by shifting two Gaussian peaks relative to each other – one due to the B-O correlation of the boroxol ring at about 2.74 Å and the other due to the Re-B correlation lying between 3.08 and 3.19 Å. The result of these qualitative trials was that the B-O correlation shifts from its value of 2.74 Å in the Pr-Nd glass to a higher value of 2.82 Å in the Nd-Pr glass while the Re-B correlation in the Pr-Nd glass shifts from 3.18 Å to a lower value of 3.08 Å in the Nd-Pr glass. The latter is similar to the value of the Nd-B correlation reported in Chapter 4 and in Section 5.7.1.

From the above observations and qualitative fits to the data, it may be concluded that when Pr is added to an Nd borate glass such that there is a predominance of Pr ions, the average Re-B correlation distance increases with a simultaneous decrease in the B-O correlation within the boroxol ring.

Table 5.7.1.1: Peak Positions and Coordination number of first four correlations of Nd-Ho doped Borate Glasses

Correlation type	Sample	Av. b sqr	Area Ce	Peak Positions (Å)	Coord. No.
				± 0.002	± 0.01
	Ho-0	0.3875	2.1306	1.366, 1.485	3.3430
1st Peak	Ho-5	0.3883	2.1089	1.366, 1.549	3.3156
B-O	Ho-15	0.3899	2.1205	1.366, 1.563	3.3476
	Ho-20	0.3907	2.0972	1.366, 1.561	3.3177
2nd Peak	Ho-0	0.3875	1.9508	2.366, 2.468	10.5873
2nd	Ho-5	0.3883	1.2117	2.366, 2.467	6.5221
Gaussian	Ho-15	0.3899	0.9944	2.366, 2.472	5.2656
Re-O	Ho-20	0.3907	1.1167	2.366, 2.478	5.8663
2nd Peak	Ho-0	0.3875	1.9350	2.366, 2.468	10.5015
2nd	Ho-5	0.3883	1.1959	2.366, 2.467	6.4371
Gaussian	Ho-15	0.3899	0.9786	2.366, 2.472	5.1824
Re-O	Ho-20	0.3907	1.1010	2.366, 2.478	5.7839
3rd Peak	Ho-0	0.3875	4.2183	2.868	6.6186
B-O	Ho-5	0.3883	3.8193	2.863	6.0049
	Ho-15	0.3899	3.8181	2.861	6.0277
	Ho-20	0.3907	3.8285	2.851	6.0565
	Ho-0	0.3875	2.6423	3.231	12.5140
4th Peak	Ho-5	0.3883	3.0801	3.244	14.4669
Re-B	Ho-15	0.3899	3.2640	3.244	15.0829
	Ho-20	0.3907	3.8160	3.242	17.4936

Table 5.7.1.2 : Areas of the second peak calculated by assuming coordination numbers of Nd-Ho doped borate glasses.

Correlation type	Sample	Conc. Ce	Boron b1	Boron b2	av b sqr	Coord. No.	Area Ce
B-B	Ho-0	0.3200	0.6650	0.6650	0.3875	3.2000	1.1686
2nd peak	Ho-5	0.3200	0.6650	0.6650	0.3883	3.2000	1.1662
2nd	Ho-15	0.3200	0.6650	0.6650	0.3899	3.2000	1.1614
Gaussian	Ho-20	0.3200	0.6650	0.6650	0.3907	3.2000	1.1590
Correlation type	**Sample**	**Conc. Ce**	**Oxygen b1**	**Oxygen b2**	**av b sqr**	**Coord. No.**	**Area Ce**
O-O	Ho-0	0.6000	0.5803	0.5803	0.3875	7.2000	3.7541
2nd peak	Ho-5	0.6000	0.5803	0.5803	0.3883	7.2000	3.7464
2nd	Ho-15	0.6000	0.5803	0.5803	0.3899	7.2000	3.7311
Gaussian	Ho-20	0.6000	0.5803	0.5803	0.3907	7.2000	3.7234
Correlation type	**Sample**	**Conc. Ce**	**Boron b1**	**Boron b2**	**av b sqr**	**Coord. No.**	**Area Ce**
B-B	Ho-0	0.3200	0.6650	0.6650	0.3875	5.0000	1.8259
2nd peak	Ho-5	0.3200	0.6650	0.6650	0.3883	5.0000	1.8222
2nd	Ho-15	0.3200	0.6650	0.6650	0.3899	5.0000	1.8147
Gaussian	Ho-20	0.3200	0.6650	0.6650	0.3907	5.0000	1.8110
Correlation type	**Sample**	**Conc. Ce**	**Oxygen b1**	**Oxygen b2**	**av b sqr**	**Coord. No.**	**Area Ce**
O-O	Ho-0	0.6000	0.5803	0.5803	0.3875	6.0000	3.1284
2nd peak	Ho-5	0.6000	0.5803	0.5803	0.3883	6.0000	3.1220
2nd	Ho-15	0.6000	0.5803	0.5803	0.3899	6.0000	3.1092
Gaussian	Ho-20	0.6000	0.5803	0.5803	0.3907	6.0000	3.1029

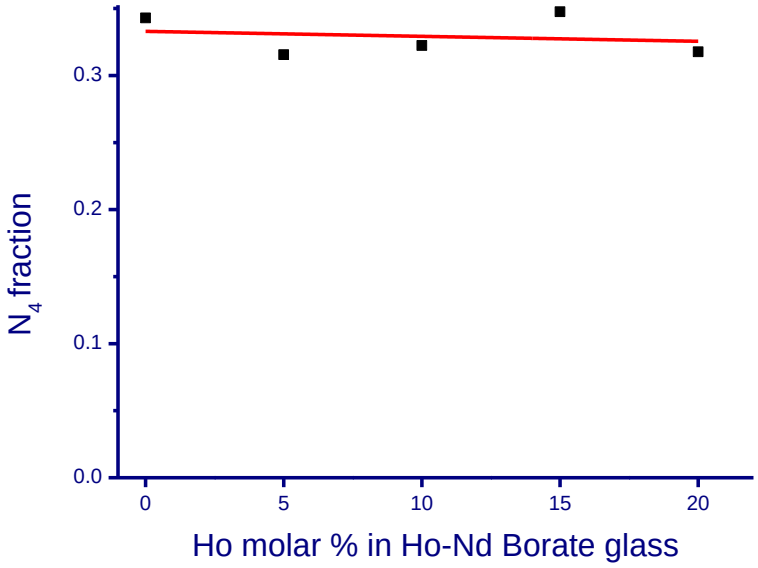

Figure 5.7.1.1: Variation of fraction of 4-fold coordinated B from 1st peak in N(r) with Ho% in Nd-Ho glasses.

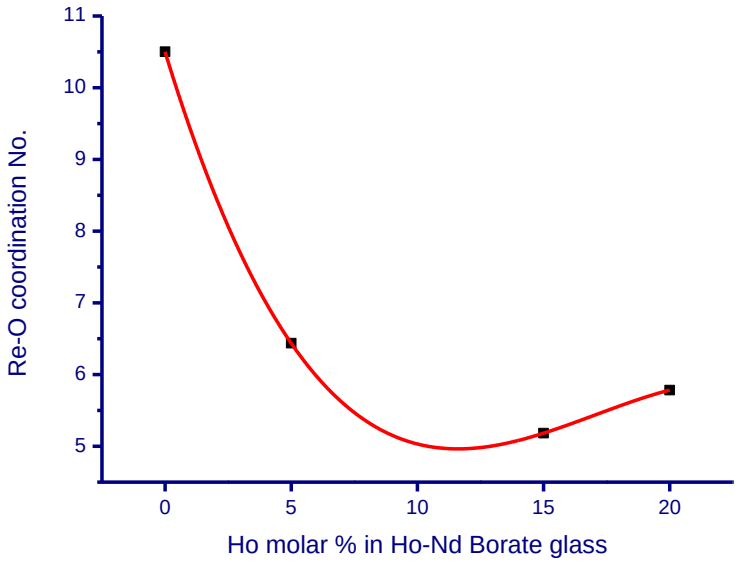

Figure 5.7.1.2: Variation of Re-O coordination from 2nd peak in N(r) with Ho% in Nd-Ho glasses.

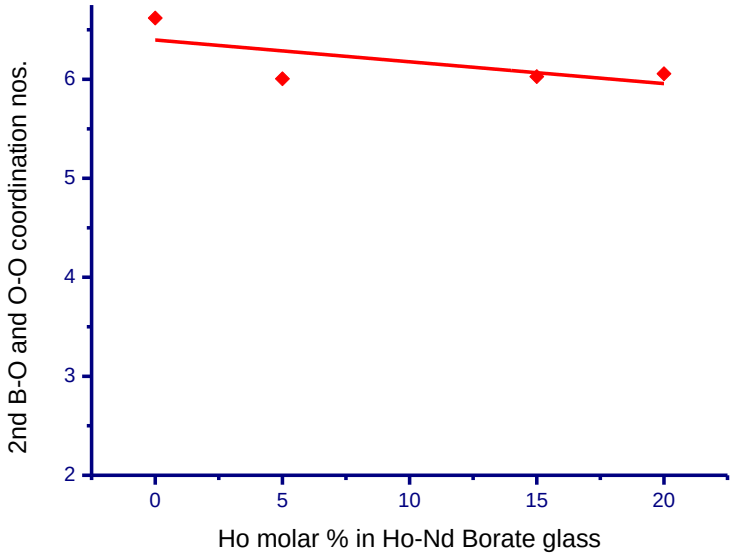

Figure 5.7.1.3: Variation of B-2ndO coordination from 3rd peak with Ho% in Nd-Ho glasses.

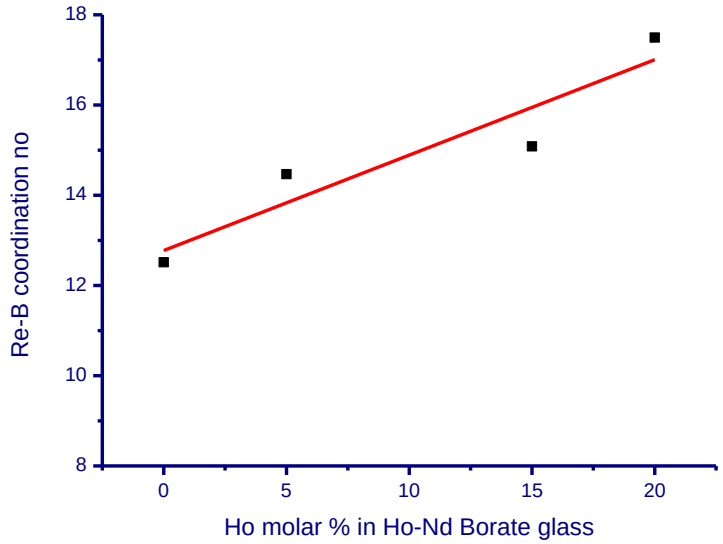

Figure 5.7.1.4: Variation of Re-B coordination from 4th peak with Ho% in Nd-Ho glasses.

References

1. Ahoussou A.P., Rogez J., Kone A., Thermochim. Acta, 441 (2006) 96.
2. Branda F., Constantini A., Fresa R., Buri A., Phys. Chem. Glasses 36 (1995) 272.
3. Constantini A., Buri A., Branda F., Solid State Ionics, 67 (1994) 175.
4. Day D.E., J. Non-Cryst. Solids 21 (1976) 343.
5. Elbers S., Strojek W., Koudelka L., Eckert H., Solid State Nucl. Magn. Reson., 27 (2005) 65.
6. Feng T. and Linzhang P., J. Non-Cryst. Solids, 112 (1989) 142.
7. Ingram M.D., Phys. Chem. Glasses 28 (1987) 215
8. Isard J.O., J. Non-Cryst. Solids 1 (1969) 235
9. Takebe H., Harada T., Kuwatara M., J. Non-Cryst. Solids 352 (2006) 709.
10. Villa M., Scagliotti M., Chiodelli G., J. Non-Cryst. Solids, 94 (1987) 101.
11. Yun Y. H., Bray P. J., J. Non-Cryst. Solids, 30 (1978) 45.
12. Zeyer-Dusterer M., Montagne L., Palavit G., Jager C., Solid State Nucl. Magn. Reson., 27 (2005) 50.

Chapter 6

Structural Studies of Coated and Compacted Microspheres of Silica Glass

Glasses can be coated in various ways by different compounds. The type and quality of a deposited film will depend on the method used, the particular compound chosen and the application of the coated surface. If a porous material is coated in its bulk, the effective surface area greatly increases as compared to a coated planar surface. In all such cases, it is important to characterize the compound after it has been successfully coated on the surface in order to check for changes in structure of the coating. For example, an oxide might change its valency state on becoming coated onto a glass surface and in such a structural change, its original physical and chemical properties might be lost.

While all the foregoing work was concerned with doping cations in the bulk of a glass, this Chapter describes the efforts at depositing several different compounds onto the surface of commercially available silica microspheres and characterizing the structures of these depositions. The coated spheres were then compacted and sintered to form porous but rigid pellets which were examined by different techniques. The effort was considered to be relevant to the making of porous active surfaces having high surface area to volume ratios. Although detailed structural analyses of the materials after being coated onto the microspheres were not undertaken, change of phase from glassy to crystalline -or vice versa-; or from one crystal phase to another were checked.

6.1 Introduction

Micro-spheres of silica having diameters from 10 to 500 μm are commercially available in a mixture of different sizes. These may be sieved and separated out into particular diameter ranges and compacted (Carrasco (2005). The compacts are useful as both sensors and sieves of particulate matter. When coated with different compounds (such as semiconductors or catalysts) and then compacted, the physical properties of these effectively porous materials may be appreciably altered.

The effort of coating the micro-spheres of silica has focused on the following materials:

(a) **Silver metal**

Materials containing silver are known to have antibacterial properties (Modak and Fox (1973), Berger et al. (1976) and Williams (1989)). Some inorganic compounds containing Ag having such properties are already in commercial use (Oloffs (1994)). Compounds releasing Ag ions over a longer time period are desirable in composite resins used for dental restorations.

(b) **Nickel metal**

The electroless deposition process has been used for Ni to produce coatings at low cost, ease of control and with excellent corrosion and wear resistance ((Gawrilov (1979), Mallory and Hadju (1991) and Riedel (1991)). Hypophosphite-reduced and dimethylamine borane (DMAB) – reduced electroless Nickel deposition (Delaunois et al. (2000), Delaunois and Lienard (2002), Chiba et al. (2003), Sankara et al. (2003), Osaka (2003), Dervos et al. (2004) and Chiba et al. (2004)) have been well used in recent years.

(c) **Zinc Oxide**

ZnO is an n-type semiconductor with a wide band gap of 3.37 eV, large exciton binding energy (60 meV), excellent chemical stability has found wide usage in photodetectors (Lu et al. (2006)),

field emission displays (Xu and Sun (2003)), light emitting diodes (Saito et al.(2002)), UV light emitters (Chen et al. (2006)), biosensors (Wang et al. (2006)).There are many methods for ZnO deposition including chemical vapour deposition, molecular beam epitaxy, RF sputtering, chemical bath deposition (CBD) etc. CBD although inexpensive prove to be reproducible only with very narrow deposition parameters (Yi et al.(2007)). The properties of ZnO depend on its morphology, microstructure which in turn determine its applications in optoelectronic devices. At present, reproducibility of ZnO crystals from CBD is still a challenge (Ouerfelli et al. (2006)).

(d) **Cadmium Sulphide**

Cds and other II-VI semiconductor compounds have wide applicability in solar cells, photoconductive sensors and other optical devices (Nadjakov et al. (1954), Hall and Meakin (1979), Hedstrom et al. (1993), Britt and Ferekides (1993)). Techniques such as evaporation, sputtering, MBE, electrodeposition and CBD have been used. The CBD technique (O'brien and Saeed, (1996)) in particular is attractive on account of the normal temperature and pressure conditions during deposition and the possibility of large-area thin CdS coatings onto glass substrates that are possible with this method.

(e) **Rare-earth borate glasses**

The Nd-Pr borate glasses described in Chapter 3 were shown to be luminescent. The effort at producing bulk luminescent glasses by coating these glasses onto silica microspheres and effectively folding these coated surfaces onto themselves to produce bulk surface emitters was the objective in these coating attempts.

The above materials ((a) to (e)) were chosen for their relevance to presently known catalytic (Nickel), bio-active (Silver), semiconducting (CdS), multi-use (ZnO) or luminescent properties

(rare-earth containing). No measurements are reported in this work on the special applications of the porous pellets coated with the above compounds as the focus here was on successfully depositing and characterizing the coatings themselves.

6.2 SAMPLE PREPARATION

6.2.1 Coating with Silver

Solutions of Silver Nitrate and Sodium Hydroxide were mixed and AgO particles precipitated out. To this a solution of ammonia was added (drop by drop) until the AgO dissolved to form Tollen's reagent. Meanwhile, a glucose solution (10 g in 10 cc) was made up and the MSG was dropped in it. The Tollen's reagent was then added slowly to the glucose solution. A coating of silver metal was observed to form on the sides of the beaker while the MSG itself was seen to have a dull grey colour.

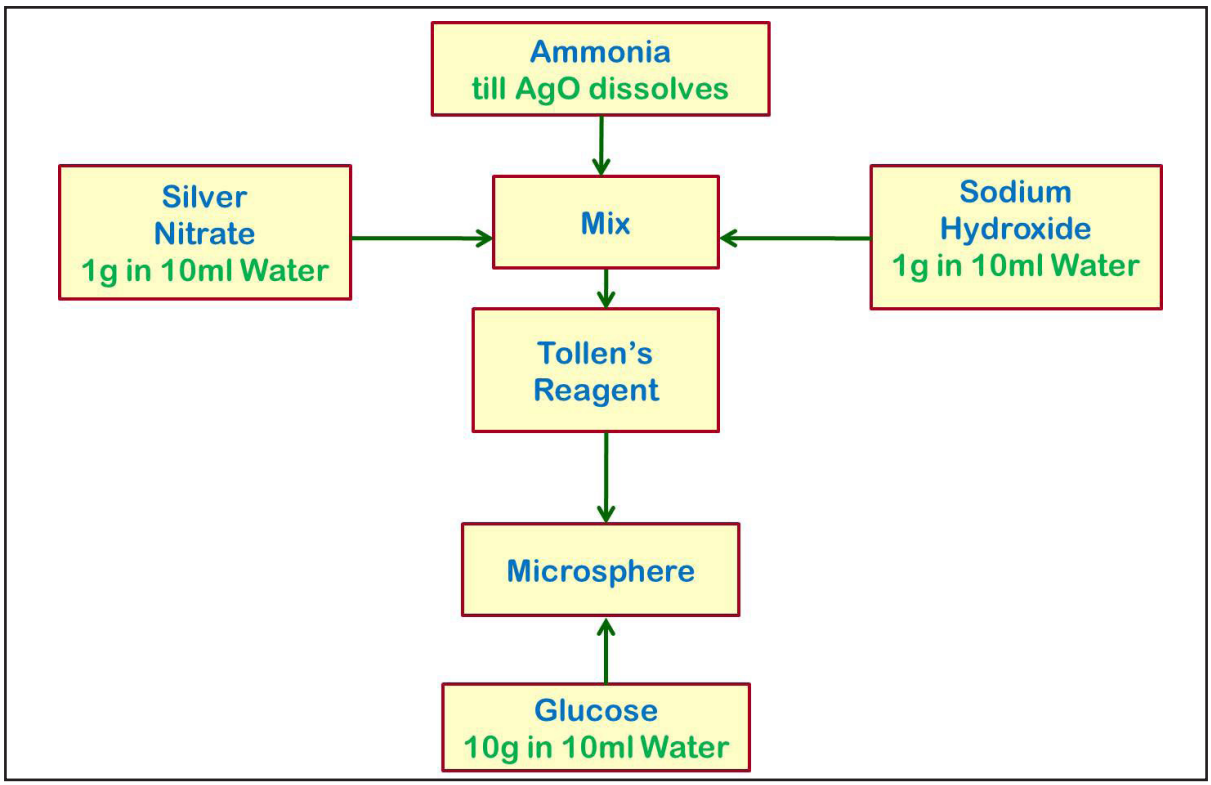

Figure 6.2.1.1: Schematic of the Silver deposition procedure

6.2.2 Coating with Nickel

To 100 ml of distilled water, 8 gm of Nickel Sulfate was added, and then 7 gm of Sodium citrate, followed by 5 drops of sodium chloride solution for wetting and the beaker was labeled A. 5 gm of Na hypo-phosphite was added to 100 ml water in beaker B (El-Mohamad (1975). The MSG were buffed in 0.1N Hydrofluoric acid. 10 ml of stannous chloride was added to these spheres and kept for a short while. The spheres were removed and then put into Palladium Chloride solution. Contents of beakers A and B were mixed and kept in water bath which was at 75 – 78 C. A few drops of concentrated ammonia were added till the solution turned blue. And then the microspheres dropped into this mixture making sure that excess $PdCl_2$ did not accompany them. Nickel deposition was observed on the spheres.

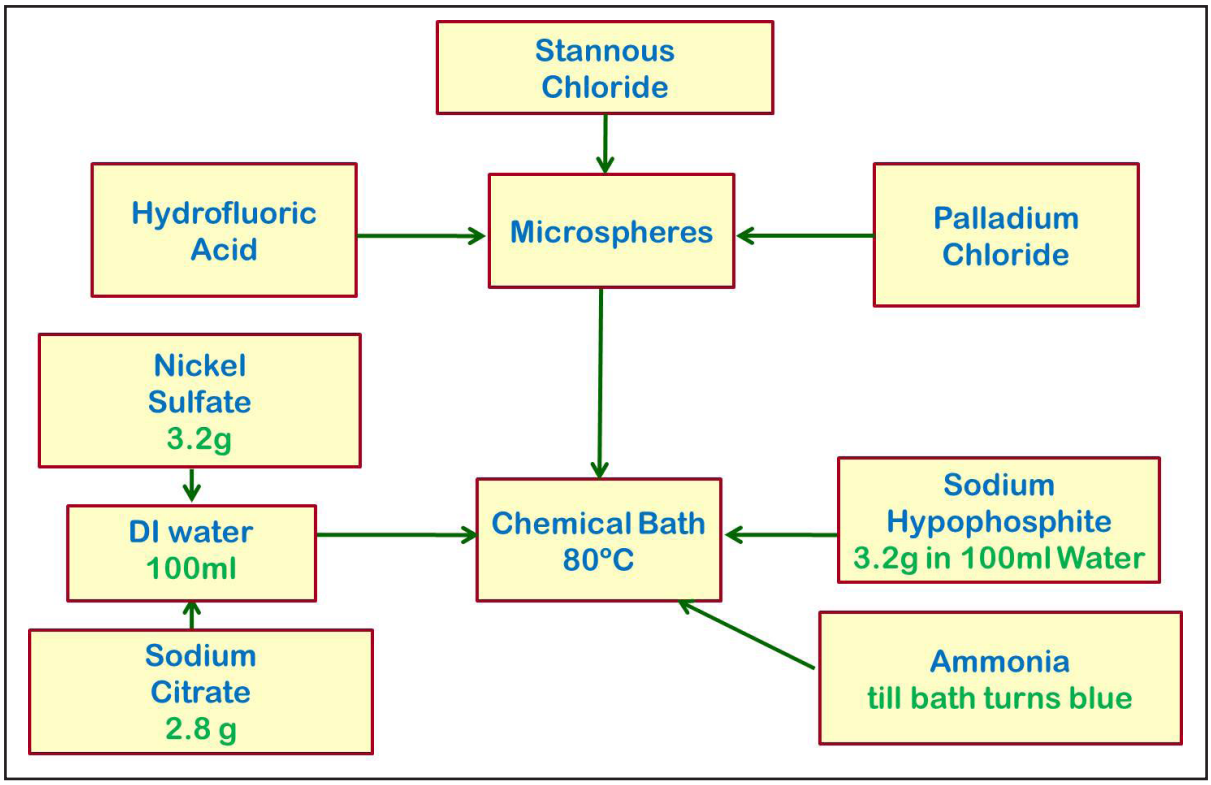

Figure 6.2.2.1: Schematic of the electroless Nickel deposition procedure.

6.2.3 Coating with Zinc Oxide

ZnO thin films were grown on microspheres by the Chemical Bath Deposition technique(Huang et al.(2009)). Before the deposition, the glass microspheres were cleaned using acetone followed by alcohol, then deionized water, each for 15 minutes. The CBD bath contained 20 ml of 0.15 mol/liter zinc sulfate as the zinc source, 20 ml of 0.05 mol/liter ammonium sulfate as the buffer agent, 40 ml of ammonia (1mol/liter) as a chelating agent for controlling the release of Zn2+ ions during the reaction and the base offering OH^-.

The glass microspheres were poured into the chemical bath for thin film growth. During CBD, the solution was maintained at a temperature between 80-85°C and its pH was at 9.5–11, while the bath was continuously stirred with a magnetic stirrer at about 25 rev/s for 20 minutes. After completion of film deposition, the glass microspheres were taken out of the solution and rinsed with deionized water.

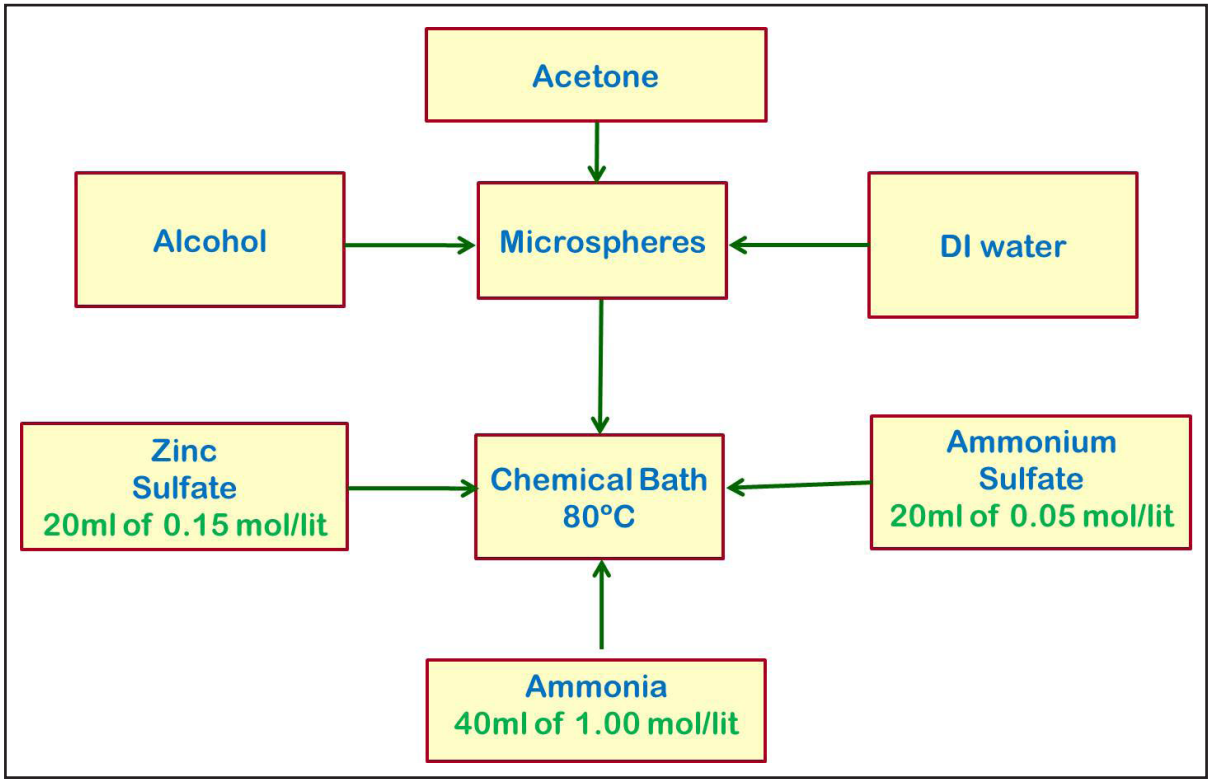

Figure 6.2.3.1: Schematic of the Chemical Bath deposition procedure of Zinc Oxide.

6.2.4 Coating with Cadmium Sulfide

CdS thin films were deposited on MSG using the CBD technique (Rami et al. (1999)). The bath concentration of various reagents used are as follows: 0.12 mol/l of 3.0ml CdCl2; 15ml of 20% NH3, 0.1 mol/l of 12ml of NH4Cl, 0.3 mol/l of 6.0ml of thiourea and 75ml of de-ionized water to make up to 111ml of solutions which were mixed in a 250ml beaker. The pH of the reaction bath was determined to be 11.15.

The MSG were dropped in the beaker. The films were deposited on the MSG and stirring it using magnetic bar and hot plate with stirrer at 80°C for 60 minutes. After the 60 minutes, the MSG was withdrawn, rinsed with distilled water, and drip dried in air. CdS thin films were observed to be deposited on the glass were uniform, well adherent to the substrates and yellow in colour.

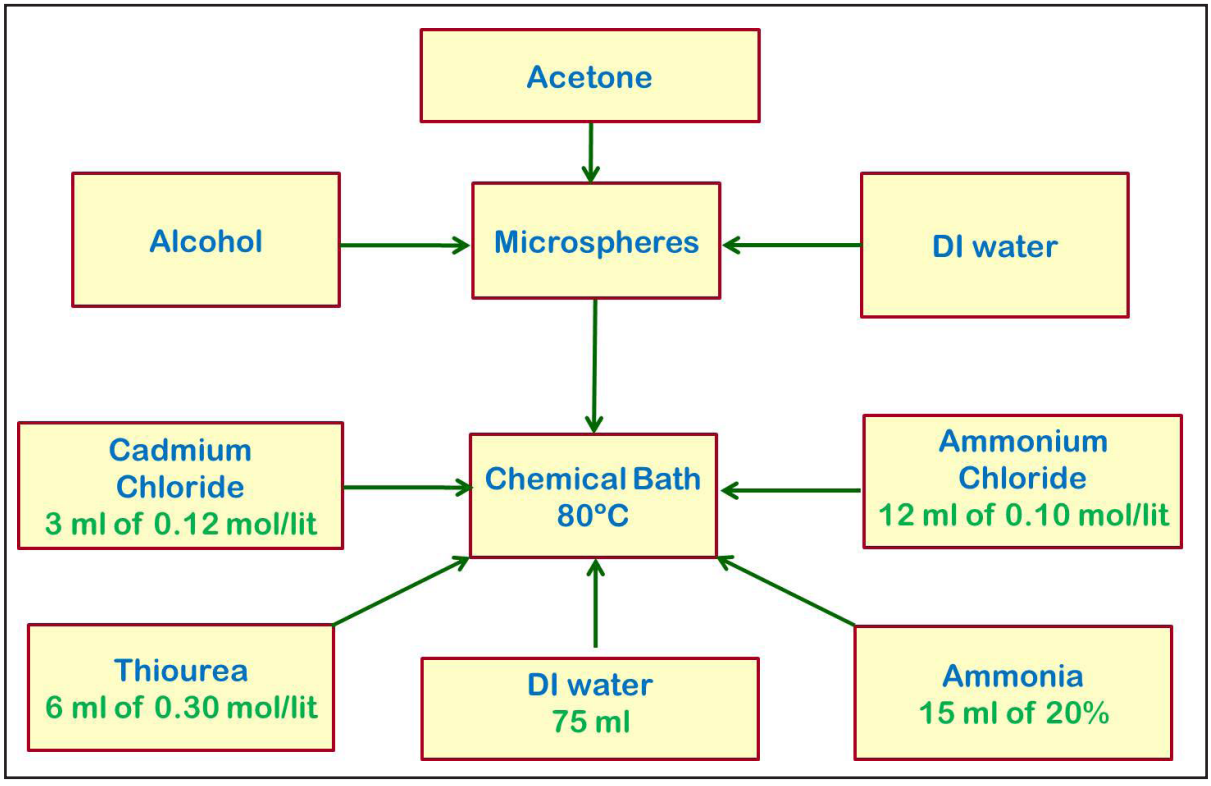

Figure 6.2.4.1: Schematic of the Cadmium Sulphide deposition procedure.

6.2.5 Coating with Rare-Earth Borate Glasses

Oxide glass is an attractive host matrix for light emitting ions because it has transparency, good mechanical strength and is chemically stable. The principal motivation of coating the microspheres with luminescent glasses was to effectively produce luminescent beads which could then be easily compacted together to form a bulk though porous luminescent material. The luminescent properties of the coatings were earlier checked and reported in Chapter 3.

6.2.6 Compacting the Coated Silica Microspheres

All the coated samples were separately mixed with Polyethylene Glycol (PEG) and ethanol and dried for 24 hours at 60ºC. After drying, 0.5g of the each of the differently coated microspheres-PEG mixture was loaded into a steel die (13 mm diameter) and kept under 2 ton pressure (2.1 x 106 Pa) for 10 minutes to produce pellets of ~ 2mm thickness and 13 mm diameter. All the pellets were sintered in air at 640 ºC for 18 hours. The schematic of the preparation process of the pellets of coated microspheres is shown in Figure 6.2.6.1. The neutron diffraction measurements required relatively large volumes of sample and for these particular experiments a specially designed die was used in which long cylinders of the compacted material were made. The diameter of these was 8 mm while the length was 40 mm.

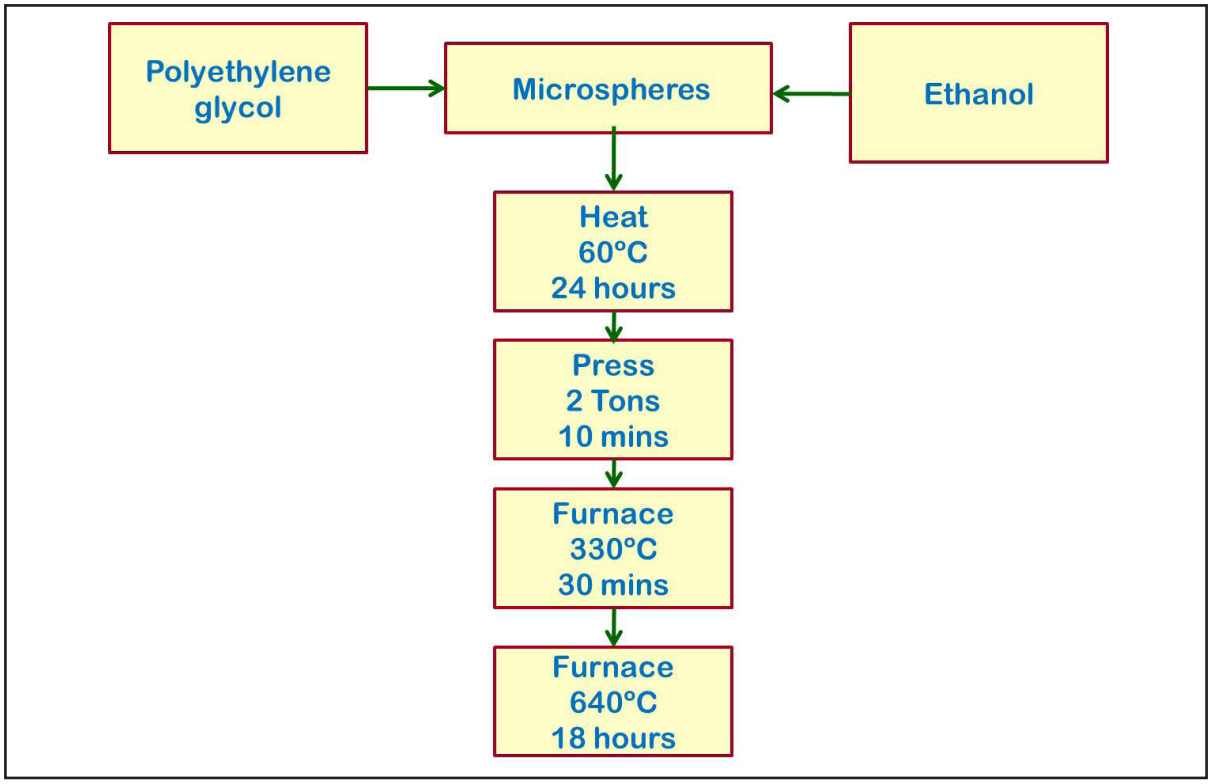

Figure 6.2.6.1: Schematic of the preparation process of the pellets of coated microspheres.

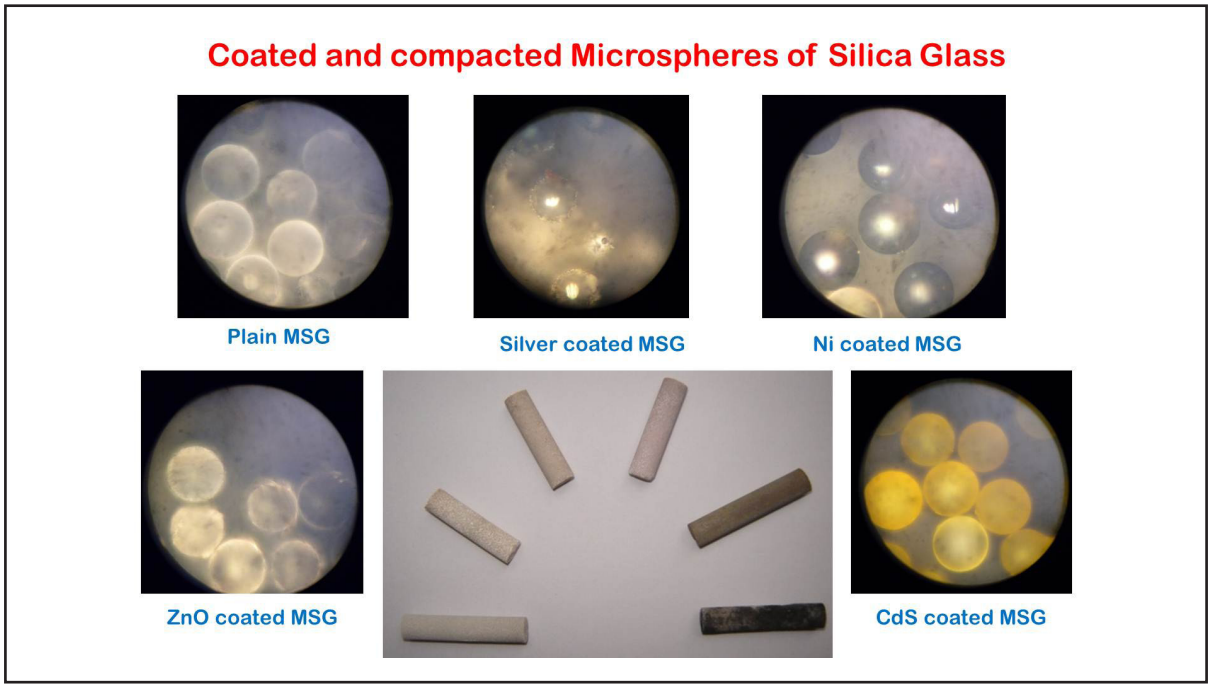

Figure 6.2.6.2: View of the cylindrical pellets and microscopic views of the coated compacts.

6.3 X-ray Diffraction

The X-ray diffraction data (using 1.54 Å incident X-rays) were obtained on both the loose microspheres that had been coated with the different compounds as well as on the compacts of these microspheres that had been sintered at 640 ^{o}C. The stacked data are shown in Figures 6.3.1 and 6.3.2.

6.4 Neutron Diffraction

Neutron diffraction measurements were made using the High Q diffractometer at Dhruva Reactor with 0.783 Å incident neutrons. The samples were all in the form of long cylinders that had been sintered as described in Section 6.2.6. Neutron diffraction patterns of Ag, Ni, ZnO and rare-earth coated and uncoated compacts of microspheres shown in Figures 6.4.1 to 6.4.4.

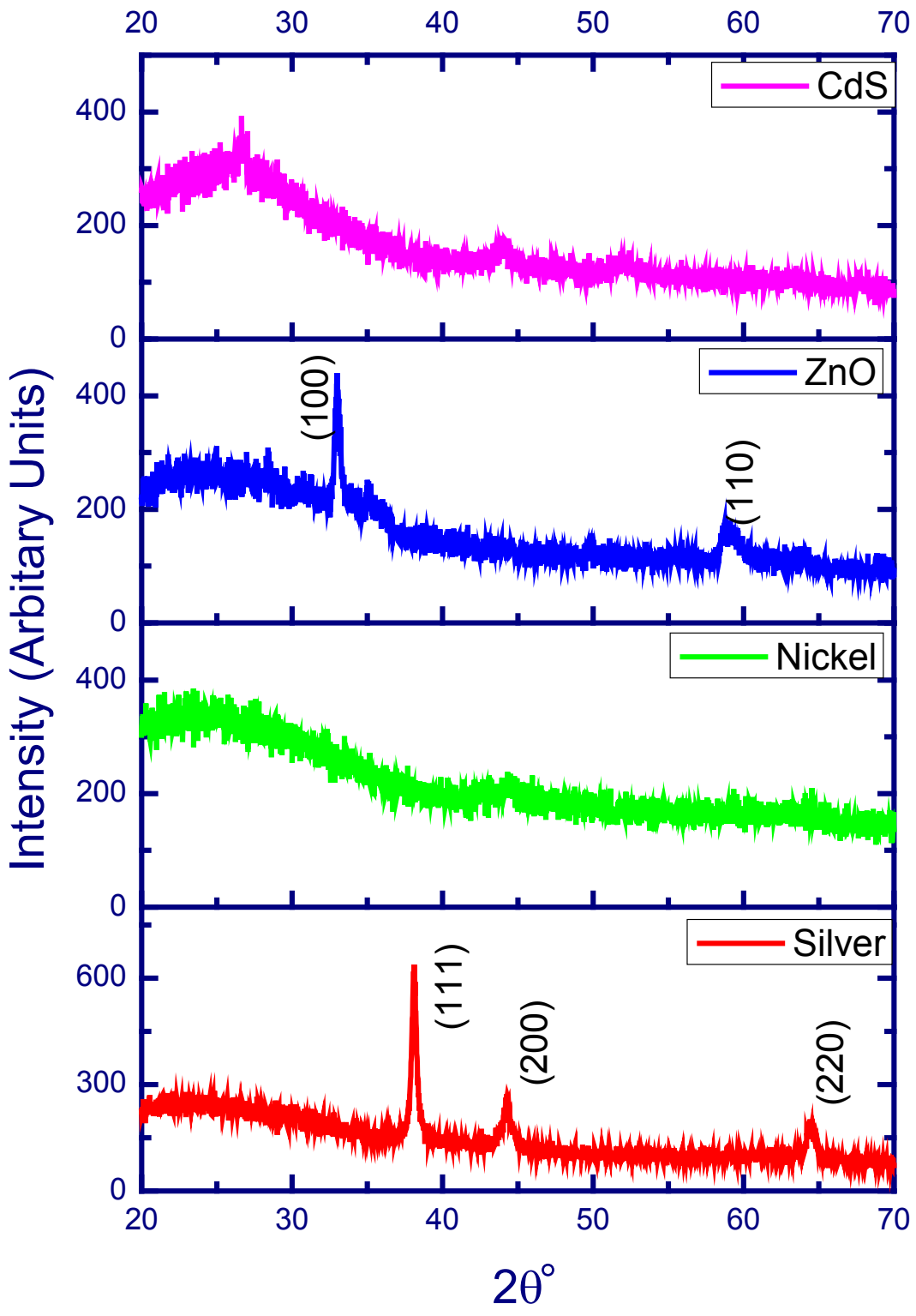

Figure 6.3.1: X-ray diffraction patterns of the coated microspheres before sintering.

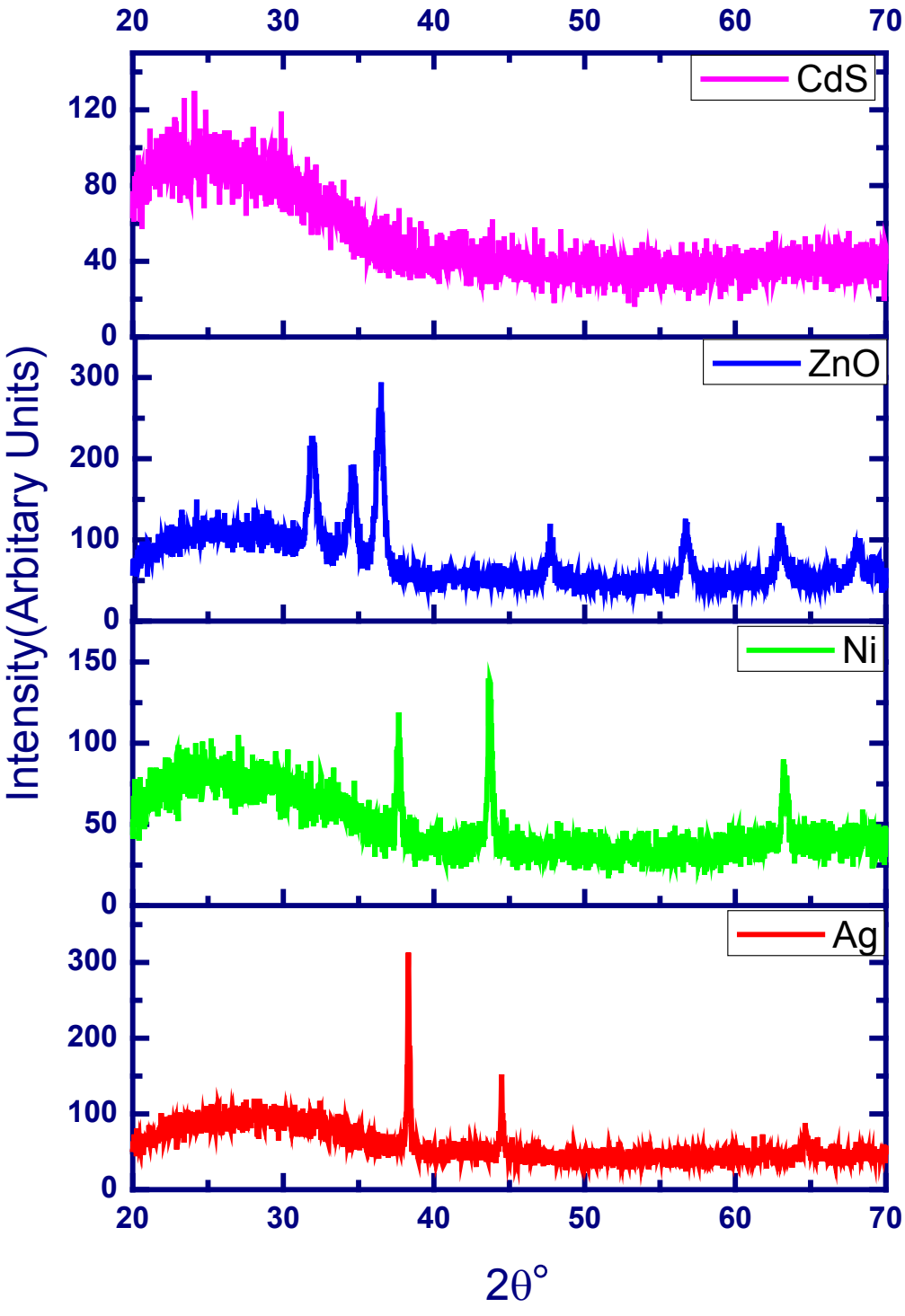

Figure 6.3.2: X-ray diffraction patterns of the coated microspheres after sintering at 640 °C.

The d-spacing for Silver and ZnO are given below :

Silver

No.	h	k	l	d [A]	2Theta	I [%]
1	1	1	1	2.35039	38.262	100.0
2	2	0	0	2.03550	44.473	45.1
3	2	2	0	1.43932	64.713	22.3

Zinc Oxide

No.	h	k	l	d [A]	2Theta	I [%]
1	1	0	0	2.80739	31.850	55.8
2	0	0	2	2.59380	34.552	41.0
3	1	0	1	2.46903	36.358	100.0
4	1	0	2	1.90514	47.698	21.8
5	1	1	0	1.62085	56.751	31.8
6	1	0	3	1.47232	63.093	28.4
7	2	0	0	1.40370	66.565	4.3
8	1	1	2	1.37454	68.168	23.5
9	2	0	1	1.35497	69.291	11.6

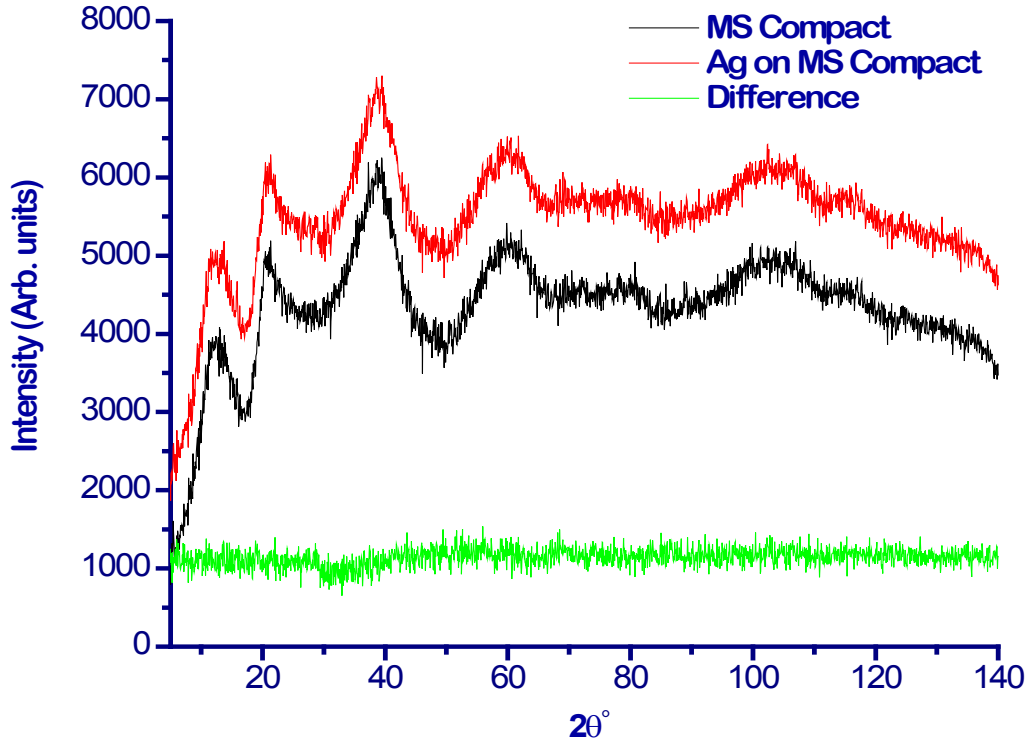

Figure 6.4.1: Neutron diffraction patterns of Ag-coated and uncoated compacts of microspheres (with arbitrary zero offsets) and their difference.

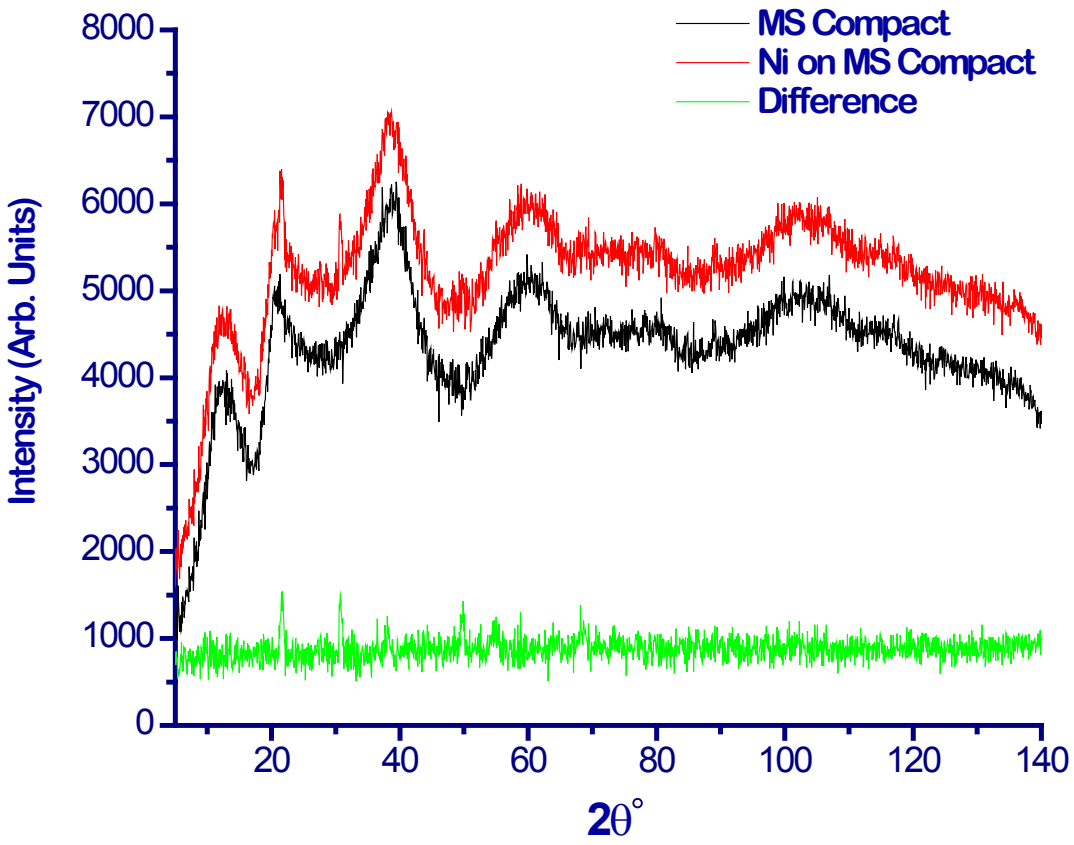

Figure 6.4.2: Neutron diffraction patterns of Ni-coated and uncoated compacts of microspheres (with arbitrary zero offsets) and their difference.

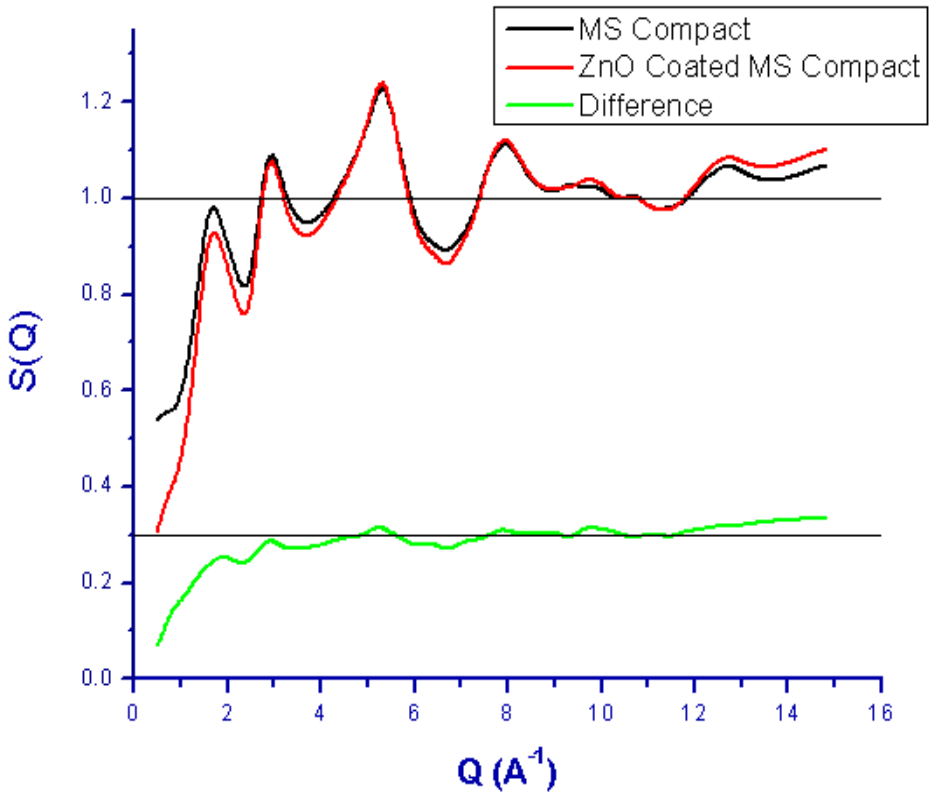

Figure 6.4.3 : Neutron diffraction S(Q) of ZnO-coated and uncoated microspheres (with arbitrary zero offsets) and their difference.

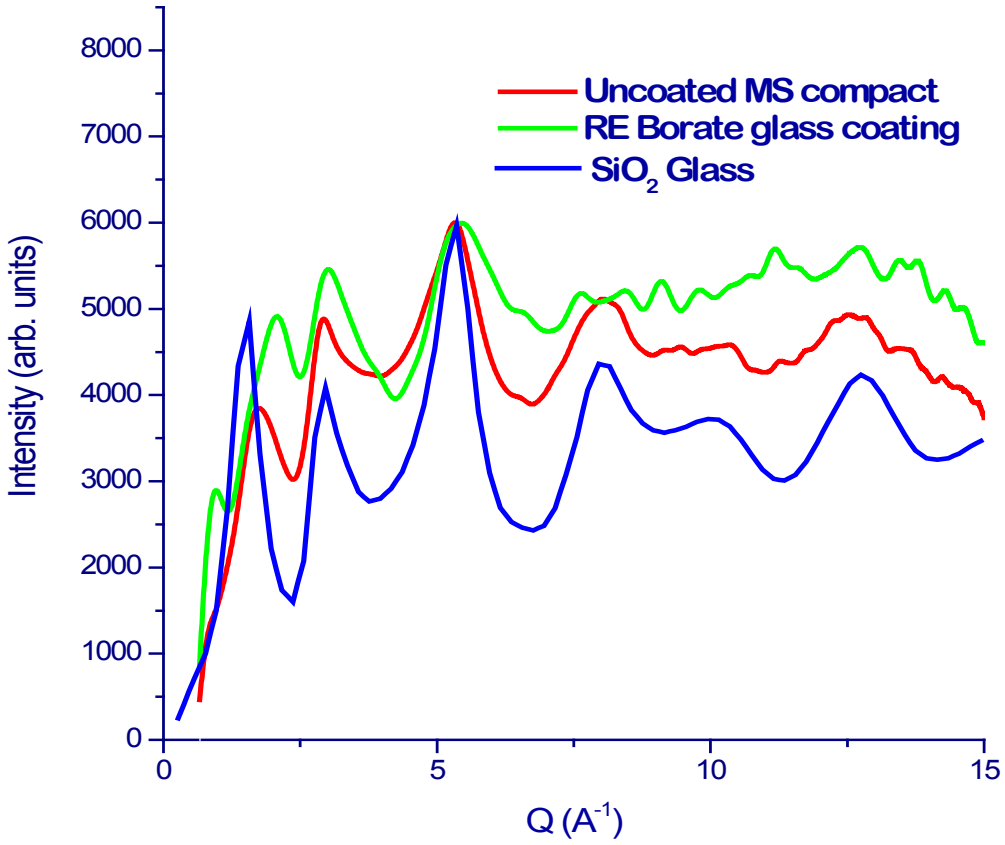

Figure 6.4.4: Neutron diffraction patterns of Nd-Pr borate glass coated onto microspheres compared with uncoated microspheres and a silica glass.

6.5 Results and Discussion

6.5.1 X-ray Diffraction Studies

It is noted that in the unsintered CdS sample, some evidence of crystallinity is present through weak Bragg reflections at 27^{o} and 44^{o} . The sintered CdS sample shows no evidence of the presence of the coated material. It is likely that this particular coated compound had evaporated during the sintering process. However, as shown in Figure 6.2.6.2 cadmium sulphide had been clearly deposited onto the microspheres by the well-known process outlined in Section 6.2.4.

The X-ray diffraction patterns relating to the deposition of ZnO and Ag - both for the unsintered and sintered samples – show that the process of sintering causes the reflection peaks to be narrower and better resolved. This may have been due to the loss of compounds (during sintering) other than ZnO and Ag that had been produced by the deposition process in each case as well as possible reduction in mosaic spread of the micro-crystals.

The diffraction data on the Ni deposited sample clearly shows three prominent reflections in the sintered sample. However, all attempts to match these peaks with expected reflections from Nickel and various Nickel compounds were unsuccessful. Nevertheless, the presence of a crystalline compound after sintering of the Nickel deposition onto the microspheres has been established.

6.5.2 Neutron Diffraction Studies

Apart from the CdS coated sample, all the above-mentioned coated samples were used in these measurements including the microspheres coated with the Nd borate glass. The diffraction patterns are shown in Figures 6.4.1, 6.4.2, 6.4.3 and 6.4.4. The diffraction pattern of the Nickel coated sample is the only one of these comparisons that shows evidence of Bragg reflection peaks superimposed on a glassy diffraction pattern due to the silica microspheres. The reason for poor signal from the coatings themselves is likely to be the fact that in a neutron diffraction

measurement, a large amount of sample is normally required for good counting statistics because of the fact that neutrons are electrically neutral particles. It is likely that all the coatings consisted of only thin layers of the deposited compounds. The Q values of the peaks at 22^{o}, 31^{o} and 50^{o} in the Nickel coated sample of Figure 6.4.2 are 3.06, 4.29 and 6.78 $Å^{-1}$ respectively. In Figure 6.3.2, the X-ray diffraction pattern of the same Ni coated sample showed peaks at 37.5^{o}, 44^{o} and 63^{o} which corresponded respectively to Q values of 2.63, 3.06 and 4.26 $Å^{-1}$. Thus the 2^{nd} and 3^{rd} peaks in the X-ray data of Figure 6.3.2 are the same reflections as the 1^{st} and 2^{nd} peaks of the difference pattern of the neutron data of Figure 6.4.2.

The comparisons of the neutron diffraction patterns in Figure 6.4.4 show the pattern of the uncoated microspheres as being similar to the pure silica pattern above the first sharp diffraction maximum (FSDP). The FSDP for the microspheres is at a slightly higher Q value indicating that the correlation length decreases from about 5 Å in pure silica to about 4 Å in the glass of the microspheres which is known to be a soda-lime-silica glass. Similarly the microspheres coated with the Nd borate glass has an FSDP at an even higher Q value corresponding to a correlation length of about 3 Å. The main diffraction features in the pattern of this glass is however quite different from that of the uncoated glass. This might have been due to the fact that the coating has a high concentration of Boron-10 which is known to be a strong neutron absorber and will result in poor counting statistics especially at higher Q values.

In conclusion it may be noted that the effort at depositing the compounds i.e. Ag, ZnO, Ni, CdS and a borate glass onto silica microspheres were successful. However, when these coated microspheres were compacted and sintered to form rigid porous pellets, only the Ag and ZnO survived the heat treatment and remained unchanged in structure. The Ni metal changed its structure and composition to some –as yet unidentified – compound of Nickel while CdS evaporated away. The coated borate glass is likely to have remained coated onto the silica microspheres as evidenced by the neutron diffraction pattern of this coated sample.

The present efforts at coating the glass microspheres have much relevance to applications of advanced catalysts, semiconductors, bacteriological control materials, UV absorption materials etc. Further characterizations of the coatings by techniques such as SANS could confirm the presence of nano-crystalline dimensions.

References

1. Berger T.J., Spadaro J.A., Chapin S.E., Becker R.O., Agents Chemother, 9 (1976) 357-8.
2. Britt J. and Ferekides C., Appl. Phys. Lett., 62 (1993) 2851
3. Carrasco M.F., Mendiratta S.K. and Ferreira J.M., Eur. Phys., J.Appl. Phys. 30 (2005) 91-99
4. Chemical Nickel Plating, U.S. Patent, El Mohamad, 3,903,319 (Sept. 2, 1975)
5. Chen P. L., Ma X. Y. and Yang D. R., Appl. Phys. Lett., 89 (2006) 111112
6. Chiba A., Haijima H., Wu W.C., Ultrasonics 42 (1–9) (2004) 617
7. Chiba, H. Haijima and Kobayashi K., Surf. Coat. Technol. 169–170 (2003) 104
8. Delaunois F. and Lienard P., Surf. Coat. Technol. 160 (2–3) (2002) 239
9. Delaunois F., Petitjean J.P., Lienard P., Jacob-Duliere M., Surf. Coat.Technol. 124 (2–3) (2000) 201
10. Dervos C.T., Novakovic J., Vassiliou P., Mater. Lett. 58 (5) (2004) 619
11. Gawrilov G.G., Chemical (Electroless) Nickel Plating, Portcullis Press Ltd, Surrey, 1979
12. Hall R.B. and Meakin J.D., Thin Solid Films, 63 (1979) 203
13. Hedstrom J., Ohlsen H., Bodegard M., Kylner A., Stolt L., Hariskos D., Ruckh M. and Schock H.-W., Proc. 23rd IEEE PVSC (1993) 364
14. Huang S.M., Bian Z.Q., Chu J. B., Wang Z. A., Zhang D.W., Li X. D., Zhu H. B. & Sun Z., J. Phys. D: Appl. Phys. 42 (2009) 055412
15. Lu C.Y., Chang S.J., Chang S.P., Lee C.T., Kuo C.F., Chang H.M., Chiou Y.Z., Hsu C.L. and Chen I.C., Appl. Phys. Lett., 89 (2006) 153101

16. Mallory G.O., Hadju J.B. (Eds.), Electroless Plating: Fundamentals and Applications, AESF, Orlando, 1991.

17. Modak S.M. and Fox C.L.J., Biochem Pharmacol, 22 (1973) 2391- 404.

18. Nadjakov G., Andreitchine R. and Borissov M., Izu. Bulg. Akad. Navk., 4 (1954) 10.

19. O'brien Poul and Saeed Tahir, J. Crystal Growth, 158 (1996) 477.

20. Oloffs C., Grosse-Siestrup C., Bisson S., Rinck M., Rudolph R., Gross U., Biomaterials 15 (1994) 753- 8.

21. Osaka T., Takano N., Kurokawa T., Kaneko T., Ueno K., Surf. Coat. Technol. 169–170 (2003) 124.

22. Ouerfelli J., Regragui M., Morsli M., Djeteli G., Jondo K., Amory C., Tchangbedji G., Napo K. and Bernede J.C., J. Phys. D: Appl. Phys., 39 (2006) 1954.

23. Rami M., Benamar E., Fahoume M., Chraibi F. and Ennaqui A., Solid State Sciences, t. 1 (1999) 179-188

24. Riedel W., Electroless Plating, ASM International, Ohio, 1991.

25. Saito N., Haneda H., Sekiguchi T., Ohashi N., Sakaguchi I. and Koumoto K., Adv. Mater., 14 (2002) 393.

26. Sankara Narayanan T.S.N., Krishnaveni K., Seshadri S.K., Mater. Chem.Phys. 82 (3) (2003) 771.

27. Wang J. X., Sun X. W., Wei A., Lei Y., Cai X. P., Li C. M. and Dong Z. L., Appl. Phys. Lett., 88 (2006) 233106.

28. Williams R.L., Doherty P.J., Vince D.G., Grashoff G.J., Williams D.F., Crit Rev Biocompat; 5 (1989) 221- 43.

29. Xu C. X. and Sun X. W., Appl. Phys. Lett. 83 (2003) 3806

30. Yi S.H., Choi S.K., Jang J.M., Kim J.A. and Jung W.G., J. Colloid and Interface Sci., 313 (2007) 705.

Chapter 7

Conclusions

7.1 Optical Studies of Rare-Earth Doped Borate Glasses

A set of 5 rare-earth borate glasses was prepared and examined by optical and X-ray diffraction methods. The essentially vitreous nature of the glasses was confirmed by the X-ray diffraction patterns in which there was no evidence of any Bragg crystalline reflections. The rare-earth ions Nd and Pr were included in the borate individually and in pairs and their UV-Visible spectra were also measured. The UV-Visible absorption spectra from the glasses possessing the single rare-earth ion types could be linearly superposed to match – in frequencies of absorption peaks - the measured spectra of those glasses having both rare-earth elements. It appears that neither rare-earth ion affects the frequencies of the UV-visible absorptions of the other. However, some small discrepancies were observed in intensities of absorption which related to the transition probabilities of 4f electrons of the rare-earth ions. The presence of one rare-earth ion type affected the absorption intensities of the other. Judd-Ofelt theory suggests that detailed transition probabilities are affected by next-nearest neighbour structures around the rare-earth ions. In order to gain some understanding of this finding, neutron diffraction studies were made on these glasses and some qualitative evidence was found for changes in structure of the glass when both rare-earth ion types are present in the borate glass – as discussed in Chapter 5.

FTIR data on these glasses confirmed the presence of B-O-B bending modes and BO_3 symmetric and asymmetric breathing modes of partially devitrified B_2O_3 glass to be also present in these glasses. As expected, the intensities of these modes were both weaker and less well-resolved in the glasses as compared to the partially crystalline sample.

Luminescent data (in the 800 nm to 900 nm range) on these glasses found the decay times

associated with emissions in the visible by Nd and Pr ions to be in the range of 1.094 to 1.225 μs. As these decay times are found to be similar to those for the same ions in a phosphate glass host, it may be concluded that luminescent levels are hardly affected by the structure of the glassy host.

7.2 Neodymium Dopant Ions in Borate Glass

Neodymium was included in a borate host glass by mixing Nd_2O_3 with B-11 boric acid in the preparation stage. The Nd fraction in the unit composition unit of the glass was varied by adding between 10 to 25 mole% of Nd_2O_3 to the starting mixture. Both neutron and X-ray diffraction data on this set of glasses were obtained. The analyses of these data sets are summarized as follows :

The first peak at 1.366 Å in the total correlation function T(r) calculated from the measured S(Q) shows a slight asymmetry in the trailing (higher r) part of the peak. In this as well as in all other diffraction data that were analysed in this work, the total radial distribution function N(r) of the MCGR calculations were used. The coordination number of oxygen around B was found to be greater than 3 for all the members of this set of glasses. The fraction of four-fold coordinated boron at 1.45 Å was seen to increase with molar percentage of the Nd_2O_3 (in a quadratic dependence) from 28% to 40% of all boron atoms being in tetrahedral coordination with oxygen.

The second peak in T(r) was ascribed to a combination of B-B together with O-O at 2.366 Å and Nd-O at about 2.5 Å. Whether the relative coordinations of B-B and O-O are 5 and 6 or 3.2 and 7.2 respectively, the Nd-O coordination number decreases quadratically with Nd_2O_3 molar % from about 9.5 to 6 coordination of oxygen around Nd. The latter decrease is proposed to be due to the coordination of Nd with the oxygen atoms belonging to the more complex structural units at lower Nd concentrations in the glass, while at higher Nd concentrations, simpler

units such as BO_3 and BO_4 would be mainly surrounding the Nd ions in the glass leading to octahedral coordination of O around Nd.

This structural model is in keeping with the assignment of the third peak in T(r) at 2.86 Å due to O-O and the fourth peak at 3.18 Å due to Nd-B. At lower Nd concentrations, the coordination of B around Nd is about twice that of O around Nd i.e. ~ 20 . The latter could be interpreted as arising from the fact that for each O of the oxygen polyhedral around the Nd ions there are two B ions. Such a situation can happen if there are more complex structural units that surround each Nd ion. At higher Nd concentrations, the coordination of B around Nd comes down to ~ 7 or one B atom for each of the O atoms in the oxygen polyhedral around Nd at these higher concentrations of Nd_2O_3. Thus, at lower Nd concentrations in the glass Nd is mainly surrounded by complex superstructural units eg. diborates, pentaborates of the borate glass while at higher Nd concentrations, simpler trigonal and tetrahedral units surround the Nd ions.

7.3 Mixed Rare-Earth Effect on Borate Glass Structure

In the preceding Chapter, a single rare-earth ion was included in a borate host glass. This was followed by incorporating two rare-earth elements together in the same host. The first pair was Nd and Ho. As with the single ion type, a series of glasses was prepared in which the concentration varied from 20 mole % of either Nd or Ho followed by an increasing percentage of the second rare-earth element with a concomitant decrease in the first type until there was only the second type at 20 mole %.

The analyses of the neutron diffraction data of these Nd-Ho glasses closely followed the approach adopted for the Nd borate glasses of Chapter 4. The first peak at 1.366 Å was ascribed to the B-O correlation. As the total concentration of rare-earth ion remained the same for all members of this series, the total B-O coordination number was found to be approximately the same with 33% of the boron atoms being in tetrahedral coordination with oxygen.

In the second peak, the weighted average of the neutron scattering lengths of Nd and Ho was used as the combined rare-earth value. The B-B and O-O correlations and coordination numbers were taken as the same as for the Nd glasses of Chapter 4. The Re-O coordination at 2.5 Å showed a decrease with increasing Ho concentration from about 10.5 (for the "only" Nd dopant) to 5.5 (for the "only" Ho dopant). These coordination numbers

The third peak was ascribed to 2nd B-O and Re-B. The variation of 2nd B-O with Ho concentration showed a slight decrease with Ho concentration and was taken as being related to this coordination in the bulk or bulk density values which were slightly lower than that of the Nd glasses. The Re-B coordination numbers increased with Ho concentration from ~ 12.5 to ~17.

Thus it may be concluded that the smallest BO_3 and BO_4 units of the borate host remain unchanged by addition of these rare-earth ions. Neither Nd nor Ho are coordinated to simpler trigonal or tetrahedral units. Nd ions appear to be surrounded by oxygen polyhedral while Ho ions have larger more complex structural units as their immediate neighbours with about three B atoms for each of the O atoms that surround the Ho ions.

The second pair of rare-earth ions included in a borate host glass was Nd with Pr. Only two concentrations in this series were prepared. The first was 18 mole % Nd_2O_3 with 2 mole % Pr_6O_{11} while the second was 8 mole % of each of these compounds. In the first the relative Nd to Pr concentration was 3:1 while in the second glass this relative concentration was 1:3. Difficulties with normalization of the S(Q) and error ripples at higher Q values led to correlation functions that could not be quantitatively interpreted. However, differences of the two total radial distribution functions were significant enough for a qualitative conclusion to be drawn.

The changes in the third and fourth peaks in T(r) of the MCGR calculations from the measured S(Q) were considered. For the Pr -Nd glass, the B-O correlation length of the boroxol ring decreases from 2.82 Å in the Nd-Pr glass to 2.74 Å. Simultaneously, the Re-B correlation length increases to 3.18 Å in the Pr-Nd glass as compared to 3.08 Å in the Nd-Pr glass.

7.4 Structural Studies of Coated and Compacted Microspheres of Silica Glass

Silica microspheres of 100 μm diameter were coated with several different compounds viz. Ag , Ni, ZnO and CdS. These coated microspheres were then mixed with polyethylene glycol, compacted under 2x 10^6 Pa (2 tonnes) and sintered at 640 ^oC for 18 hours to produce rigid but porous compacts. All four types of coating were observed under X100 magnification to be uniformly deposited. In addition to these compounds, a fifth coating consisting an Nd-borate glass was also prepared.

X-ray diffraction patterns of the unsintered and sintered samples confirmed the Ag, ZnO and CdS samples to be crystalline and having the Bragg reflection planes expected of these compounds. Although the Ni coating was shown to be crystalline, the structure was not matching with any of the commonly known compounds of Nickel. After sintering, the CdS sample was no longer present on the microspheres while the other compounds showed the same reflections but with better angular resolution.

Neutron diffraction patterns were also obtained for these coated samples. The Nickel coated sample was seen to have several weak reflections superimposed on a glassy background. The positions of these peaks on a Q scale were in agreement with the same peaks measured by X-ray diffraction on both the sintered and un-sintered Ni sample. The diffraction patterns for the other crystalline compounds were too weak to be observed as the quantity deposited onto the microspheres was not sufficient to be observed with neutrons. The S(Q) functions for Nd-borate glass, the uncoated microspheres and pure silica were compared . The first sharp diffraction peak for each of these samples showed a correlation length to progressively decrease from 5 Å to 3 Å in going from the pure silica to the Nd-borate coated glass.

The bulk properties and potential uses of these coated microspheres which have been compacted

and sintered to form rigid yet porous pellets are yet to be investigated. They hold much promise in various applications such as high performance catalysts, anti-microbial filters, semiconductors, luminescent materials etc.

In Conclusion

This work has dealt with the investigation of structures of rare-earth doped borate glasses by X-ray and neutron diffraction. Much useful information up to and including the second nearest -neighbour correlations has been obtained. These parameters are truly representative of the bulk average structures and are of fundamental relevance to physical properties of these glasses. Further investigations of these structures can be carried out by techniques such as : Raman scattering to determine the presence and relative proportions of the different structural units in the glass; Boron- NMR for the structural environments around Boron; EXAFS for the local structural environments of the rare-earth ions; and SANS to check for possible nano-clustering of the rare-earth ions at higher concentrations. Computer simulation studies on these glasses, based on the diffraction data presented in this work would also be valuable in clarifying structural ambiguity in the second and third neighbour correlation distances.

Bibliography

1. Ahoussou A.P., Rogez J., Kone A., Thermochim. Acta, 441 (2006) 96.
2. Ajroud M., Haouari M., Ben Ouada H., Maaref H., Brenier A. and Garapon C., J. Phys. Condens. Matter, 12 (2000) 3181-3193
3. Alben R. and Boutron P., Science, 187 (1975) 430
4. Barton L., Brinza D., Frease R.A. and Longcor F.L., J. Inorg. Nucl. Chem. 39 (1977) 1845.
5. Bell R.J. and Dean P., Phil. Mag. 25 (1972) 1381
6. Berger T.J., Spadaro J.A., Chapin S.E., Becker R.O., Agents Chemother, 9 (1976) 357-8.
7. Blech I.A. and Averbach B.L., Phys. Rev. 137 (1965) A 1113
8. Branda F., Constantini A., Fresa R., Buri A., Phys. Chem. Glasses 36 (1995) 272.
9. Bray P.J. and Silver A.H., Modern aspects of the vitreous state, Vol. 1, ed., Mackenzie J.D. (Butterworths, Washington, 1960) p. 92
10. Bray P.J., Feller S.A., Jellison G.E. Jr. and Yun Y.H., J. Non-Crystalline Solids 38-39 (1980) 93
11. Bray P.J., Gravina S. and Lee D., in: Boron-rich Solids, ed. Emin D., Aselage T.L. and Morosin B., Al P Conf. Proc. 231 (1991) 271
12. Britt J. and Ferekides C., Appl. Phys. Lett., 62 (1993) 2851
13. Carrasco M.F., Mendiratta S.K. and Ferreira J.M., Eur. Phys., J.Appl. Phys. 30 (2005) 91-99
14. Chakraborty I.N., Shelby J.E., and Condrate R.A. Sr., J. Am. Ceram. Soc., 67 (1984) 782
15. Chakraborty I.N., Day D.E., Lapp J.C., and Shelby J.E., J. Am. Ceram. Soc., 68 (1985) 368
16. Chemical Nickel Plating, U.S. Patent, El Mohamad, 3,903,319 (Sept. 2, 1975)
17. Chen P. L., Ma X. Y. and Yang D. R., Appl. Phys. Lett., 89 (2006) 111112
18. Chiba, H. Haijima and Kobayashi K., Surf. Coat. Technol. 169–170 (2003) 104
19. Chiba A., Haijima H., Wu W.C., Ultrasonics 42 (1–9) (2004) 617

20. Chiodelli C., Magistris A., Villa M., and Björkstam J.L., J. Non-Cryst. Solids 51 (1982) 143

21. Cocking S.J. and Heard C.R.T., U.K.A.E.A., Rept. A.E.R.E. (1965) 5016

22. Compton A.H. and Allison S.K., X-rays in Theory and Experiment, Van Nostrand Rainhold, New York, (1935)

23. Constantini A., Buri A., Branda F., Solid State Ionics, 67 (1994) 175.

24. Cromer D.T and Mann J.B., Acta Cryst. A24 (1968) 321

25. Dalba G., Fornasini P., Rocca F., Bernieri E., Burratini E., and Mobilio S., J. Non-Cryst. Solids, 91 (1987) 153

26. Dalba G., Fornasini P., Rocca F., J. Non-Cryst. Solids, 123 (1990) 310

27. Davis E.A., Wright H., Doran N.J. and Nex C.M.M., J. Non-Crystalline Solids 32 (1979) 257.

28. Day D.E., J. Non-Cryst. Solids 21 (1976) 343.

29. De Sousa B., and Singh M., M.Sc. Project Report, 2004, Goa University

30. Debye P., Ann. Phys. 46 (1915) 809

31. Delaunois F., Petitjean J.P., Lienard P., Jacob-Duliere M., Surf. Coat.Technol. 124 (2–3) (2000) 201

32. Delaunois F. and Lienard P., Surf. Coat. Technol. 160 (2–3) (2002) 239

33. Dervos C.T., Novakovic J., Vassiliou P., Mater. Lett. 58 (5) (2004) 619

34. Dunlevey F.M. and Cooper A.R., Bull. Am. Ceram. Soc. 51 (1972) 374

35. Dunlevey F.M. and Cooper A.R., The structure of non-crystalline materials, ed., P.H. Gaskell (Taylor and Francis, London, 1977) p. 211

36. Edwards J.O. and Ross V.J., J. Inorg. Nucl. Chem. 15 (1960) 329

37. Elbers S., Strojek W., Koudelka L., Eckert H., Solid State Nucl. Magn. Reson., 27 (2005) 65.

38. Elliott S.R, Physics of Amorphous Materials, Longman, Harlow, 1990

39. Elliott S.R., Phil. Mag. B37 (1978) 435

40. Enderby J.E., Physics of Simple Liquids, (1968) Eds. Temperly H.N.V., Rowlinson J.S. and Rushbrooke G.S. (North-Holland, Amsterdam), Chap. 14

41. Evans D.L. and King S.V., Nature 212 (1966) 1353

42. Faber T. E. and Ziman J. M., Phil. Mag. 11 (1965) 153

43. Fajans F. and Barber S.W., J. Am. Chem. Soc. 74 (1952) 2761

44. Feller S.A., Dell W.J., and Bray P.J., J. Non-Cryst. Solids 15 (1982) 21

45. Feng T. and Linzhang P., J. Non-Cryst. Solids, 112 (1989) 142.

46. Fischer H. E., Barnes A. C and Salmon P. S., Rep. Prog. Phy. 69 (2006) 233-199

47. Fournet G., Handbuch der Physik vol 32 (Berlin: Springer) (1957) pp 238–320

48. Galeener F. L., in : The Structure of Non-Crystalline Materials, P.H. Gaskell, J. M. Parker and E. A. Davis (Eds.), Taylor and Francis, New York (1983) 343

49. Galeener F., Lucovsky G., and Mikkelsen J.C., Jr., Phys. Rev. B8 (1980) 3983

50. Galeener F.L. and Geissberger A.E., J. Phys. (Paris) Coll. C 9 (1982) 343.

51. Galeener F.L. and Thorpe M.F., Phys. Rev. B 28 (1983) 5802

52. Gawrilov G.G., Chemical (Electroless) Nickel Plating, Portcullis Press Ltd, Surrey, 1979

53. Goubeau J. and Keller H., Z. Anorg. Allg. Chem. 272 (1953) 303

54. Gravina S.J., Bray P.J. and Petersen G.L., J. Non-Cryst. Solids 123 (1990) 165

55. Greaves G.N. and Davis E.A., Phil. Mag. 29 (1974) 1201

56. Green R.L., J. Am. Ceram. Soc. 25 (1942) 83

57. Griscom D.L., in: Borate Glasses: Structure, Properties, Applications, Eds. Pye L.D., Frechette V.D. & Kreidl N.J., Plenumney York (1978) 11

58. Hall R.B. and Meakin J.D., Thin Solid Films, 63 (1979) 203

59. Hannon A.C., Grimly D.I., Hulme R.A., Wright A.C., Sinclair R.N., J. Non-Cryst. Solids, 177 (1994) 299-316

60. Hannon A.C., Sinclair R.N., Blackman J.A., Wright A.C. and Galeener F.L., J. Non-Cryst. Solids 106 (1988) 116

61. Hannon A.C., Wright A.C. and Sinclair R.N., in: Fundamentals of Glass Science and Technology 1993 (Stazione Sperimentale del Vetro, Venice, 1993) p. 479 (Suppl. Riv. Staz. Sper. del Vetro XXII1 1993)

62. Hayashi S. and Hayamizu, J. Non-Cryst. Solids 11 (1989) 214

63. Hedstrom J., Ohlsen H., Bodegard M., Kylner A., Stolt L., Hariskos D., Ruckh M. and Schock H.-W., Proc. 23rd IEEE PVSC (1993) 364

64. http://www.isis2.isis.rl.ac.uk/RMC/mcgr.htm

65. Huang S.M., Bian Z.Q., Chu J. B., Wang Z. A., Zhang D.W., Li X. D., Zhu H. B. & Sun Z., J. Phys. D: Appl. Phys. 42 (2009) 055412

66. Ingram M.D., Phys. Chem. Glasses 28 (1987) 215

67. Isard J.O., J. Non-Cryst. Solids 1 (1969) 235

68. Izumitani T., Toratani H. and Kuroda H., J. Non-Cryst.Solids 47 (1982) 87

69. Jacobs R.R. and Weber M.J., IEEE J. Quantum Electron.QE-12 (1976) 102

70. Jellison G.E. Jr. and Bray P.J., Sol. St. Commun. 19 (1976) 517

71. Jellison G.E. Jr., Panek L.W., Bray P.J. and Rouse G.B. Jr., J. Chem. Phys. 66 (1977) 802

72. Johnson P.A.V., Wright A.C. and Sinclair R.N., J. Non-Cryst. Solids 50 (1982) 281

73. Judd B.R., Phys. Rev. 127 (1962) 750

74. Kamitsos E.I., Patsis A.P., Karakassides M.A., and Chryssikos G.D., J. Non-Cryst. Solids 126 (1990) 52

75. Kanehisa M.A. and Elliott R.J., Mater. Sci. Eng. B 3 (1989) 163

76. Kim K.S. and Bray P.J., J. Nonmetals, 2 (1974) 95

77. Krogh-Moe J., Acta Cryst. 9 (1956) 951

78. Krogh-Moe J., Arkiv Kemi 14 (1959) 31

79. Krogh-Moe J., Phys. Chem. Glasses, 3 (1962) 1

80. Krogh-Moe J., Phys. Chem. Glasses, 6 (1965) 46

81. Krogh-Moe J., J. Non-Cryst. Solids, 1 (1969) 269

82. Krupke W.F., IEEE J. Quantum Electron. QE-10 (1974) 450

83. Kumari S. and Pereira N., M.Sc. Project Report, 2003, Goa University

84. Labarre J.-F., Graffeuil M., Faucher J.-P., M. Pasdeloup and Laurent J.-P., Theoret. Chim. Acta 11 (1968) 423

85. Licheri G., Musini A., Pashina G., Piccaluga G., Pinna G., and Magistris A., J. Chem. Phys. 85 (1986) 500

86. Lomer W. M. and Low G. G., Thermal Neutron Scattering ed P A Egelstaff (London and New York: Academic) (1965) chapter 1

87. Lorch E., J. Phys. C: Solid State Phys. 2 (1969) 229

88. Lorösch J., Couzi M., Pelous J., Vacher R., and Levasseur A., J. Non-Cryst. Solids, 69 (1984) 1

89. Lowther J.E., J. Phys. C, 7 (1974) 4393-4402

90. Lu C.Y., Chang S.J., Chang S.P., Lee C.T., Kuo C.F., Chang H.M., Chiou Y.Z., Hsu C.L. and Chen I.C., Appl. Phys. Lett., 89 (2006) 153101

91. Mallory G.O., Hadju J.B. (Eds.), Electroless Plating: Fundamentals and Applications, AESF, Orlando, 1991.

92. Marion J.E. and Weber M.J., Eur. J. Solid State Inorg. Chem. 28 (1991) 271

93. Milberg M.E., J. Appl. Phys. 29 (1958) 64

94. Modak S.M. and Fox C.L.J., Biochem Pharmacol, 22 (1973) 2391- 404.

95. Moorthy L.R., Jayasimhadri M., Radhapathy A. & Ravikumar R.V.S.S.N., Mater. Chem. Phys., 93 (2005) 455-460

96. Moorthy L.R., Rao T.S., Jayasimhadri M., Radhapathy A., & Murthy D.V.R.,

Spectrochimica Acta Part A, 60 (2004) 2449-2458

97. Mott N. F., Elements of Wave Mechanics (Cambridge: Cambridge University Press), (1962)

98. Mozzi R.L. and Warren B.E., J. Appl. Cryst. 3 (1970) 251

99. Nadjakov G., Andreitchine R. and Borissov M., Izu. Bulg. Akad. Navk., 4 (1954) 10.

100. Norman N., Acta Cryst., 10 (1957) 370

101. O'brien Poul and Saeed Tahir, J. Crystal Growth, 158 (1996) 477.

102. Ofelt G.S., J. Chem. Phys. 37 (1962) 511

103. Oloffs C., Grosse-Siestrup C., Bisson S., Rinck M., Rudolph R., Gross U., Biomaterials 15 (1994) 753- 8.

104. Osaka T., Takano N., Kurokawa T., Kaneko T., Ueno K., Surf. Coat. Technol. 169–170 (2003) 124.

105. Ouerfelli J., Regragui M., Morsli M., Djeteli G., Jondo K., Amory C., Tchangbedji G., Napo K. and Bernede J.C., J. Phys. D: Appl. Phys., 39 (2006) 1954.

106. Paalman N.H. and Pings C.J.; J. Appl. Phys. 33 (1962) 2635

107. Pashina G., Piccaluga G., and MAgini M., J. Chem. Phys. 81 (1984) 6201

108. Petkov V., J. Appl. Cryst. 22 (1989) 387

109. Placzek G., Phys. Rev. 86 (1952) 377

110. Pusztai L. and McGreevy R.L., Physica B, 357 (1997) 234-236

111. Ramesh Rao N., Krishna P.S.R., Basu S., Dasannacharya B.A., Sangunni K.S. and Gopal E.S.R., J. Non-Crystalline Solids, 240 (1998) 221-231

112. Rami M., Benamar E., Fahoume M., Chraibi F. and Ennaqui A., Solid State Sciences, t. 1 (1999) 179-188

113. Rawson H., Inorganic Glass-Forming Systems, Academic Press (1967)

114. Riedel W., Electroless Plating, ASM International, Ohio, 1991.

115. Risen W.M. Jr., J. Non-Cryst. Solids 76 (1985) 97

116. Saito N., Haneda H., Sekiguchi T., Ohashi N., Sakaguchi I. and Koumoto K., Adv. Mater., 14 (2002) 393.

117. Salmon P. S., Proc. R. Soc. Lond. A (1994) 445 351–65

118. Sankara Narayanan T.S.N., Krishnaveni K., Seshadri S.K., Mater. Chem.Phys. 82 (3) (2003) 771.

119. Serafini A. and Labarre J.F., J. Mol. Structure 26 (1975) 129

120. Shikerkar A.G., Desa J.A.E., Krishna P.S.R., and Chitra R., J. Non-Cryst. Solids, 270 (2000) 234- 246

121. Shin Y.B. and Heo J., J. Non-Cryst. Solids, 253 (1999) 23

122. Soper A.K. and Egelstaff P.A., Nucl. Instrum. Meth. (1980) 415

123. Squires G.L., Introduction to the Theory of Thermal Neutron Scattering (Cambridge: Cambridge University Press) (1978)

124. Svanson S.E., Forslind E. and Krogh-Moe J., J. Phys. Chem. 66 (1962) 174

125. Takebe H., Harada T., Kuwatara M., J. Non-Cryst. Solids 352 (2006) 709.

126. Tanabe S., Ohyagi T., Soga N. and Hanada T., Phys. Rev. B46 (1992) 3305

127. Thijsse B.J., J. Appl. Cryst. 17 (1984) 61

128. Tuller H.L. and Button D.P., in Transport-Structure Relations in Fast Ion and Mixed Conductors, ed. by Poulsen F.W., Hessel-Andersen N., Clausen K., Skaarup S., and Toft Soerensen O., (Risø National Laboratory, Denmark, (1985)

129. van Hove L., Phys. Rev. 95 (1954) 249–62

130. Varshneya Arun, Fundamentals of Inorganic Glasses, Soc. of glass Tech. (2006)

131. Villa M., Scagliotti M., Chiodelli G., J. Non-Cryst. Solids, 94 (1987) 101.

132. Vineyard G.H., Phys. Rev. 96 (1954) 93

133. Wang J. X., Sun X. W., Wei A., Lei Y., Cai X. P., Li C. M. and Dong Z. L., Appl. Phys. Lett., 88 (2006) 233106.

134. Warren B.E., Krutter H. and Morningstar O., J. Am. Ceram. Soc. 19 (1936) 202

135. Williams R.L., Doherty P.J., Vince D.G., Grashoff G.J., Williams D.F., Crit Rev Biocompat; 5 (1989) 221- 43.

136. Williams S.J. and Elliott S.R., Proc. R. Soc. (London) A 380 (1982) 427

137. Windisch C.F. Jr. and Risen W.M. Jr., J. Non-Cryst.Solids 48 (1982) 325

138. Wright A. C., Advances in Structure Research by Diffraction Methods, 5 (1974) 1-84

139. Wright A. C., Nucl. Instrum. Methods, 176 (1980) 623–5

140. Wright A.C., Phy.Chem. Glasses: Eur. J. of Glass Sci. Technol. B, 51(1) (2010) 1-39

141. Wright A.C., Sumner D.J. and Clare A.G., in: The Structure of Non-Crystalline Materials 1982, ed. Gaskell P.H., Parker J.M. and Davis E.A. (Taylor and Francis, London, 1982) p. 395

142. Xu C. X. and Sun X. W., Appl. Phys. Lett. 83 (2003) 3806

143. Yarnel J.L., Katz M.J., Wenzel R.G. and Koenig S.H., Phys. Rev. A7 (1973) 2130

144. Yi S.H., Choi S.K., Jang J.M., Kim J.A. and Jung W.G., J. Colloid and Interface Sci., 313 (2007) 705.

145. Yiannopoulos Y. D., Chryssikos G. D. & Kamitsos E. I., Phys. Chem. Glasses, 42 (3) (2001) 164–72

146. Yun Y. H., Bray P. J., J. Non-Cryst. Solids, 30 (1978) 45.

147. Zachariasen W.H., J. Am. Chem. Soc. 54 (1932) 3841

148. Zeyer-Dusterer M., Montagne L., Palavit G., Jager C., Solid State Nucl. Magn. Reson., 27 (2005) 50.

149. Zachariasen W.H., J. Am. Chem. Soc. 54 (1932) 3841

150. Zeyer-Dusterer M., Montagne L., Palavit G., Jager C., Solid State Nucl. Magn. Reson., 27 (2005) 50.

Appendix

Publications

1. "Optical Properties of Pr and Nd Ions in a Borate Glass", J. A. Erwin Desa, Wilson A. Vaz, Brenda L. De Souza and Manju Singh, Glass Technology: European Journal of Glass Science and Technology, Part A Volume 50 Number 4, August 2009.

In Preparation

1. "Neodymium Dopant Ions in Borate Glass", Wilson Vaz, J.A. Erwin Desa, P.S.R. Krishna and A.B. Shinde.

Conference Presentations

1. "Rare Earth Oxides in a Borate Host Glass", J.A.Erwin Desa, Wilson Vaz, Brenda De Souza and Manju Singh; "The 6th International Conference on Borate Glasses, Crystals and Melts (BORATE 2008)", Egret Himeji, Japan, August 18-22, 2008.
2. "Optical Absorption, Luminescence and Raman Spectroscopic Studies of Rare-Earth Doped Phosphate Glasses", J.A.Erwin Desa, Wilson Vaz, Alka Sawaikar, P.R. Sarode, and S.K. Mendiratta; "International Conference on Multifunctional Oxide Materials (ICMOM 2009)", Himachal Pradesh University, Shimla, UP, April 16-18, 2009.
3. "Structures of Coated and Compacted Microspheres of Silica", Wilson Vaz, J.A. Erwin Desa, P.S.R. Krishna and A.B. Shinde; "Conference on Neutron Scattering and Mesoscopic Systems (CNSMS 2009)", International Centre/Goa University, Goa, October 12 - 14, 2009.
4. "Structural Studies of Coated and Compacted Glass Microspheres", Wilson Vaz, J.A. Erwin Desa, P.S.R. Krishna, A.B. Shinde; "XXII International Congress on Glass (ICG 2010)", Salvador da Bahia, Brazil, September 20-25, 2010.

5. "Optical Studies of Neodymium And Praseodymium Doped Phosphate Glasses", J.A.Erwin Desa, Wilson Vaz, Alka Sawaikar, P.R. Sarode, and S.K. Mendiratta; "XXII International Congress on Glass (ICG 2010)", Salvador da Bahia, Brazil, September 20-25, 2010.

6. "Structural Studies of Compacted Glass Microspheres", Wilson Vaz, J.A. Erwin Desa, P.S.R. Krishna, A.B. Shinde; "International Conference on Specialty Glass & Optical Fiber: Materials, Technology & Devices (ICGF 2011)", Central Glass & Ceramic Research Institute, Kolkata, August 4-6, 2011.

7. "Structures of Porous Compacts of Coated Glass Microspheres", Wilson Vaz, J.A. Erwin Desa, P.S.R. Krishna, A.B. Shinde; "4th International Conference on Porous Media (INTERPORE 2012)", Purdue University, West Lafayette, Indiana, U.S.A., May 14-16, 2012.

8. "Neutron Diffraction Studies Of Rare-Earth Doped Borate Glasses", Wilson Vaz, J.A. Erwin Desa, P.S.R. Krishna And A.B. Shinde; "2nd International Symposium On Neutron Scattering (ISNS 2013)", BARC, Mumbai, January 14-17, 2013.

Workshops Attended

1. School on "Neutrons as Probes of Condensed Matter", BARC, Mumbai, October 5 -10, 2009.

2. Arun Varshneya Class on "Fundamentals of Glass Science and Technology", Salvador da Bahia, Brazil, September 20-25, 2010.